Liquid water flow in snow and hydrological implications

THÈSE N^O 6441 (2015)

PRÉSENTÉE LE 27 FÉVRIER 2015
À LA FACULTÉ DE L'ENVIRONNEMENT NATUREL, ARCHITECTURAL ET CONSTRUIT
LABORATOIRE DES SCIENCES CRYOSPHÉRIQUES
PROGRAMME DOCTORAL EN GÉNIE CIVIL ET ENVIRONNEMENT

ÉCOLE POLYTECHNIQUE FÉDÉRALE DE LAUSANNE

POUR L'OBTENTION DU GRADE DE DOCTEUR ÈS SCIENCES

PAR

Nander WEVER

acceptée sur proposition du jury:

Prof. N. Geroliminis, président du jury
Prof. M. Lehning, Prof. M. Parlange, directeurs de thèse
Prof. K. Nishimura, rapporteur
Prof. P. Perona, rapporteur
Prof. M. van den Broeke, rapporteur

(EPFL
ÉCOLE POLYTECHNIQUE
FÉDÉRALE DE LAUSANNE

Suisse
2015

We are a way for the Cosmos to know itself.

— Carl Sagan

Acknowledgements

Scientific papers and this PhD thesis, that is what the scientific community can see from my work over the last few years. But for me personally, the more interesting part were not those end products, but the process of getting them. Finding my way in the snow sciences in the last four years has been a rich experience. At the SLF, the atmosphere is very encouraging to explore the snow related sciences in all its aspects.

I am especially grateful to my thesis-director Michael Lehning for being an excellent guide in this process. I enjoyed the freedom in my work and our effective meetings. Your enthusiasm when I presented results or ideas was without exception encouraging. You always gave me a positive feeling that I was on the right track and I always left with new ideas. I have been impressed many times with your quick switching between the big picture and the small details. Thank you also for offering me to join the research expedition to the Antarctic sea ice as a field assistant. I have beautiful memories of the frozen world in the twilight, while battling the elements, or was it rather the laser-scanner? It was a great experience!

I would also like to thank all employees of the institute for interesting discussions about snow related processes. In particular I am thankful to my group leader Charles Fierz for all the fruitful discussions we had about snow processes and the possibilities and impossibilities to simulate them in SNOWPACK. I gained a lot of insights in the fascinating processes guiding the snow cover from the first snow flake to the last melt form. I will always look to the snow cover with different eyes in the future.

During my examination on 27 October, the exam committee was creating a warm atmosphere which resulted in interesting discussions, for which I highly acknowledge Prof. Nikolaos Geroliminis, Prof. Michael Lehning, Prof. Marc Parlange, Prof. Paolo Perona, Prof. Michiel van den Broeke and Prof. Kouichi Nishimura.

Finally, the countless adventurous days in the snowy mountains around Davos together with my dear colleagues and friends will remain in my memory forever. Snow not only is an interesting and versatile field of study, but also provides unforgettable joy and inspiration to the mind. A big thanks to all for being such pleasant companions!

Davos, 27 November 2014.   Nander Wever

Abstract

The presence of a snow cover has a strong impact on hydrological processes. It alters the lower boundary of the atmosphere considerably, while shielding the underlying soil from atmospheric influences for extended periods of time. Consequently, the behaviour of the snow cover has a strong impact on, for example, soil moisture and streamflow. In this thesis, the role of the snow cover as an interface between the atmosphere and the soil is assessed. One important aspect is the snowmelt and subsequent flow of liquid water in snow. It determines when meltwater is released from the snowpack and starts contributing in other hydrological processes. In mountainous terrain, liquid water flow in snow is also important in wet snow avalanche formation. Complex flow processes, such as ponding of liquid water inside the snowpack and lubrication at the snow-soil interface, may weaken existing weak layers or set in motion glide snow avalanches.

An implementation of a solver for Richards Equation (RE) in the one-dimensional, physics based, multi-layer snow cover model SNOWPACK is discussed. This equation for liquid water flow in variably saturated porous media provides the model with a consistent description of liquid water flow in the snow-soil continuum, including phase changes. For soil, a freezing point depression approach for phase changes was implemented, as well as a description of heat advection by liquid water flow under the presence of a temperature gradient.

The SNOWPACK model was validated by comparing snow cover simulations for the sites Weissfluhjoch (2540 m) and Col de Porte (1325 m) with an extensive data set of over a decade of meteorological and snowpack measurements. Solving RE for snow appeared to improve the estimation of liquid water runoff from the snowpack, especially on sub-daily time scales and in deep, stratified snow covers. The onset of snowpack runoff in spring was better predicted when using RE instead of the conventional bucket-type approach. On the sub-daily time scale, the timing of peak runoff was predicted more accurately using RE. These results suggest that the understanding of hydrological processes in snow dominated catchments could benefit from solving RE for the snowpack. For Weissfluhjoch, SNOWPACK simulations were also compared to snow profiles, snow temperature measurements and data from upward looking ground penetrating radar, to assess the representation of the internal snowpack structure. In the main winter season, high agreement was found for the temporal evolution of snow water equivalent, snow density, temperature profiles and, to a lesser extent, grain size and type. In the melt season, a comparison with measured snow temperatures suggested that simulations with RE provide a better representation of the movement of the meltwater front through the snowpack than with the bucket scheme. However, this result is only partly supported

Abstract

by the progress of the meltwater front as detected in the radar data. The bucket scheme seems to provide a better overall agreement here, although still large discrepancies exist. In contrast, measured snowpack runoff started consistently earlier than the radar detected arrival of the melt water front at the snowpack base. That suggests that preferential flow is playing a significant role in the onset of snowpack runoff and that simulations with RE cover (unintentionally) some preferential flow effects. Simulations with RE also reproduced liquid water ponding on microstructural inhomogeneities in the snowpack.

The depletion rate of snow water equivalent in spring appeared to be overestimated in the simulations. Although it could not be excluded that errors in diagnosing the surface energy fluxes are playing a role, there were strong indications that the densification process of the snowpack in spring is not adequately simulated, as simulated snow density in spring was typically much lower than measured. This could potentially have a strong impact on the energy input in the snowpack, as light upper snow layers may provide isolation for deeper snow layers, while at the same time, shortwave radiation may penetrate deeper in the snowpack, efficiently bringing heat inside the snowpack. Furthermore, the radar data suggests that a snowpack is able to retain more meltwater than predicted by either one of the water transport schemes. These problems deserve attention in future SNOWPACK developments.

The revised soil module of SNOWPACK was verified by comparing soil moisture measurements for 7 stations in the area of Davos, that were equipped with soil moisture sensors at several depths, with distributed SNOWPACK simulations using the spatially explicit Alpine3D model. Given the uncertainties in soil properties and soil moisture measurements, soil moisture was simulated with varying degrees of success. By investigating cross-correlations between the different sites for measurements and Alpine3D simulations, it was found that the spatially distributed simulations were able to explain a part of the spatial variability in the measurements. This could be mainly attributed to the spatial variability of the snow cover and snow melt. Preliminary results also suggest that streamflow simulations in Alpine3D could benefit from accurate soil moisture simulations.

Finally, the improved SNOWPACK model was used to simulate the snow cover development at 14 sites in two areas in Switzerland that encountered severe flooding in October 2011, when a large snowfall was followed by a significant warming and large rainfall. Thick snow covers (>50 cm) were found to have had significant capacity for liquid water storage, creating a time lag of several hours between the onset of rainfall and the onset of snowpack runoff, whereas shallow snow covers reacted much quicker. Interestingly, it was found that once thick snow covers produced runoff, peak runoff rates exceeded runoff rates from shallow snowpacks and also exceeded the sum of rainfall and snowmelt rates. This suggests that snow settling, wet snow metamorphism and liquid water flow provide an interaction with each other that potentially can enhance snowpack outflow. This model result could not yet be validated with measurements, but may have important consequences for understanding the contribution of snowpack runoff in flood events.

Key words: snow cover, liquid water flow, mountain hydrology, soil moisture, numerical modelling

Zusammenfassung

Die Schneedecke spielt eine wichtige Rolle bei hydrologischen Prozessen. Sie ändert die untere Randbedingung für die Atmosphäre und gleichtzeitig schirmt sie für längere Zeit den Boden vom Atmosphäreneinfluss ab. Deswegen hat die Anwesenheit einer Schneedecke unter anderem starke Auswirkungen auf die Bodenfeuchte und den Abfluss von Fliessgewässern. In dieser Studie wird die Rolle der Schneedecke als Schnittstelle zwischen der Atmosphäre und des Bodens genauer untersucht. Eine wichtige Kompenente ist hier unter anderem die Schneeschmelze und der daraus resultierende Wassertransport im Schnee, da aus der Schneedecke freigegebenes Wasser nachfolgend zu verschiedensten hydrologischen Prozessen beiträgt. Zusätzlich ist die Wasserströmung im Schnee in Berggebieten besonders wichtig für die Bildung von Nasschneelawinen. Komplexe Strömungseffekte, wie an bestimmten Schneeschichten aufstauendes Wasser innerhalb der Schneedecke und die Entstehung einer Schmierschicht am Schnee-Boden-Übergang, können Schwachschichten innerhalb der Schneedecke auslösen oder die ganze Schneedecke als Gleitschneelawine in Bewegung bringen.

Im Folgenden wird die Implementierung eines Lösers für die Richards-Gleichung (RG) in das eindimensionale, physikalisch basierte Schneedeckenmodell SNOWPACK diskutiert. Diese Gleichung für die Wasserströmung in ungesättigten porösen Medien gibt dem Modell die Möglichkeit, die Wasserströmung in stimmiger Weise für das Schnee-Boden Kontinuum zu beschreiben und dabei Phasenübergänge zu berücksichtigen. Für Böden sind Phasenübergänge anhand des Konzepts der Gefrierpunktserniedrigung implementiert, weiterhin wird Wärme-Advektion bedingt durch Wasserströmung abgebildet, wenn es einen Temperaturgradienten gibt.

Das SNOWPACK-Modell wurde mittels eins Vergleichs von Schneedeckensimulationen für die Standorte Weissfluhjoch (2540 m) und Col de Porte (1325 m), welche langjährige Messreihen von meteorologischen Grössen und Schneedeckeninformationen besitzen, validiert. Es hat sich gezeigt dass die RG die Abschätzung des Abflusses aus der Schneedecke verbessert, insbesondere für stündliche Zeitskalen und in dicken, stark geschichteten Schneedecken. Der Beginn des Abflusses aus der Schneedecke im Frühling wird mit der RG besser abgebildet, wenn verglichen mit einem konventionellen Eimer-Verfahren. Gleichzeitig verbessert die RG die Vorhersage der täglichen Spitzenablüsse aus der Schneedecke. Diese Ergebnisse weisen darauf hin, dass das Verständnis hydrologischer Prozesse in schneereichen Einzugsgebieten von der Anwendung der RG für die Wasserbewegung innerhalb einer Schneedecke profitieren kann. Für die Station Weissfluhjoch wurden die SNOWPACK-Simulationen zusätzlich mit manuell aufgenommenen Schneeprofilen, Messreihen von Schneetemperaturen und Daten

eines nach oben gerichteten Bodenradars verglichen. So konnte die korrekte Abbildung der inneren Struktur der Schneedecke im Modell analysiert werden. Im Hochwinter wurde eine hohe Übereinstimmung für die zeitliche Entwicklung des Schneewasseräquivalentes, der Schneedichte, der Temperaturprofile, und, in geringerem Masse, der Korngrösse und -form gefunden. Ein Vergleich mit gemessenen Schneetemperaturen während der Schmelzphase im Frühling hat darauf hingewiesen, dass der Durchgang der Schmelzwasserfront mit RG besser abgebildet wird als mit dem Eimer-Verfahren. Dieses Ergebnis wird von der aus den Radardaten abgeleiteten Bewegung der Schmelzwasserfront aber nur teils bestätigt. Das Eimer-Verfahren scheint im Allgemeinen besser mit den Radardaten übereinzustimmen, obwohl es auch hier grosse Abweichungen gibt. Jedoch fängt gemessener Abfluss aus der Schneedecke früher an, als man aus der Ankunft der Schmelzwasserfront in den Radardaten erwarten würde. Daraus ist anzunehmen, dass präferenzielles Fliessen eine wichtige Rolle zu Beginn des Schmelzwasserabflusses spielt und Simulationen mit RG die präferenziellen Fliessprozesse teilweise (eher unbeabsichtigt) abdecken. Simulationen mit RG reproduzieren aber auch das Aufstauen des Wassers an Schichten mit stark unterschiedlichen Eigenschaften in ihrer Microstruktur.

Der simulierte Abbau der Schneedecke im Frühling findet schneller statt als beobachtet. Es konnte nicht ausgeschlossen werden, dass Fehler bei der Bestimmung der Energieflusse an der Schneeoberfläche eine Rolle spielen, aber eine konsistente und signifikante Unterschätzung der Schneedichte im Frühling weist stark darauf hin, dass die Setzung und Verdichtung des Schnees zu diesem Zeitpunkt unterschätzt wird. Das könnte potenziell grosse Folgen für die Energiezufuhr an der Schneedecke haben, da die leichten oberen Schneeschichten eine isolierende Schicht für das innere der Schneedecke bilden. Gleichzeitig kann kurzwellige Strahlung tiefer in der Schneedecke eindringen und so auf effiziente Weise die Schneedecke aufwärmen. Weiterhin gibt es Hinweise in den Radardaten, die andeuten, dass Schneedecken vielleicht mehr Schmelzwasser festhalten können als simuliert wird. Diese Probleme verdienen Aufmerksamkeit bei zukünftigen Entwicklungen von SNOWPACK.

Das überarbeitete Bodenmodul von SNOWPACK wird anhand eines Vergleichs von simulierter Bodenfeuchte mit Messungen an sieben Stationen in der Landschaft Davos und verteilten SNOPWACK-Simulationen mittels des räumlich-expliziten Alpine3D-Modells validiert. Angesichts der grossen Unsicherheiten in Bodenparametern als auch Bodenfeuchtemessungen, wird auch die Bodenfeuchte mit unterschiedlichem Erfolg simuliert. Kreuzkorrelationen zwischen einzelnen Messstationen in gemessener und simulierter Bodenfeuchte zeigen aber, das Alpine3D in der Lage ist, ein Teil der räumlichen Variabilität in den Messungen zu erklären. Das scheint vor allem mit der räumlichen Varibilität in Schneedeckenverteilung und Schneeschmelze zusammen zu hängen. Erste Ergebnisse zeigen auch, dass die Abflussmodellierung in Alpine3D von genaueren Bodenfeuchtesimulationen profitieren könnte.

Zuletzt ist das überarbeitete SNOWPACK Modell für Schneedeckensimulationen an 14 Standorten in zwei Regionen in der Schweiz angewendet worden, die im Oktober 2011 von schweren Überschwemmungen betroffen waren. Ein Grossschneefall wurde damals abgelöst von starker Erwärmung und grossen Regenmengen. Es wurde festgestellt, dass dicke Schneedecken (über 50 cm) mehr Speicherkapazität für Schneeschmelze und Regenwasser boten und dass dies

den Beginn des Wasserabflusses aus der Schneedecke um mehrere Studenten verzögert hat. Dünne Schneedecken zeigten eine viel schnellere Reaktion. Interessant war, dass sobald dickere Schneedecken Abfluss produzierten, deren Abflussspitzen höher lagen als in die dünnere Schneedecken und zudem auch höher als die Summe von Regen- und Schmelzraten. Dies weisst darauf hin, dass das Zusammenspiel von Schneesetzung, Nassschneemetamorphose und Wasserströmung als Reaktion den Abfluss aus der Schneedecke verstärken können. Dieses Modellergebnis konnte noch nicht mit Messungen bestätigt werden, hat aber potenziell wichtige Konsequenzen für das Verstehen des Beitrags von Schneedeckenabluss zu Überschwemmungen.

Stichwörter: Schneedecke, Wasserströmung, Gebirgshydrologie, Bodenfeuchte, Numerische Modellierung

Contents

Contents

List of Symbols

Symbol	Units	Description
b	mm w.e.	intercept
c	J kg^{-1} K^{-1}	specific heat
c_p	J kg^{-1} K^{-1}	specific heat of soil particles
f	–	tuning factor
g	m s^{-1}	gravitational acceleration
h	m	pressure head
h_w	m	pressure head associated with liquid water
K	m s^{-1}	hydraulic conductivity
$K_{\mathrm{L}h}$	m s^{-1}	hydraulic conductivity of the isothermal part for liquid water
$K_{\mathrm{L}T}$	m s^{-1}	hydraulic conductivity for liquid water under a thermal gradient
K_sat	m s^{-1}	saturated hydraulic conductivity
$K_{\mathrm{T}h}$	m s^{-1}	total hydraulic conductivity of the isothermal part
$K_{\mathrm{T}T}$	m s^{-1}	total hydraulic conductivity of the thermal part
$K_{\mathrm{v}h}$	m s^{-1}	hydraulic conductivity of the isothermal part for water vapour
$K_{\mathrm{v}T}$	m s^{-1}	hydraulic conductivity for water vapour under a thermal gradient
L	J kg^{-1}	latent heat of fusion
m	–	van Genuchten parameter
M_cum	mm w.e.	cumulative snow melt sum
n	–	van Genuchten parameter
N_iter	–	number of iterations for convergence in Picard scheme
P_cum	mm	cumulative precipitation sum
q	m s^{-1}	snowpack runoff
Q_cc	J m^{-2}	total cold content of the snowpack
Q_cum	mm w.e.	cumulative snowpack runoff
Q_L	W m^{-2}	latent heat flux
Q_LWnet	W m^{-2}	net longwave radiation
Q_P	W m^{-2}	heat advection by liquid precipitation
Q_S	W m^{-2}	sensible heat flux
Q_sum	W m^{-2}	upper boundary heat flux
r_es	m	equivalent sphere radius
r_g	m	classical grain size
s	m^3 m^{-3} s^{-1}	source or sink

List of Symbols

Sc	–	correction factor (*Ippisch et al.*, 2006)
T	K	soil temperature
T_{melt}	K	melting temperature of water
T^*	K	melting point of the soil water
z	m	vertical coordinate (positive upwards)
z_0	m	surface roughness length
α	m^{-1}	van Genuchten parameter
α_{r}	–	regression coefficient for precipitation
β_{r}	–	regression coefficient for snow melt
γ	rad	slope angle
Δt_{new}	s	new time step
Δt_{old}	s	old time step
Δz	m	vertical grid spacing
$\Delta \theta$	m^3 m^{-3}	change in θ between Picard iterations
ϵ_h	m	convergence criterion for h
ϵ_θ	m^3 m^{-3}	convergence criterion for θ
Θ	–	saturation
θ	m^3 m^{-3}	liquid water content
θ_{h}	m^3 m^{-3}	water holding capacity
θ_{i}	m^3 m^{-3}	ice content
θ_{r}	m^3 m^{-3}	residual liquid water content
θ_{r}^{t}	m^3 m^{-3}	residual liquid water content at current time step
$\theta_{\mathrm{r}}^{t-1}$	m^3 m^{-3}	residual liquid water content at previous time step
θ_{s}	m^3 m^{-3}	saturated liquid water content
θ_{T}	m^3 m^{-3}	sum of liquid water and water vapour content
λ	W m^{-1} s^{-1}	thermal conductivity of soil particles
μ	kg m^{-1} s^{-1}	dynamic viscosity
ρ	kg m^{-3}	dry density of the snowpack
ρ_{i}	kg m^{-3}	density of ice
ρ_{p}	kg m^{-3}	density of soil particles
ρ_{w}	kg m^{-3}	density of water

1 Introduction

1.1 Motivation

On average 43% of the Northern Hemisphere land area is continuously or seasonally covered with snow (*Kapnick and Delworth*, 2013). For the meteorologist, the snow cover alters the lower boundary of the atmosphere (*Cohen and Rind*, 1991). For example, the presence of a snow cover strongly influences the surface albedo, and consequently, the energy budget of the earth's surface. Radiative cooling of the snow cover due to outgoing longwave radiation often results in stably stratification in the surface layer of the atmosphere. For the hydrologist, the snow cover rather is an upper boundary for the soil (*Edwards et al.*, 2007). The snow cover provides a shield for the soil in winter time, reducing its exposure to the atmosphere for a significant part of the year. This directly influences the moisture and temperature fluxes at the top of the soil. The solid precipitation that falls in winter is mainly stored in the snowpack, apart from occasional melt or rain-on-snow events. In spring, when snowmelt starts, there is a strong water flux infiltrating the soil, which impacts sub-surface flow, ground water flow and eventually streamflow. Also overland flow from snowmelt may occur. In this thesis, the snow cover is studied in particular in its role as an interface between the atmosphere and the soil.

1.1.1 Streamflow and Flood Risks

Snow is an important component in the hydrological cycle. A snow cover stores precipitation in the winter months, releasing it again in spring when the snow melts. It thereby serves as an important fresh water supply for lowlands adjacent to mountainous regions (*Viviroli et al.*, 2007). Many studies focus on the role of the snow cover on streamflow. For example, for hydropower, it is not only important to know the spatial distribution of snow water equivalent, as an indicator of possible future discharge, but also the temporal dynamics of the contribution of snowmelt to streamflow (*Basso and Botter*, 2012). In mountainous terrain, the relation between snowmelt and discharge is complex, due to differences in altitude and spatial variability in received solar radiation from variability in slope angle and slope azimuth (see Figure 1.1). In light of the expected future climate change, these questions receive increased

1

attention (e.g., *Bavay et al.* (2013)).

Interactions between the snow cover and hydrological processes also regularly result in peak discharge and flooding. For example, the January 1995 flood of the Rhine River was not only attributed to unusual high rainfall amounts in the basin of the Rhine, but also to additional snowmelt in some parts of the basin due to unusual high air temperatures for the time of the year. The melt water caused the soil to be saturated and become impervious (*Fink et al.*, 1996; *Disse and Engel*, 2001). However, the contribution of the Alps to this event was considered to be small (*Disse and Engel*, 2001). This was different in May 1999. Following the snow rich winter season of 1998-1999, snowmelt in spring caused again a peak discharge of the Rhine. This event was caused by an unfortunate combination of circumstances, when strong snowmelt of the unusual thick snow cover was accompanied by heavy precipitation in upstream parts of the basin of the Rhine (*Forster and Hegg*, 2000; *Disse and Engel*, 2001).

Figure 1.1: The Dischma catchment near Davos during spring snowmelt, when snowmelt patterns are dominated by differences in altitude, slope aspect and angle.

The floods from the Rhine serve as an example of regional interactions between snowmelt, soil moisture and streamflow. Those processes have also been identified in other parts of the world, like for instance for the Mississippi and Missouri River (*Maurer and Lettenmaier*, 2003; *Koster et al.*, 2010). However, many examples of flooding events indicate that this interaction is not only effective on large scales. In October 2011, heavy rainfall and warming following shortly after heavy snowfall caused flooding in many mountainous regions in the Swiss Alps (*Badoux et al.*, 2013; *Rössler et al.*, 2014). In *Wever et al.* (2014), which is part of this thesis as Chapter 5, it is shown that already at the point scale, the snow cover contributed significant amounts of melt water in addition to the incoming rainfall. Moreover, modelled peak snowpack runoff rates were found to exceed the sum of precipitation and melt rates, likely as a result from interactions between snow settling, wet snow metamorphism and liquid water flow. In contrast, in the flooding event in October 2000 in the Southern Swiss Alps, the decrease in snowfall limit during the precipitation event was identified as having reduced the potential peak discharge of the Rhône River (*Federal Office for Water and Geology*, 2002). In other affected regions during this event, the snow cover potentially contributed additional

liquid water to runoff (*Weingartner et al.*, 2003). These contrasting examples of the role of a snow cover in hydrological processes indicate that modelling the snow cover is a delicate exercise and this provides a strong motivation to study the modelling of liquid water flow in snow in relation with both atmospheric forcing as well as underlying soil in more detail.

1.1.2 Wet Snow Avalanches

In steep mountainous terrain, avalanches pose a threat to infrastructure and civilization. Also wet snow may release as an avalanche. These wet snow avalanches are particularly dangerous as often the entire snowpack to the ground is released, which results in large release volumes (*McClung and Schaerer*, 2006). Furthermore, the presence of liquid water makes the flow heavy and dense, and long runout distances have been observed.

When the liquid water content of snow is low and the air forms a continuous path through the pore space (pendular regime), the sintering between individual crystals is reasonably effective resulting in strong bonds between crystals (*Colbeck*, 1979). When liquid water content increases to the point where the liquid water forms a continuous path through the pore space (funicular regime), this sintering process is severely disrupted and the snow looses its strength rapidly (*Colbeck*, 1997).

Different values for the transition between the pendular and funicular regime are reported. In *Colbeck* (1979), a value of 7% is mentioned, whereas *Denoth* (1982) found in laboratory experiments values in the range of $13-18\%$ for new, fine-grained snow and $7-12\%$ for old, coarse grained snow. Above these values, the snow is described as slush snow and the strength of the snowpack is strongly reduced. The funicular regime is often associated with slush avalanches, which are typically observed at high latitudes (*McClung and Schaerer*, 2006).

It is not necessary for snow to be in the funicular regime to release as a wet snow avalanche. For example, liquid water flow may also weaken existing weak layers in the snowpack. One process that may strongly influence the strength of weak layers is ponding of liquid water on capillary barriers. In strongly stratified snow, contrasting microstructural properties (e.g., grain size or density), cause discontinuities in hydraulic properties. When the suction of the upper layer is higher than the lower layer, as for example with new snow on top of old snow, liquid water infiltrating the snowpack starts ponding on the transition between those layers (*Waldner et al.*, 2004). In *Techel et al.* (2011) and Figure 6.1, this effect is visualized using a dye-tracer. This process continues until the pressure head of the liquid water exceeds the suction pressure of the layer below and water continuous its way down. Because two contrasting layers in the snowpack that may act as capillary barriers often also form a weak layer, the presence of liquid water at these capillary barriers may disrupt the weak layer and trigger an avalanche. The loss of strength due to wetting has been verified for weak layers consisting of faceted crystals or depth hoar (*Techel et al.*, 2011).

The two most common sources of liquid water in the snowpack are snowmelt and rainfall.

Figure 1.2: An example of capillary suction at the base of the snowpack in a glide snow crack (photo: C. Mitterer).

Rainfall is considered to be particularly dangerous, as it adds mass to the snowpack. This additional mass has been found to strongly reduce the strength of a snowpack and may even trigger the failure of dry weak layers deeper in the snowpack before the liquid water reaches those (*Conway and Raymond*, 1993; *McClung and Schaerer*, 2006).

A special category of wet snow avalanches are gliding snow avalanches. The gliding surface of these type of avalanches is by definition the ground surface, causing a full-depth snowpack release. They are most frequently observed on grassy slopes and are sometimes preceded by the formation of a glide crack. Often it is considered that lubrication at the snowpack base triggers the snow gliding (*McClung and Schaerer*, 2006). Long grass may even be more efficient in serving as a gliding surface (*McClung and Schaerer*, 2006). Figure 1.2 shows a detail of the interface between the ground and a snow cover in a glide crack of a gliding snow avalanche. Interestingly, the brownish water indicates that significant amounts of water that has been in contact with soil, were held back or even sucked up in the snowpack by capillary forces. This water may have increased the lubrication which has set in motion the gliding snow avalanche.

An interesting distinction between wet snow and gliding snow avalanches that is sometimes made is that for wet snow avalanches, the heat and liquid water that is driving the avalanche formation process is progressing from the top of the snowpack, whereas for gliding snow avalanches, the ground heat flux and basal melt of the snowpack is the driving process. Gliding snow avalanches provide a clear example where the understanding of the avalanche formation process requires understanding of the soil processes.

1.2 Context

1.2.1 Modelling the Snow Cover

For an adequate simulation of the hydrological cycle in snow covered areas, most hydrological models have at least a simple snow model[1]. The simplest approach is to have a single-layer snow model, with a constant density (e.g., UEB model (*Tarboton and Luce*, 1996)). A common method to calculate snowmelt is to use a temperature-index or degree-day approach, in which the snowmelt is determined solely from air temperature using a factor relating air temperature or degree-days to snowmelt. Examples of hydrological models where this approach is used are the TOPMODEL (*Ambroise et al.*, 1996) or SWAT (*Fontaine et al.*, 2002). Note that most temperature-index based models do not use a constant factor, but take for example the yearly cycle in solar radiation into account (*Hock*, 1999; *Walter et al.*, 2005). This provides a simple, yet effective way to improve snowmelt estimates. Although a temperature-index approach has been found to be successful, it does not work for high temporal resolutions (sub-daily time scales), or in mountainous terrain, where spatial variability in snowmelt is large, depending on slope angle, shadowing and reflection effects (*Hock*, 2003). Furthermore, this approach can only be applied successfully if extensive calibration is performed, for example using discharge measurements (*Kumar et al.*, 2013). But even with thorough calibration, a well constructed physics based multi-layer snowpack model that solves the energy balance for snowmelt, seems to be able to provide a more accurate estimate of the seasonal evolution of snow water equivalent than temperature-index or degree day models (*Essery and Etchevers*, 2004; *Kumar et al.*, 2013).

Some single-layer snow models indeed solve the full energy balance (e.g., *Tarboton and Luce* (1996); *Zanotti et al.* (2004)) and it has been shown that even simple approaches for solving the energy balance may already provide satisfying melt rates (*Walter et al.*, 2005; *Essery et al.*, 2013). Variations on single-layer snow models have been introduced, for example by using a two-layer snow model, with a new snow layer and an old snow layer (e.g., ISNOBAL (*Marks et al.*, 1999)). In the hydrological community, the insight that more sophisticated snow models are required to simulate catchments where snow plays an important role, lead to the development of hydrological models with even more complex snow models (e.g., the multi-layer snow model in the SHAW model (*Flerchinger and Saxton*, 1989) or GEOtop (*Endrizzi et al.*, 2013)). The catchment scale hydrological model CATHY has been recently coupled to a three layer snow scheme that accounts for phase changes, snow settling and liquid water flow (*Yang and Niu*, 2003; *Niu et al.*, 2014).

Finally, there are detailed multi-layer physics based snow models, like for example SNTHERM (*Jordan*, 1991), CROCUS (*Brun et al.*, 1989; *Vionnet et al.*, 2012), and SNOWPACK (*Lehning et al.*, 2002a,b; *Wever et al.*, 2014). Their development was not primarily driven by hydrological applications, but also by for example assessing avalanche risks for avalanche warning services (*Brun et al.*, 1989; *Lehning et al.*, 1999; *Schirmer et al.*, 2009), or to serve in remote sensing

---

[1]This section is not meant to provide an exhaustive overview of existing snow models.

applications (*Fily et al.*, 1999). Nevertheless, they also have been successful in hydrological applications, for example in the Alpine3D model framework (*Lehning et al.*, 2006; *Bavay et al.*, 2009) or in meso-scale and global surface schemes (*Vionnet et al.*, 2012).

1.2.2 Modelling Liquid Water Flow in Snow

As for determining snowmelt, the model approaches for determining the liquid water flow also widely vary. In soils, the most common approach to model liquid water flow is by treating soil as a porous matrix, and solve the balance between gravity and capillary forces. This is described by the famous, widely used Richards Equation (RE), which describes water flow in variably saturated porous media (*Richards*, 1931). The analogue between the soil matrix and the ice matrix is evident and has been recognized for a long time (*Waterhouse and Bunten*, 1969; *Colbeck*, 1972). In contrast with the field of soil hydrology, the full RE has seldom been solved for a snow cover, but virtually all snow models account for the fact that capillary suction may retain a part of the melt water in the snowpack.

When the liquid water content increases further, models route melt water downward after exceeding the threshold water content (often referred to as irreducible water content) that is associated with capillary forces. This approach is commonly referred to as a bucket scheme. The melt water leaving the snowpack is then provided to the other hydrological components in the model. In many models, water moves down instantaneously, like SNOWPACK (*Bartelt and Lehning*, 2002; *Wever et al.*, 2014) and later versions of CROCUS (*Vionnet et al.*, 2012), whereas other models implement attenuation in water movement, taking into account finite hydraulic conductivities, like the SHAW model (*Flerchinger and Saxton*, 1989). Another common approach is to use the gravitational component of the RE, as in the SNTHERM model (*Jordan*, 1991) or the early versions of CROCUS (*Brun et al.*, 1989). Most studies find that the bucket scheme works rather well, as for typical levels of saturation in snow, the capillary forces acting against gravity play a minor role in the flow of liquid water (*Colbeck*, 1972).

However, a detailed look at examples of liquid water in snow reveal that this is not the complete picture. For example, clear indications of capillary suction have been observed in laboratory experiments with flooding snow on sea ice (*Massom et al.*, 2001). Also the earlier mentioned field observations in glide cracks of gliding snow avalanches revealed capillary forces seemingly causing upward water movement in snow (Figure 1.2). Furthermore, the many observations of water ponding on capillary barriers inside the snowpack (e.g., *Waldner et al.* (2004); *Techel et al.* (2011)) cannot be simulated with the approaches described above. By approximating water fluxes as provided by RE, *Hirashima et al.* (2010a) suggested that RE is describing those kind of processes. This motivated us to extend the effort by *Hirashima et al.* (2010a) and implement a solver for the full RE for the soil-snowpack continuum.

Almost all snow models for hydrological applications are one-dimensional. A few multi-dimensional snow models have been presented (e.g., *Illangasekare et al.* (1990); *Hirashima et al.* (2014)), so far mainly studying idealized snowpacks on an experimental basis. As will

be discussed later, multi-dimensional models seem to be necessary to simulate certain flow features with a physics based approach, like preferential flow.

1.2.3   Modelling the Underlying Soil

Just as the atmosphere is posing a marked boundary condition on top of the snowpack, so does the soil from below. The SNOWPACK model has originally been designed as a pure snow model where the lower boundary temperature in the model was provided by prescribing the upper soil temperature. Shortly afterwards, the model was extended with a full soil module (*Luetschg et al.*, 2004) in order to assess the influence of the soil on the lower boundary of the snowpack. The strongest forcing of the soil to the snowpack is provided by the heat flux from the soil, which is generally directed upwards. However, the snowpack also influences the temperature distribution in soil. For example, it has been observed that soil below a shallow show cover is experiencing more soil freezing than below a deep snow cover (*Shanley and Chalmers*, 1999; *Bayard et al.*, 2005). Furthermore, melt water from the snow influences the soil moisture state of the underlying soil during the snow season (*McNamara et al.*, 2005; *Bales et al.*, 2011; *Kumar et al.*, 2013), and thereby the amount of energy needed for soil freezing in colder periods.

For soil, the liquid water flux from the snowpack provides an important boundary condition. As discussed above, accurate modelling of snow water equivalent at the basin scale was found to improve streamflow estimations. However, many studies also found that this is not sufficient. The degree of saturation of the soil seems to strongly determine the final effect of snowpack runoff on streamflow (*McNamara et al.*, 2005; *Seyfried et al.*, 2009; *Bales et al.*, 2011). Streams were found to react strongly on snowmelt episodes when the underlying soil is wet. The reaction speed of streamflow to snowmelt may also be expected to depend on the underlying soil. For example, in alpine terrain, soils are generally highly permeable, resulting in short reaction times (*Weingartner et al.*, 2003). These studies suggest that it is necessary to have an adequate soil model in addition to the snow model, when relating snowmelt to other components of the hydrological cycle or to streamflow. This topic is further discussed in Chapter 4.

In the bucket schemes for meltwater runoff, all water that is considered excess in the snowpack, is allowed to leave the snowpack and infiltrate the soil. However, the extension of the SNOWPACK model with RE, as discussed in Chapter 2, changes this process description. The amount of melt water leaving the snowpack may now dependent on the soil state. For example, if the soil has a high clay content, the model simulates ponding of liquid water at the base of the snowpack during the afternoon peak snowpack runoff (see Figure 1.3b). This effect also shows up in the simulations if an impedance on hydraulic conductivity in the soil would be applied when the soil is frozen (see Figure 1.3c), but is absent in the reference simulation using a typical soil type found in alpine terrain (see Figure 1.3a).

These examples of two-way interactions in both heat and liquid water flow between the snow
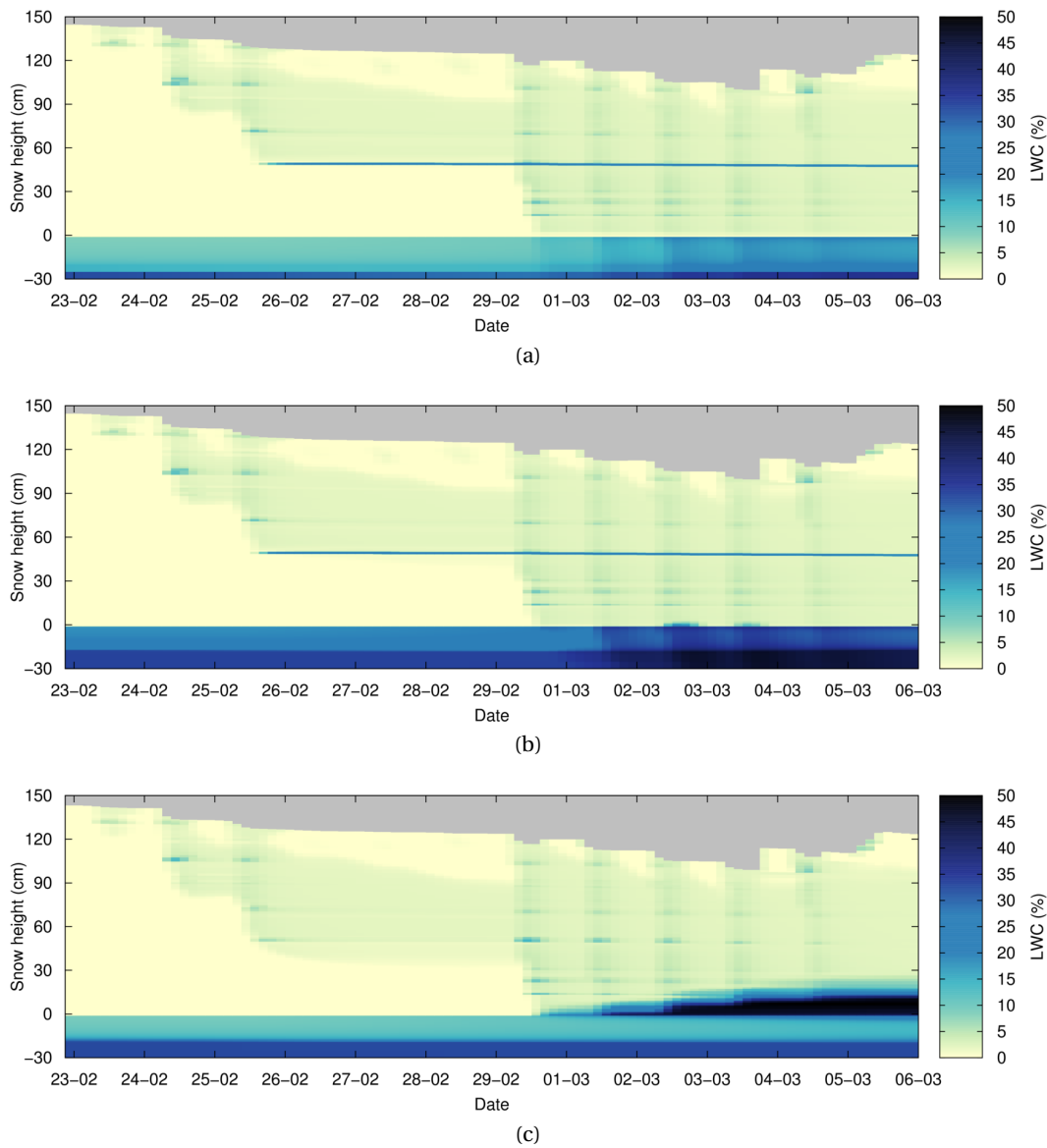
(a)

(b)

(c)

Figure 1.3: Example simulations of liquid water content (LWC) in snow for the Uf den Chaiseren station using RE (see Chapter 4), for (a) the reference simulation using silty loam as soil type, (b) using silty clay as soil type, leading to ponding at the base of the snowpack in the late afternoon on March 2 and 3, (c) using ice impedance on hydraulic conductivity in silty loam soil, following *Hansson et al.* (2004), resulting in strong ponding at the snow-soil interface. The snow-soil interface is located at $y = 0$. In (a) and (b), water ponding near a buried surface hoar layer around 50 cm can be seen. In (c) this layer is not as outspoken due to a different course of events in the beginning of the simulations due to ice impedance on hydraulic conductivity in the frozen soil.

Figure 1.4: Map of the Alps, showing the location of the measurement sites Weissfluhjoch (Switzerland) and Col de Porte (France).

and the underlying soil suggest that simulations would benefit from a model description that treats the snowpack and soil as a continuum. An increasing interest to use SNOWPACK in the Alpine3D model framework to simulate hydrological processes and streamflow (e.g., *Lehning et al.* (2006); *Bavay et al.* (2009)), provides our last motivation to study the relationship between a snow cover and the underlying soil.

1.3 Summary of Contents

In Section 1.1, it has been motivated and hypothesized that solving liquid water flow in the snow-soil continuum using RE is expected to be a valuable extension to the physics based snowpack model SNOWPACK. In Chapter 2, the various water transport models for the SNOWPACK model are discussed and compared. In particular, the implementation of the solver for the full RE in one-dimension for the snow-soil continuum, including phase changes, is described. Model simulations of snowpack runoff were compared with snow lysimeter measurements at two alpine sites: Weissfluhjoch (2540 m) and Col de Porte (1325 m) (see Figure 1.4). The studied period consisted of 14 and 17 snow seasons, respectively. At both sites, improvements were found in several aspects of snowpack runoff. This was especially evident on the sub-daily time scale, but RE also showed a higher agreement regarding daily runoff sums and the onset of snowpack runoff in spring. The improvements for Weissfluhjoch were found to be larger than for Col de Porte. We hypothesized that this may be caused by a difference in typical snowpack structure. Weissfluhjoch is at a much higher altitude than

Col de Porte, and as a consequence, the snowpack at Weissfluhjoch is below freezing most of the winter season. This leads to a very strong stratification in the snowpack. At Col de Porte, snowmelt and rainfall may occur during the whole winter season. The snowpack is in a wet state for extended periods of time. As we also found that the differences between water transport schemes got smaller for Weissfluhjoch when the snowpack there is isothermal and wet, we concluded that solving RE in particular improves liquid water flow in deep, stratified snow covers and at the onset of snowmelt. To our knowledge it was also the first study testing the performance of a physics based snowpack model in predicting snowpack runoff for such a long measured time series.

The fact that RE provided a demonstrable improvement when considering snowpack runoff, raised the question of what the implications are for the internal snowpack microstructure. Moreover, the hydraulic properties of snow are strongly dependent on microstructural snowpack parameters (*Yamaguchi et al.*, 2010, 2012; *Katsushima et al.*, 2013), making it necessary to verify those modelled parameters with observed profiles. Over a decade of consistent snow related measurements are available at the WFJ, combined with standardized automated meteorological measurements as well as manual snow profiles. This allows for a thorough verification of the snowpack model for multiple snow seasons. To our knowledge, this has not been done so far for a physics based snowpack model. Solving liquid water flow in soil using RE also required some adaptations of the soil freezing and thawing process as simulated by the model. When soil is unsaturated, liquid water is present even below the freezing temperature of water. This is called the freezing point depression. In SNOWPACK, the approach by *Dall'Amico et al.* (2011) is followed. For a closed energy balance of the soil, also the heat advection by liquid water flow in soil under a temperature gradient needed to be taken into account. In Chapter 3, the updated soil module is described in detail and is also being validated as well as possible for the site Weissfluhjoch. This aims to answer the question to what extent SNOWPACK is able to simulate the soil in such a way that it provides a realistic lower boundary condition for the snowpack. Furthermore, a correct representation of the vertical temperature profile in the snowpack is an indication that the heat flow through the snowpack is correctly modelled, which in turn will influence the state of the underlying soil.

The comparison with field data is presented in Chapter 3. It showed that during the main winter season, snow height, snow water equivalent, snow temperature distributions and snow density as well as their temporal evolution are well simulated in the model and the influence of the two water transport schemes is small. In the melt season, a more pronounced underestimation of snow density of about $100\,\mathrm{kg\,m^{-3}}$ was found, accompanied by an increasing bias in snow water equivalent. As the net energy balance seems to be satisfyingly diagnosed during the main winter season, the analysis suggests that the process descriptions in SNOWPACK have particular difficulties in accurately simulating the densification during spring. A too low snow density will result in a deeper penetration of shortwave radiation, effectively providing heat to the snowpack. Furthermore, heat conductivity will be underestimated, and it may be that the simulated snowpack in spring is therefore too isolated to be able to release heat during night.

The RE approach for water flow reproduced ponding over capillary barriers and also provided a closer agreement with measured snow temperatures in spring, suggesting a better simulation of the movement of the melt water front through the snowpack. A comparison with the meltwater front as detected by an upward looking ground penetrating radar, showed that simulations with RE provide a higher agreement in the beginning of the melt season, whereas simulations with the bucket scheme show a closer agreement of the meltwater front reaching the base of the snowpack. The radar data also suggests that more liquid water is retained in the snowpack than simulated by the model, which may contribute to overestimating snow depletion rates in the simulations.

In Chapter 4, the circle in studying the snowpack as an interface between soil and the atmosphere is closed by a more in-depth verification of the updated soil module by analysing soil moisture simulations and measurements for seven stations that were installed in the vicinity of Davos. It was found that the distributed SNOWPACK simulations in the Alpine3D model framework for the Davos area simulated soil moisture variations at measurement sites with varying degree of success. At some stations, temporal soil moisture variations are well captured, especially in the upper soil layers, even though the soils were initialized with the same hydraulic properties. At a few stations, measurements seem to be influenced by fluctuating ground water levels, which is not considered in this study. At two stations, the soil appeared to have high volumetric water contents, which reduces the sensitivity of the sensors. Soil freezing seems to be overestimated in SNOWPACK, possibly by neglecting vegetation or inadequate soil thermal or hydraulic properties. Nevertheless, the Alpine3D model appeared to be able to reproduce spatial variability found in the measurements, mainly related to snow distribution and spatial variability in snowmelt. In summer, the spatial variability in the simulations was much smaller than in the measurements. Using the recently developed travel time distribution approach (*Comola et al.*, 2014), streamflow from the Dischma catchment in the Davos area is calculated and compared to measurements. Routing the flux at the top of the soil to streamflow, was found to have a lower agreement with observed streamflow than the flux below either 30 or 60 cm of soil. This preliminary result indicates that the new soil module could potentially contribute to improved streamflow simulations using Alpine3D.

Finally, Chapter 5 describes a study with the SNOWPACK model of a marked rain-on-snow event in autumn 2011 in the Swiss Alps that caused wide-spread flooding. A large snowfall of locally more than 1 m was followed by intense rain a day later. By carrying out simulations of the snow cover during this event, insights have been gained of how the modelled processes and RE modulate incoming rainfall and snowmelt when generating snowpack runoff. It has been found that deep snow covers (over 50 cm), that were still dry, initially absorbed important amounts of rain and melt water, before the snowpack runoff started. In shallow snow covers, snowpack runoff started much sooner after the onset of rainfall and snowmelt. However, it turned out that once deep snowpacks produced runoff, the runoff rate was higher than in shallow snow covers, and in both, the maximum runoff rate was also higher than the sum of snowmelt and rainfall rates. The analysis of the model simulations suggested that this is related to the dynamics of the liquid water storage of the snow cover. It seems that a combination

of snow settling, wet snow metamorphism and associated changes in hydraulic properties (e.g., water retention and hydraulic conductivity) may be the cause for the enhanced outflow of liquid water from the snowpack. This result is difficult to verify experimentally, although it may have significant consequences for the understanding of the flood risks from snowmelt and rain-on-snow events.

2 Solving Richards Equation for snow improves snowpack meltwater runoff estimations in detailed multi-layer snowpack model

Nander Wever[1,3], Charles Fierz[1], Christoph Mitterer[1], Hiroyuki Hirashima[2], Michael Lehning[1,3]

[1] WSL Institute for Snow and Avalanche Research SLF, Davos Dorf, Switzerland.

[2] Snow and Ice Research Center, NIED, Japan.

[3] CRYOS, School of Architecture, Civil and Environmental Engineering, EPFL, Lausanne, Switzerland.

Summary

The runoff from a snow cover during spring snowmelt or rain-on-snow events is an important factor in the hydrological cycle. In this study, three water balance schemes for the 1 dimensional physically-based snowpack model SNOWPACK are compared to lysimeter measurements at two alpine sites with a seasonal snow cover, but with different climatological conditions: Weissfluhjoch (WFJ) and Col de Porte (CDP). The studied period consists of 14 and 17 yr, respectively. The schemes include a simple bucket-type approach, an approximation of Richards Equation (RE), and the full RE. The results show that daily sums of snowpack runoff are strongly related to a positive energy balance of the snow cover and therefore, all water balance schemes show very similar performance in terms of Nash-Sutcliffe efficiency (NSE) coefficients (around 0.63 and 0.72 for WFJ and CDP, respectively) and r^2 values (around 0.83 and 0.72 for WFJ and CDP, respectively). An analysis of the runoff dynamics over the season showed that the bucket-type and approximated RE scheme release meltwater slower than in the measurements, whereas RE provides a better agreement. Overall, solving RE for the snow cover yields the best agreement between modelled and measured snowpack runoff, but differences between the schemes are small. On sub-daily time scales, the water balance schemes behave very differently. In that case, solving RE provides the highest agreement between modelled and measured snowpack runoff in terms of NSE coefficient (around 0.48 at

both sites). At WFJ, the other water balance schemes loose most predictive power, whereas at CDP, the bucket-type scheme has an NSE coefficient of 0.39. The shallower and less stratified snowpack at CDP likely reduces the differences between the water balance schemes. Accordingly, it can be concluded that solving RE for the snow cover improves several aspects of modelling snow cover runoff, especially for deep, sub-freezing snow covers and in particular on the sub-daily time scales. The additional computational cost was found to be in the order of a factor of 1.5-2.

2.1   Introduction

The presence of a snow cover has a strong impact on the hydrological cycle. The snow cover can delay the routing from precipitation to streamflow on time scales from a few hours or days to several months and many studies have shown the importance of the snow cover for accurate runoff and streamflow modelling (e.g. *Seyfried et al.* (2009); *Koster et al.* (2010); *Mahanama et al.* (2012)). Furthermore, the effects of rain-on-snow (ROS) events on runoff from catchments are strongly dependent on the state of the snow cover (*Marks et al.*, 2001; *Mazurkiewicz et al.*, 2008). The use of physically-based snowpack models in hydrological modelling is increasing, with varying degrees of model complexity. Studies have shown that by using physically-based snowpack models, the determination of (spatial distribution of) snow water equivalent and discharge at basin outlets improves (*Marks et al.*, 1999; *Zanotti et al.*, 2004). A correct description of water flow through a snowpack is not only important to improve meltwater runoff estimations, but also helps to improve the understanding of wet snow avalanche formation (*Conway and Raymond*, 1993; *Mitterer et al.*, 2011a).

An important coupling between the snow cover and surface or sub-surface flow is provided by meltwater runoff at the base of the snowpack. For an accurate assessment of the snowpack runoff, it is important to have a good understanding of water movement through a snowpack. Water transport in snow is a complex process, because in general, the snow cover consists of many layers that may vary in temperature, density as well as in grain size and type. Experimental studies have shown that microstructural properties of the snowpack strongly influence the hydraulic properties of snow (*Shimizu*, 1970; *Colbeck*, 1974; *Marsh*, 1991; *Yamaguchi et al.*, 2010). Where a snow layer with small grains is on top of a layer with coarse grains, these differences in hydraulic properties will lead to the formation of capillary barriers at the interface (*Jordan*, 1996; *Waldner et al.*, 2004; *Peitzsch et al.*, 2008; *Mitterer et al.*, 2011a). Also lateral flow along these capillary barriers, ice lenses or other dense parts of the snow cover has been identified (*Peitzsch et al.*, 2008). Field experiments also have repeatedly observed the existence of preferential flow paths, which can provide a more efficient water transport mechanisms than matrix flow alone (e.g. *Kattelmann*, 1985; *Schneebeli*, 1995; *Katsushima et al.*, 2013).

For modelling the water flow through the snowpack, capillary effects are often neglected and many models follow a bucket-type approach (e.g. *Flerchinger and Saxton*, 1989; *Jin et al.*, 1999; *Marks et al.*, 1999; *Boone and Etchevers*, 2001; *Vionnet et al.*, 2012). These water balance

schemes are easy to implement and computationally very efficient, making them very suitable for distributed modelling. Richards Equation (*Richards*, 1931), hereafter denoted as RE, is often applied to soils to describe variably saturated matrix flow. However, its application potential for snowpacks has already been identified in literature (*Colbeck*, 1972, 1974; *Jordan*, 1983a; *Illangasekare et al.*, 1990; *Hirashima et al.*, 2010a). *Jordan* (1996) and *Hirashima et al.* (2010a) found that RE was able to reproduce the formation of capillary barriers as observed in laboratory experiments and snow profiles.

Compared to the knowledge of hydraulic properties in various types of soil, measurements to derive hydraulic properties in natural snow are restricted to a few studies (*Shimizu*, 1970; *Colbeck*, 1974; *Marsh*, 1991; *Yamaguchi et al.*, 2010). Except for the study by *Colbeck* (1974), these studies were focussed on wet snow. Other snow types are more difficult to investigate, because in the presence of liquid water, snow metamorphism is rapid and the transition to wet snow types almost immediate.

Several snowpack models that describe liquid water transport on the basis of RE have been developed. Some model studies were restricted to idealised snowpacks to quantify the effects of water percolation in snow (*Illangasekare et al.*, 1990; *Jordan*, 1996; *Daanen and Nieber*, 2009). When neglecting capillary forces, the resulting gravity flow in RE, as proposed by *Colbeck* (1972) in the kinematic wave model, has been used in earlier versions of CROCUS (*Brun et al.*, 1989) and the current version of SNTHERM (*Jordan*, 1991; *Davis et al.*, 2001). *Hirashima et al.* (2010a) developed a water balance scheme where downward water flow by Darcy's law is approximated assuming stationary and equilibrium flow properties. To our knowledge, the full RE has not been used in a physically-based snow cover model to model water flow in snow in simulations of full snow seasons, forced by meteorological field measurements. In this study, the implementation of a solver for RE in the physically-based snowpack model SNOWPACK (*Bartelt and Lehning*, 2002; *Lehning et al.*, 2002b,a) is described, where the snowpack and soil are treated as a continuous column. The model is applied on two alpine measurement sites with a seasonal snow cover and contrasting climatological conditions: Weissfluhjoch (WFJ) near Davos, Switzerland and Col de Porte (CDP) near Grenoble in France. In simulations of 14 and 17 snow seasons respectively, the bucket scheme, *Hirashima et al.* (2010a) scheme and the full RE are compared with lysimeter measurements of snowpack runoff. The focus will be primarily on the timing and magnitude of snowpack runoff.

2.2 Theory and numerical formulations

Several methods to model water flow in snow have been developed. The three that are compared here, will be discussed below.

2.2.1 Bucket scheme

In the so-called bucket scheme, a threshold water content (water holding capacity, θ_h) is defined, above which all the liquid water exceeding this threshold in a layer is transported downward in the snowpack or soil, regardless of the storage capacity of lower layers (*Bartelt and Lehning*, 2002). The downward moving water is either stored at one of the lower layers (if possible), or is drained from the model domain. In SNOWPACK, the water holding capacity varies per layer according to (*Coléou and Lesaffre*, 1998):

$$
\theta_h = \begin{cases}
0.0264 + 0.0099 \frac{(1-\theta_i)}{\theta_i}, & \theta_i \leq 0.23 \\
0.08 - 0.1023\,(\theta_i - 0.03), & 0.23 < \theta_i \leq 0.812 \\
0, & \theta_i > 0.812
\end{cases}
\tag{2.1}
$$

where θ_i is the volumetric ice content of the snow ($\mathrm{m^3\,m^{-3}}$).

2.2.2 Richards equation

RE describes water movement in variably saturated porous media (*Richards*, 1931). For a 1-dimensional column, RE can be written in a mixed-form, which can be discretized in a finite difference approximation that ensures perfect mass balance (*Celia et al.*, 1990):

$$
\frac{\partial \theta}{\partial t} - \frac{\partial}{\partial z}\left(K(\theta)\left(\frac{\partial h}{\partial z} + \cos\gamma\right)\right) + s = 0,
\tag{2.2}
$$

where θ is the volumetric liquid water content (LWC, $\mathrm{m^3\,m^{-3}}$), K is the hydraulic conductivity ($\mathrm{m\,s^{-1}}$), h is the pressure head (m), z is the vertical coordinate (m, positive upwards and perpendicular to the slope), γ is the slope angle and s is a source/sink term ($\mathrm{m^3\,m^{-3}\,s^{-1}}$).

For applying Eq. (2.2), a water retention curve has to be specified that relates θ to h. For snow, it is common to take the *van Genuchten* (1980) model:

$$
\theta = \theta_r + (\theta_s - \theta_r)\frac{\left(1 + (\alpha|h|)^n\right)^{-m}}{\mathrm{Sc}},
\tag{2.3}
$$

where θ_r is the residual water content ($\mathrm{m^3\,m^{-3}}$), θ_s is the saturated water content ($\mathrm{m^3\,m^{-3}}$) and α is a fit coefficient that is related to the maximum pore size in the medium. m and n are additional fit parameters that are related to the pore size distribution. Sc is a correction factor proposed by *Ippisch et al.* (2006), who have shown the necessity of using an air entry pressure when $n \leq 2$. Here, the correction is applied for all values of n, with an air entry pressure of 0.0058 m, corresponding to a largest pore size of 5 mm.

Two parameterizations for the *van Genuchten* (1980) model have been published recently: *Daanen and Nieber* (2009) fitted the water retention curve based on several published experiments that were collected by *Marsh* (1991) and *Yamaguchi et al.* (2010) retrieved water

retention curves from several snow samples in laboratory experiments. *Daanen and Nieber* (2009) determined the parameters α and n for the van Genuchten model to be:

$$\alpha = 30(2r_g) + 12, \tag{2.4}$$

and

$$n = 0.800(2r_g) + 3, \tag{2.5}$$

where r_g is the mean grain radius (mm), corresponding to the classical grain size definition (*Fierz et al.*, 2009). In this study we (primarily) refer to this classical grain size of a snow layer as the average size of its grains, where the size of a single grain or particle is its greatest extension measured in millimetres (*Fierz et al.*, 2009; *Baunach et al.*, 2001). This has to be distinguished from the optical equivalent grain size that is related to the specific surface area of snow (see, for example, *Carmagnola et al.*, 2014; *Fierz et al.*, 2009).

The parameterization for α proposed by *Yamaguchi et al.* (2010) is:

$$\alpha = 7.3(2r_g) + 1.9. \tag{2.6}$$

For n, the original parameterization by *Yamaguchi et al.* (2010) was modified by *Hirashima et al.* (2010a) to be able to extend the parameterization beyond grain radii of 2 mm:

$$n = 15.68e^{(-0.46(2r_g))} + 1, \tag{2.7}$$

where, for numerical stability, the upper grain radius limit is set to be 5 mm in this study.

In both parameterizations, the van Genuchten parameter m is chosen as:

$$m = 1 - (1/n). \tag{2.8}$$

Note that both parameterizations for the van Genuchten model for snow differ significantly. Therefore, both are taken into consideration in this study, where the *Hirashima et al.* (2010a) modifications of the *Yamaguchi et al.* (2010) parameter set will be referred to as Yamaguchi and the *Daanen and Nieber* (2009) parameter set as Daanen.

To apply the van Genuchten model, also θ_s and θ_r need to be defined. For θ_s, it is common to take it equal to the pore space:

$$\theta_s = (1 - \theta_i)\frac{\rho_i}{\rho_w}. \tag{2.9}$$

Note that the correction factor at the right hand side ensures that there is enough space when liquid water freezes and thereby expands. For θ_r, *Colbeck* (1974) experimentally found a value of 0.07. Gravity drainage experiments by *Yamaguchi et al.* (2010) showed values around 0.02, suggesting that additional suction could reduce θ even more. Cold fresh snow is initially

completely dry and also phase changes can reduce θ below θ_r, causing singularities in the van Genuchten model (Eq. 2.3).

To circumvent these problems, a pragmatic strategy was implemented for determining θ_r: first, new snow layers were initialized with a very small value for θ of $\epsilon_\theta/10$, where ϵ_θ is the convergence criterion (see Appendix A). This means that new snow layers are initialized in a dry state from the perspective of the convergence criterion. Then, the residual water content for the current time step (θ_r^t) is scaled between 0 and 0.02 according to:

$$\theta_r^t = \min \langle 0.02, \max \langle \theta_r^{t-1}, f \cdot \theta \rangle \rangle , \tag{2.10}$$

where f is a tuning factor, taken as 0.75 and θ_r^{t-1} is the residual water content from the previous time step.

For determining the hydraulic conductivity, the van Genuchten-Mualem model is used (*Mualem*, 1976; *van Genuchten*, 1980):

$$K(\theta) = K_{sat}\Theta^{1/2} \left[1 - \left(1 - \Theta^{1/m} \right)^m \right]^2 , \tag{2.11}$$

where K_{sat} is the saturated hydraulic conductivity ($\mathrm{m\,s^{-1}}$) and Θ is the effective saturation:

$$\Theta = \frac{\theta - \theta_r}{\theta_s - \theta_r}. \tag{2.12}$$

For K_{sat}, the proposed equation by *Shimizu* (1970) has been widely used for a long time:

$$K_{sat} = \left(\frac{\rho_w g}{\mu} \right) \left[0.077 \left(\frac{r_g}{1000} \right)^2 \exp \left(-0.0078 \theta_i \rho_i \right) \right] , \tag{2.13}$$

where ρ_w and ρ_i are the density of water ($1000\,\mathrm{kg\,m^{-3}}$) and ice ($917\,\mathrm{kg\,m^{-3}}$), g is the gravitational acceleration (taken as $9.8\,\mathrm{m\,s^{-2}}$) and μ is the dynamic viscosity (taken as $0.001792\,\mathrm{kg\,(m\,s)^{-1}}$).

Recently, *Calonne et al.* (2012) proposed a slightly different equation, based on calculations from tomography images:

$$K_{sat} = \left(\frac{\rho_w g}{\mu} \right) \left[0.75 \left(\frac{r_{es}}{1000} \right)^2 \exp \left(-0.013 \theta_i \rho_i \right) \right] , \tag{2.14}$$

where r_{es} is the equivalent sphere radius (m).

The largest difference between the parameterization of *Shimizu* (1970) and *Calonne et al.* (2012) is in the range of snow with low density and new snow or decomposing and fragmenting snow particles (*Calonne et al.*, 2012). In the presence of liquid water, wet snow metamorphism is rapid and also densification occurs, which quickly reduces the differences between both parameterizations. We found that results marginally improve when using the equation from *Calonne et al.* (2012), so results presented here exclusively use Eq. (2.14). For this, we determine

the optical grain radius from the simulated grain size following *Vionnet et al.* (2012) and use this as an approximation of r_{es}.

In SNOWPACK simulations, the typical microstructural evolution of the snowpack results in an increase in snow grain radius when snow ages or experiences melt-freeze cycles. This will increase the saturated hydraulic conductivity. However, settling of the snow cover and subsequent melt cycles will increase the density, which will decrease the hydraulic conductivity. In the simulations, the first effect is dominating, as grain size will generally increase by a factor 3–8, thus influencing K_{sat} by a factor 9 to 64 over a snow season. Snow density will increase by a factor 2–5, influencing K_{sat} by a factor 5 to 25 over a snow season for typical snow densities. Field experiments have shown that different temperature regimes may result in a different microstructural evolution of the snowpack and hence of K_{sat} (*Domine et al.*, 2013).

2.2.3 NIED scheme

Hirashima et al. (2010a) developed a water balance scheme for the SNOWPACK model based on approximating the water transport by fluxes derived from Darcy's law by assuming stationary flow properties for a time step and equilibrium in water flow between two layers. RE is not explicitly solved and only downward water movement is possible. *Hirashima et al.* (2010a) also used the earlier discussed modified water retention curve for the van Genuchten model by *Yamaguchi et al.* (2010). The study focussed primarily on the internal snowpack processes and achieved the reproduction of capillary barriers on the interface between layers with different grain sizes. In this study, we will refer to this water balance scheme as NIED.

2.3 Data and methods

2.3.1 Data Weissfluhjoch

The experimental site at the Weissfluhjoch (WFJ, 46.83° N, 9.81° E) is located at an altitude of 2540 m in the Swiss Alps near Davos. During the winter months, almost all precipitation falls as snow at this altitude. As a consequence, a continuous seasonal snow cover builds up every winter, with a maximum snow height ranging from 153–366 cm over the period 1934–2012. The measurement site is located in an almost flat part of a southeast oriented slope (γ is taken equal to 0).

The dataset contains air temperature, relative humidity, wind speed and direction, incoming and outgoing longwave and shortwave radiation, surface temperature, soil temperature at a few cm below the surface, snow height and precipitation from a heated rain gauge. The dataset has been quality checked, by replacing missing values with values from backup sensors or by applying various interpolation methods (*Schmucki et al.*, 2014). The precipitation was corrected for undercatch during snowfall and windy conditions by using a correction proposed by *Førland et al.* (1996). The relationship for a Finnish H&H-90 gauge was taken, as it was

empirically found to estimate precipitation at WFJ best, when comparing seasonal maximum measured snow water equivalent (SWE) in biweekly manual snow profiles to modelled SWE at the same date.

The experimental site is equipped with a lysimeter, which measures the liquid water runoff from the snowpack. The surface area of the squared lysimeter is $5\,m^2$ and since 2001, it is measuring at a resolution of $0.16\,kg\,m^{-2}$ (before $0.20\,kg\,m^{-2}$). Data is collected at $10\,min$ intervals. The lysimeter is enclosed by a $60\,cm$ high wall to reduce lateral flow effects near the soil-snow interface. However, lateral flow along capillary barriers within the snow cover or other, more impermeable layers (e.g. melt-freeze crusts) higher in the snowpack may still affect the measurements. The lysimeter is expected to collect additional meltwater advected by lateral flow mechanisms, as the device is located close to the lowest part of the site.

The studied period for WFJ is from 1 September 1996 to 30 September 2010. This period, consisting of 14 full winter seasons, is chosen based on data-availability and quality of the lysimeter measurements.

2.3.2 Data Col de Porte

The experimental station Col de Porte (CDP, 45.30° N, 5.77° E) is located in the Chartreuse range in France and is operated by MeteoFrance. The datasets of hourly measurements and the snowpack evaluation data have been published and described in *Morin et al.* (2012). The station is located at $1325\,m$ altitude and, as a consequence, experiences a warmer climate than WFJ. The snow cover produces snowpack runoff more often during the snow season and ROS events are more frequent than at WFJ. Due to these frequent wetting cycles, we expect the snowpack to be less stratified at CDP than at WFJ. A snow cover builds up for at least several weeks every winter season at this site, but is interrupted by complete melt in some years. With typical maximum snow heights ranging from 68–207 cm over the period 1993–2011, snow covers at CDP are generally less deep than at WFJ.

The dataset contains a set of very similar measurements as at WFJ: air temperature, specific humidity, wind speed and direction, incoming and outgoing longwave and shortwave radiation, surface temperature, several soil temperatures, snow height and precipitation from a heated rain gauge. The precipitation data in the CDP dataset is already corrected for undercatch and the precipitation amounts are separated in rain and snow, as described in *Morin et al.* (2012). The SNOWPACK model accepts only a single value as precipitation input and decides based on a temperature threshold of $1.2\,°C$ whether the precipitation should be considered rain or snow. Therefore, we adjusted the CDP dataset to an air temperature above $1.2\,°C$ in case only rainfall was reported, and an air temperature below $1.2\,°C$ in case snow fall was reported. Mixed precipitation was provided as a sum to SNOWPACK and depending on the air temperature considered as rain or snowfall.

CDP is equipped with both a $5\,m^2$ and a $1\,m^2$ lysimeter. *Kattelmann* (2000) shows that smaller

lysimeters exhibit significantly larger inaccuracies. Also in this study we found that the larger lysimeter provided highest agreement for all water balance schemes, and we will only use the data from the $5\,\text{m}^2$ lysimeter. The dataset from CDP is used here for the period from 1 September 1994 to 31 July 2011 (17 winter seasons), determined by the data availability of the $5\,\text{m}^2$ lysimeter.

2.3.3 Methods

Model description

The 1-dimensional mixed form of RE (Eq. 2.2) is solved by a Picard iteration scheme (*Celia et al.*, 1990), adapted for a variable grid spacing based on *Rathfelder and Abriola* (1994). The scheme has the property of an easy numerical implementation that is globally convergent. In Appendix A, several aspects of the numerical implementation are discussed.

When using RE, the snowpack and the soil are considered as a single continuous column. There are no special boundary conditions for the lowest snow layer or upper-most soil layer. The snowpack runoff, defined as all liquid water leaving the snowpack at the bottom, is calculated in a model postprocessing step by evaluating Darcy's law at the interface between the snowpack and the soil:

$$q = K\left(\frac{\partial h}{\partial z} + \cos\gamma\right) \approx K^{i+1/2}\left(\frac{h^{i+1} - h^i}{\Delta z} + \cos\gamma\right), \tag{2.15}$$

where q is the snowpack runoff (m s^{-1}), positive values denoting downward water movement. The right hand side describes the numerical implementation, where i denotes the upper-most soil element and $i + 1$ the lowest snow element, $K^{i+1/2}$ is the hydraulic conductivity at the interface between element i and $i + 1$, and h^i and h^{i+1} are the pressure heads in the top soil and bottom snow element, respectively. Δz is the vertical grid spacing. In the rest of the paper, snowpack runoff will be treated from a mass balance perspective, denoting downward water movement (snowpack outflow) with a negative value.

For the snowpack, the layer thickness varies per layer and with time. When there is solid precipitation, new snow layers are added on top of the domain with an initial thickness of 2 cm. Over time, settling of the snow reduces the layer thickness. When a snow layer gets smaller than a specified minimum height or the ice content decreases below a specified minimum value, it is joined with the layer above (in case it is the lowest snow layer) or below (all other cases). When two adjacent snow layers get similar properties, they are also merged (*Bartelt and Lehning*, 2002).

The model is run in 15 min time steps. Processes are described sequentially, assuming stationary snowpack behaviour in these 15 min. First, new snow is added to the snowpack at the beginning of a time step when solid precipitation occurs. Then, the change in temperature distribution over the time step is calculated, after which phase changes are executed based

on the new temperature profile at the end of the time step. Then the water balance routine is executed. For runs with the bucket or NIED scheme, first the snowpack water flow is calculated. The sum of snowpack runoff over the time step is expressed as an average runoff from the snowpack over the time step, which is then used as a specified flux (second type) boundary condition (*McCord*, 1991) for RE for the soil part. For runs with RE scheme for both snowpack and soil, the soil-snow column is calculated as a continuous column. After the calculation of water transport is finished, the new snowpack state will undergo phase change again when necessary, mainly to freeze percolating meltwater and rain water. The time step is finalised by calculating the internal snowpack metamorphism, as described in *Lehning et al.* (2002a). Note that water transport by the NIED scheme is internally calculated with a time step of 1 min. The solver for RE uses a variable time step (see Appendix A for details).

The latent heat associated with rain, evaporation/condensation and sublimation/deposition is applied as a Neumann boundary flux for the temperature equation. In case of rain, evaporation or condensation, the liquid water flux itself is used as a specified flux boundary condition for the water balance schemes. During deposition, surface hoar may be formed on the snow cover (*Stössel et al.*, 2010). In case of evaporation or sublimation, the implementation of the boundary condition require different treatments, depending on water balance scheme. In the bucket and NIED simulations, the latent heat flux is first used to evaporate liquid water from the snowpack. Remaining energy is then used to sublimate the ice matrix, respecting the fact that evaporation is more favoured by the lower energy required for evaporation. When RE is used for the snowpack, the specified flux at the upper boundary is actively limited. A maximum evaporative flux is allowed, based on an imaginary limiting pressure head outside the model domain (see Appendix A). If the evaporative flux exceeds this value, the flux is limited to this value. The excess energy is used to sublimate the ice matrix. Note that the actual mass exchange differs whether evaporation/condensation or sublimation/deposition occurs, because of the difference in latent heat involved. This may cause a slightly different mass balance of the snowpack in the different simulations.

2.3.4 Simulation setup

The SNOWPACK model is driven by the measured precipitation amounts. Measured precipitation is assumed to be rain when the air temperature was higher than 1.2 °C and snow otherwise. The net radiation is determined from the incoming and outgoing longwave and shortwave radiation and, consequently, albedo is derived from the measured shortwave radiation components. Absorption of penetrating shortwave radiation is treated as a source term for the temperature equation in the top snow layers. The surface energy balance is evaluated using the net longwave radiation and calculated latent and sensible heat fluxes using a common form of Monin–Obukhov bulk formulation (*Lehning et al.*, 2002b). Atmospheric stability is estimated from the difference in measured air and surface temperature. The net heat flux is used as a Neumann boundary condition for the temperature equation. In the simulations, a roughness length (z_0) of 0.002 m was used for WFJ (*Stössel et al.*, 2010) and 0.015 m for CDP

(*Essery et al.*, 2013).

In all simulations, the water flow in the soil is solved using RE. Soil freezing was not considered and the soil temperature was bounded by $0\,°C$. This assumption is supported by snow profiles of seasonal snow covers, where ground heat creates close to melting conditions at the snow-soil interface.

For WFJ simulations, a soil of 1.5 m depth is used, divided into 30 layers of varying thickness. This setup ensures that choices for lower boundary conditions in the soil are only marginally impacting the snow cover. Typical soil properties for gravel/coarse sand were taken ($\theta_r = 0.01$, $\theta_s = 0.35$, $\alpha = 3.5\,\text{m}^{-1}$, $n = 4.5$ and $K_{sat} = 3.171 \cdot 10^{-6}\,\text{m s}^{-1}$). At the lower boundary, a water table is prescribed as a Dirichlet boundary condition for RE and a constant upward soil heat flux of $0.06\,\text{W m}^{-2}$ is prescribed as Neumann boundary condition for the temperature equation. Although in reality, the water table is expected to be deeper at WFJ, the gravel/coarse sand material will make the influence of the water table on snowpack runoff negligible small.

At CDP, the ground heat flux is an important factor in the energy balance of the snowpack, due to the low elevation and consequently warmer soil of the site. To take this into account in the simulations, a soil of 10 cm depth was used, divided into 10 layers, and measured soil temperatures at 10 cm depth were applied as a Dirichlet boundary condition for the lower boundary. Although *Morin et al.* (2012) reports a substantial loam content for the soil at CDP, we used the same soil as for WFJ to prevent ponding conditions in the shallow soil. At the lower boundary, a free drainage Neumann boundary condition was applied for solving RE.

Analysis

For both sites, the model simulations and lysimeter measurements are analysed for the 24, 12, 6, 3 and 1 h time scales and, only for WFJ, also for the 0.5 h time scale. Runoff values were constructed by summing the 15 min model output resolution or the 10 min (WFJ)/1 h (CDP) lysimeter measurement resolution to the respective time scales, starting at 00:00 h (midnight) local time. We restrict the analysis in this study only to periods with a snow cover on the ground during the winter season. We will refer to these periods as snow seasons, where the snow seasons are denoted by the year in which they end (e.g. 1997 denotes winter season 1996–1997). Summer snowfalls are ignored in the analysis.

To determine the beginning and end of a snow season at WFJ, it is assumed that on 1 March a snow cover is always present. Then, it is searched both forward and backward in time in the measurements and simulations until all have snow-free conditions. These mark the start and end of the snow season. The melt season at WFJ is defined here as the period from 1 March to the melt out date. In the measurements from the lysimeter, one cannot distinguish snowpack runoff with a snowpack present and rain without a snowpack. Using measured snow height to determine the end of the snow season appeared to be somewhat cumbersome as measurement inaccuracies make it difficult to determine when the surface is

snow free. Moreover, the rain gauge used to derive precipitation amounts, the snow height sensor and the lysimeter are located several metres apart. Given the spatial variability of the snow cover thickness, the snow height sensor cannot be regarded as fully representative for the snow height at the lysimeter. Therefore, the snowpack runoff measured by the lysimeter was assumed to come from the snowpack as long as a snow cover was present in the simulations and consequently, the lysimeter runoff may include rainfall in snow-free conditions, if the duration of the simulated snow cover exceeds the real snow cover presence.

At CDP, the snow cover may melt completely during the winter season in some years. Therefore, we define the start of the snow season here as the first snowfall that contributed to the snow cover present at 31 December. If at May 1, no snow cover is present, it is looked backward in time to find the last day where a snow cover is present in either the measurements or one of the simulations. Else, we look forward in time, to find the last day a snowcover is present. The lysimeter data from CDP is cleaned by the providers such that it only reports values when a snow cover is present. However, if the snow cover still exists in the simulations and the lysimeter is already snow-free, rainfall will be added to snowpack runoff in the simulations, but is not reported by the lysimeter. Therefore, rainfall was added to the lysimeter series when there was no measured snow cover, but still a snow cover in one of the simulations.

To assess the added value of the water balance schemes, the performance of modelled snowpack runoff is compared to a constructed runoff series that consists of the modelled LWC production (snowmelt, refreezing and rain input). This LWC production is calculated for each time step as the average of the four simulation variants. It represents the case where the sum of snowmelt and rain input is routed to runoff immediately and it will be referred to as average LWC production (avg. LWC prod.).

To quantify the accuracy of the modelled snowpack runoff, Nash-Sutcliffe model efficiency coefficients (NSE, *Nash and Sutcliffe*, 1970) are calculated for all time scales. These are only determined over the winter snow season. To calculate an NSE coefficient over all snow seasons, the snow seasons are analyzed sequentially by removing the intermediate summer periods.

All simulations were run on the same desktop computer as a single-core process. The increase in computational time by using RE for the snow cover is significant but not excessive: the additional effort for water transport is of the same order as the total seasonal snow cover simulation without RE. For WFJ, the simulations with the bucket scheme for snow took on average about 1.5 min per year and the NIED scheme took about 1.7 min per year. Solving RE for snow increased the average simulation time to 3.1 min per year for RE (Yamaguchi) and 2.7 min per year for RE (Daanen). CPU times for CDP are about half as those for WFJ, as a result of the shallower snowpack.

2.4 Results and discussion

The discussion of the results will first focus on the seasonal and daily time scale and afterwards on sub-daily time scales. Table 2.1 shows the snow season period and the maximum measured snow height for each year. In the studied period, the snow season at WFJ is mostly starting in October, and the melt out date is mostly between mid-June and mid-July. The maximum measured snow height ranges from 182 cm in 2005 to 356 cm in 1999. At CDP, the snow season is shorter than at WFJ and is roughly between November and April/May. Also the maximum snow height reached is lower than at WFJ, and ranges from 68 cm in the years 2001 and 2007 to 207 cm in 1999.

Table 2.1 also shows the seasonal average difference between measured and modelled snow height. The year-to-year variability indicates that using measured precipitation to drive snowpack simulations has some inherent inaccuracies and the main problem is that the over- or underestimation of a single precipitation event will persist throughout the rest of the snow season. It is noteworthy that snow height also varies between the different schemes, although these variations are smaller than the year-to-year ones. The snow height variations between simulations can be explained by differences in mass loss due to runoff and by differences in settling, as a result of varying vertical LWC and density distributions due to the different water balance schemes. Although the differences between simulations are rather small, RE with Yamaguchi's parameterization shows the smallest deviation from measured snow height, whereas Daanen's parameterization seems to cause slower settling and higher snow heights. This is especially visible in the simulations for WFJ.

Figure 2.1 shows that the cumulative runoff sum from the snowpack exhibits much smaller variations between simulations than the snow height, indicating that there is only a small difference in modelled snow water equivalent. As the precipitation input is the same for all simulations, the slightly varying cumulative runoff sums are mainly caused by differences in evaporation/condensation or sublimation/deposition. The reasons for these differences are, first, that the LWC in the surface layer will influence the surface temperature, especially due to variations in time needed to refreeze at night. These differences in surface temperature in the evening hours may influence sensible and latent heat exchange and may cause differences in energy input into the snow cover between simulations. Second, the partitioning of latent heat between sublimation and evaporation is different between the water balance schemes. Because of the difference in latent heat associated with sublimation or evaporation, mass gain or loss will be smaller in case of sublimation/deposition than in evaporation/condensation. Note that in practise, the albedo of the snow cover, and thus the energy balance, is also influenced by the LWC in the surface layer. This influence is not present here, because measured albedo is used to drive simulations at both sites.

At both sites, the agreement between measured and modelled cumulative sum of snowpack runoff is limited (see Fig. 2.1), although most year-to-year variability is captured. The under-catch correction was verified for both sites by comparing the seasonal maximum measured
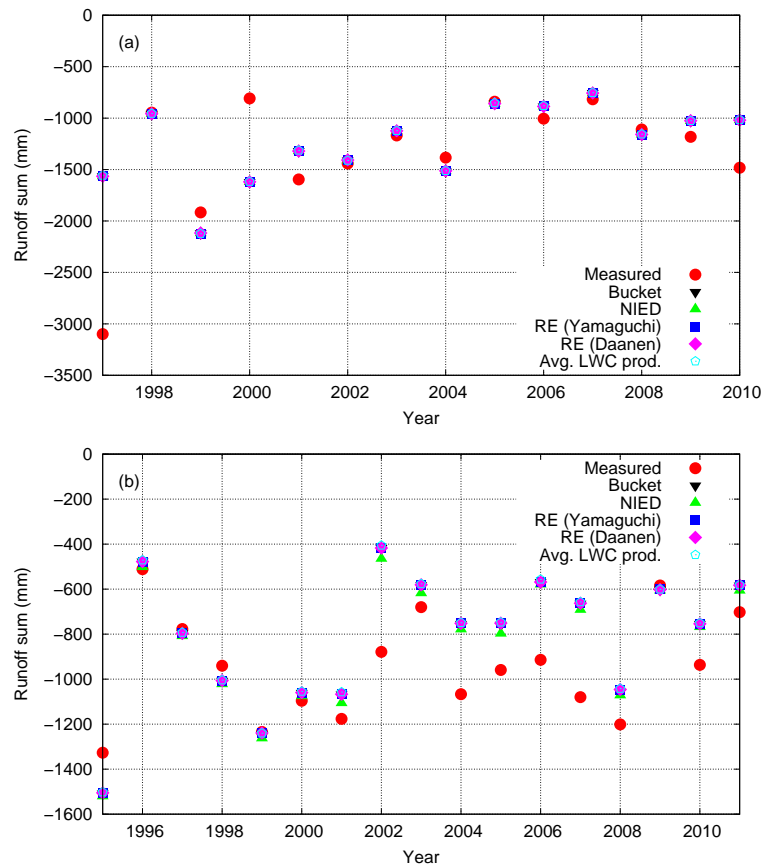
Figure 2.1: Measured and modelled snowpack runoff sums (mm) over the snow seasons for WFJ **(a)** and CDP **(b)**.

SWE in snow pits to the modelled SWE at the same date. No systematic over- or underestimation was found, which suggests that the estimation of precipitation does not show a bias. The overestimation of snow height at WFJ and the underestimation of the snow height at CDP (see Table 2.1) are likely related to the modelling of new snow density and snow compaction over time.

The discrepancies between modelled and measured runoff may also be caused by an unrepresentative snowpack state at the lysimeter or inhomogeneous flow features like flow fingering and flow over ice lenses. The accuracy of the undercatch correction for solid precipitation (*Goodison et al.*, 1998) may also vary from year-to-year. Furthermore, the deviations are likely a general expression of the fact that snow height can vary over short distances, mainly caused by heterogeneity in wind fields (e.g. *Winstral et al.*, 2002; *Mott et al.*, 2010). However, the deviation between measured and modelled snowpack runoff is suspiciously large at WFJ in the years 1997 and 2000. These differences seem to be too large to be explained by lateral flow effects or inhomogeneous snow redistribution, and the agreement between measured and modelled snow height for these years (see Table 2.1) suggest that precipitation input is also

not the cause of the differences. In both cases, the consistency between maximum measured snow height and modelled snowpack runoff indicates that the most probable source of error is in the measured snowpack runoff. This likely is either a malfunctioning of the lysimeter or a strongly unrepresentative snowpack state at the lysimeter.

2.4.1 Daily time scale

For snow season 1998 at WFJ, all water balance schemes show rather good performance compared to other years and also the measured runoff sum is in good agreement with the modelled runoff sum. Therefore, this year is used as an example. Figure 2.2a shows the cumulative snowpack runoff in the melt season. As can be seen, the lysimeter registers the first melt water at the base of the snowpack earlier than any of the model schemes. The simulations with RE produce runoff soon after the first measured runoff, whereas the bucket and NIED simulations show some delay. For the rest of the melt season, there are no important differences. Because the bucket and NIED simulations withhold the water too much in the snowpack compared to the lysimeter and the simulations with RE, the daily outflow near the end of the season becomes higher than in simulations with RE. General runoff dynamics and alternating phases with high and low runoff are represented well in all simulations, although in some periods, discrepancies in runoff amounts between measurements and model exist.

Figure 2.3 shows the NSE coefficients for daily sums of snowpack runoff for both WFJ and CDP for the respectively 14 and 17 yr individually. It shows that for the daily time scale, differences between the various models are much smaller than year-to-year differences in NSE coefficients. Furthermore, the spread between simulations is larger at CDP than WFJ. For both sites, it can be seen that when the agreement between modelled and measured snowpack runoff is lower, all water balance schemes have a lower agreement with measured snowpack runoff (and vice versa). The fact that NSE coefficients for the average LWC production follow the same pattern is an indication that for these years, sources of error causing variation of NSE coefficients may be related to the estimation of meltwater production as determined by a positive energy balance and a possibly sometimes inaccurate partitioning of precipitation in rain and snow. The representation of internal snowpack structure and accompanying hydraulic properties in the model seem to play a less pronounced role, which may also imply that the model does not reproduce adequately enough year-to-year variations in internal snowpack structure that influence water flow.

On the other hand, lysimeter measurements are known to be notoriously difficult, as found in experiments by *Kattelmann* (2000). Discrepancies between measured and modelled snowpack runoff should therefore not be attributed solely to an inaccurate representation of the snow cover or energy balance in the model. For example, due to lateral flow in the snowpack, the effective area from which meltwater is collected may differ from the actual area of the lysimeter (*Kattelmann*, 2000). Furthermore, the walls around the lysimeter to prevent preferential flow along the base of the snowpack may influence the snow cover at the start of the snow season.
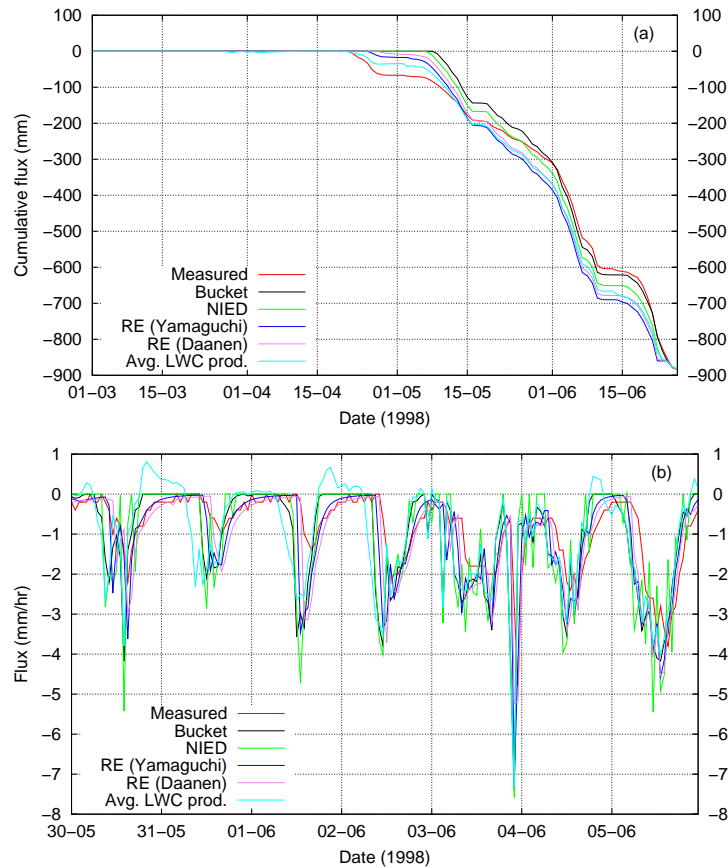
Figure 2.2: Cumulative snowpack runoff at WFJ for the lysimeter measurements and the various water balance schemes for the 1998 melt season **(a)** and hourly snowpack runoff for the lysimeter measurements and the various water balance schemes for one week during the 1998 melt season **(b)**.

The lysimeter may collect more snow due to wind effects and snowmelt can be reduced due to the shadowing effect of the wall. This may lead to a non-representative snow cover inside the lysimeter.

The three years with a very low NSE coefficient for WFJ are also likely related to measurement problems. Typical causes for low NSE values are a consistent over- or underestimation (bias) and poor timing of meltwater peaks (*McCuen et al.*, 2006). For the years 1997 and 2000, the low NSE coefficients are for an important part caused by the bias between modelled and measured seasonal snowpack runoff (see Fig. 2.1). For the year 2005, it appears as if the lysimeter was obstructed for quite some time, after which half the seasonal sum of snowpack runoff passed through the device in few days time (not shown).

In terms of NSE coefficient, RE does reproduce measured snowpack runoff best at both sites, although differences are marginal. At WFJ, RE achieves an NSE coefficient of 0.63 and 0.62 for
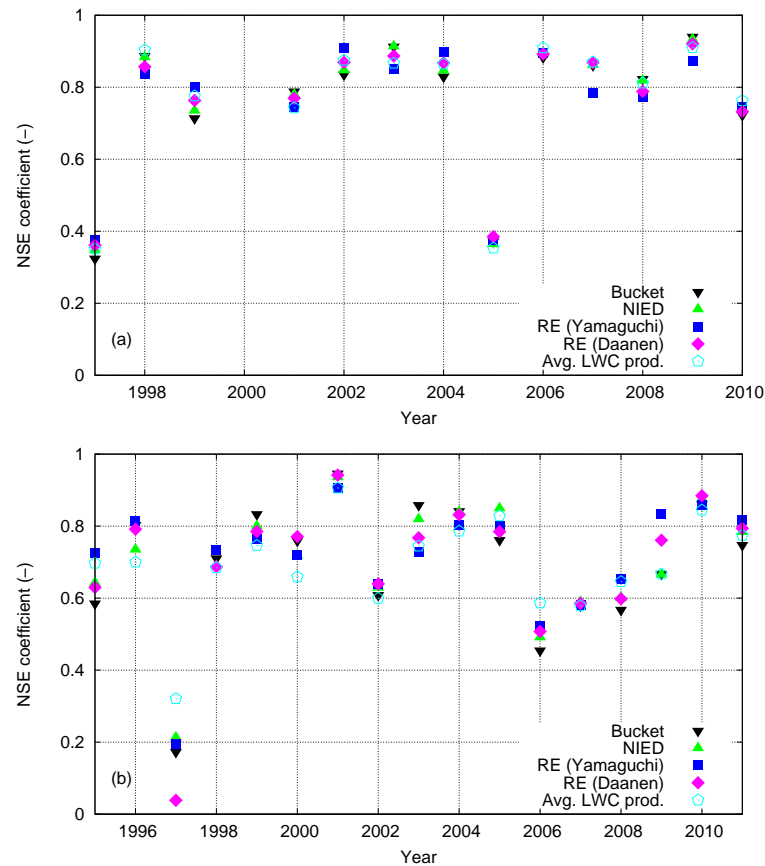
Figure 2.3: NSE coefficients (model vs. measured) for the snow seasons for the 24 h time scale for WFJ **(a)** and CDP **(b)**. The NSE coefficients for snow season 2000 for WFJ are negative and not shown.

Yamaguchi's and Daanen's parameterization, respectively, over all 14 snow seasons. Bucket and NIED schemes also exhibit very similar performance with NSE coefficients of 0.61 and 0.62, respectively. For CDP, NSE coefficients for the daily time scale are higher than for WFJ. RE achieves an NSE of 0.72 and 0.71 for Yamaguchi's and Daanen's parameterization, respectively. NSE coefficients for the bucket and NIED scheme are 0.70 and 0.72, respectively. The fact that the different water balance schemes have very similar performance on the daily time scale and have an NSE coefficient very similar to the one for the average LWC production is an indication that once the snowpack is isothermal, meltwater production near the surface is transported downward within the day in all models and that this is in good agreement with the measurements. This is noted already in literature (e.g. *Colbeck*, 1972; *Brun et al.*, 1989; *Davis et al.*, 2001).
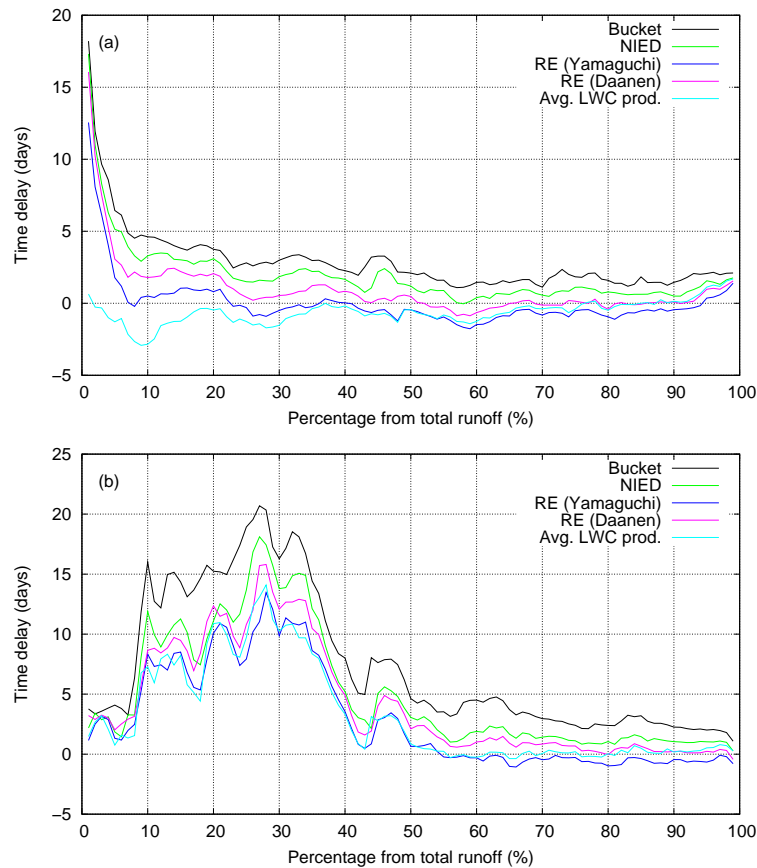
Figure 2.4: Average delay over all simulated years between modelled and observed snowpack runoff as a function of percentage of total melt season snowpack runoff (for WFJ **(a)**, starting 1 March) or total snow season snowpack runoff (for CDP, **b**).

2.4.2 Timing of seasonal runoff

To assess the performance of the water balance schemes in simulating the dynamics of the snowpack runoff over the season, it was determined at which date a certain percentage of the total cumulative snowpack runoff was reached. This was also done for the measurements. Then the difference between measured and modelled date was determined. Figure 2.4 shows the time delay in days between modelled and measured snowpack runoff. A positive delay means that modelled cumulative snowpack runoff arrives later in time than the measured one. For example: 20 % of total snowpack runoff is delayed by 1 day in the RE (Yamaguchi) simulations and 4 days in the bucket simulations. For CDP, the comparison is made over the complete snow season, as important melt and snowpack runoff events occur throughout the season. At WFJ, melt and subsequent snowpack runoff occurs either at the early start of the snow season (October or November), or after the beginning of March. So for WFJ, the comparison is made for the spring melt season only.

As can be seen, all models are strongly underestimating the arrival date of the first few percent of the total snowpack runoff in the melt season at WFJ, up to about 18 days for the bucket and NIED scheme. Average LWC production in the models is in fairly good agreement with measured snowpack runoff, suggesting that the first surface melt is almost directly accompanied by snowpack runoff. This fast arrival of meltwater at the base of the snowpack in the measurements likely results from the more efficient transport mechanism of preferential flow paths compared to matrix flow. Several experiments have shown that water flow in snow is not horizontally homogeneous (e.g. *Conway and Benedict*, 1994; *Waldner et al.*, 2004; *Katsushima et al.*, 2013). The 1-D approach in this study cannot resolve preferential flow paths by flow fingering, as observed in several experiments. Preferential flow paths will be able to transport water downward faster than horizontally uniform matrix flow, as simulated here. However, Fig. 2.4 suggest that this may involve only about 5 % of cumulative seasonal snowpack runoff. Note that this does certainly not imply that preferential flow cannot have a more pronounced effect on the internal snowpack microstructure or wet snow avalanche formation.

After the start of snowpack runoff, the simulations with RE quickly show very little delay with measured snowpack runoff. For values of about 5 % and above, the dynamical snowpack runoff during the melt season is adequately simulated with RE. The fact that the delay is fairly constant after about 25 % shows that the daily amount of meltwater leaving the snowpack is in quite good agreement with measured values. The delayed snowpack runoff in the bucket and NIED scheme persist for almost the entire season. Apparently, bucket and NIED are retaining meltwater in the snowpack too long, releasing it later in the melt season.

At CDP, the first modelled snowpack runoff in the snow season is in rather good agreement with the measurements. This is likely a result of the fact that the snowpack is still very shallow when these snowpack runoff events occur. Afterwards, there arises a marked delay, visible in all water balance schemes, but most pronounced in the bucket scheme. In this period, extending from about 8–40 % of the snowpack runoff, more snowpack runoff is measured than modelled. This may be an expression of efficient preferential flow paths. After about 40 %, all water schemes are fairly constant compared to the beginning of the snow season. It may be concluded that the variations in the RE and NIED schemes are smaller than in the bucket scheme, showing that they provide better representation of the runoff dynamics throughout the snow season.

2.4.3 Sub-daily time scales

Figure 2.2b shows the hourly flux of snowpack runoff for one week during the melt season of the example snow season 1998. A daily returning peak in melt water outflow, associated with the daily cycle in melt, is visible. During 3 June a ROS event occurred with 14 mm of rain. The daily onset of runoff and timing of the peak flux is better reproduced by simulations with RE. The figure also shows that RE is able to reproduce the recession curve in the evening hours and the night. Although the NIED scheme does not reproduce this for WFJ in this case, *Hirashima*

et al. (2010b) found that the recession curve is reproduced in the NIED scheme for warm snow regions such as the central part of Japan.

In Fig. 2.5, NSE coefficients for the various water balance schemes are shown for sub-daily time scales. It is clear that for smaller time scales, the NSE coefficients decrease for all water balance schemes. On the 12 and 24 h time scales, all schemes produce more or less similar results at both sites. For the 1 h time scale, RE (Yamaguchi) achieves a still reasonable NSE coefficient of 0.49 for WFJ, where the bucket and NIED scheme have NSE coefficients of 0.17 and 0.07, respectively. The decrease in NSE coefficient for the bucket and NIED schemes must be mainly caused by poor timing of the meltwater release, as the daily sums of modelled snowpack runoff do not show large differences (see Fig. 2.3). At CDP, the RE scheme achieves a similar NSE coefficient for the 1 h time scale as at WFJ (respectively 0.47 and 0.44 for the Yamaguchi and Daanen parameterization). On the other hand, the bucket scheme achieves a much better NSE coefficient than at WFJ (0.39). Although an exact reason for the contrasting results was not found, we think it is a confirmation of the fact that once the snowpack is isothermal, differences in water balance schemes are rather small. These snowpack conditions are more frequent at CDP than at WFJ. Moreover, the shallower and less stratified snowpack at CDP likely reduces the differences between the water transport as calculated by the different schemes.

The constructed runoff series from the average LWC production shows a strong decrease in NSE coefficient on the smaller time scales, indicating the importance of taking into account travel time and intermediate storage in the snow cover for sub-daily time scales.

Figure 2.6 shows that the NSE coefficients for hourly sums of snowpack runoff exhibit variation from year to year. For bucket and NIED simulations, NSE coefficients for hourly snowpack runoff are close to zero or even negative for WFJ, indicating that the model has poor performance on the hourly time scale. RE shows a much better agreement with measurements than the other two schemes for most years, with Yamaguchi's parameterization being the best. At CDP, RE has overall the best performance, although the spread between the RE and bucket scheme is much smaller than at WFJ. Year-to-year variability at CDP seems to be smaller than at WFJ, maybe caused by a smaller year-to-year variation in internal snowpack structure.

2.4.4   Timing of hourly runoff

The NSE coefficients for WFJ simulations on the hourly time scale were close to 0 or even negative for the bucket and NIED schemes, which was ascribed to poor timing of the meltwater release in the bucket and NIED simulations. To quantify the timing of snowpack runoff, lag correlations were calculated between each of the simulations and the measured snowpack runoff. The time span was limited to -12 and $+12$ h, to prevent correlations with the daily cycle. Table 2.2 shows the time lag belonging to the highest lag correlation, with negative values indicating the snowpack runoff is too early in the day in the simulations. For WFJ, the bucket and NIED schemes have about 1–2 h too early snowpack runoff compared to measured
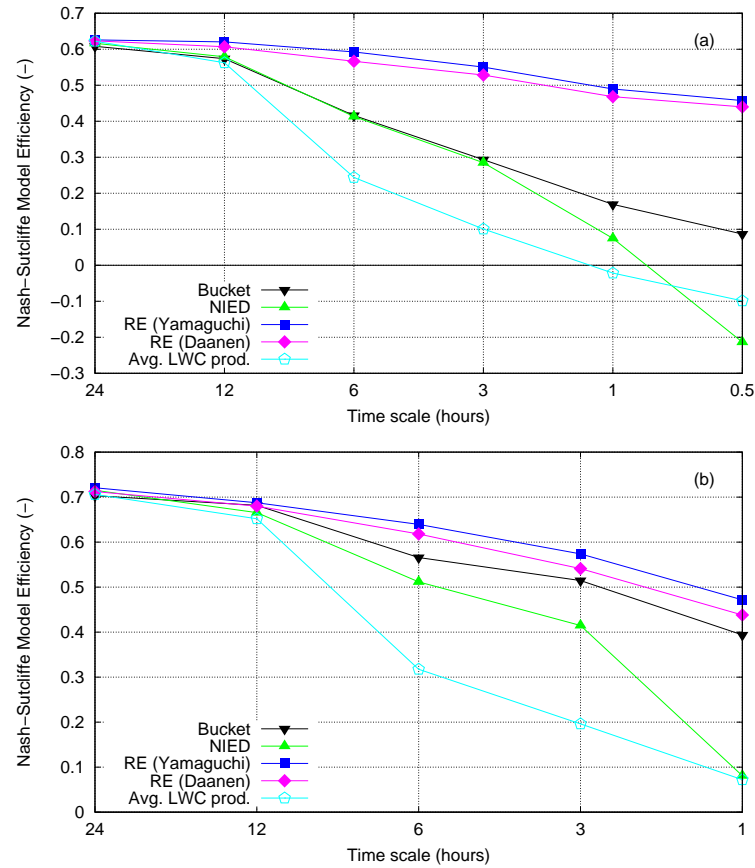
Figure 2.5: NSE coefficients (model vs. measured) over all snow seasons for the studied water balance schemes for different sub-daily time scales for WFJ **(a)** and CDP **(b)**.

snowpack runoff, while both simulations with RE show fairly good agreement in timing. Yamaguchi's parameterization seems to provide the best agreement with the measurements. The time lag between the average LWC production and measured snowpack runoff is about 1–3.5 h, showing the importance of the travel time through the snow cover for the sub-daily time scale. At CDP, the bucket and NIED schemes provides the best timing of the peak in meltwater release, whereas the Daanen's parameterization is worst. As can be seen by the low time lag value for the average LWC production, the snowpack at CDP is reacting much quicker to melt than at WFJ, probably due to a shallower and less stratified snowpack. Furthermore, when the modelled density of the snowpack is too high, as suggested by the underestimation of snow height at CDP (see Table 2.1), hydraulic conductivity is estimated too low (Eq. 2.14). This will result in an overestimation of travel time through the snowpack in simulations with RE.

The simulations with RE for WFJ did not show a significant time lag between lysimeter measurements and modelled snowpack runoff. The existence of preferential flow paths in snow would give the expectation that a time lag would exist when modelling matrix flow alone.
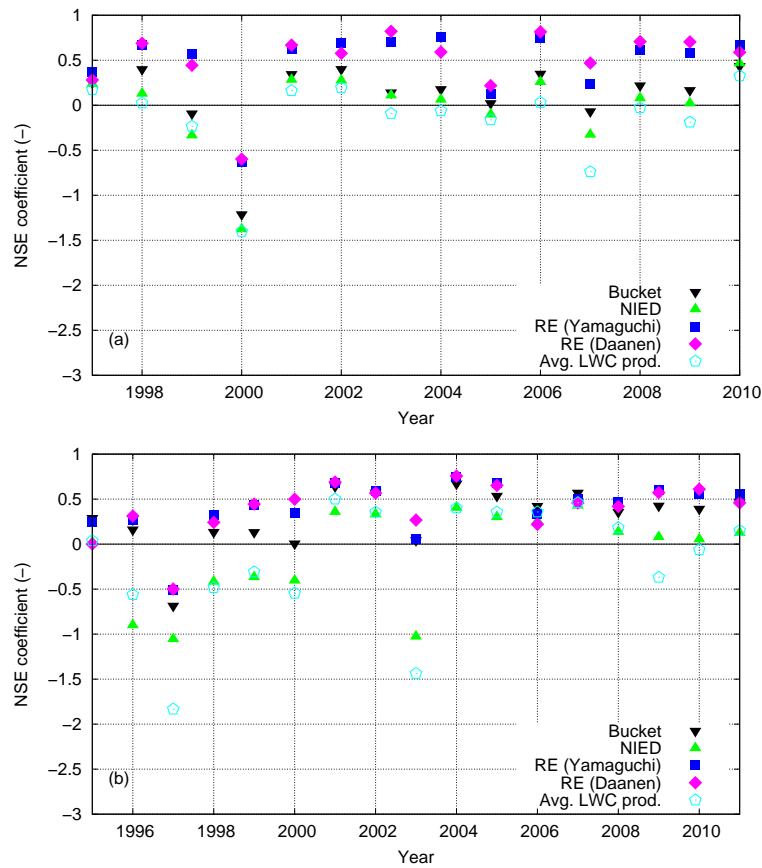
Figure 2.6: NSE coefficients (model vs. measured) for the snow seasons for the 1 h time scale for WFJ **(a)** and CDP **(b)**.

Only the simulations for CDP show a tendency towards a positive time lag when using RE. Three issues may play a role here. First, the strategy for choosing $\theta_r < \theta$ results in a direct participation of all liquid water in water transport. This may be a simplification of reality that would compensate for the error of neglecting preferential flow paths in the model. Second, it is possible that experiments to derive parameterizations for the water retention curve and hydraulic conductivity already incorporate preferential flow effects due to the measurement setup in which average flow behaviour is observed. Finally, the simulation results can be interpreted as that the existence of preferential flow paths is not essential for correctly modelling snowpack runoff, because the amount of water involved in preferential flow is small. However, this is not supported by results from other studies (e.g. *Marsh*, 1999, 2006).

2.4.5 Relation modelled and measured runoff

Figures 2.7 and 2.8 show scatter density plots for both the bucket scheme and RE (Yamaguchi) model for both the 24 h and 1 h time scale. In the figures for WFJ, the years 1997, 2000 and
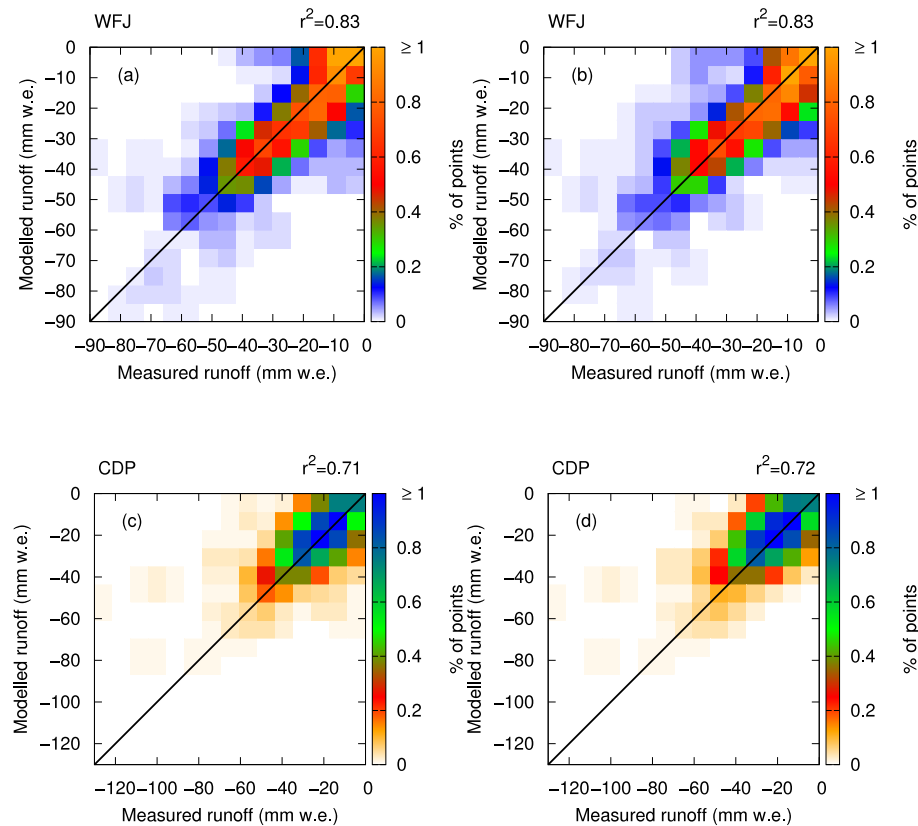
Figure 2.7: Density scatter plots for modelled versus measured snowpack runoff (mm) for the 24 h time scale for the bucket scheme **(a, c)** and RE (Yamaguchi) scheme **(b, d)** for both WFJ **(a, b)** and CDP **(c, d)**. In colour are shown the percentages in the specific region, cut off at 1 %. Data is divided in 15 × 15 bins. For an improved distinction between WFJ and CDP results, the colour scale for CDP is inverted.

2005 are left out, as the earlier discussed high discrepancy between modelled and measured snowpack runoff for these years appeared to be identifiable as outliers. The figures show the relative distribution of combinations of measured and modelled snowpack runoff for the 11 remaining snow seasons and for the 17 snow seasons at CDP.

For the 24 h time scale, the scatter density plots for both water balance schemes look very similar, in contrast to the 1 h time scale. Combined with an almost equal r^2 value, this confirms the conclusion that all water balance schemes have almost equal performance on the daily time scale. This conclusion can be drawn for both sites.

The distribution for the 1 h time scale shows that for WFJ, modelled snowpack runoff with the RE (Yamaguchi) scheme agrees better with measured snowpack runoff than the bucket scheme. This is also expressed by the much higher r^2 value. In contrast with WFJ, the results for

the 1 h time scale in terms of r^2 are almost similar for CDP for both schemes. Besides the main distribution along the diagonal where modelled snowpack runoff equals measured snowpack runoff, two distinct features are found. First, the bucket scheme seems to produce considerable amounts of snowpack runoff (-2 to $-5\,\text{mm}\,\text{h}^{-1}$) when there is almost no snowpack runoff measured. This effect was not present on the 24 h time scale, so it likely originates from the fact that the bucket scheme is releasing meltwater too early on the hourly time scale. Here, the neglect of travel time through the snowpack in the bucket scheme plays an important role. For WFJ, this is supported by the lag correlation (see Table 2.2). Interestingly, the effect is also visible at CDP, where no time lag was found. This apparent contradiction originates from the difference between both statistical methods. Second, another small effect is that especially in the RE (Yamaguchi) scheme, there is snowpack runoff observed on the order of -2 to $-4\,\text{mm}\,\text{h}^{-1}$, where at the same time the modelled snowpack runoff is close to zero. Interestingly, these two features are visible in simulations for both sites, although it does not result in the same difference in r^2 value between both water balance schemes.

2.5   Conclusions

A comparison of measured snowpack runoff by a lysimeter and 3 water balance schemes for the physically-based snowpack model SNOWPACK has shown that simulating water flow through a snow cover using RE achieves the best agreement with an acceptable increase in computation effort. The water balance schemes were tested for two alpine sites with a seasonal snow cover in a different climatological regime. For WFJ, NSE coefficients for simulations with RE were higher on both the daily and sub-daily time scales when compared to bucket and NIED simulations. The strongest improvement is on the sub-daily time scales. This is also supported by r^2 values between measured and modelled runoff. At CDP, the improvement in NSE coefficient when using RE compared to the bucket scheme is modest, and absent in the r^2 value. At both sites, NSE coefficients vary from year-to-year, quite synchronously: years with lower NSE coefficients have low NSE coefficients in all water balance schemes and vice versa. This indicates that measurements of either snowpack runoff or meteorological forcing have systematic errors that also vary from year to year. On the other hand, the specific implementation of modelled processes will also introduce errors that may have varying effects from year-to-year, depending on the snowpack structure.

The timing of meltwater arrival at the base of the snowpack and the runoff dynamics throughout the season also improved with RE, for both the daily and the sub-daily time scale. On the seasonal time scale, bucket and NIED simulations seem to retain the meltwater in the snowpack too long, underestimating the arrival of meltwater at the base of the snowpack in the early stages of the melt season. This was particularly found at WFJ, where there is a thick snow cover with strong layering and a clearly distinguishable dry, cool snowpack phase and a melting snowpack phase. At CDP, where melt is occurring frequently, it was found that especially in the middle of the winter, more snowpack runoff is measured than modelled. This is most pronounced in the bucket scheme. This may be caused by preferential flow paths, that
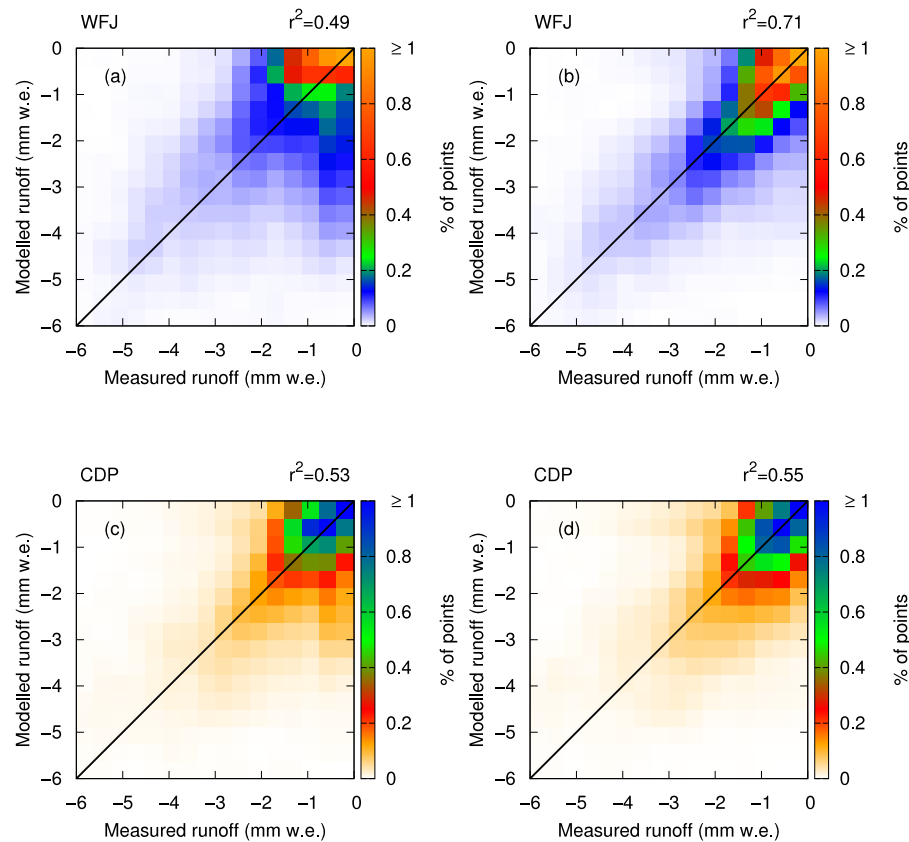
Figure 2.8: Density scatter plots for modelled versus measured snowpack runoff (mm) for the 1 h time scale for the bucket scheme **(a, c)** and RE (Yamaguchi) model **(b, d)** for both WFJ **(a, b)** and CDP **(c, d)**. In colour are shown the percentages in the specific region, cut off at 1 %. Data is divided in 15 × 15 bins. For an improved distinction between WFJ and CDP results, the colour scale for CDP is inverted.

provide efficient water transport to the bottom of the snowpack and which are not modelled. The results from both sites confirm that after the snow cover has become isothermal, the snowpack runoff is mainly determined by the meltwater production near the surface due to a positive energy balance and all water balance schemes route this water to snowpack runoff within the day, causing similar performance on the daily time scale.

For the sub-daily time scale, lag correlation coefficients showed that bucket and NIED simulations release meltwater too early in the day compared to measured snowpack runoff at WFJ. This is mainly because the water balance schemes in these two simulations either do not incorporate or else underestimate travel time of liquid water through the snowpack. This result is in contrast with the observations on the seasonal time scale, where it was found that these schemes retain meltwater too long. Apparently, the bucket and NIED scheme

require too much time to bring the snowpack to isothermal conditions, by propagating melt water downward too slowly. But once the snowpack is isothermal and wet in these schemes, additional meltwater produced during daytime is propagated downwards too quickly.

For RE, the timing of both seasonal and daily snowpack runoff is in better agreement with measured snowpack runoff. At CDP, the bucket and NIED schemes showed a better agreement of the estimation of the peak water outflow. Of the two parameterizations of the water retention curve in the van Genuchten model, Yamaguchi's parameterization has on average the best representation of travel time, whereas Daanen's parameterization causes a little too slow travel time.

It was generally found that using RE improved modelled snowpack runoff estimations more for the high alpine site WFJ than for the lower site CDP. We propose that the shallower snowpack at CDP reduces the differences arising from using different water balance schemes. Furthermore, the frequent melt cycles occurring at CDP are homogenizing the snowpack, reducing the stratification. The absence of strong inhomogeneities in the snowpack reduces the advantage the RE would have of explicitly taking differences in capillary suction between layers into account.

This study has shown that solving RE for snow is improving several aspects of modelled snowpack runoff considerably, especially for deep, sub-freezing snow covers, which mainly form at high altitude. Yamaguchi's parameterization shows the best overall performance, especially in terms of NSE coefficients. In the simulations for WFJ, the LWC distribution in the snowpack seems to cause slower settling in SNOWPACK, overestimating snow heights when using Daanen's parameterization. This will be a drawback in some applications, especially if snow depth is used to calculate winter precipitation (*Lehning et al.*, 2002b). Note that this study did neither consider the internal snowpack microstructure nor the LWC or density distribution, but focussed only on snowpack runoff. The use of RE may have a considerable effect on these internal snowpack properties.

2.6   Outlook

As was pointed out by *Marsh* (1999), there is a strong need for a better understanding and improved models to describe the complex water flow in natural snow covers. This study has shown that when solely looking at snowpack runoff, improving water balance schemes has an important consequence for the accuracy of snowpack runoff modelling. We also found that the available van Genuchten parameterizations have different effects on modelled snowpack runoff, although they are both based on experiments. Because the number of experimental studies analysing liquid water flow in snow is limited, the results in this study suggest that more experiments for different snow types are welcome as there is potential for the improvement of the model performance of water flow in snow. New measurement techniques are available (*Walter et al.*, 2013), which allow the detailed investigation of water flows including preferential flows in snow. This will help to solve the open question on the

importance of preferential versus matrix flow, which has been raised in this study. Moreover, the improvement in performance regarding snowpack runoff suggests that a deeper analysis on the effects on the internal microstructure of the snow, such as the formation of melt-freeze crusts is needed.

2.7 Appendix

Solving RE for snow involves some numerical challenges. Generally, many layers form in deep seasonal snowpacks such as at Weissfluhjoch, which can cause strong inhomogeneities in grain size and density. For numerical models, these inhomogeneities may impact numerical performance. Here, the specific numerical implementation will be discussed with some best practice methodology.

2.7.1 Time step control

To be able to simulate a complete snow season with optimal numerical performance, it is unavoidable to use variable time steps, as the dry snowpack in the winter months can be treated with much larger time steps than the spring snowmelt or ROS events. Infiltration fronts of meltwater in dry snow or soil require small time steps, because Picard iteration is known to have slow convergence for these situations (*Paniconi and Putti*, 1994). Therefore, we divide the SNOWPACK time step of 15 min in smaller time steps with variable length for solving RE, by applying the time stepping approach proposed by *Paniconi and Putti* (1994). Based on the number of iterations needed to achieve convergence in the Picard iteration scheme (N_{iter}), the new time step Δt_{new} is based on the previous time step Δt_{old} according to (determined by trial and error):

$$\Delta t_{\text{new}} = \begin{cases} 1.25\Delta t_{\text{old}}, & N_{\text{iter}} \leq 5 \\ \Delta t_{\text{old}}, & 5 < N_{\text{iter}} \leq 10 \\ 0.5\Delta t_{\text{old}}, & 10 < N_{\text{iter}} \leq 15 \\ \text{back} - \text{step}, & N_{\text{iter}} > 15 \end{cases} \tag{2.16}$$

When a back-step is performed, the time step is repeated with a smaller time step: $\Delta t_{\text{new}} = f_{\text{bs}}\Delta t_{\text{old}}$, with $f_{\text{bs}} = (1/3)^{n_{\text{sb}}}$ and n_{sb} being the number of sequential back-steps (for 1st back-step: $n_{\text{sb}} = 1$). Back steps are not only performed when $N_{\text{iter}} > 15$, but also when (i) change in pressure head between iterations exceeds a prescribed value (10^3 m) or (ii) the mass balance is violated (mass balance error > 0.1 $\text{kg}\,\text{m}^{-12}$). Both are early signs of growing numerical instabilities due to a too large time step. Doing a backstep immediately saves computation time by not executing all 15 iterations.

2.7.2 Convergence criterion

To determine convergence of the solution, the absolute change in solution between two iterations is required to be below a certain threshold. In the proposed Picard iteration by *Celia et al.* (1990), convergence is checked by a threshold value for the change in pressure head ($\Delta h < \epsilon_h$). However, *Huang et al.* (1996) have found that for non near-saturated conditions, determining convergence based on a threshold for θ ($\Delta\theta < \epsilon_\theta$) will also work and will generally improve convergence considerably, especially in dry conditions as often found in the snowpack. However, close to saturation and in ponding conditions, determining convergence based on θ is not possible and the pressure head condition should be used. Therefore, it is set that where $\Theta > 0.99$, the pressure head criterion is used and the θ criterion elsewhere. The θ criterion at low saturation can cause very inaccurate pressure head estimations and consequently large errors in the flux determined by Eq. (2.15). To achieve an accurate estimation of the snow-soil interface flux, convergence in the upper-most soil layer and lowest snow layer is always judged by the pressure head criterion. Values for ϵ_h and ϵ_θ are set to $1 \cdot 10^{-3}$ m and $1 \cdot 10^{-5}$ m^3 m^{-3} respectively, based on *Huang et al.* (1996).

2.7.3 Treatment of dry and refreezing snow layers

Fresh snow is dry below freezing and refreezing can cause the formation of dry layers. This gives a singularity in the Van Genuchten model for $\theta \leq \theta_r$, associated with an infinitely low pressure head. This problem is circumvented by initialising these new dry snow layers with a very low pressure head. First, in case $\theta < \theta_r + \frac{\epsilon_\theta}{10}$, θ_r was determined by setting it equal to:

$$\theta_r = \begin{cases} 0, & \theta \leq \frac{\epsilon_\theta}{10} \\ \theta - \frac{\epsilon_\theta}{10}, & \theta > \frac{\epsilon_\theta}{10} \end{cases} \tag{2.17}$$

Then, the following algorithm was used to determine the initial pressure head for dry snow layers: for each layer, the pressure head associated with $\theta = \theta_r + \frac{\epsilon_\theta}{10}$ was determined, so not detectable by the convergence criterion. The smallest value found for pressure head was chosen to initialise dry snow layers with. The associated tiny amount of LWC was created by melting the ice matrix. To prevent a continuously refreezing and subsequent melting of these tiny amounts of water in the snow cover, refreezing of meltwater in snow was only allowed for LWC exceeding 0.01 %. This value is small enough not to influence other snowpack calculations (e.g. wet snow metamorphism). The initialisation value of the pressure head was also used to determine the maximum allowed evaporative flux at the top of the domain, by prescribing it for an imaginary grid point outside the model domain.

2.7.4   Hydraulic conductivity at the interface between nodes

The finite difference approach to solve RE uses the center point of snowpack layers as nodes. The scheme therefore requires an estimation of the hydraulic conductivity at the interface between two layers. In literature, several methods to approximate hydraulic conductivity at the interface nodes between layers have been proposed (e.g. harmonic averaging, geometric averaging, see for example *Szymkiewicz and Helmig*, 2011). Several approaches were tested, but many yield very bad numerical performance and many tests would not complete within reasonable time. Main problems arise at interfaces where the hydraulic conductivity varies over several orders of magnitude (dry fresh snow layers on top of old snowpack). Most proposed averaging methods tend to put more weight on the lowest value for K. Arithmetic mean was found to work best, as it will effectively smooth large gradients in hydraulic conductivity. We suggest that the limited knowledge of hydraulic properties of snow is likely to influence calculation results stronger than errors arising from inaccurate approximations of the hydraulic conductivity at the interface nodes.

Acknowledgements

Edited by: F. Dominé

Chapter 2. Solving Richards Equation for snow improves snowpack meltwater runoff estimations in detailed multi-layer snowpack model

Table 2.1: Duration[a], maximum measured snow height and seasonal average difference in measured and modelled snow height[b] for all snow seasons.

Site	Snow season	Season Duration[a]	Maximum measured snow height (cm)	Average difference snow height (cm)[b]			
				Bucket	NIED	RE (Yamaguchi)	RE (Daanen)
WFJ	1997	05-09–23-07	257	6	3	4	11
	1998	09-10–26-06	203	−8	−9	−8	−2
	1999	11-09–01-08	356	29	26	27	38
	2000	25-09–04-07	288	21	19	15	31
	2001	30-10–08-07	289	−20	−21	−18	−13
	2002	30-08–27-06	225	17	15	12	23
	2003	21-09–15-06	245	3	3	7	14
	2004	03-10–25-07	262	31	30	32	42
	2005	04-11–23-06	182	7	6	6	14
	2006	15-11–25-06	207	−2	−3	−2	5
	2007	31-10–10-06	190	−11	−11	−10	−5
	2008	17-10–30-06	288	0	0	2	11
	2009	27-10–01-07	267	−7	−8	−8	1
	2010	09-10–03-07	217	2	1	5	11
	1995	18-12–18-05	191	3	1	2	4
	1996	27-12–19-04	135	0	−3	−2	0
	1997	17-11–27-04	127	17	15	15	17
	1998	29-11–11-05	158	8	5	5	7
	1999	10-11–14-05	207	−20	−23	−21	−20
	2000	15-11–04-05	148	−14	−16	−16	−14
	2001	14-12–02-05	68	0	0	0	1
	2002	21-12–03-04	123	−14	−15	−16	−15
CDP	2003	28-11–19-04	139	−4	−6	−6	−4
	2004	26-11–30-04	153	−12	−13	−13	−10
	2005	28-11–02-05	168	1	0	0	2
	2006	22-11–02-05	158	−5	−6	−4	−3
	2007	05-12–11-04	68	−2	−3	−4	−3
	2008	08-11–08-05	140	11	9	10	12
	2009	20-11–23-04	143	−6	−7	−6	−5
	2010	29-11–25-04	105	−1	−2	−1	0
	2011	06-11–07-04	72	9	8	10	10

[a] The snow season duration is formatted in DD-MM and denotes the period for which a snow cover existed in either the measurements or one of the model variants.
[b] A positive value denotes an overestimation of snow height in the model compared to measured snow height (and vice versa).

Table 2.2: Lag correlation coefficients (hours) for modelled snowpack runoff compared to measured snowpack runoff. Negative values mean the measured snowpack runoff should be shifted back in time to match modelled snowpack runoff.

Site	Snow season	Bucket	NIED	RE (Yamaguchi)	RE (Daanen)	Avg. LWC prod.
				Lag correlation with measured runoff (hours)		
WFJ	1997	−1	−2	0	0	−2.5
	1998	−1	−1	0	0	−1
	1999	−0.5	−2.5	0	0.5	−3
	2000	−3	−3	0	0	−4
	2001	−1.5	−1.5	−0.5	0	−2.5
	2002	0	−0.5	0	0	−0.5
	2003	−0.5	0	0	0	−0.5
	2004	−2	−2	0	0.5	−2
	2005	−1.5	-1.5	−1	−1	−1.5
	2006	−1	−1	−1	0	−3.5
	2007	−1.5	-1.5	−0.5	0	-4
	2008	−2	−1.5	−1	−0.5	−2
	2009	−2.5	-2.5	−0.5	0	−3.5
	2010	−1	−1	0	0	−1.5
CDP	1995	0	0	1	2	0
	1996	0	0	0	1	−1
	1997	0	0	1	2	−1
	1998	0	0	1	1	−1
	1999	0	0	0	1	−1
	2000	0	0	0	0	0
	2001	0	0	0	0	0
	2002	0	0	0	1	−1
	2003	0	0	0	0	−1
	2004	0	0	0	1	−1
	2005	0	0	0	1	−1
	2006	0	0	1	2	−1
	2007	0	0	0	1	0
	2008	0	0	1	1	0
	2009	0	0	0	1	−1
	2010	0	0	0	0	0
	2011	0	0	1	1	0

3 Verification of the multi-layer SNOW-PACK model with different water transport schemes

Nander Wever[1,2], Charles Fierz[1], Lino Schmid[1], Achim Heilig[3], Michael Lehning[1,2]

[1] WSL Institute for Snow and Avalanche Research SLF, Davos Dorf, Switzerland.

[2] CRYOS, School of Architecture, Civil and Environmental Engineering, EPFL, Lausanne, Switzerland.

[3] Institute of Environmental Physics, University of Heidelberg, Germany.

Summary

The widely-used detailed SNOWPACK model has undergone constant development over the years. A notable recent extension is the introduction of a Richards Equation (RE) solver as an alternative for the bucket-type approach for describing water transport in the snow and soil layers. Also continuous updates of snow settling and new snow density parametrisations have changed model behaviour. This study presents a detailed evaluation of model performance against an abundant multi-year data set from Weissfluhjoch Davos, Switzerland, with a focus on those internal variables, which are influenced by liquid water dynamics. The data set is collected by automatic meteorological and snowpack measurements, manual profiling, and radar data from an upward looking ground penetrating radar. During the main winter season, snow height, SWE, snow temperature distributions and snow density as well as their temporal evolution are well simulated in the model and the influence of the two water transport schemes are small. The RE approach reproduces internal differences over capillary barriers but fails to predict enough grain growth since the growth routines have been calibrated using the bucket scheme in the original SNOWPACK model. In the melt season, a more pronounced underestimation of snow density of about $100 \, \mathrm{kg \, m^{-3}}$ is found, accompanied by an increasing SWE bias. The radar data suggests that more liquid water is retained in the snowpack than simulated by the model. These analyses suggest that the process descriptions in SNOWPACK

have particular difficulties in accurately simulating the combined effect of snow settling under the influence of liquid water flow, the surface energy balance and penetrating shortwave radiation in the melt season. The discrepancies between the simulations and the field data are generally larger than the differences between the two water transport schemes. Nevertheless, the detailed comparison of the internal snowpack structure shows that the timing of internal temperature and water dynamics is adequately and better represented with the new RE approach when compared to the conventional bucket scheme, although the radar-deduced wetting front movement is better reproduced by the bucket scheme.

3.1   Introduction

The one-dimensional physics based snowpack model SNOWPACK (*Lehning et al.*, 2002a,b) has been used in many studies to assess various aspects of the snow cover. Recently, the model has been extended with a solver for Richards Equation (RE) in the snowpack and soil, which improved the simulation of liquid water flow in snow from the perspective of snowpack runoff (*Wever et al.* (2014), see Chapter 2). In that study, a comparison between snowpack runoff measured by a snow lysimeter and modelled snowpack runoff showed a higher agreement when simulating liquid water flow with RE, especially on the sub-daily time scale. Also the arrival of meltwater at the base of the snowpack in spring was better reproduced when using RE to solve liquid water flow in snow. However, these results were solely based on the liquid water leaving the snowpack. It raised questions to what extend the two water transport schemes differ in the simulation of the internal snowpack structure and if the improvements in snowpack runoff estimations with RE are also consistent with simulations of the internal snowpack.

For many applications, especially in hydrological studies, the primary variables of interest are snow water equivalent (SWE) and snowpack runoff, as the first provides possible future meltwater and the latter provides the liquid water that directly participates in hydrological processes. However direct measurements of SWE are relatively sparse, as SWE is rather time consuming to measure directly. Snow height measurements on the other hand are relatively easy to measure either manually or automatically and consequently, long climatological records of snow height are available. Methods have been developed to relate snow height to SWE (*Jonas et al.*, 2009; *Sturm et al.*, 2010). Snow density is another parameter that is variable in time and space (*Bormann et al.*, 2013) and rather cumbersome to measure in the field. Although it is seldom of primary interest, it may serve wide applications as an intermediate parameter between a property that is observed and a property that one is interested in. For example, proper estimates of snow density will increase the accuracy of translating snow height in SWE. Furthermore, snow density is required for correctly interpreting ground penetrating radar signals (*Heilig et al.*, 2009, 2010; *Okorn et al.*, 2014) or translating dielectric measurements to liquid water content, as for example with the Snow Fork (*Sihvola and Tiuri*, 1996), or the Denoth meter (*Denoth*, 1994).

Apart from bulk snowpack properties, there is also a demand for detailed snowpack models to assess the layering and microstructural properties of the snowpack, for example with the purpose of avalanche forecasting. Contrasting snowpack layers with respect to, for example, density, grain shape or grain size can act as weak layers where avalanches may release. Also the presence of liquid water can reduce the strength of a snowpack considerably, depending on grain shape (*Colbeck*, 1982; *Techel et al.*, 2011). When snowpack models are used to understand wet snow avalanche formation, it is important that the model can reproduce capillary barriers, at which liquid water may pond (*Baggi and Schweizer*, 2009; *Hirashima et al.*, 2010a; *Mitterer et al.*, 2011a). Also the arrival of meltwater at the bottom of the snowpack is considered to be a good indicator for the onset of wet snow avalanche activity. However, reliable liquid water content (LWC) measurements for the snowpack are difficult to obtain. Some attempts for continuous monitoring are promising (*Avanzi et al.*, 2014; *Schmid et al.*, 2014), but are not yet operational. Recently, advances have been made with using upward looking ground penetrating radar (upGPR) to assess the progress of the meltwater front in snow covers and first attempts have been made to derive liquid water amounts from the signal (*Mitterer et al.*, 2011b; *Okorn et al.*, 2014; *Schmid et al.*, 2014). We also consider temperature measurements taken during manual snow profiling as a reliable and precise way to determine which part of the snowpack has become isothermal and likely had liquid water in it due to infiltration or snowmelt.

As with snow density, snow temperatures are rarely of primary interest in snow studies. However, a correct representation of the temperature profile of the snowpack is required, as it determines the snow metamorphism (grain shape and size) and settling rates (*Lehning et al.*, 2002a). Temperature gradients drive moisture transports and have a strong influence on the grain growth (*Colbeck*, 1982; *Domine et al.*, 2013). Furthermore, temperature profiles are an indicator of whether the combination of the surface energy balance, the ground heat flux, and the internal heat conductivity of the snowpack is correctly approximated.

In this study, the SNOWPACK model is extensively verified for several bulk properties of the snowpack and against snow profiles made in the field, with the aim to verify the representation of the internal microstructure. Time series of soil and snow temperatures and snow lysimeter measurements from the Weissfluhjoch (WFJ) near Davos, Switzerland, are used to validate snowpack temperature profiles and snowpack runoff in the simulations. Furthermore, 4 years of upGPR data at WFJ is used to qualitatively asses the liquid water flow in the snowpack in comparison with model simulations. This study has a special focus on those snowpack variables that are influenced by liquid water flow and is limited to snow height, SWE, liquid water runoff from the snow cover, snow density, snow temperature, and grain size and shape, as for these, validation data is available. Internally, the SNOWPACK model also uses additional state variables, like sphericity, dendricity and bond size (*Lehning et al.*, 2002a).

3.2 Theory

The theoretical basis of the SNOWPACK model regarding the heat advection equation and snow settling has been discussed in *Bartelt and Lehning* (2002). The treatment of the snow microstructure and several parametrisations, like for snow viscosity, snow metamorphism and thermal conductivity are presented in *Lehning et al.* (2002a). Some of those parametrisations have been refined in later versions of SNOWPACK. The treatment of the meteorological forcing for determining the energy balance at the snow surface is discussed in *Lehning et al.* (2002b). Finally, the liquid water transport schemes are presented and verified in *Wever et al.* (2014). Here, we will outline theoretical aspects not discussed in the aforementioned literature.

3.2.1 Water retention curves

To solve RE, a water retention curve has to be specified. Here, the van Genuchten model is used (*van Genuchten*, 1980), where the water retention curve is described with several parameters: residual water content (θ_r), saturated water content (θ_s) and parameters α (m^{-1}), n and m. Also, the saturated hydraulic conductivity K_{sat} (m s^{-1}) needs to be specified. In SNOWPACK, the ROSETTA class average parameters (*Schaap et al.*, 2001) are implemented to provide these parameters for various soil types.

For snow, the parametrisation for α in the van Genuchten model as proposed by *Yamaguchi et al.* (2010) reads:

$$\alpha = 7.3(2r_g) + 1.9, \tag{3.1}$$

where $2r_g$ is the classical grain size (m), which is defined as the average maximum extent of the snow grains (*Fierz et al.*, 2009). For n, the original parametrisation by *Yamaguchi et al.* (2010) was modified by *Hirashima et al.* (2010a) to be able to extend the parametrisations beyond grain radii of 2 mm:

$$n = 15.68e^{(-0.46(2r_g))} + 1. \tag{3.2}$$

Here, we will abbreviate this parametrisation of the water retention curve as Y2010. This parametrisation has been used in *Wever et al.* (2014).

The Y2010 parametrisation was determined for snow samples with similar densities. In *Yamaguchi et al.* (2012), an updated set of experiments was described for a wider range of snow density and grain size, leading to the following parametrisation of the van Genuchten parameters:

$$\alpha = 4.4 \cdot 10^6 \left(\frac{\rho}{2r_g}\right)^{-0.98}, \tag{3.3}$$

and

$$n = 1 + 2.7 \cdot 10^{-3} \left(\frac{\rho}{2 r_{\mathrm{g}}} \right)^{0.61}, \tag{3.4}$$

where ρ is the dry density of the snowpack (kg m^{-3}). This parametrisation will be referred to as Y2012. Both parametrisations will be compared here. θ_{r} and θ_{s} are defined as described in *Wever et al.* (2014) and K_{sat} is parametrised following *Calonne et al.* (2012):

$$K_{\mathrm{sat}} = \left(\frac{\rho_{\mathrm{w}} g}{\mu} \right) \left[0.75 \left(\frac{r_{\mathrm{es}}}{1000} \right)^2 \exp \left(-0.013 \theta_{\mathrm{i}} \rho_{\mathrm{ice}} \right) \right], \tag{3.5}$$

where ρ_{w} and ρ_{ice} are the density of water (1000 kg m^{-3}) and ice (917 kg m^{-3}), respectively, g is the gravitational acceleration (taken as 9.8 m s^{-2}), μ is the dynamic viscosity (taken as 0.001792 kg (m s)$^{-1}$), θ_{i} is the volumetric ice content (m^3 m^{-3}) and r_{es} is the equivalent sphere radius (m), approximated by the optical radius, which in turn can be parametrised using grain size, sphericity and dendricity (*Vionnet et al.*, 2012).

In both parametrisations and for soil layers, the van Genuchten parameter m is chosen as:

$$m = 1 - (1/n), \tag{3.6}$$

such that the Mualem-model has an analytical solution (*van Genuchten*, 1980). We correct the water retention curve using the approach by *Ippisch et al.* (2006) for taking into account the air entry pressure. As in *Wever et al.* (2014), an air entry pressure of 0.0058 m was used, corresponding to a largest pore size of 5 mm.

The method to solve RE requires the calculation of the hydraulic conductivity at the interface nodes. It is common to take the arithmetic mean (denoted AM) of the hydraulic conductivity of the adjacent elements, although other calculation methods have been proposed (e.g., *Szymkiewicz and Helmig* (2011)). Here, we compare the default choice of AM with the geometric mean (denoted GM), as proposed by *Haverkamp and Vauclin* (1979), to investigate the possible influence of the choice on averaging method on the simulations of liquid water flow.

3.2.2 Soil Freezing and Thawing

Due to the isolating effects of thick snow covers and the generally upward directed soil heat flux, soil freezing at WFJ is mostly limited to autumn and the beginning of the snow season, when the snow cover is still shallow. To solve phase changes in soil, we follow the approach proposed by *Dall'Amico et al.* (2011). They express the freezing point depression in soil as a

function of pressure head as:

$$T^* = T_{\text{melt}} + \frac{g T_{\text{melt}}}{L} h,$$

(3.7)

where T^* is the melting point of the soil water (K), T_{melt} is the melting temperature of water (273.15 K), L is the latent heat associated with the phase transition from ice to water (J kg^{-1}) and h is the pressure head (m).

When the soil temperature T (K) is at or below T^*, the soil is in freezing or thawing state. Then, the pressure head associated with liquid water h_{w} (m) can be expressed as:

$$h_{\text{w}} = h + \frac{L}{g T^*} \left(T - T^* \right),$$

(3.8)

where h is the total pressure head of the soil (m). The van Genuchten model provides the relationship between pressure head and LWC:

$$\theta = \theta_{\text{r}} + (\theta_{\text{s}} - \theta_{\text{r}}) \frac{\left(1 + (\alpha|h_{\text{w}}|)^n \right)^{-m}}{Sc},$$

(3.9)

where θ is the volumetric LWC (m^3 m^{-3}). Consequently, the ice part can be expressed as:

$$\theta_{\text{i}} = \theta_{\text{r}} + (\theta_{\text{s}} - \theta_{\text{r}}) \frac{\left(1 + (\alpha|h|)^n \right)^{-m}}{Sc} - \theta,$$

(3.10)

where Sc is the correction proposed by *Ippisch et al.* (2006).

In *Dall'Amico et al.* (2011), a splitting method is introduced to solve both the heat advection equation and RE for liquid water flow in a semi-coupled manner. We approach the problem by finding the steady state solution for T, θ and θ_{i} in Equations 3.8, 3.9 and 3.10. This steady state solution is found numerically by using the Bisect-Secant method (*Dekker*, 1969), where the starting points for the method are taken as all ice melting and all liquid water freezing, respectively. In soil, liquid water flow can advect heat when a temperature gradient is present. In the soil module of SNOWPACK, heat advection associated with the liquid water flow is calculated after every time step of the RE solver, before assessing soil freezing and thawing.

3.3 Methods and Data

3.3.1 Data (1): Meteorological Time Series

The SNOWPACK model is forced with a meteorological data set from the experimental site at the Weissfluhjoch (WFJ) at an altitude of 2540 m in the Swiss Alps near Davos. During the winter months, a continuous seasonal snow cover builds up at this altitude. The measurement site is located in an almost flat part of a south-east oriented slope.

The data set contains air temperature, relative humidity, wind speed and direction, incoming and outgoing longwave and shortwave radiation, surface temperature, soil temperature at the interface between the snowpack and the soil, snow height, and precipitation from a heated rain gauge. An undercatch correction is applied for the measured precipitation (*Wever et al.*, 2014). From September 2013 onwards, soil temperatures are measured at 50, 30 and 10 cm depth. The experimental site is also equipped with a snow lysimeter with a surface area of 5 m^2, as described in *Wever et al.* (2014). The rain gauge and snow lysimeter are measuring at an interval of 10 minutes, whereas most other measurements are done at 30 minute intervals. Therefore, only the 30 minute sums of precipitation and snow lysimeter measurements are used here.

In the area surrounding WFJ, field data to validate soil freezing and thawing is lacking. For modelling the snowpack, the most important influence of the soil is the heat flux that is provided at the lower boundary of the snowpack. For this purpose, we will use the temperature measured at the interface between the soil and the snowpack to validate the soil module. This temperature measurement is influenced by soil freezing and thawing. Our primary interest here is the investigation to what degree the soil module as now in SNOWPACK is capable of providing a realistic lower boundary for the snowpack.

SNOWPACK can be forced with either measured precipitation amounts or with measured snow height. In precipitation driven simulations (Precip driven), measured precipitation is assumed to be snowfall when the air temperature is below 1.2 °C and rain otherwise. For these type of simulations, the study period is from October 1, 1996 to July 1, 2014 (1 week after melt out date), consisting of 18 full snow seasons. In case of snow height driven simulations (HS driven), an additional threshold for relative humidity and a maximum value for the temperature difference between the snow surface and the air is used to determine whether snowfall is possible. Then, snowfall is assumed to occur when measured snow height is exceeding the modelled snow height (*Lehning et al.*, 1999), in combination with a parametrisation for new snow density (*Schmucki et al.*, 2014). In both modes, new snow layers are added for each 2 cm of new snow. An uninterrupted, consistent dataset for this type of simulations is available from October 1, 1999 to July 1, 2014, consisting of 15 full snow seasons. The last snow season (2014) of the studied period has the most data available and will be used as the example snow season to detail how SNOWPACK simulates the snow cover.

Many processes in SNOWPACK are based on physical descriptions that require calibration, for example for wet and dry snow settling, thermal conductivity and new snow density. For this purpose, specially collected datasets with some additional detailed snowpack measurements from snow seasons 1993, 1996, 1999 and 2006 have been used when constructing the model. Snow metamorphism processes were mainly calibrated against laboratory experiments (*Baunach et al.*, 2001).

3.3.2   Data (2): Manual Snow Profiles

Every two weeks, around the 1st and 15th of each month respectively (depending on weather conditions), a manual full depth snow profile is taken at the WFJ, following the guidelines from *Fierz et al.* (2009). Measurements include snow temperature at a resolution of 10 cm, and snow density in steps of approximately 30 cm. Density is determined by taking snow cores using a 60 cm high aluminium cylinder with a cross-sectional area of 70 cm^2 and weighting the snow core using a calibrated spring. Grain size (following the classical definition of average maximum extent of the snow grains) and grain shape are evaluated by the observer using a magnifying glass. An observer may report two grain shapes when a mixture is present, where the first one reported is considered the most abundant shape. The observers also provide hand estimations of snow hardness and wetness. The snow profiling is carried out in the morning hours, starting around 9:00 local time. One of the first measurements involves the temperature in the top of the snowpack, although, depending on the time of year, the measurement may be influenced by the sunrise.

3.3.3   Data (3): Upward Looking Ground Penetrating Radar

An upGPR is located at the measurement site at about 10 m distance from the meteorological station (*Heilig et al.*, 2009, 2010; *Mitterer et al.*, 2011a; *Okorn et al.*, 2014). It has been operational from 15 December 2010 onwards and provides data for 4 snow seasons overlapping with the model simulations in this study. From the data, the wetting front is manually determined, based on the presence of a daily cycle in the travel time of the radar signal between the radar and the layers in the snowpack (*Schmid et al.*, 2014). These daily cycles are caused by variations in permittivity due to changes in LWC. The total amount of liquid water in the snowpack can be estimated as a percentage of the total snow cover mass (*Schmid et al.*, 2014). This requires a precise estimation of the snow height above the radar, which is ensured with a separate snow height sensor in the direct vicinity of the radar. However, for shallow snow covers (< 1 m), inaccuracies in snow height measurements result in imprecise estimates of LWC.

3.3.4   Methods (1): Model Setup

For the simulations in this study, the SNOWPACK model is solving the energy balance at the snow surface. The turbulent fluxes are calculated using the stability correction functions as in *Stössel et al.* (2010). This is an adequate approximation for most of the snow season, when the snow surface cooling due to net outgoing long wave radiation is causing a stable stratification. The surface albedo is calculated from the ratio of measured incoming and reflected shortwave radiation. The net longwave radiation budget is also calculated from the difference in measured incoming and outgoing long wave radiation. The aerodynamic roughness length (z_0) of the snow is fixed to 0.002 m.

The soil at WFJ consists of coarse material with some loam content, as was observed when

Table 3.1: Average bulk snowpack statistics for various simulation setups for all simulated snow seasons. Differences are calculated as modelled value minus measured value, ratios are calculated as modelled value divided by measured value.

Variable	Bucket	RE-Y2010AM	RE-Y2012AM	RE-Y2012GM	Bucket	RE-Y2012AM
	HS driven (2000-2014)				Precip driven (1997-2014)	
RMSE HS (cm)	4.16	3.98	4.11	4.12	20.79	23.04
Difference HS (cm)	1.36	0.87	0.91	0.93	-0.88	-5.00
RMSE SWE (mm w.e.)	39.36	39.83	39.86	39.57	84.59	98.80
Difference SWE (mm w.e.)	-5.99	-6.94	-9.98	-8.61	-15.45	-35.63
Ratio SWE (mm w.e.)	1.01	1.00	0.99	0.99	1.00	0.94
Ratio runoff sum (-)	1.07	1.14	1.13	1.13	0.98	0.98
NSE 24 hours (-)	0.70	0.73	0.73	0.73	0.68	0.67
NSE 1 hour (-)	0.13	0.57	0.58	0.58	0.06	0.42
r^2 24 hrs runoff sum (-)	0.83	0.85	0.85	0.85	0.84	0.83
r^2 1 hour runoff sum (-)	0.47	0.75	0.76	0.75	0.48	0.69
Lag correlation for runoff (hrs)	-1.47	-0.20	-0.17	-0.13	-1.72	-0.44
RMSE cold contents (kJ/m^2)	664	582	580	588	960	876
Difference cold contents (kJ/m^2)	-108.5	35.1	-18.5	-23.4	-73.9	43.5
r^2 cold contents (-)	0.90	0.92	0.92	0.92	0.83	0.86
r^2 isothermal part (-)	0.74	0.87	0.87	0.85	0.75	0.86
Mass balance error (kg/m^2)	0.01	0.01	0.01	0.01	0.15	0.05
Energy balance error (W/m^2)	0.04	0.05	0.06	0.05	-0.05	0.06
CPU time (min)	1.42	3.62	3.67	3.96	1.51	3.98

installing the soil temperature sensors. The ROSETTA class average parameters for the loamy sand class are taken for the van Genuchten parametrisation of the water retention curve for the soil ($\theta_r = 0.049$ m^3 m^{-3}, $\theta_s = 0.39$ m^3 m^{-3}, $\alpha = 3.475$ m^{-1}, $n = 1.746$, $K_{sat} = 1.2176 \cdot 10^{-5}$ m s^{-1}). For the thermodynamic properties, the specific heat for the soil constituents was set to 1.0 kJ kg^{-1} K^{-1} and the heat conductivity to 0.9 W m^{-1} K^{-1}. The total soil depth in the model is taken as 3 m, with a layer spacing of 1 cm in the top layers and 40 cm for the lowest layer. The dense layer spacing in the top of the soil is necessary to describe the large gradients in soil moisture and temperature occurring here. At the lower boundary, a water table is prescribed, together with a Neumann boundary condition for the heat advection equation, simulating a constant geothermal heat flow of 0.06 W m^{-2}.

All simulations are run on the same desktop computer as a single-core process, using a model time step of 15 minutes. In the solver for RE, the SNOWPACK time step may be subdivided in smaller time steps when slow convergence is encountered (*Wever et al.*, 2014). The computation time is in the order of a few minutes per year, where RE takes about twice as much time as the bucket scheme (*Wever et al.*, 2014). Checks of the overall mass and energy balance reveal that the mass balance for all simulations is satisfied well within 1 mm w.e. and the energy balance error is generally around 0.05 W m^2 (see Table 3.1). We consider these errors to be well acceptable for our purpose.

3.3.5 Methods (2): Analysis

The analysis of the simulations is done per snow season. Here, the snow season is defined as the main consecutive period with a snow cover of at least 5 cm on the ground. The snow season at WFJ generally starts in October or November and lasts until June or July. The snow season is denoted by the year in which they end. Summer snowfalls are ignored in this study.

The snow season at the WFJ is characterized by an early phase at the end of autumn or beginning of winter, when the snow cover is still relatively shallow and occasionally melt or rain on snow events are occurring. From the end of November to mid March can be defined as the accumulation period, in which snowpack runoff is virtually absent and the snowpack temperature is below freezing. This implies that in this period, all precipitation is added to the snow cover as solid mass, either by rain refreezing inside the snowpack, or by snowfall. Small amounts of snowmelt occurring near the surface refreeze during night or deeper in the snowpack. Therefore, the increase in SWE between the biweekly profiles can be used to verify the undercatch correction in case the SNOWPACK model is driven with measured precipitation from the heated rain gauge, and to verify the combined effect of the parametrised new snow density and snow settling in case snow height is used to derive snow fall amounts. The final phase is the melting phase, starting in April in most snow seasons, when the snowpack is isothermal and wet and producing snowpack runoff.

The snow temperature sensors may be influenced by penetrating shortwave radiation in the snowpack. Therefore, snow temperature measurements are only analysed when the measured snow height is at least 20 cm above the height of the sensor. Comparing snow temperatures between snow seasons was done by first standardising the measurement time of the temperature series between 0 and 1, for the start and end of the snow season, respectively. Then the data was binned in steps of 0.01 and bin averages were calculated. These series were then used for calculating the average and standard deviation between snow seasons. The same procedure was followed for snow height.

To compare manual snow profiles with the model simulations, several processing steps are required (*Lehning et al.*, 2001). The snow height at the snow pit is generally different from the simulated snow height. This is not only due to the model not depicting the snowpack development perfectly but also because the snow pit is made at some distance from the snow height sensor which is used to drive the simulations. Therefore, we scale the simulated profile to the observed profile by adjusting each layer thickness, without adjusting the density. This implies that mass may be added or removed from the modelled domain. Then, the model layers are aggregated to match the number and thickness of the layers in the observations. Model layers are assigned to observed layers based on the centre height of the model layer. The typical thickness of a model layer is around 2 cm, so possible round-off errors are expected to be small. For temperature, the matching with modelled layer temperatures is achieved by linear interpolation from the measured temperature profile to the centre point of the modelled layer.

The cold content of the snowpack is the amount of energy necessary to bring the snowpack to 0 °C, after which an additional energy surplus will result in net snowmelt. The total cold content Q_{cc} (J m^{-2}) of the snowpack is defined in discrete form as the sum of the cold content of each layer:

$$Q_{cc} = \sum_{i=1}^{n} \rho_i c_i \Delta z_i \left(T_i - T_{melt}\right),$$

$\qquad$ (3.11)

where i is an index to a snow layer, n is the number of snow layers in the domain, ρ_i is the density of the layer (kg m^{-3}), c_i is the specific heat of the layer (J kg^{-1} K^{-1}), Δz_i is the layer thickness (m) and T_i is the temperature of the layer (K). The cold content is calculated for both the observed and modelled profiles, where the modelled profile is first aggregated onto the observed layer spacing with the procedure described above.

Observers may report a primary and secondary grain shape. For determining plotting colour, it is common to take a 70% vs 30% mixing ratio from the colours assigned to the grain shapes (*Fierz et al.*, 2009). Here, we mix the colours evenly half and half, in order to make a comparison with the modelled profiles easier. Generally, determining grain shape is having a subjective component. We would therefore consider it to be a good agreement when SNOWPACK is simulating as main shape either one of the primary or secondary observed grain shapes or vice versa.

3.4 Results and Discussion

When presenting the results for the different snowpack related variables, first the results for the example snow season 2014 are shown, followed by an analysis of the complete study period. Figures for the other snow seasons can be found in the online Supplement. The results from the upGPR data are shown last, as they consist of a much shorter period.

3.4.1 Snow Height and Snow Water Equivalent

Figure 3.1 shows the snow height for several simulation setups. Per construction, the snow height driven simulations provide a high degree of agreement between measured and modelled snow height. The general tendency of the precipitation driven simulations is to follow the measured snow height, although it can be clearly seen that some precipitation events are overestimated, whereas others are underestimated. These differences are caused by inaccuracies when measuring solid precipitation with a rain gauge (*Goodison et al.*, 1998), imperfections in the undercatch correction, or the effect of aeolian wind transport causing either erosion or accumulation of snow at the measurement site. As snow drift is mainly occurring close to the surface, the rain gauge is rather insensitive to these effects as its installation height is higher than the typical depth of a drifting snow layer. On the other hand, at WFJ, snow drift is expected to play a relatively small role. Furthermore, a rain gauge inter-comparison project
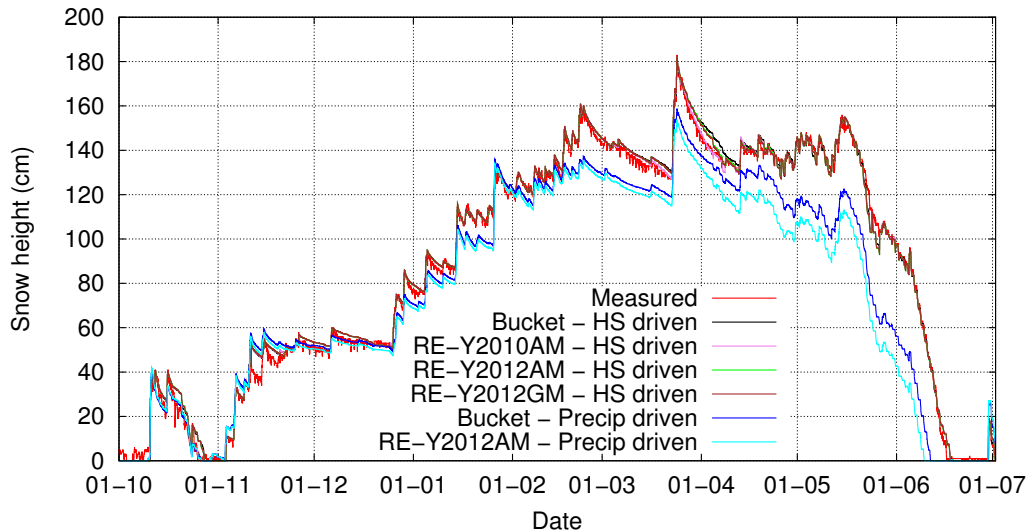
Figure 3.1: Measured and modelled snow height for different model setups for the example snow season 2014.

by MeteoSwiss is currently carried out at WFJ, which may allow for a better understanding of important effects and an improved undercatch correction in the future.

As listed in Table 3.1, the RMSE of snow height for all simulated snow seasons is significantly larger for precipitation driven simulations than for snow height driven ones. Furthermore, the difference between measured and modelled snow height tends to be negative, denoting an underestimation of snow height by the model. In the Supplement Figures 3.18 and 3.19, snow height for various model setups are shown for each snow season. Typical year-to-year variability of inconsistencies in the precipitation driven simulations are present, whereas the snow height driven simulations follow the measured snow height more closely. In Figure 3.2, the average snow height difference is shown for all simulated snow seasons, relative to the standardized date in the snow season. It shows that the underestimation of the snow height is occurring mainly near the end of the snow season, thus during the melt season. This does not necessarily imply that the melt rates are overestimated, as snow height is the combined result of snow accumulation, settling and melt.

SWE is generally a better indicator of snow accumulation and snowmelt than snow height. A comparison between observed SWE in manual profiles and modelled SWE (Figure 3.3a) shows that the agreement between both is high. The linear fits between the data points show that on average, the prediction of SWE in the model is accurate, for both snow height and precipitation driven simulations. The scatter is larger for precipitation driven simulations and there seems to be an underestimation of low SWE values and an overestimation of high ones. The modelled SWE is a result of several effects: (i) snowfall amounts, which rely on an accurate estimation of new snow density in case of snow height driven simulations or an
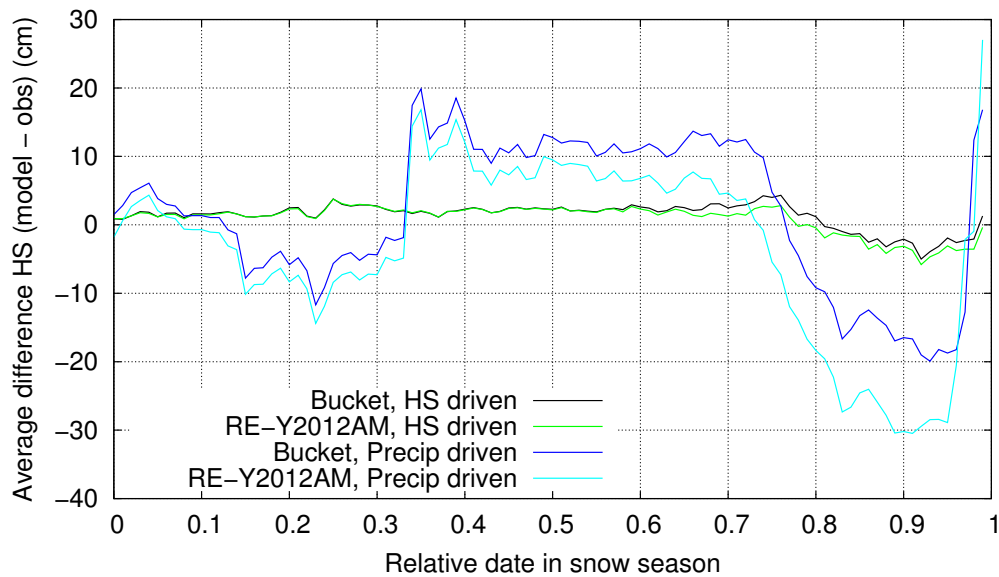
Figure 3.2: Difference in modelled and measured snow height relative to the snow season. For every snow season, the first day with a snow cover is set at 0, the last day at 1.

adequate undercatch correction in case of precipitation driven simulations, (ii) snow settling, in case of snow height driven simulations, (iii) snowmelt and (iv) liquid water flow in snow and subsequent snowpack runoff. To separate the effect of liquid water flow and snowpack runoff, Figure 3.3b shows the increase in SWE during the accumulation phase of the snow season at the WFJ, when only factors (i), (ii), and (iii) are playing a role. The snow height driven simulations are on average providing a high degree of agreement with the measured increase in SWE during the accumulation phase, with only a marginal difference between the bucket scheme and RE scheme. Here, it needs to be mentioned that in snow height driven simulations, the snow settling formulation is able to compensate for errors in the estimation of new snow density and vice versa. For example: when new snow is initialized with a too high density, and thus too much mass is added, the snow settling will be underestimated and consequently, the next snow fall amount is also underestimated. Because the snowfall amounts in precipitation driven simulations are independent of settling of the snow cover, the increases in SWE are independent of the predicted settling. The results show that in the accumulation phase, the combined effect of new snow density and snow settling is providing a slightly underestimated SWE increase, whereas the opposite is found for precipitation driven simulations.

Figure 3.4 shows the difference in SWE between model simulations and the snow profiles for all simulated snow seasons. The difference in snow height driven simulations is rather small, compared to precipitation driven simulations. All simulations show that in the melt phase, the model underestimates the SWE. This points towards either an overestimation of melt rates, or

57

(a) (b)
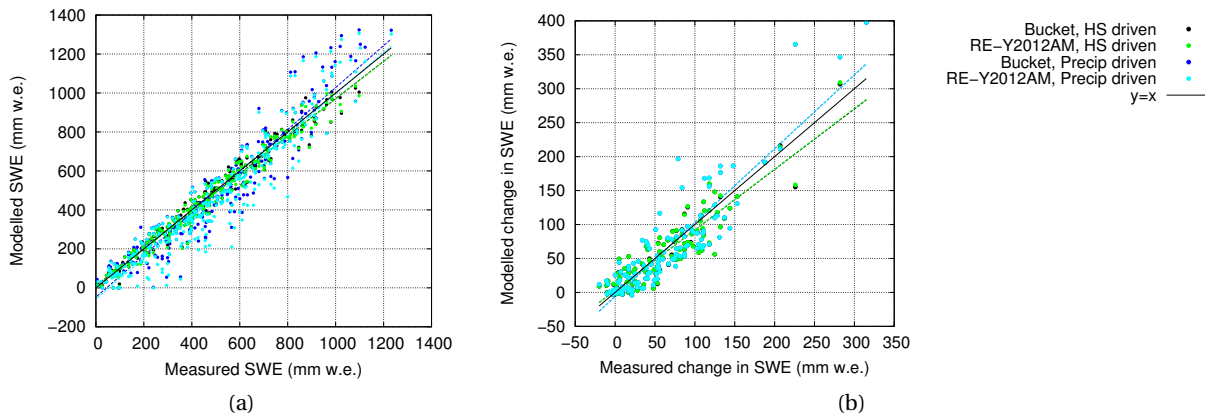
Figure 3.3: Comparison of measured and modelled SWE (mm w.e.) (a) and increase in SWE in the biweekly profiles and the simulations during the accumulation phase (b). The blue and green dots in Figure (b) perfectly overlap.
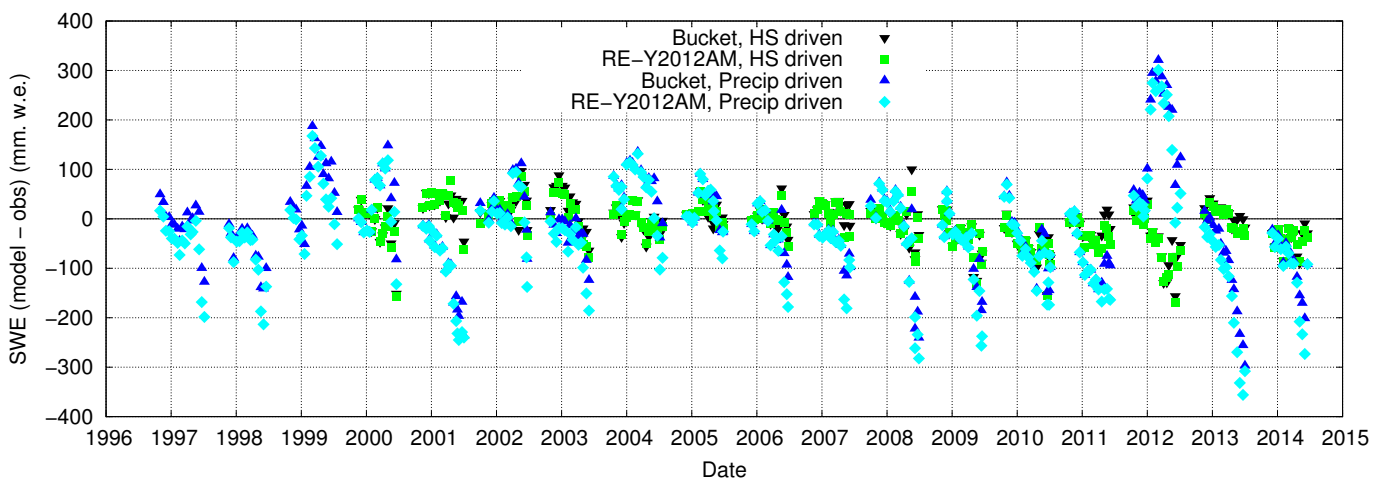
Figure 3.4: Difference in modelled and observed snow water equivalent in the biweekly profiles.

a too quick release of meltwater at the base of the snowpack, or a combination of both. The fact that the discrepancies for the precipitation driven simulations are larger than for the snow height driven ones, is related to the underestimation of snow height during the melt phase. In the snow height driven mode, a too strong decrease in snow height during snowmelt is compensated for by a continuous adding of fresh snow in case the snowfall conditions are met.
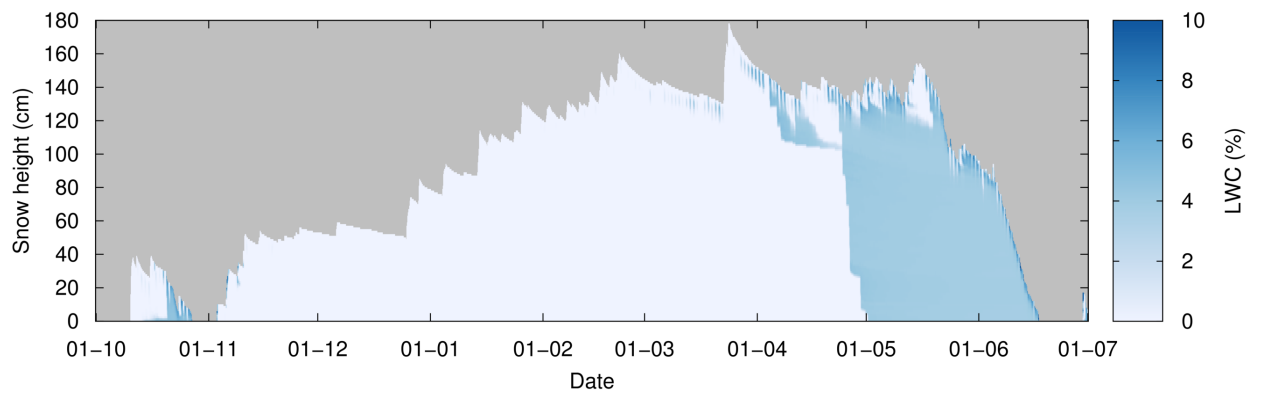
(a)
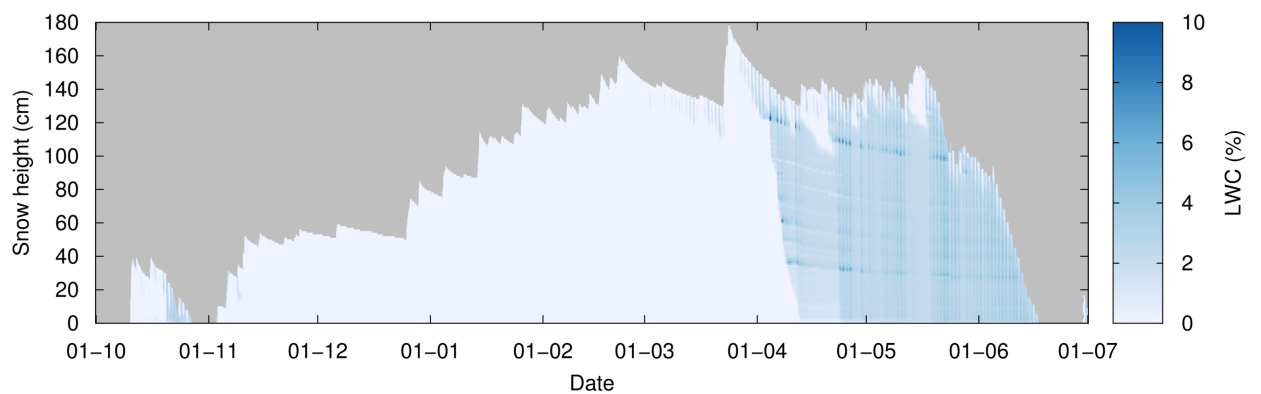
(b)

Figure 3.5: Snow LWC (%) for the snow height driven simulation with the bucket scheme (a) and with RE-Y2012AM (b).

3.4.2 Liquid Water Content and Snowpack Runoff

Figures 3.5a and 3.5b show the distribution of liquid water inside the snowpack for the example snow season for the bucket scheme and RE, respectively. It shows that liquid water is present during the beginning of the snow season and during the melt season, which is a typical pattern for WFJ. The simulations with RE show a quicker downward routing of meltwater from the surface, where the meltwater is produced, than the simulations with the bucket scheme. Furthermore, the latter provides a rather homogeneous LWC distribution throughout the snowpack, except for the lighter surface elements, where LWC is significantly higher. A daily cycle is not visible, except for layers close to the surface. With RE, there is both a strong

variation in the vertical direction as well as in time. Marked accumulations of liquid water can be seen at transitions between layers with different characteristics. These accumulations peak to around 10% LWC and are occurring during the first wetting of the snowpack and above capillary barriers inside the snowpack. This is also observed in real snowpacks (*Techel and Pielmeier*, 2011) and is thought to be an important factor in wet snow avalanche formation. This effect is particularly present during the first wetting, as later in the melt season, the wet snow metamorphism reduces the contrast between microstructural properties, and the increase in hydraulic conductivity when the snowpack below the capillary barrier gets wet, reduces its working as a barrier. The RE scheme also introduces a strong daily cycle in LWC in the simulations. The results for other snow seasons can be found in the Supplement Figures 3.20, 3.21 and 3.22, and they illustrate that the differences between both water transport schemes found in the example snow season are consistent for other snow seasons as well.

Direct comparison of these model results with measurements is difficult, as continuous, non-destructive observations of LWC are not available. However, snowpack runoff is strongly coupled to the LWC distribution. Snowpack runoff at the measurement site WFJ is typically occurring in the melt season and in some snow seasons during autumn when early snow falls may be alternately followed by short melt episodes or rain on snow events. This is illustrated by the cumulative runoff curves in the Supplement Figures 3.23 and 3.24. Table 3.1 shows the ratio of modelled to measured snowpack runoff. Snowpack runoff from precipitation driven simulations is on average 2% less than observed, whereas snow height driven simulations show about 8-14% more runoff than is observed. From the snow height driven simulations, simulations with RE again have higher runoff sums than the simulations with the bucket scheme. This behaviour is found in most simulated snow seasons, as shown by Figure 3.25 in the Supplement. The overestimation of total runoff in snow height driven simulations is caused by the previously described mechanism where the snow height driven simulations add snow layers in spring when the snow height decrease is overestimated. The approach is inadequate during the melt season, as these new snow layers have low densities compared to the rest of the snowpack and snow settling will quickly reduce the modelled snow height again below the measured one. As the wet snow settling is a little stronger when using RE, this effect is slightly larger for those simulations.

A common measure to quantify the agreement between measured and modelled snowpack runoff is the Nash-Sutcliffe model efficiency (NSE, *Nash and Sutcliffe* (1970)), which is shown in Table 3.1 and Figures 3.26 and 3.27 in the Supplement for completeness. Snowpack runoff is discussed in detail in *Wever et al.* (2014). NSE coefficients increase for simulations with RE, especially on the 1 hour time scale, as well as the r^2 value. The NSE coefficients and r^2 values tend to be lower for precipitation driven simulations than for snow height driven ones, especially in the simulations with RE. This likely is a result of a more accurate prediction of travel time of liquid water through the snowpack in snow height driven simulations. This is also indicated by the difference in time lag correlation (see Table 3.1) between precipitation driven simulations and snow height driven ones. The best timing of snowpack runoff on the hourly time scale is achieved with snow height driven simulations with RE.

3.4.3 Soil Temperatures

At WJF, soil temperatures are available at three depths, but only for the last snow season in this study (see Figure 3.6a). The simulated soil temperatures are satisfactory simulated, although the soil never showed temperatures well below 0 °C. However, it is primarily important in this study that the soil as modelled by SNOWPACK serves as an adequate lower boundary condition for the snowpack simulations. For this purpose, we can examine the soil temperature in the topmost soil part at the snow-soil interface, which is available for the snow seasons 2000-2014 (see Figure 3.6b). For most of the time when a snow cover is present, the interface temperature at the snow-soil interface is close to 0 °C, except in the beginning of the snow season when the snow cover is still shallow. This is common for deep alpine snowpacks due to the isolating effect of thick snow covers and the generally upward directed soil heat flux. The figure shows that the simulations capture the variability in early season soil-snow interface temperature to a high degree in most years.

3.4.4 Snow Temperatures

Figures 3.7a and 3.7b show the temperature distribution inside the snowpack for the example snow season for the bucket scheme and RE, respectively. In the Supplement Figures 3.28, 3.29 and 3.30 the other snow seasons are shown. In every snow season, the snowpack temperature at WFJ is below freezing for an extended period of time and for these periods, no noticeable differences are found between simulations with the bucket scheme or RE. As a result of the differences in liquid water flow depicted in Figures 3.5a and 3.5b, the parts of the snowpack that are isothermal differ significantly. Table 3.1 shows that the r^2 value between the relative part of the snowpack that is isothermal in the observations and the simulations increases from 0.74 to 0.87 when solving liquid water flow with RE.

The temperature distribution of the snowpack is strongly related to the combination of the net energy balance of the snowpack and the snow density. Density influences temperature through the thermal inertia of dense snow layers and through the strong dependence of thermal conductivity on density. Errors in either the energy balance or snow density may result in errors in snow temperature. For this reason, the cold content of the snowpack can be considered a more robust method to check the energy balance of the snow. Table 3.1 shows that the RMSE in cold content in the snow height driven simulations is highest for the bucket scheme. The RMSE of around 670 kJ m^{-2} can be considered equivalent to 2 mm w.e. snowmelt. This shows that the estimation of cold content in the simulations is adequate when, for example, estimating the onset of snowmelt and refreezing capacity inside the snowpack. The higher RMSE for precipitation driven simulations can be associated with the higher discrepancy between measured and modelled snow height. The bias in the cold content is small compared to the RMSE, denoting that the average simulated energy input in the snowpack is accurate compared to its temporal variation. This conclusion is only valid for the period when the snowpack temperature is below freezing, as in the melt season, the
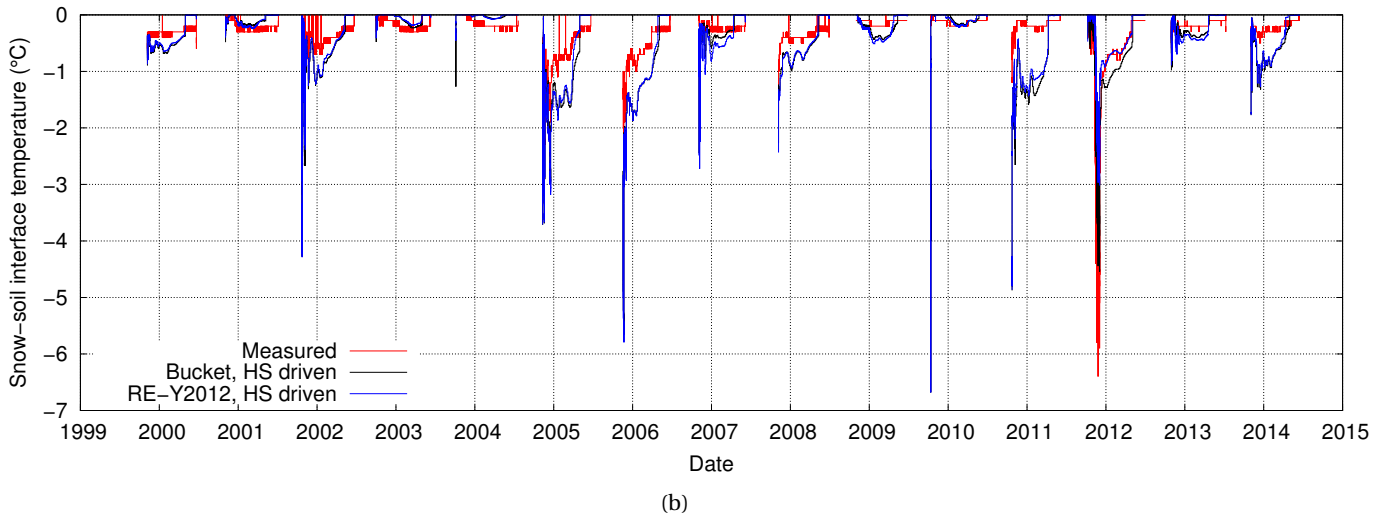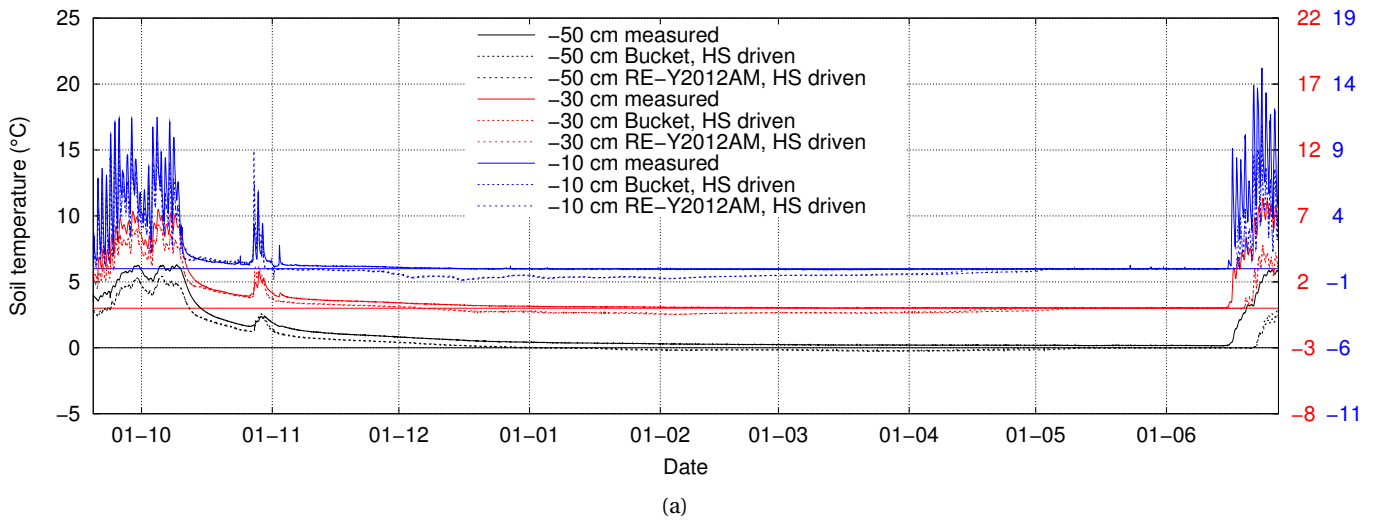
(a)

(b)

Figure 3.6: Measured and modelled soil temperatures at 10, 30 and 50 cm below the surface for the example snow season 2013-2014 (a) and measured and modelled snow-soil interface temperature for snow seasons 2000-2014 (b). Only the snow height driven simulations with the bucket scheme and RE-Y2012AM are shown.

cold content is by definition 0 J m^{-2}. Furthermore, the surface energy balance is normally a self-balancing process, which is disrupted when phase changes occur.

Figure 3.8a shows the measured and modelled snow temperatures at three heights for the example snow season 2014. The change of snow temperatures over the snow season is adequately captured. There is almost no difference between simulations with the bucket scheme or RE, except for the timing when the snowpack gets isothermal, associated with the meltwater front moving through the snowpack. For this example snow season, simulations with RE seem
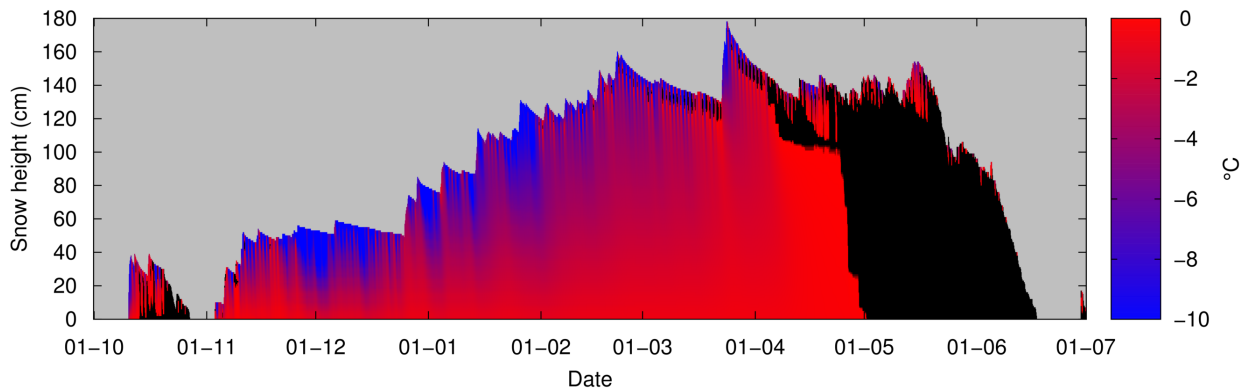
(a)
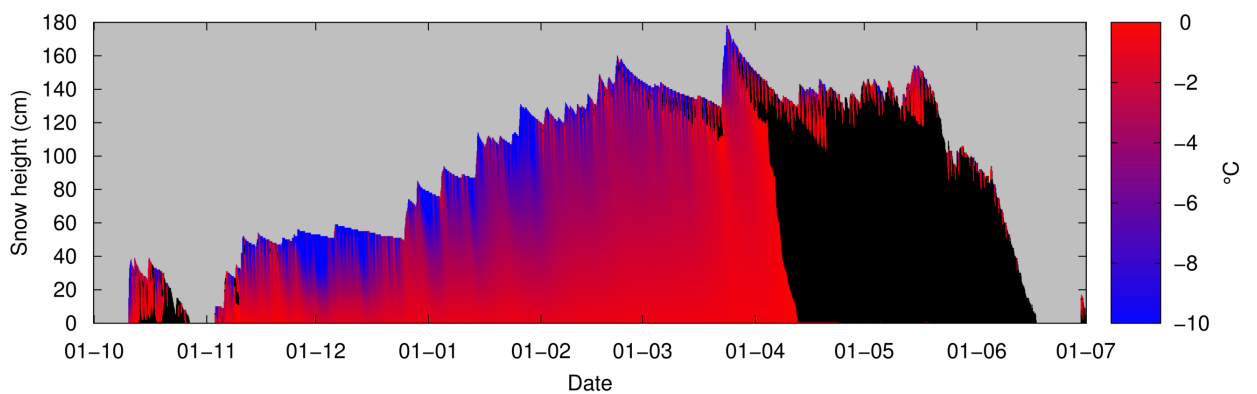
(b)

Figure 3.7: Snow temperature (°C) for the snow height driven simulation with the bucket scheme (a) and with RE-Y2012AM (b). Snow at exactly 0 °C is coloured black to mark areas of the snowpack that are likely melting or wet.

to better capture when the snowpack becomes 0 °C, suggesting a better prediction of the movement of the meltwater front through the snowpack. In the Supplement Figures 3.31 and 3.32, results for each snow season are shown. In most snow seasons, simulations with the RE scheme provide a better agreement with measured temperatures in spring than the bucket scheme. However, in some snow seasons (e.g., 2001 and 2011), simulations with RE show an increase in snow temperature before the measured temperature increases, which suggest a too fast simulated progress of the meltwater front. This will be investigated later in detail using the upGPR data.

(a)
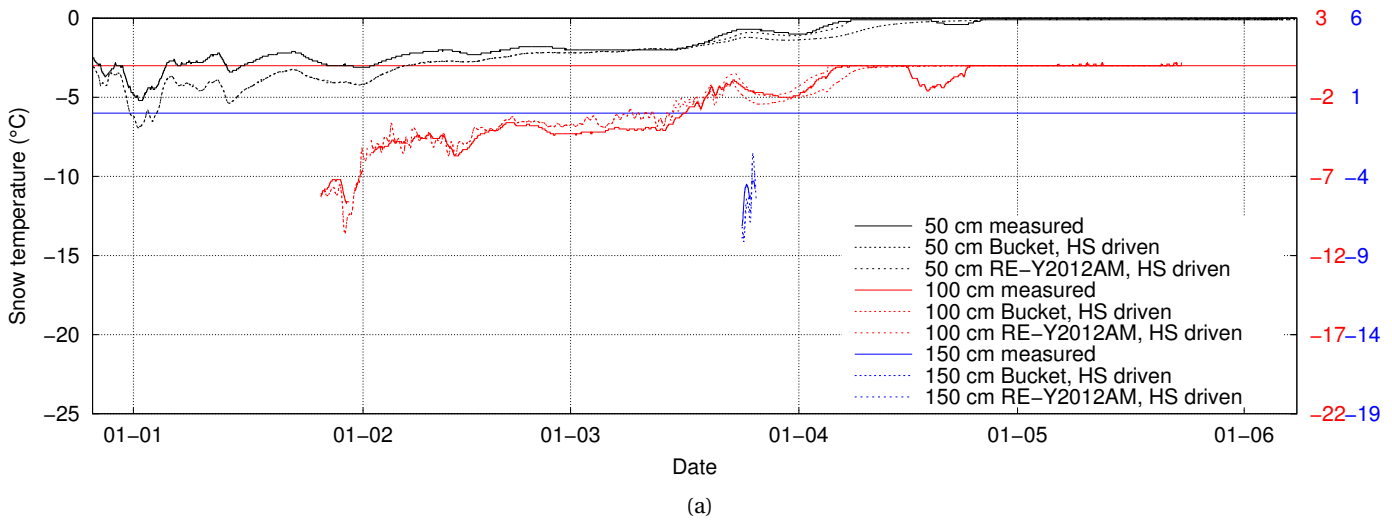
Figure 3.8: Measured and modelled snow temperatures at 50, 100 and 150 cm above the surface for snow height driven simulations for the example snow season 2014. Only the simulations with the bucket scheme and RE-Y2012AM are shown. Values are only plotted when the snow height was at least 20 cm more than the height of the temperature sensor.

In Figure 3.9a and 3.9b, the average and standard deviation, respectively, of the difference between modelled and measured temperatures are shown, determined over all 15 snow seasons of the snow height driven simulations, plotted as a function of the relative date in the snow season. During the main winter season, the temperatures at 50 and 100 cm height are on average up to 0.5 °C lower in the model than in the measurements, whereas the temperature at 150 cm is on average up to 1.0 °C too high in the simulations. Interestingly the snow surface temperature is generally underestimated, whereas the highest snow temperature sensor is too warm. This suggests that the snow layers near the top of the snowpack have a too low density in the simulations. This results in a higher isolation of the snowpack, causing heat from inside to escape at a slower rate, allowing the surface to cool more.

The standard deviation of the difference between modelled and measured temperatures shows an increase with height above the ground. This can be attributed to higher temporal variations in temperature in the upper snowpack due to highly variable surface energy fluxes. The standard deviation for the snow and snow-soil interface temperature typically is less than 1.0 °C, and decreases towards the melt season. For the surface temperature, the standard deviation is typically high in the beginning and the end of the snow season. In the beginning of the snow season, lower snow densities, low air temperatures and reduced incoming shortwave radiation allows for a strong radiative cooling of the snow surface, which may be relatively delicate to simulate correctly. In the melt season, discrepancies in the time the snow surface needs to refreeze at night may contribute to the increase in standard deviation between modelled and measured surface temperatures.
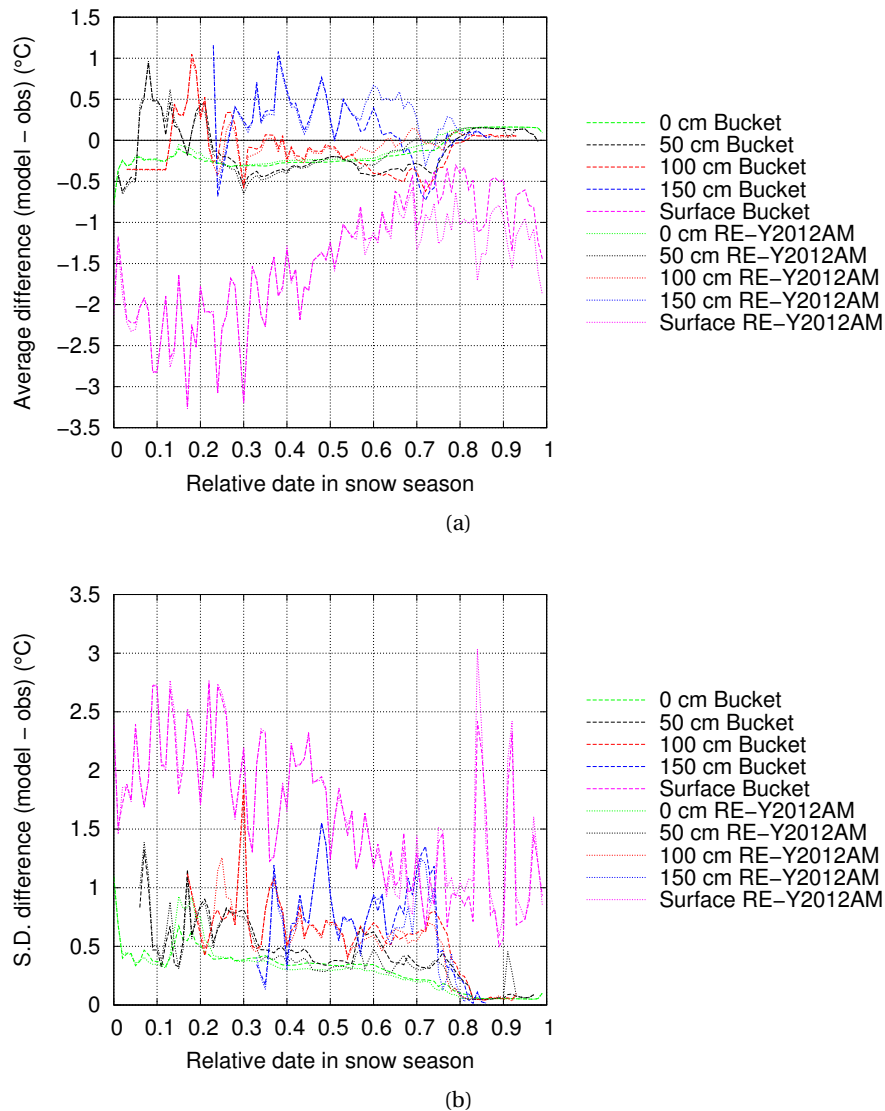
(a)

(b)

Figure 3.9: Average (a) and standard deviation (S.D.) (b) of the difference between modelled and measured snow temperatures, surface temperature and ground temperature (°C) relative to the snow season. For every snow season, the first day with a snow cover is set at 0, the last day at 1. The statistics are determined over the 15 snow seasons with snow height driven simulations.

Figure 3.9a also shows that in the beginning of the melt season, the difference between snow temperatures simulated with RE and measurements is on average smaller than with the bucket scheme at 0, 50 and 100 cm depth, suggesting a better timing of the movement of the meltwater front through the snowpack and the associated temperature increase to 0 °C. The reason why this is not expressed in the temperature series at 150 cm is unclear.
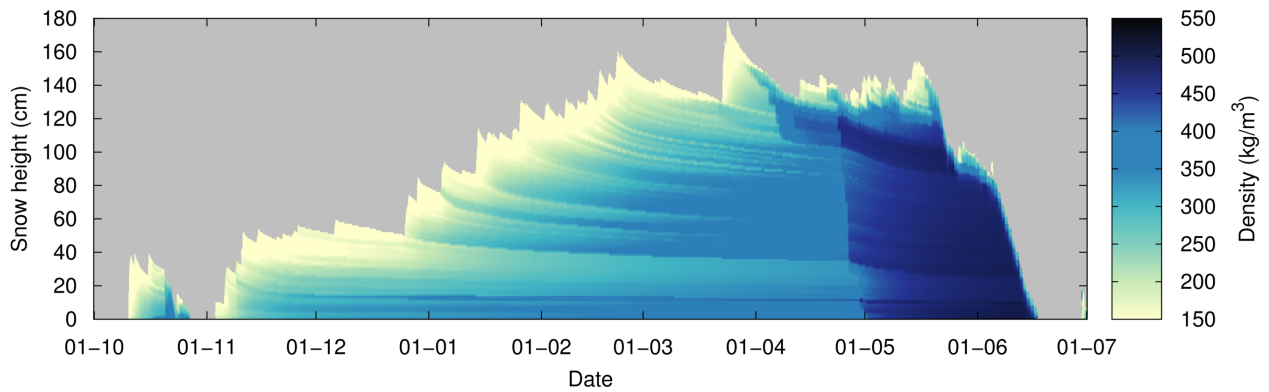
(a)
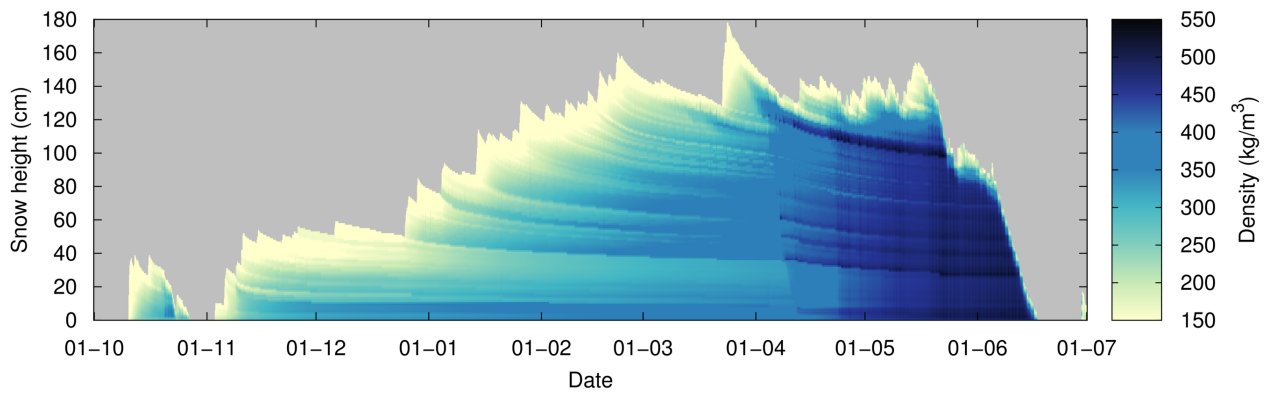
(b)

Figure 3.10: Snow density (kg m^{-3}) for the snow height driven simulation with the bucket scheme (a) and with RE-Y2012AM (b).

3.4.5   Density

Figures 3.10a and 3.10b show snow density profiles for the bucket scheme and RE, respectively, for the example snow season. In Supplement Figures 3.33, 3.34 and 3.35, the other snow seasons are shown. Differences in density mainly arise when liquid water is involved. The accumulation and subsequent partial refreeze of meltwater at some layers form denser parts, whereas other layers remain light because less meltwater is retained. This type of stratification is known to happen, although verification is difficult, because density is sampled at a low spatial resolution in the field.

(a)

(b)
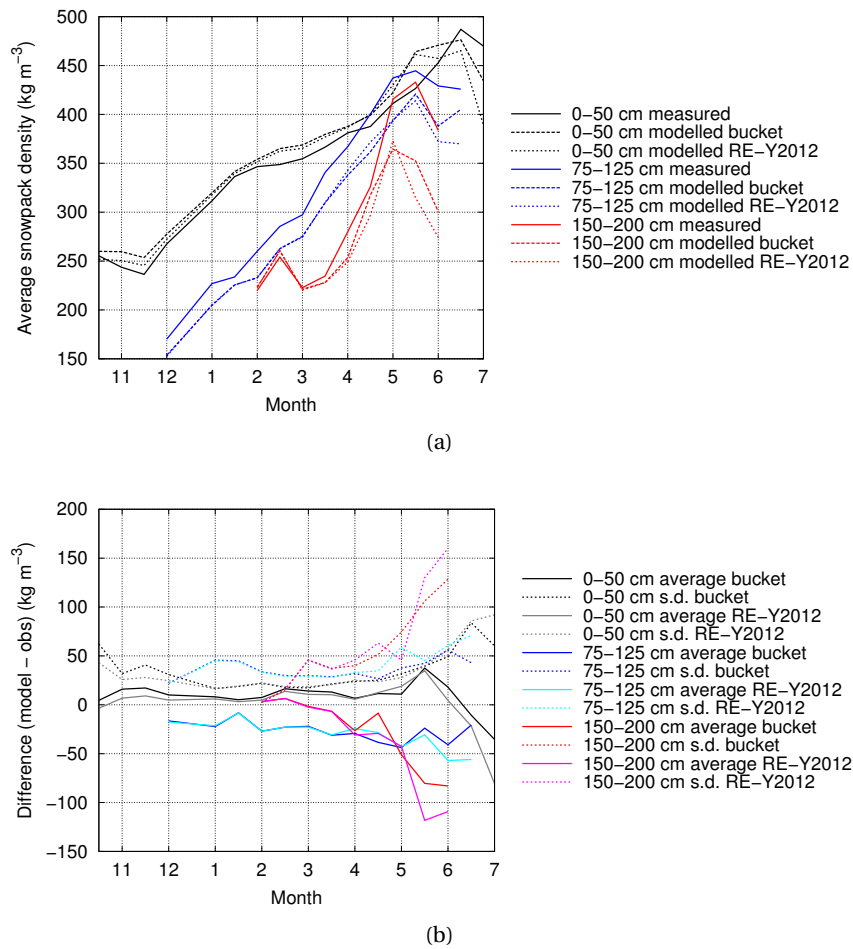
Figure 3.11: Average simulated and measured snow density (kg m^{-3}) (a) and average and standard deviation (s.d.) of the difference between simulated and measured snow density (kg m^{-3}) (b), relative to the snow season for the lower, middle and upper part of the snowpack. For every snow season, the first day with a snow cover is set at 0, the last day at 1. The statistics are determined over the 15 snow seasons with snow height driven simulations.

In Figure 3.11a, average snow density as observed in the manual profiles is compared with the modelled snow densities for the snow height driven simulations for the period 1999-2013. Generally, the seasonal trend in snow density is captured well in the model. Discrepancies between modelled and observed profiles are larger than the differences arising from the different water transport schemes. In general, SNOWPACK overestimates the density near the base of the snow cover, while it underestimates the density of the upper part of the snowpack. This is consistent for all simulated snow seasons, as illustrated in Supplement Figure 3.36. It supports the argumentation in the previous section. These over- and underestimations are larger than the differences between water transport schemes. In Figure 3.11b, the average and standard deviation of the difference between simulated and observed density is shown,

determined over the 15 snow seasons of the snow height driven simulations. Average discrepancies in snow densities are less than 25 kg m^{-3}, increasing to 50-100 kg m^{-3} near the end of the melt season. The standard deviation of the discrepancies is less than 50 kg m^{-3}, increasing to 100-150 kg m^{-3} near the end of the melt season. This illustrates that the new snow density parametrisation and the snow settling formulation is able to provide accurate predictions of snow density, but that the densification process during the melt season, where in the observations higher densities are observed than simulated, is not well understood in terms of the physical descriptions in SNOWPACK.

3.4.6 Snow microstructure

The simulated snow microstructure is analysed first for grain shape, followed by grain size. The modelled grain shape profiles for the example snow season for the bucket scheme (Figure 3.12a and RE (Figure 3.12b) show that differences mainly arise from liquid water flow, as can be seen in the distribution of melt forms and crusts. In Supplement Figures 3.38, 3.39 and 3.40, grain shape profiles can be found for all simulated snow seasons. The effect of liquid water flow on the prevalence of melt forms is consistent when comparing with the distribution of LWC (Supplement Figures 3.20, 3.21 and 3.22). For the main part of the snow season, grain shapes are similar between both simulations. In the melt season, the simulation with RE shows a larger fraction of melt forms in the profile, due to the quicker downward transport of liquid water. Figure 3.13 shows the observed profiles and the profiles for the same date as modelled with either the bucket scheme and RE for all available snow seasons. Both simulations and the observations agree on the general patterns: new snow and precipitation particles are found in the early snow season and in the upper part of the snowpack. After metamorphism taking place, those grains develop in either rounded or faceted crystals. Melt forms mainly show up in spring when liquid water is infiltrating the snowpack. The bucket and RE scheme show little difference, except for the parts of the snowpack that have melt forms. The differences between the water transport schemes are much smaller than the difference with the observations. Another noticeable feature from the observed profiles is the sometimes inconsistent jumping

Table 3.2: Correlation coefficients and (in brackets) t-values between profile average simulated and observed grain size, and relative simulated and observed parts of the snowpack containing the listed grain shape, for various simulation setups.

Grain shape	Bucket	RE-Y2010AM	RE-Y2012AM	RE-Y2012GM	Bucket	RE-Y2012AM
	HS driven (2000-2014)				Precip driven (1997-2014)	
Average grain size	0.75 (17.5)	0.74 (17.0)	0.74 (17.2)	0.74 (17.1)	0.64 (12.9)	0.62 (12.2)
New snow and precip. particles	0.77 (19.1)	0.80 (20.6)	0.80 (20.6)	0.79 (20.3)	0.75 (17.7)	0.74 (17.1)
Rounded grains	0.63 (12.6)	0.61 (12.1)	0.61 (12.2)	0.62 (12.4)	0.59 (11.4)	0.60 (11.5)
Faceted crystals, depth hoar	0.61 (12.0)	0.61 (12.0)	0.60 (11.8)	0.60 (11.7)	0.61 (11.9)	0.59 (11.3)
Melt forms	0.93 (41.2)	0.95 (45.4)	0.95 (45.7)	0.95 (47.0)	0.93 (39.0)	0.93 (40.6)
Ice layers	0.00 (0.0)	0.00 (0.0)	0.00 (0.0)	0.00 (0.0)	0.00 (0.0)	0.00 (0.0)
Crusts	0.63 (12.8)	0.61 (12.2)	0.61 (11.9)	0.63 (12.7)	0.64 (13.0)	0.67 (14.1)

in grain shape between two subsequent profiles. It illustrates the typical subjectivity of the observer to judge the grain shape, which was also found in *Lehning et al.* (2001).

The best agreement is achieved in new snow and precipitation particles and melt forms, as indicated by the high r^2 value for the relative part of the snowpack containing these grain shapes (see Table 3.2). These grain shapes provide the smallest challenges to simulate. The discrepancies between SNOWPACK and observations regarding rounded and faceted crystals are larger, indicated by the lower r^2 value. This discrepancy is also visually present in Figures 3.13. However, SNOWPACK is able to capture some of the year-to-year variability. For example, the simulations capture the abundance of faceted crystals in snow season 2010 and 2011 well, whereas it also captures the presence of rounded grains in the upper half of the snowpack in snow season 2001.

A discrepancy is also found close to the base of the snowpack, where in the SNOWPACK model crusted melt forms prevail, although the observed profiles show either crusted melt forms turning into depth hoar (e.g., snow season 2003), or only depth hoar (e.g., snow season 2010). These melt forms originate from melt episodes in the early snow season and apparently, SNOWPACK is not simulating the transition of these layers into depth hoar, which is observed in the profiles. To resolve this discrepancy, an appropriate heuristic function to describe the transformation from melt forms to depth hoar needs to be developed. Another discrepancy is the absence of ice lenses in the simulations, although they are commonly present in the observed profiles. In some cases, crusts are simulated near ice lenses in the observed profiles. The process of the formation of ice lenses is often considered to be related with the horizontal water movement at capillary barriers (*Techel et al.*, 2011) and it may be that a one-dimensional model approach is not adequate to simulate these processes.

Grain size plays an important role in liquid water flow, as it has a strong influence on the water retention curves (Equations 3.1-3.4). Figures 3.14a and 3.14b show modelled grain size profiles for the example snow season for the bucket scheme and RE, respectively. Differences between the schemes are mainly found in the melt season where the bucket scheme produces slightly larger grains. This is associated with the higher liquid water content in that scheme (Figure 3.5a) compared to RE (Figure 3.5b). This results in a stronger wet snow grain growth rate. Figure 3.14b also illustrates the cause of the liquid water accumulation found near a height of 120 cm in the beginning of April in Figure 3.5b. The layer below the ponding water consisted of significantly larger grains and was creating a capillary barrier for the liquid water. The comparison with the grain microstructure in Figure 3.12b shows that these large grains arose from a melt crust that formed just before the last large snowfall in that snow season. In the Supplement Figures 3.41, 3.42 and 3.43, results are shown for each snow season and a comparison with the LWC distribution (see Supplement Figures 3.20, 3.21 and 3.22) shows that capillary barriers are a typical occurrence in simulations with RE for the deep, non-isothermal, stratified snow cover as found at WFJ.

Figures 3.15a and 3.15b show the average and standard deviation, respectively, of the grain

sizes from the manual profiles and the simulations for the snow seasons 2000-2014. Most distinguishable is the steady increase in grain size towards and in the melt season. Both simulations do show an increase in grain size near the end of the snow season, although the average observed grain size is often underestimated. The underestimation of grain size in simulations with RE compared to the bucket scheme is consistent for most snow seasons and results from lower LWC values in the snowpack and, consequently, lower wet snow grain growth rates. This contributes to a reduced r^2 value for grain size (see Table 3.2). Most of the variation in grain size that exists before the wetting of the snow starts, remains present throughout the snow season in the simulations. However, the vertical variation of grain size typically decreases during the melt season, as shown in Figure 3.15b. Also opposite trends can be found, partly caused by snow falls during the melt season. The simulations tend to provide a decrease of the standard deviation in the melt season and the agreement with the observations varies from year to year. Especially large variations in grain size in the profiles are not captured in the simulations.

(a)

(b)

Precipitation Particles

Decomposing and fragmented
precipitation particles

Rounded grains

Faceted crystals

Depth hoar

Surface hoar
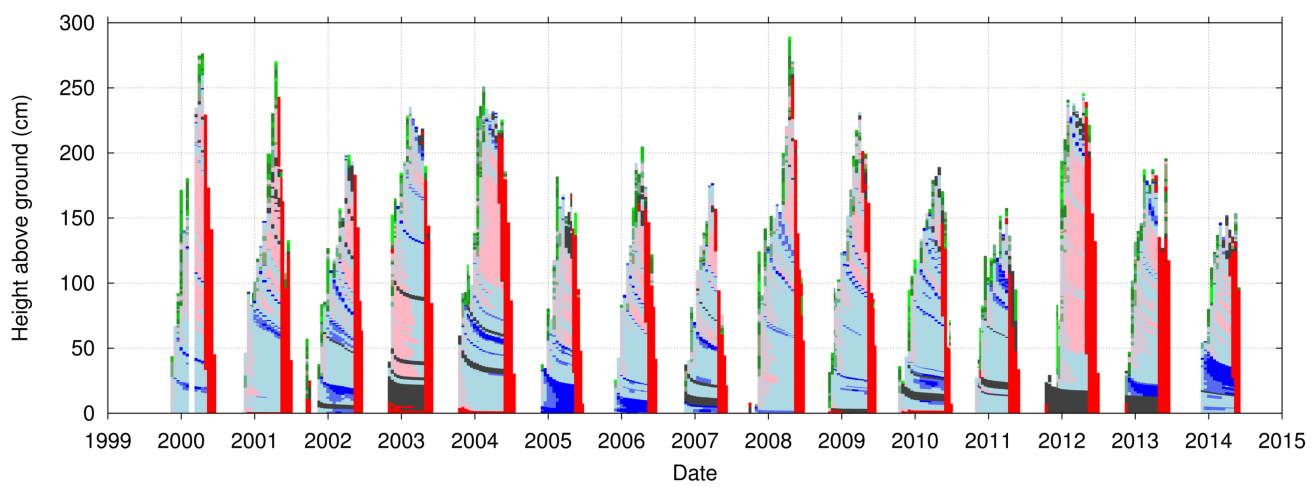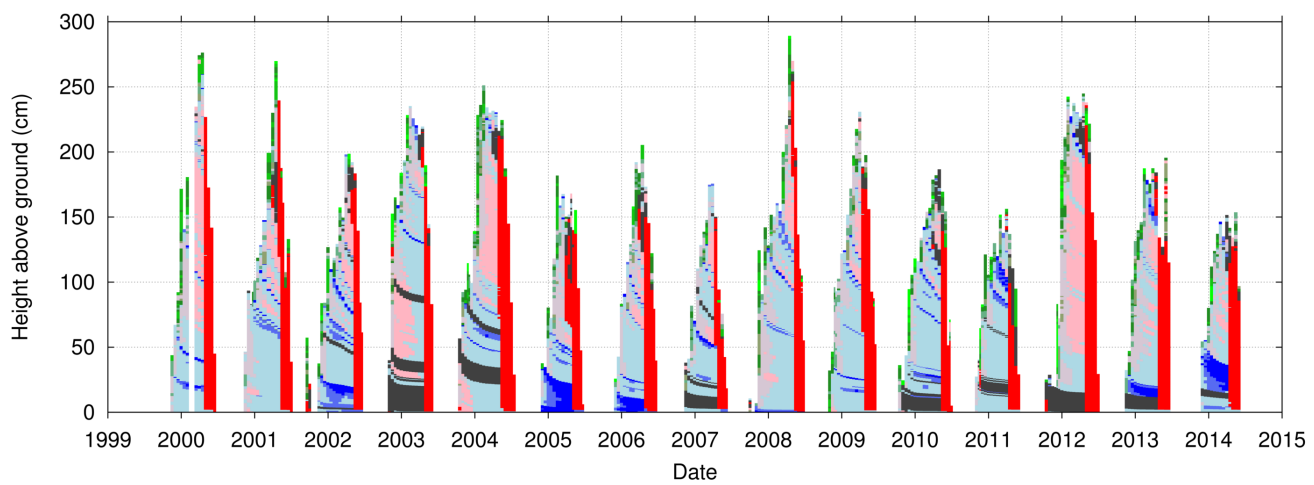
Melt forms
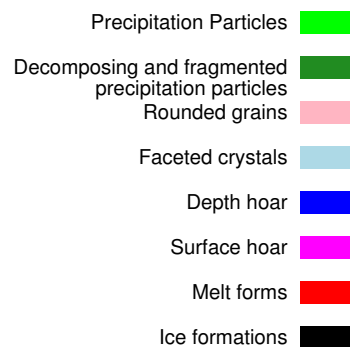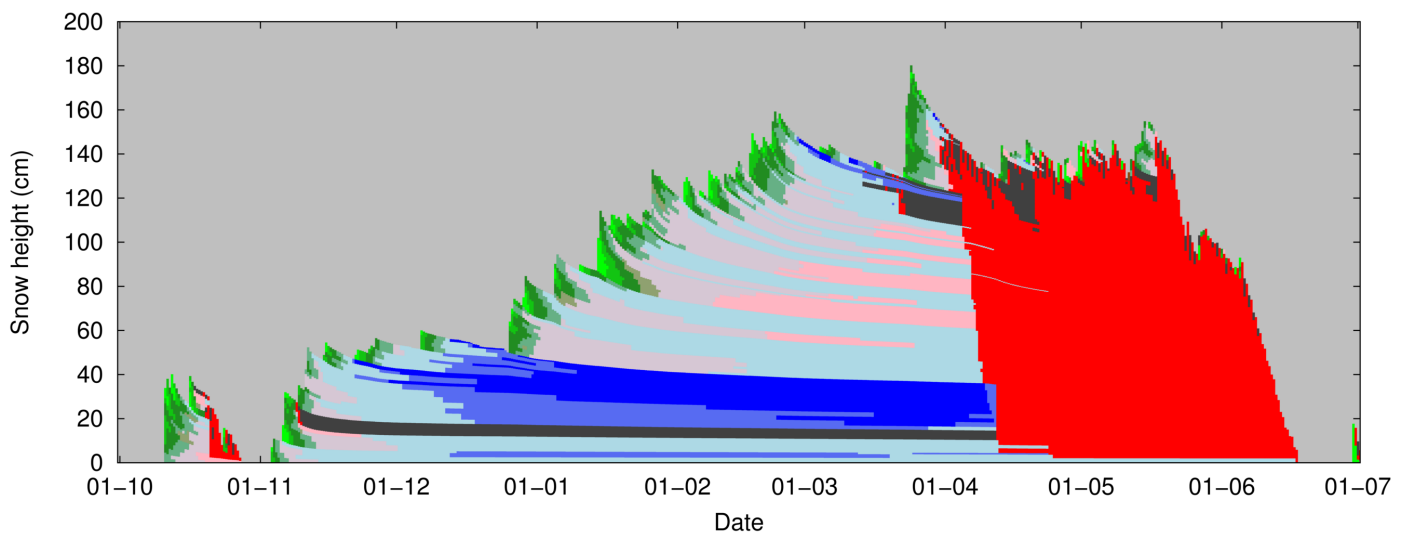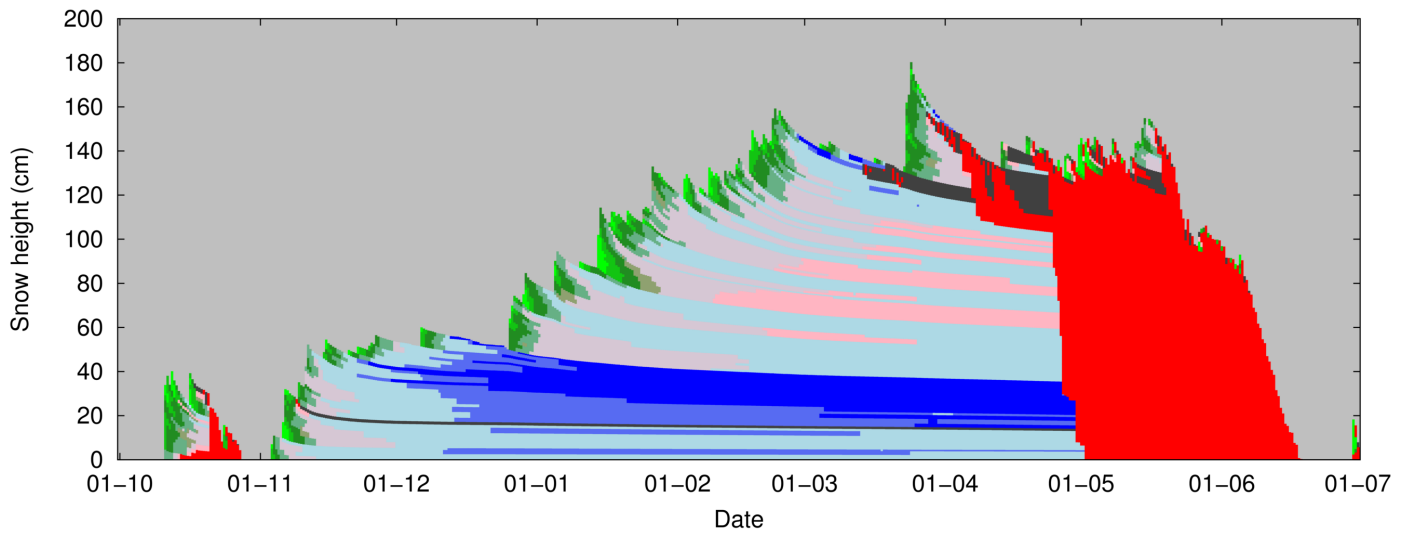
Ice formations

(c)

Figure 3.12: Grain shapes for the snow height driven simulation with the bucket scheme (a) and with RE-Y2012AM (b) for the example snow season 2014. Crusts and ice lenses are summarized as *Ice formations*.
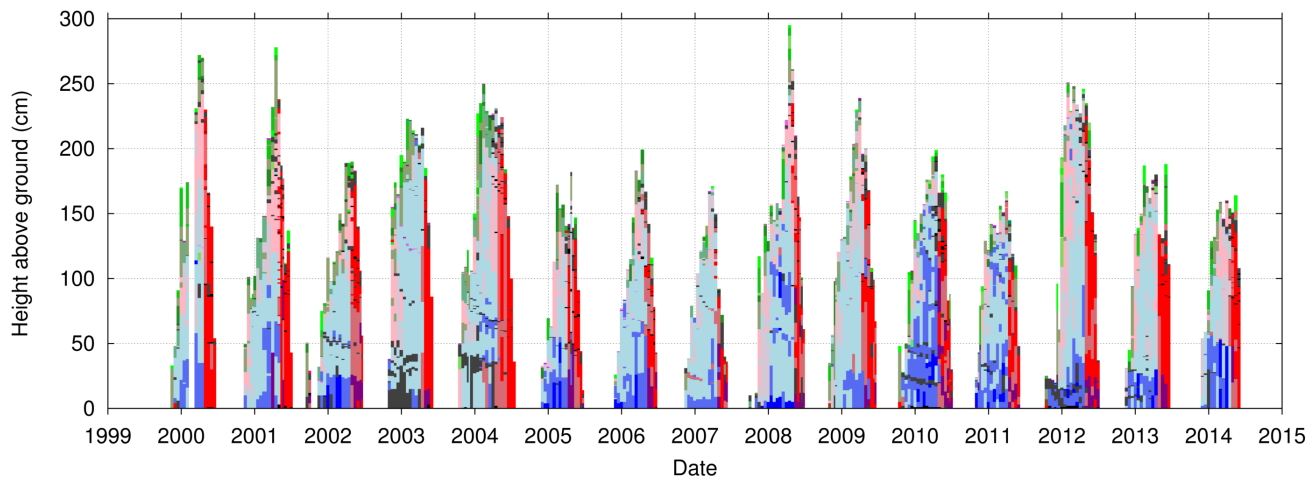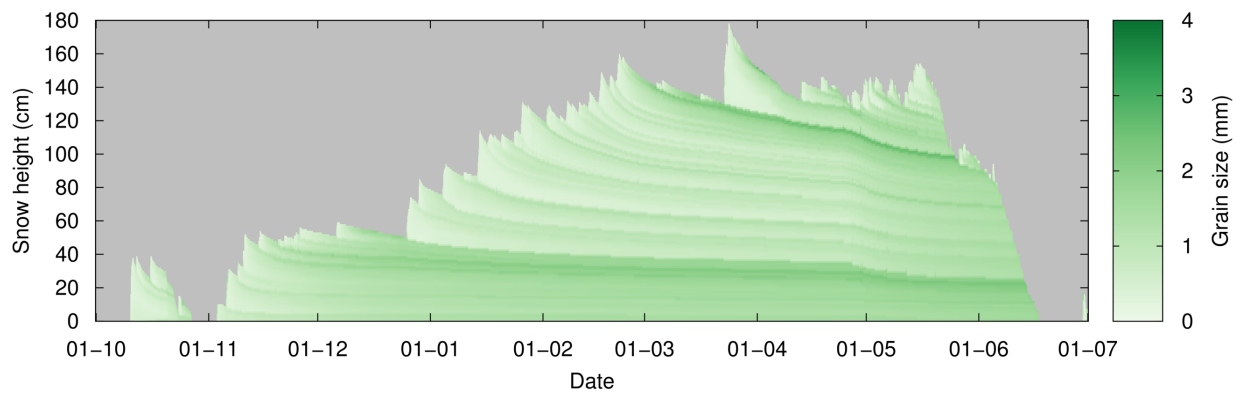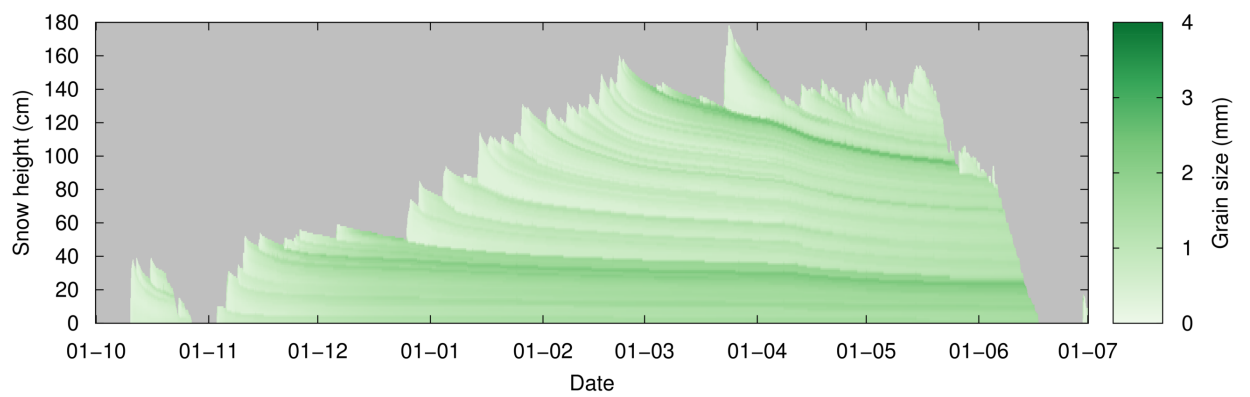
Figure 3.13: Grain shapes in the observed profiles (a), snow height driven simulations with the bucket scheme (b) and RE-Y2012AM (c). A legend is provided in Figure 3.12.
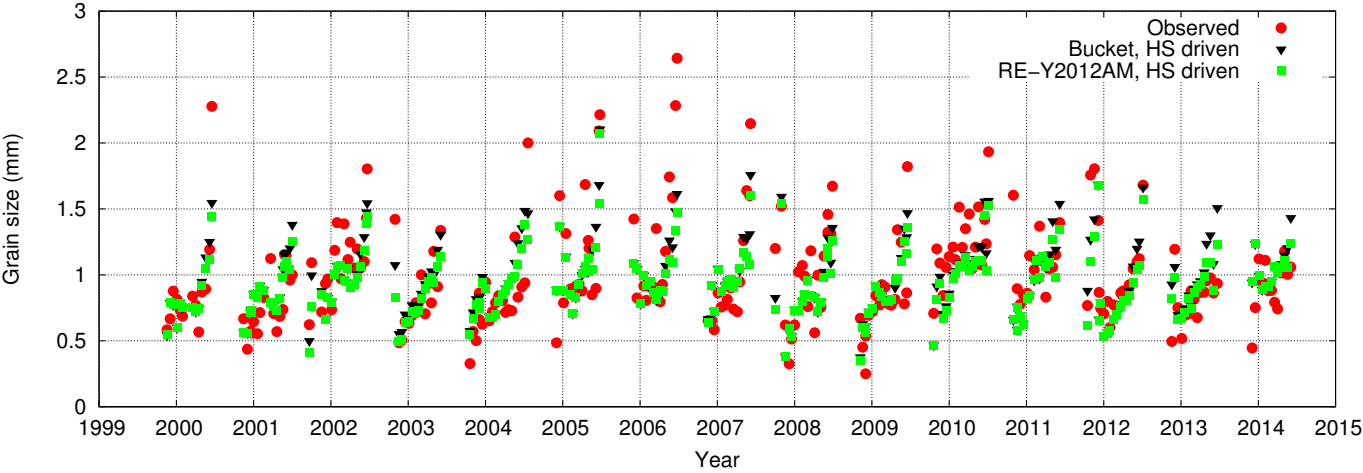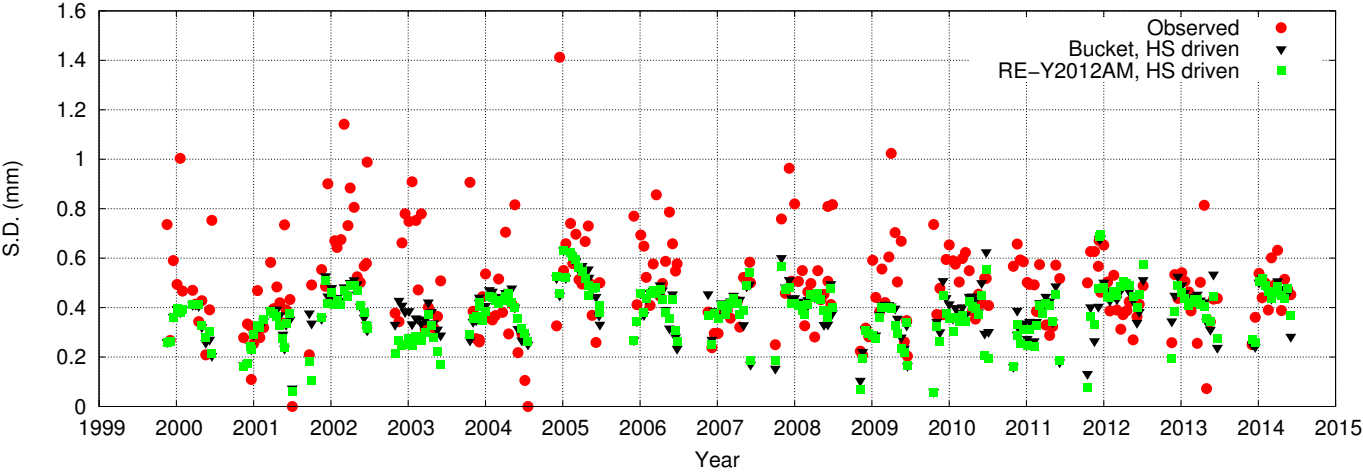
72

(a)

(b)

Figure 3.14: Grain size for the snow height driven simulation with the bucket scheme (a) and with RE-Y2012AM (b) for the example snow season 2014.

(a)

(b)

Figure 3.15: Average (a) and standard deviation (S.D.) (b) of observed and modelled grain size (mm).
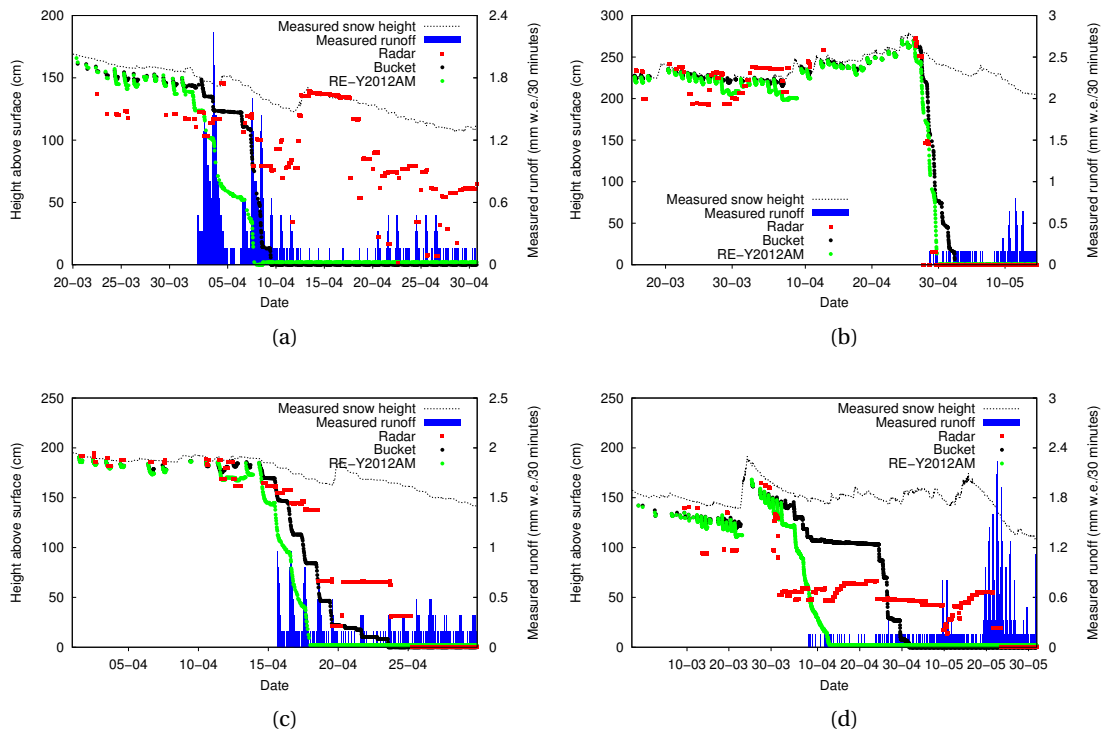
Figure 3.16: Snow height (dashed line) and the position of the meltwater front as detected from the upGPR data (red dots), modelled with the bucket scheme (black dots) and RE-Y2012AM (green dots) for snow season 2011 (a), 2012 (b), 2013 (c) and 2014 (d). Measured snowpack runoff is denoted by blue bars. The simulations were snow height driven. (Data kindly provided by Lino Schmid.)

3.4.7 Radar

For the four snow seasons 2011-2014, a more in-depth comparison of the water transport schemes is possible by analysing the upGPR data. From this data, the progress of the meltwater front through the snowpack can be determined (*Schmid et al.*, 2014). Figure 3.16 compares the position of the meltwater front determined from the upGPR data with the simulations using the bucket scheme and RE for the four snow seasons. When the meltwater front reaches the bottom of the snowpack, snowpack runoff can be expected. For this reason, snowpack runoff is also plotted in these figures. The wetting front is only plotted when the radar signal indicated that parts of the snowpack were wet, or when the snowpack in the simulations was partly wet. When a preferential flow path forms just above the radar, they could potentially be detected. The scatter observed in snow season 2011 may be attributed to this. In that season, the progress of the meltwater front as detected by the radar was also interrupted by a short cooler period with fresh snow. The detected meltwater front jumps back to the surface, whereas in the simulations the snowpack below the fresh snow remains wet. Here, it likely
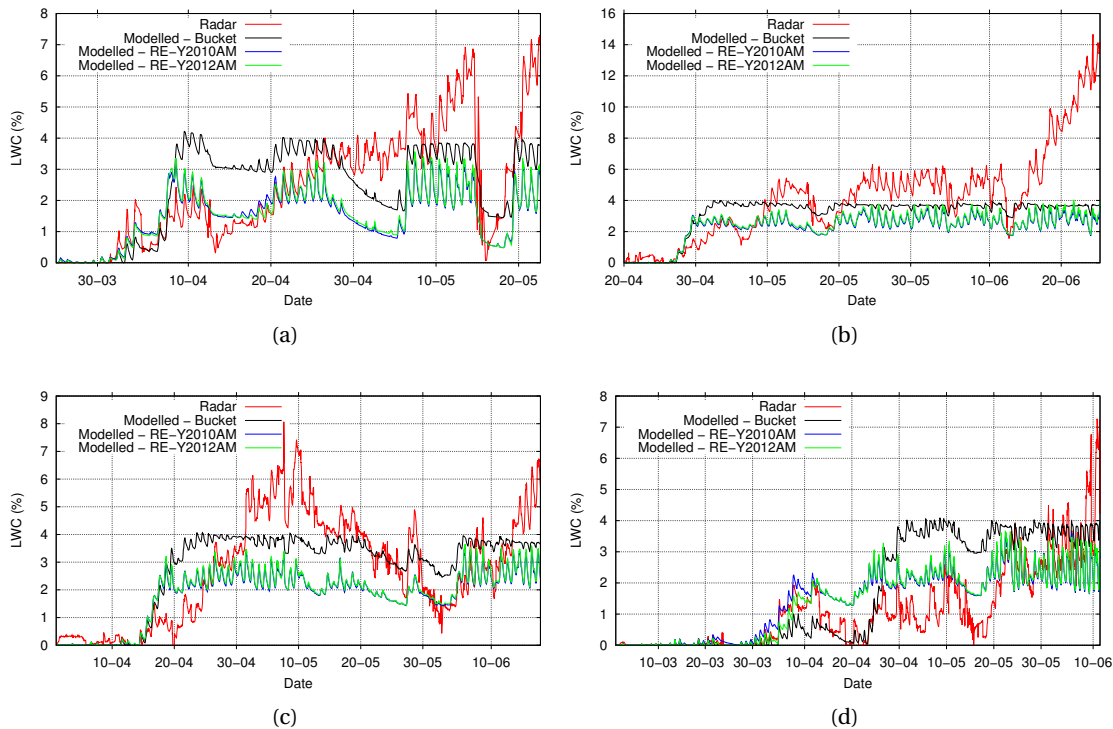
Figure 3.17: Total LWC (%) of the snowpack as determined from the upGPR data (red), modelled with the bucket scheme (black), RE-Y2010AM (blue), and RE-Y2012AM (green) for snow season 2011 (a), 2012 (b), 2013 (c) and 2014 (d). The simulations were snow height driven. (Data kindly provided by Achim Heilig.)

plays a role that changes in LWC are required for analysing the radar signal. These are likely to have been absent when the new snow was covering the old snowpack.

It is noticeable that the consistency between the position of the observed meltwater front and the onset of measured snowpack runoff is very limited. An exception is snow season 2012, for which the results are consistent to a high degree. The progress of the meltwater front through the snowpack is accurately modelled by RE, and only slightly less accurate by the bucket scheme for this snow season. The snow lysimeter measurements show runoff almost directly at the time the meltwater front as detected from the upGPR reaches the soil. It is important to note however, that the progress of the meltwater front is much quicker than in the other snow seasons. Firstly, due to large snow falls in that snow season, the snow stratification was rather homogeneous, limiting the amount of possible capillary barriers or impermeable layers in the snowpack that could hinder the progress of the meltwater front. The relatively homogeneous stratification can also be found in snow density (Supplement Figure 3.35), grain shape (Supplement Figure 3.40) and grain size (Supplement Figure 3.43). Second, the onset of the snowmelt was initiated by a very warm period, leading to sufficient snowmelt to infiltrate

the complete snowpack in a short amount of time. These factors all provide less challenges for the model.

For the other snow seasons, the figures show that there are not only discrepancies between the observations and model results, but also between the observed progress of the meltwater front in the upGPR data and the measured snowpack runoff. In these three snow seasons, snowpack runoff started earlier than the arrival of the meltwater front at the base of the snowpack. This is indicative for the existence of preferential flow paths bringing meltwater down efficiently. The amount of snowpack runoff measured before the arrival of the meltwater front is highly variable. In snow season 2011, high amounts of snowpack runoff were observed, whereas in snow season 2014, only marginal amounts were observed. In that snow season, there is a strong increase observed in snowpack runoff close to the moment of the arrival of the meltwater front at the snowpack base.

When looking at the modelled progress of the meltwater front, simulations with the RE scheme are always simulating a faster progress of the front. In the beginning of the melt season, when the meltwater front is disappearing regularly during night, the depth to which the liquid water infiltrates the snowpack is underestimated with the bucket scheme. The RE scheme does show larger infiltration depths, mostly in agreement with the upGPR data. However, the speed with which the meltwater front finally progresses through the snowpack during the main melt phase is largely overestimated by both the bucket and the RE scheme. However, the presence of measured snowpack runoff would support a faster progress of the meltwater front. The analysis of the upGPR data strongly suggests that the convenient improvement in the accuracy of simulated snowpack runoff with RE is partly caused by (unintentionally) mimicking some preferential flow effects. Whether this is caused by parametrisations of the water retention curve or hydraulic conductivity, or the chosen implementation in SNOWPACK, remains unclear. This was also discussed in *Wever et al.* (2014). However, the bucket scheme may seem to better coincide with the meltwater front in the radar data, it may as well be argued that the differences between both water transport schemes are smaller than the discrepancies with the radar data. It is likely that the limits of one-dimensional models will prevent a correct simulation of both snowpack runoff as the internal snowpack structure at the same time.

Figure 3.17 shows the LWC as determined from the upGPR signal and the different water transport schemes. Visually there is more consistency than with the meltwater front. The start of snowmelt in spring, causing an increase in LWC, seems to well coincide between the radar data and the model. Simulations with the RE-scheme show a clear daily cycle that is in amplitude comparable to the upGPR signal. The bucket scheme exhibits a much smaller amplitude. This difference in model behaviour arises from the fact that once the snowpack is isothermal and wet in the bucket scheme, only refreezing will change the LWC of the snowpack, whereas in the RE scheme, LWC decreases slowly during the evening hours and the night when meltwater production has stopped, due to recession processes. This was also observed in *Wever et al.* (2014). An other difference is that the LWC variations during the melt season are much smaller in both simulations than in the upGPR data. The latter shows peaks up to

$7 - 8\%$. In snow season 2011-2012, the LWC peaks even at 14%, which may be considered rather high compared to typical values reported in literature (*Techel and Pielmeier*, 2011). In the simulations, the maximum LWC decrease slowly in the bucket approach towards the end of the melt season as a result of the snow densification process. In the bucket scheme, water retention is described to decrease with increasing density. In the updated parametrisation of *Yamaguchi et al.* (2012), a higher snow density leads to an increased water retention for the same suction. Therefore, the RE simulations show a slight increase in daily maximum LWC during the melt season. However, the magnitude of these changes is much smaller than observed. The fact that the simulations have lower maximum LWC values than detected by the radar may provide a part of the explanation for the overestimation of SWE depletion rates in the melt season (Figure 3.4).

3.5 Conclusions

The one-dimensional physics based multi-layer SNOWPACK model has been validated against measured time series and manual snow profiles for the measurement site WFJ in the Swiss Alps near Davos. Two water transport schemes, the bucket and RE scheme, were taken into consideration as well as two modes to provide the precipitation forcing for the simulations: snow height driven (15 snow seasons) and precipitation driven (18 snow seasons). Along with the implementation of the solver for RE, the soil module of SNOWPACK has also been updated. Comparing simulated and measured temperatures at the snow-soil interface confirmed that the updated soil module can provide a correct lower boundary for the snowpack simulations.

The snow height driven simulations provide good agreement with measured snow height (RMSE about 4 cm) and, during the accumulation phase of the snow cover, with SWE. This indicates that the model adequately simulates the combination of snow settling and new snow density. For precipitation driven simulations, the SWE in the accumulation phase exhibits a slightly larger spread than in snow height driven simulations, which is mainly caused by deficiencies in the precipitation undercatch correction and possibly snow drift effects. This results in a lower RMSE for snow height (20-23 cm). For the simulations at WFJ, SNOWPACK consistently overestimates the depletion rate of SWE during the spring melt season, resulting in an underestimation of SWE of typically 200 mm w.e. near the end of the snow season, accompanied by an underestimation of snow height up to 30-40 cm. In snow height driven simulations, this is compensated for by simulating regular snowfalls in order to match measured snow height. This procedure has as a drawback that too much mass is added to the snowpack in spring, resulting in an about 8-14% overestimation of cumulative runoff over the snow season, whereas precipitation driven simulations provide on average 2% less snowpack runoff than measured.

The comparison of simulated snow density with snow density measurements made in snow profiles has shown that both the average snow density and the seasonal trend is well simulated in SNOWPACK during the main winter season. Average bias is around 25 kg m^{-3} and the

density of deep snow layers is slightly overestimated, whereas the density of upper layers is slightly underestimated. The discrepancies grow in the melt season, when SNOWPACK underestimates snow density on average up to 100 kg m^{-3}. This suggest that the densification in spring, likely under influence of liquid water flow, is not adequately captured by SNOWPACK.

Modelled and measured snow temperatures showed a satisfying agreement with average discrepancies of around 0.5 °C. The discrepancies in the surface temperature were found to be larger, likely associated with the above mentioned underestimation of snow density in the upper layers and consequently the effect on thermal conductivity. The discrepancy in the cold content of the snow cover from simulations and field measurements was found to be small, suggesting that the surface energy balance and the soil heat flux are on average satisfactory estimated. However, this conclusion only holds for the main winter period, as the defined cold content can only be used to assess energy budgets of snow that is below freezing. The average difference between simulated and measured snow temperature in the melt season was smaller in simulations with RE than with the bucket scheme, suggesting a better prediction of the progress of the meltwater front through the snowpack.

The model provides consistent simulations of grain size and shape. Grain size is observed to increase near the end of the snow season due to metamorphism, while the vertical variations decrease. This is also reproduced by the simulations. A comparison between the grain shapes found in the profiles showed that melt forms are best predicted, followed by new snow grains. These clearly provide less challenge to simulate. Simulations with RE showed a slightly increased correlation for melt forms. Larger discrepancies between simulations and observed profiles arise for rounded and faceted crystals, independent of the used water transport scheme. The observed formation of faceted crystals near the bottom of the snowpack is often not captured in the simulations when melt forms from the beginning of the snow season are present.

The temporal evolution and the vertical distribution of the LWC in the snowpack differ significantly between the bucket scheme and RE. The latter provides a faster downward propagation of the meltwater front. A higher correlation coefficient and NSE coefficient between simulated and measured snowpack runoff indicates a better agreement of simulations with RE than the bucket scheme. RE also provides a higher r^2 value for the isothermal part of the snowpack compared to the manual snow profiles, suggesting a better simulation of the progress of the meltwater front through the snowpack. A comparison with the upGPR measurements has shown that larger depths to which meltwater infiltrates the snowpack in the early melt phase as simulated with RE is confirmed in some snow seasons. The final progress of the meltwater front in the upGPR measurements turns out to be slower than simulated with either the bucket scheme or RE. Here, it should be noted that the detected position of the meltwater front in the upGPR and the measured onset of snowpack runoff is inconsistent as well, likely associated with the existence of preferential flow paths. The high agreement between simulations with RE and snowpack runoff suggests that RE is accidentally mimicking preferential flow effects. The bucket scheme seems to have a higher agreement with the meltwater front in the radar

data, but differences between both schemes are relatively small. The results suggest that the ability of a one-dimensional approach to correctly estimate both snowpack runoff as well as the internal snowpack structure in wet snow conditions is rather limited. As the simulation of ponding of liquid water on capillary barriers and crusts is only captured with RE and not with the bucket scheme, RE seems promising however for the ability of SNOWPACK to assess wet snow avalanche risks.

The validation has shown that SNOWPACK has sufficient agreement with measurements for snow temperatures, snow density, grain size and shape in the main winter season for a wide range of applications. However, the above mentioned discrepancy in the depletion rates of SWE in spring deserves attention in future model development. The depletion rate is the result of many interacting processes. First of all, it is strongly coupled to snowmelt, and thus dependent on the surface energy fluxes. Given the high agreement in cold content in the main winter season, errors in diagnosing the surface energy balance due to uncertainties in atmospheric stability and measurement errors in radiation, wind speed or air temperature, seems to be small on average. We would argue that the insufficient simulation of the densification during spring is more important here. A too low snow density will result in a deeper penetration of shortwave radiation, effectively providing heat to the snowpack. Furthermore, heat conductivity will be underestimated, and it may be that the simulated snowpack in spring is therefore too isolated to be able to release heat during night. Finally, the simulations seem to retain less liquid water than is observed in the upGPR data. This suggest a too fast release of meltwater by the snowpack, which may contribute to overestimating SWE depletion rates.

The analyses show that the differences in temperature profiles, snow density and grain size and shape between water transport schemes are negligible when the snowpack is dry. This shows that the implementation of RE as described in *Wever et al.* (2014) is adequate for its purpose of improving liquid water content and snowpack runoff simulations. We found that the Y2012 water retention curve provides better results than the Y2010 parametrisation, whereas different averaging methods to determine the hydraulic conductivity at the nodes seem to have little influence. In general, several aspects of the simulations related to liquid water flow do improve with RE, although often, the differences between simulations tend to be smaller than differences between the simulations and the observations.

Acknowledgements

Supplement

This supplement belongs to:
Verification of the multi-layer SNOWPACK model with different water transport schemes

Authors: Nander Wever[1], Charles Fierz[1], Lino Schmid[1], Achim Heilig[3], Michael Lehning[1,2]

[1] WSL Institute for Snow and Avalanche Research SLF, Davos Dorf, Switzerland.
[2] CRYOS, School of Architecture, Civil and Environmental Engineering, EPFL, Lausanne, Switzerland.
[3] Institute of Environmental Physics, University of Heidelberg, Germany.

(a) 1999-2000

(b) 2000-2001

(c) 2001-2002

(d) 2002-2003

(e) 2003-2004

(f) 2004-2005

(g) 2005-2006

(h) 2006-2007
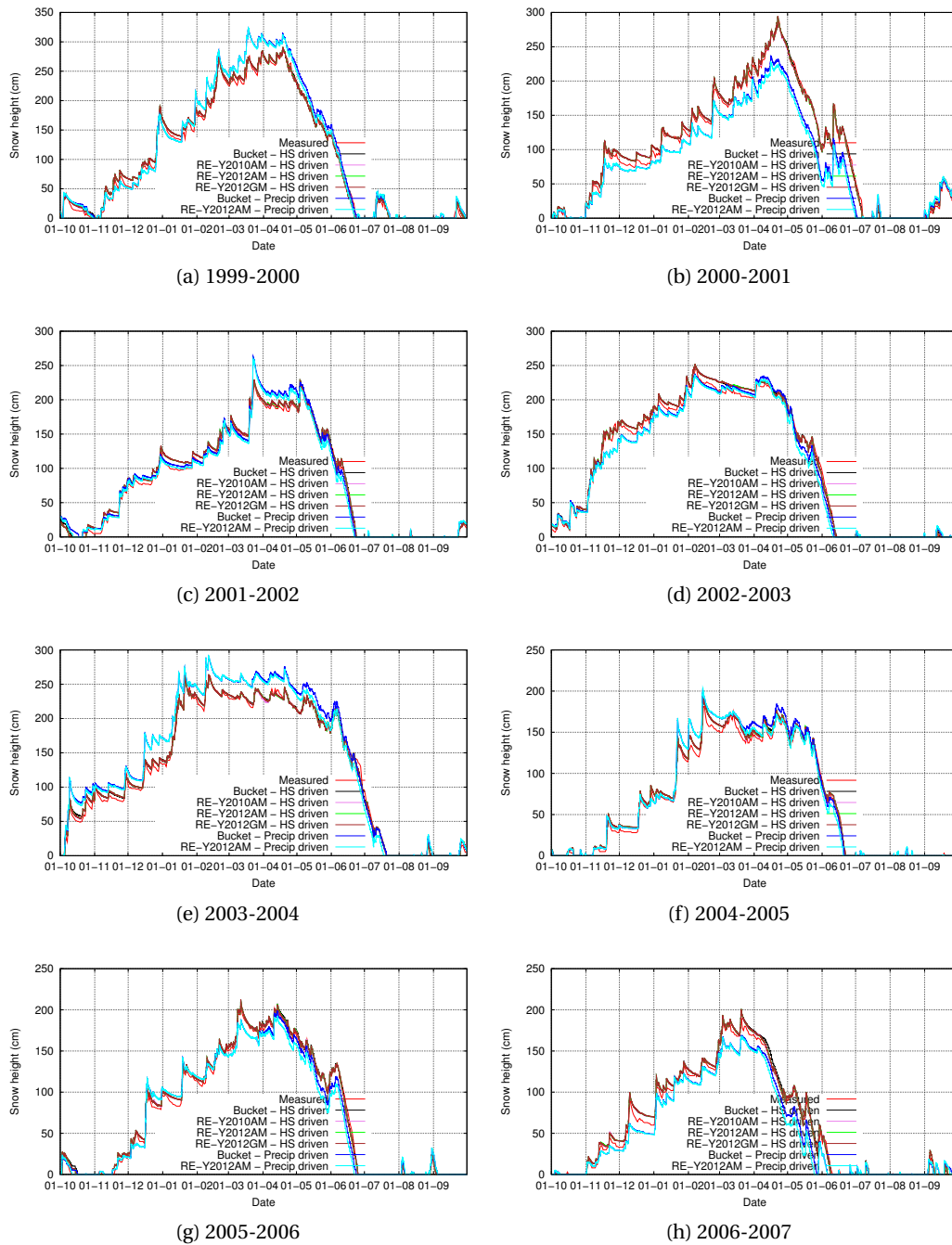
Figure 3.18: Measured and modelled snow height for different model setups.

(a) 2007-2008

(b) 2008-2009

(c) 2009-2010

(d) 2010-2011

(e) 2011-2012

(f) 2012-2013

(g) 2013-2014
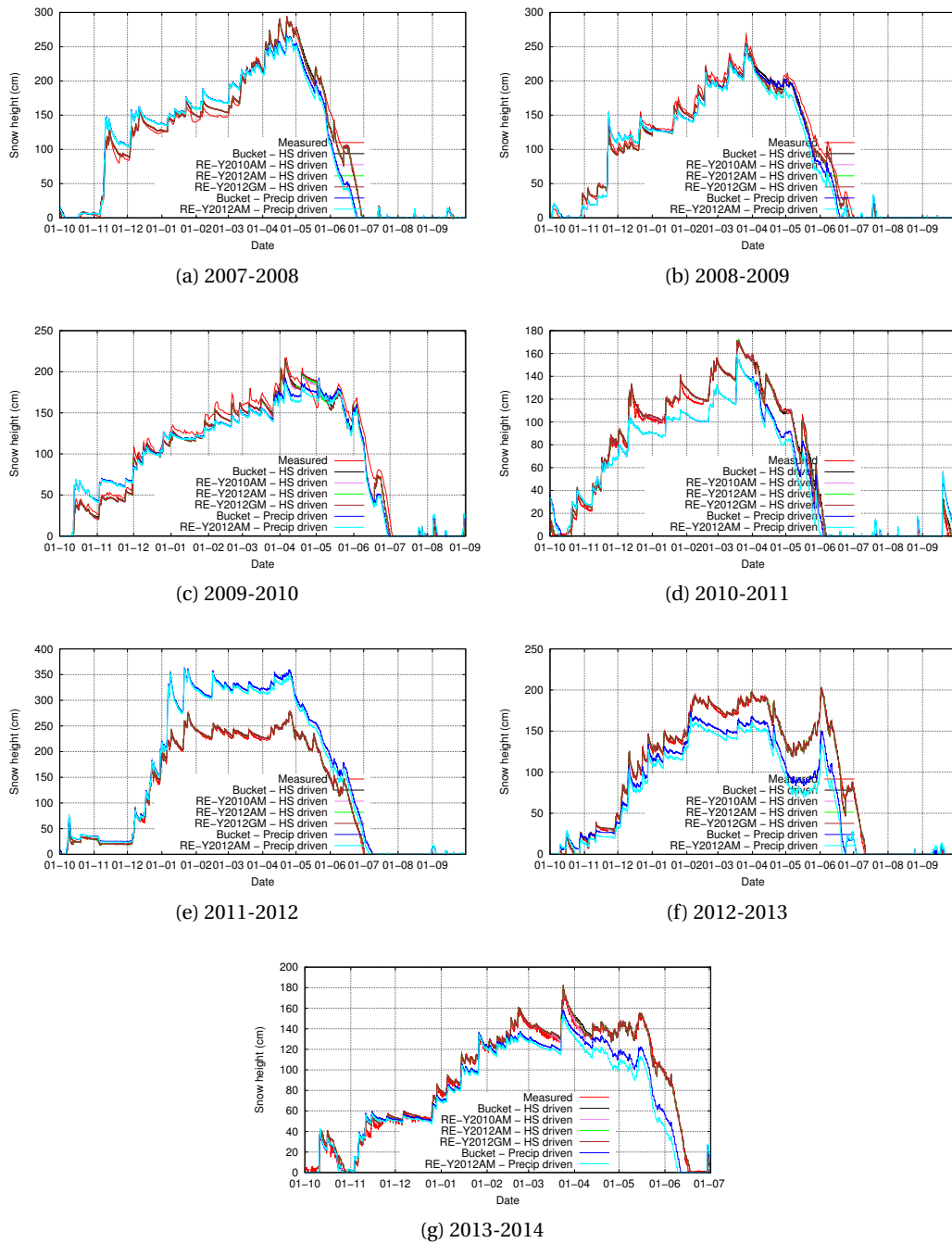
Figure 3.19: Measured and modelled snow height for different model setups, continued.

(a) 1999-2000

(b) 1999-2000

(c) 2000-2001

(d) 2000-2001

(e) 2001-2002

(f) 2001-2002

(g) 2002-2003

(h) 2002-2003

(i) 2003-2004

(j) 2003-2004
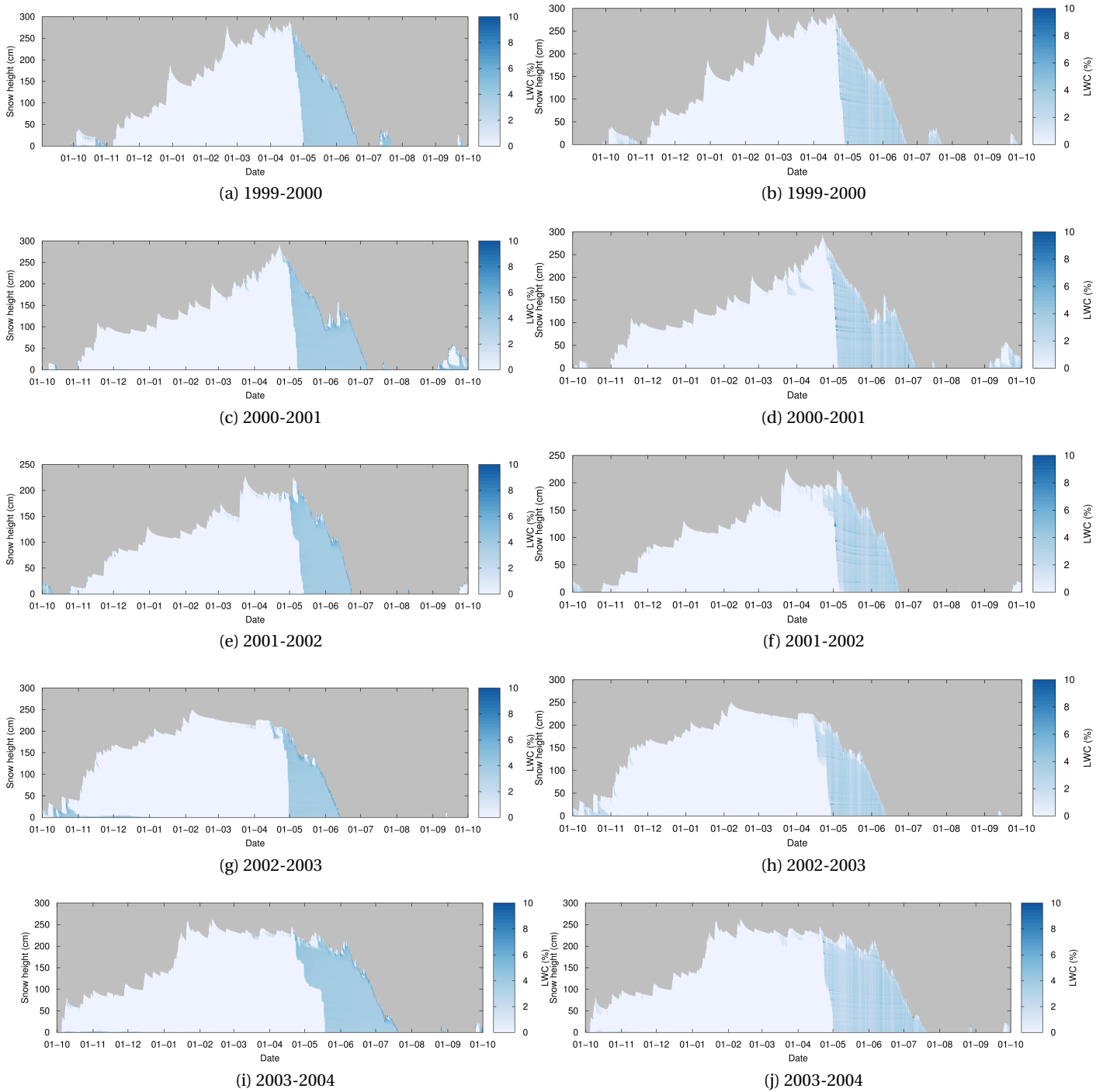
Figure 3.20: LWC (%) for the simulations with the bucket scheme (left), and with RE-Y2012AM (right).

(a) 2004-2005

(b) 2004-2005

(c) 2005-2006

(d) 2005-2006

(e) 2006-2007

(f) 2006-2007

(g) 2007-2008

(h) 2007-2008

(i) 2008-2009

(j) 2008-2009
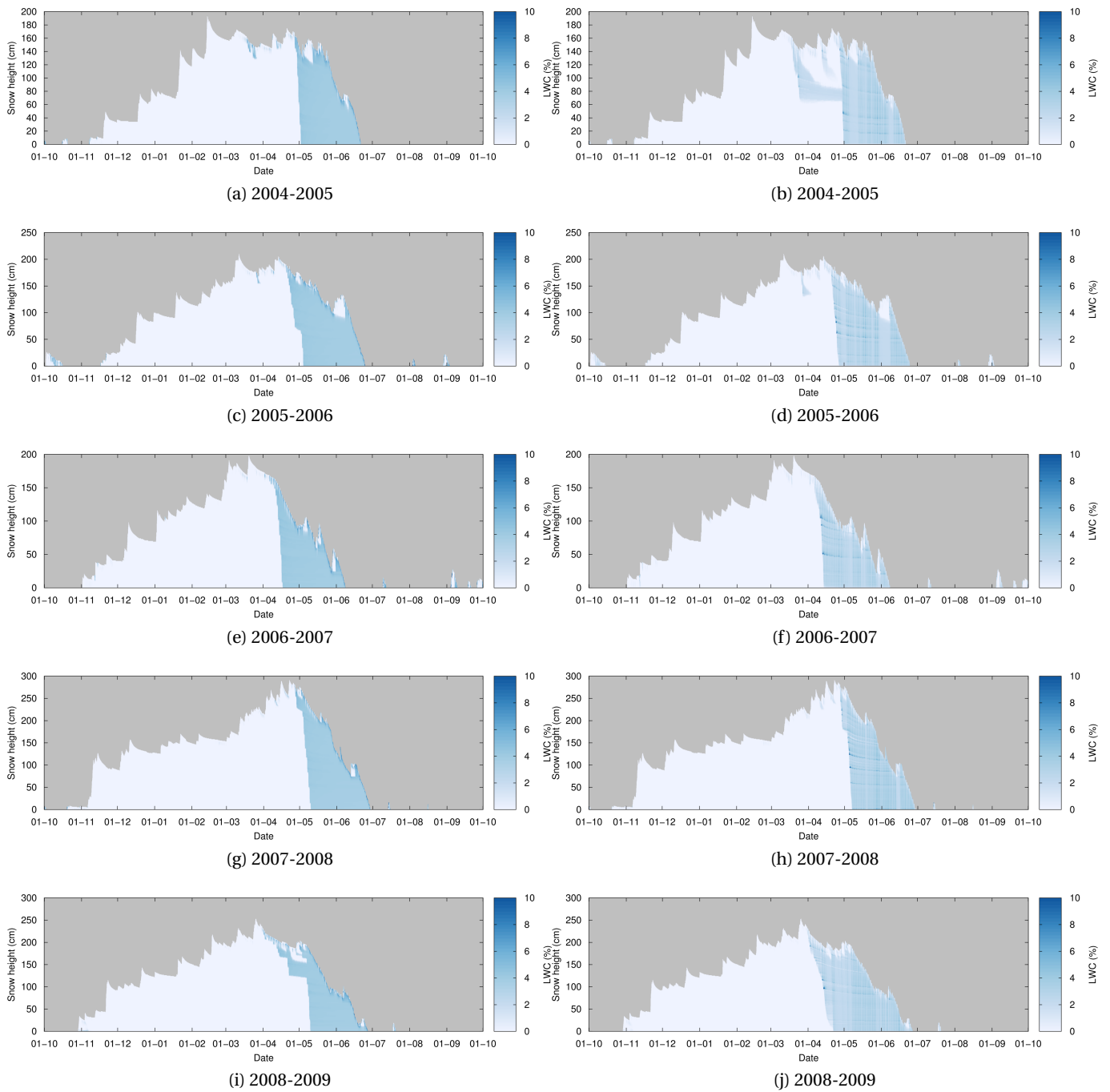
Figure 3.21: LWC (%) for the simulations with the bucket scheme (left), and with RE-Y2012AM (right), continued.

(a) 2009-2010

(b) 2009-2010

(c) 2010-2011

(d) 2010-2011

(e) 2011-2012

(f) 2011-2012
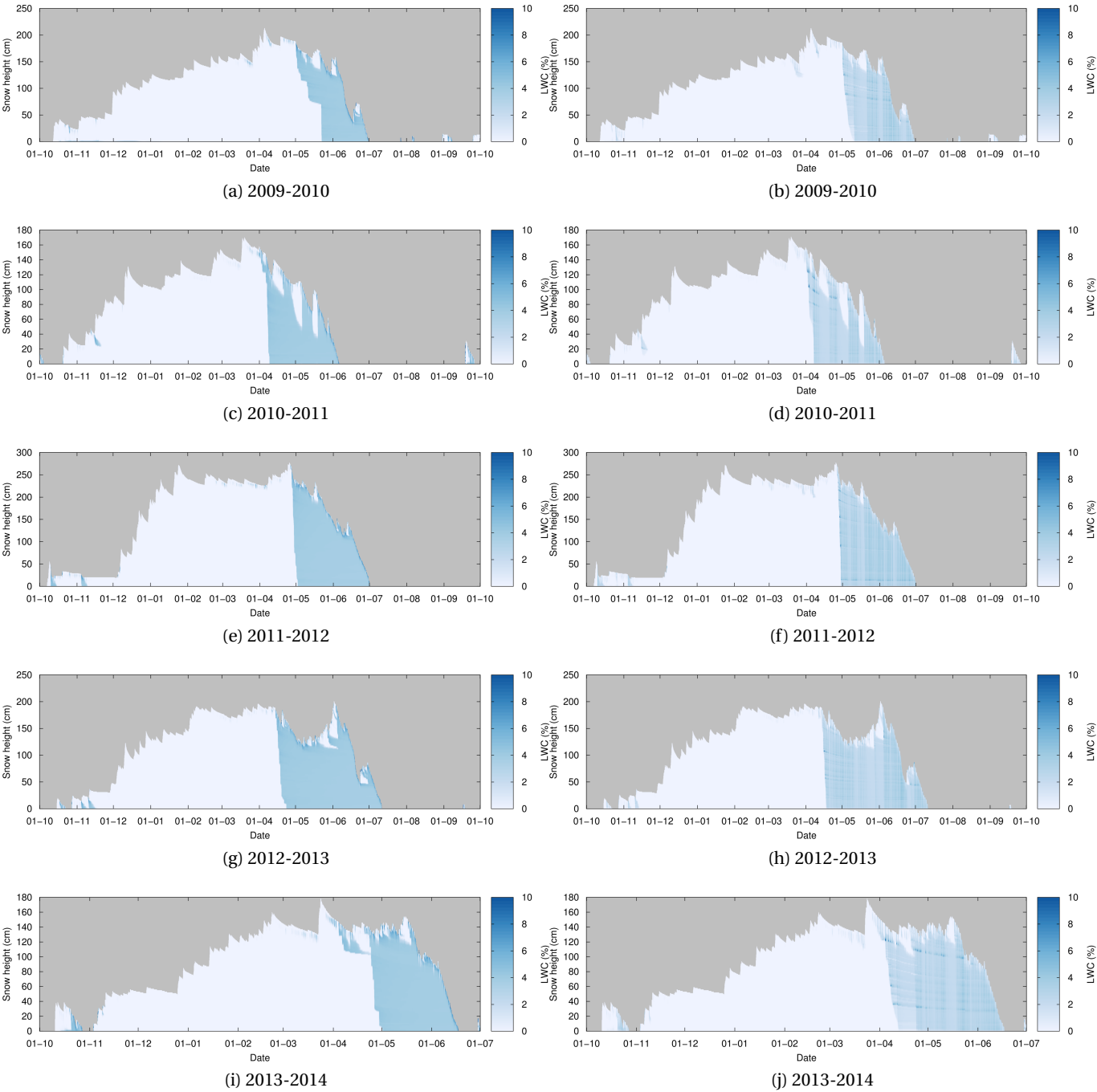
(g) 2012-2013

(h) 2012-2013

(i) 2013-2014

(j) 2013-2014

Figure 3.22: LWC (%) for the simulations with the bucket scheme (left), and with RE-Y2012AM (right), continued.
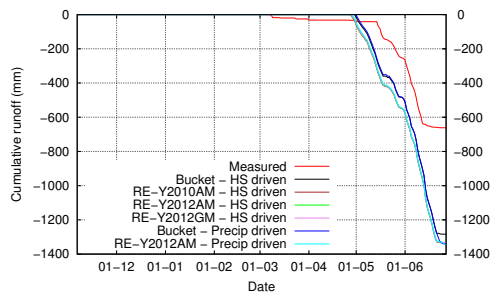
(a) 1999-2000
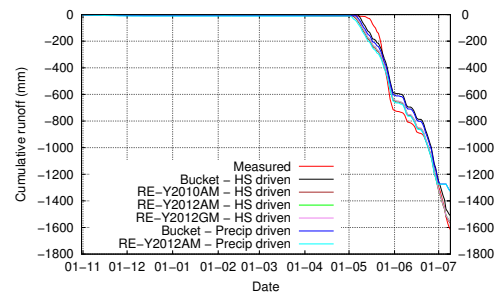
(b) 2000-2001
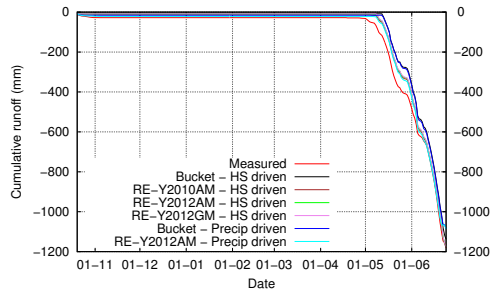
(c) 2001-2002
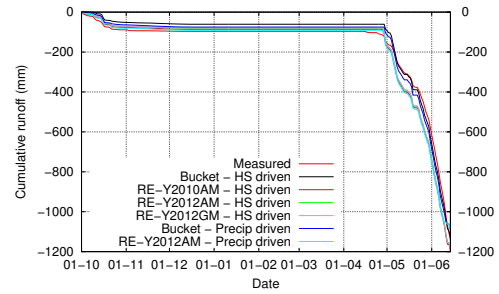
(d) 2002-2003
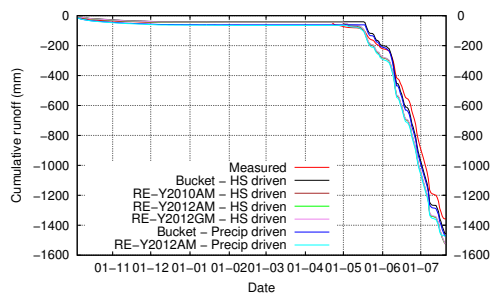
(e) 2003-2004
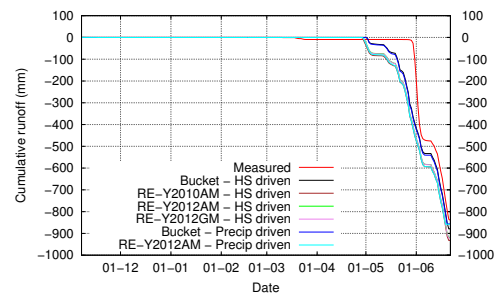
(f) 2004-2005

(g) 2005-2006

(h) 2006-2007

Figure 3.23: Cumulative runoff (mm. w.e.).

(a) 2007-2008

(b) 2008-2009

(c) 2009-2010

(d) 2010-2011

(e) 2011-2012

(f) 2012-2013

(g) 2013-2014
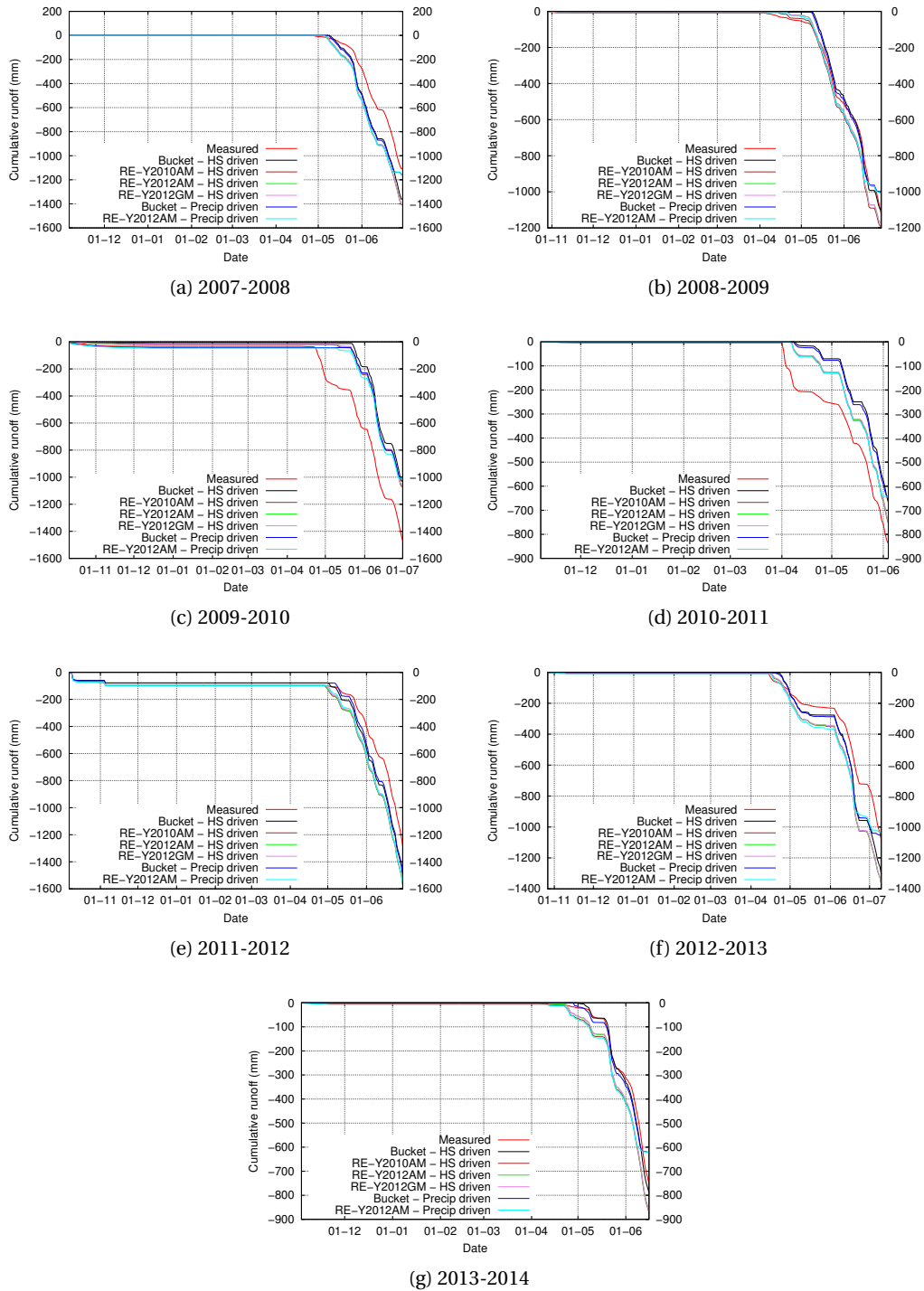
Figure 3.24: Cumulative runoff (mm. w.e.), continued.
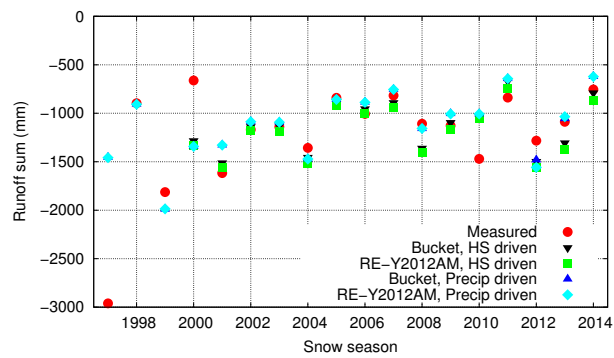
Figure 3.25: Seasonal runoff sums from the perspective of the snowpack mass balance (negative values denote snowpack outflow).
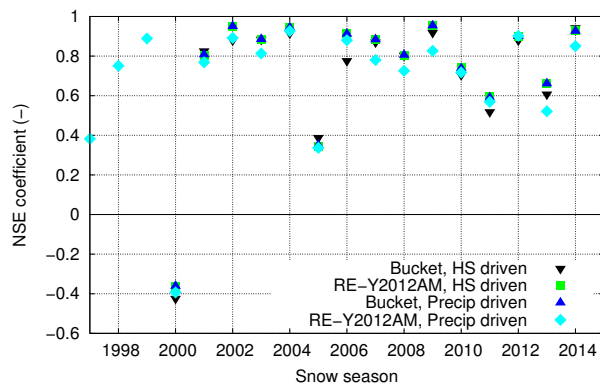
Figure 3.26: Nash-Sutcliffe model efficiency coefficients for daily runoff sums.
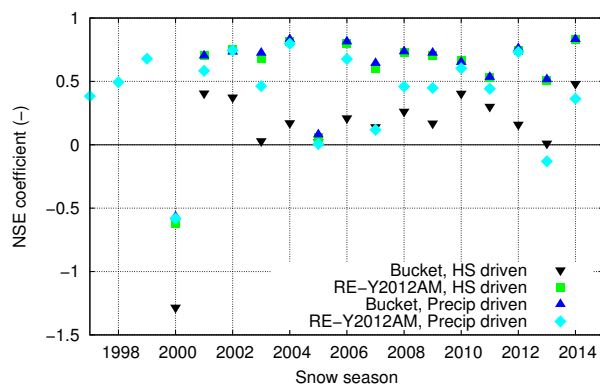
Figure 3.27: Nash-Sutcliffe model efficiency coefficients for hourly runoff sums.

(a) 1999-2000

(b) 1999-2000

(c) 2000-2001

(d) 2000-2001

(e) 2001-2002

(f) 2001-2002

(g) 2002-2003

(h) 2002-2003

(i) 2003-2004

(j) 2003-2004
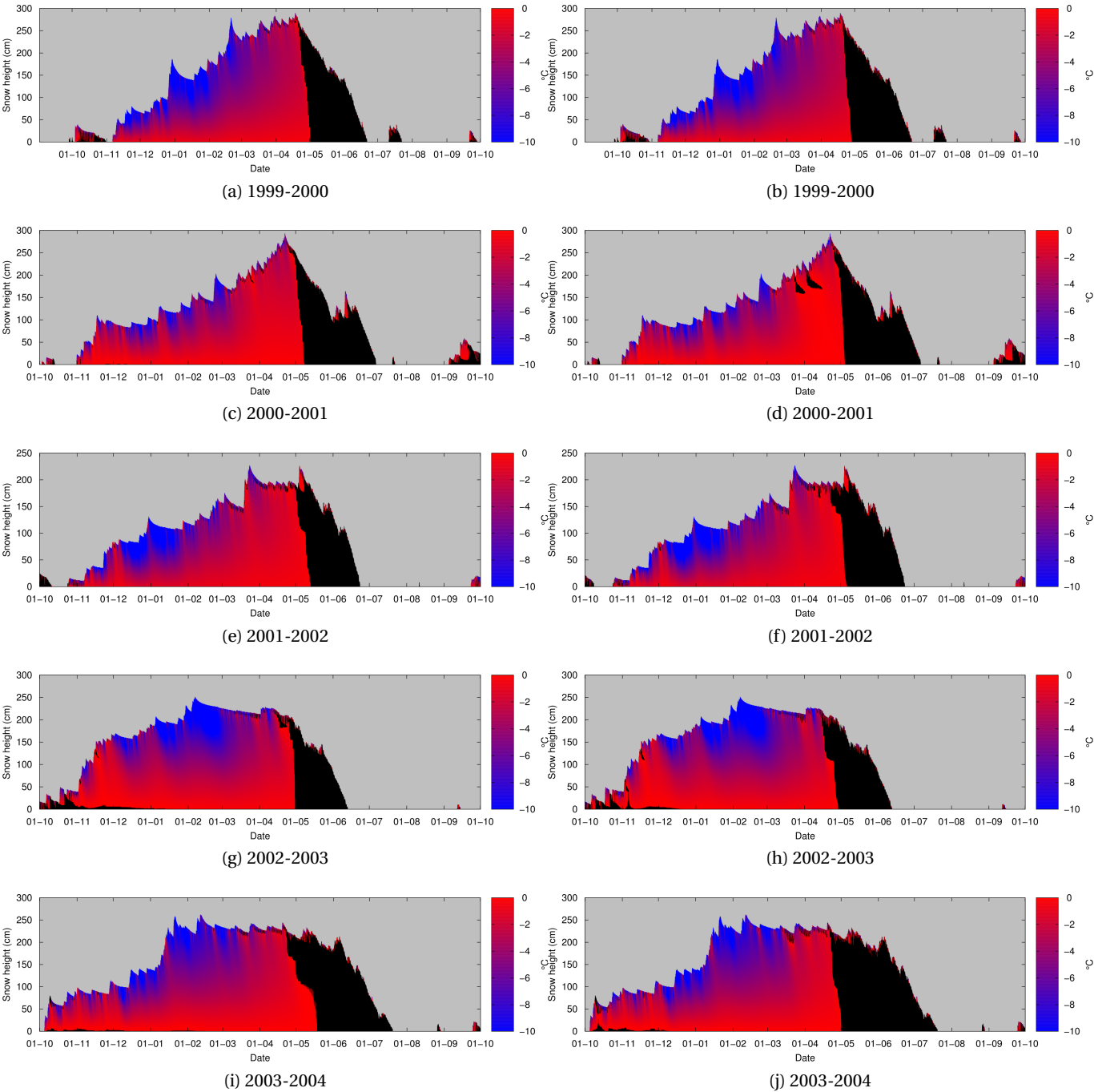
Figure 3.28: Snow temperature (°C) for the simulations with the bucket scheme (left), and with RE-Y2012AM (right). Snow at exactly 0 °C coloured black to mark areas of the snowpack that are melting or wet.

(a) 2004-2005

(b) 2004-2005

(c) 2005-2006

(d) 2005-2006

(e) 2006-2007

(f) 2006-2007

(g) 2007-2008

(h) 2007-2008

(i) 2008-2009

(j) 2008-2009
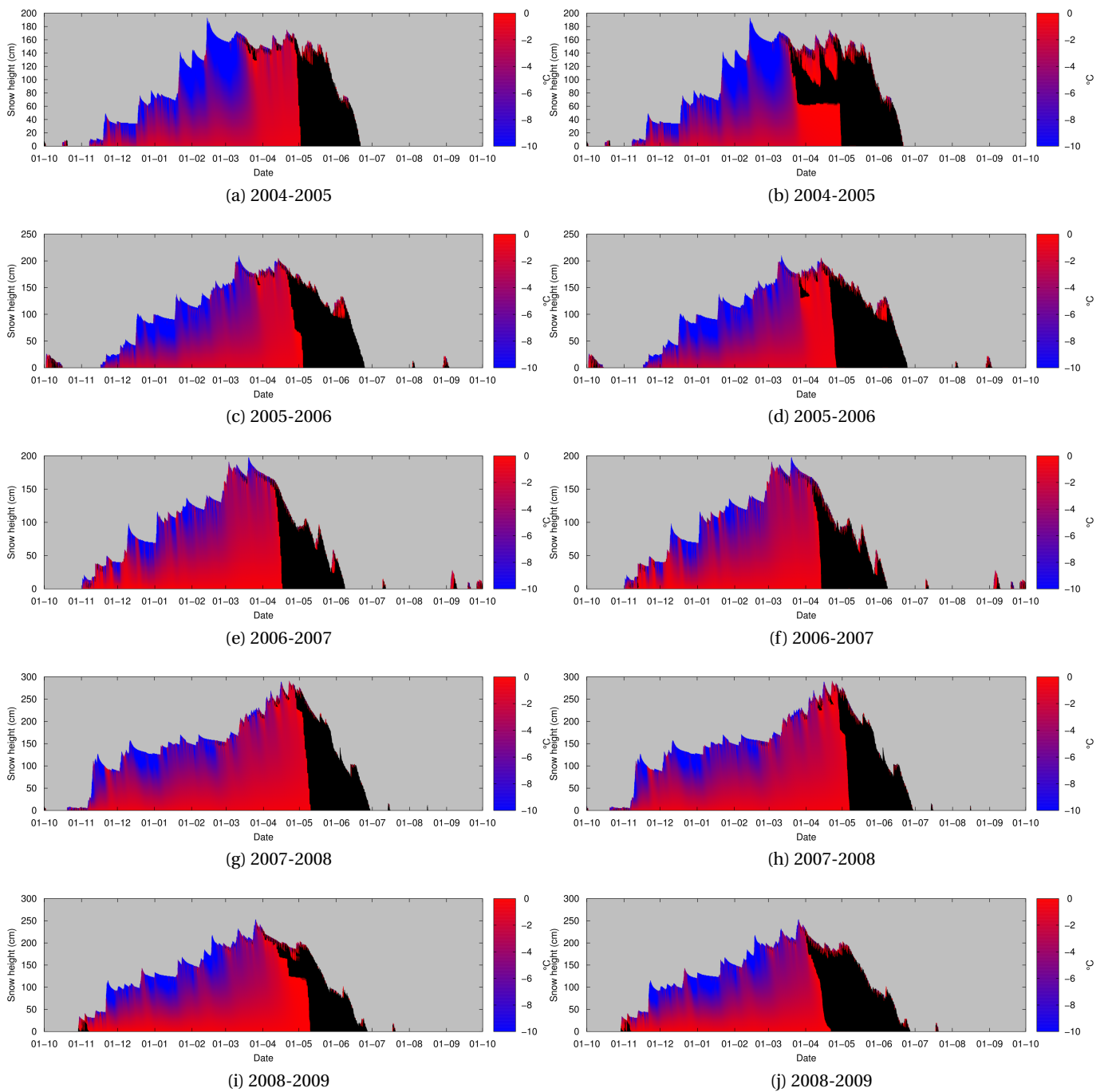
Figure 3.29: Snow temperature (°C) for the simulations with the bucket scheme (left), and with RE-Y2012AM (right), continued. Snow at exactly 0 °C coloured black to mark areas of the snowpack that are melting or wet.

(a) 2009-2010

(b) 2009-2010

(c) 2010-2011

(d) 2010-2011

(e) 2011-2012

(f) 2011-2012

(g) 2012-2013

(h) 2012-2013

(i) 2013-2014

(j) 2013-2014
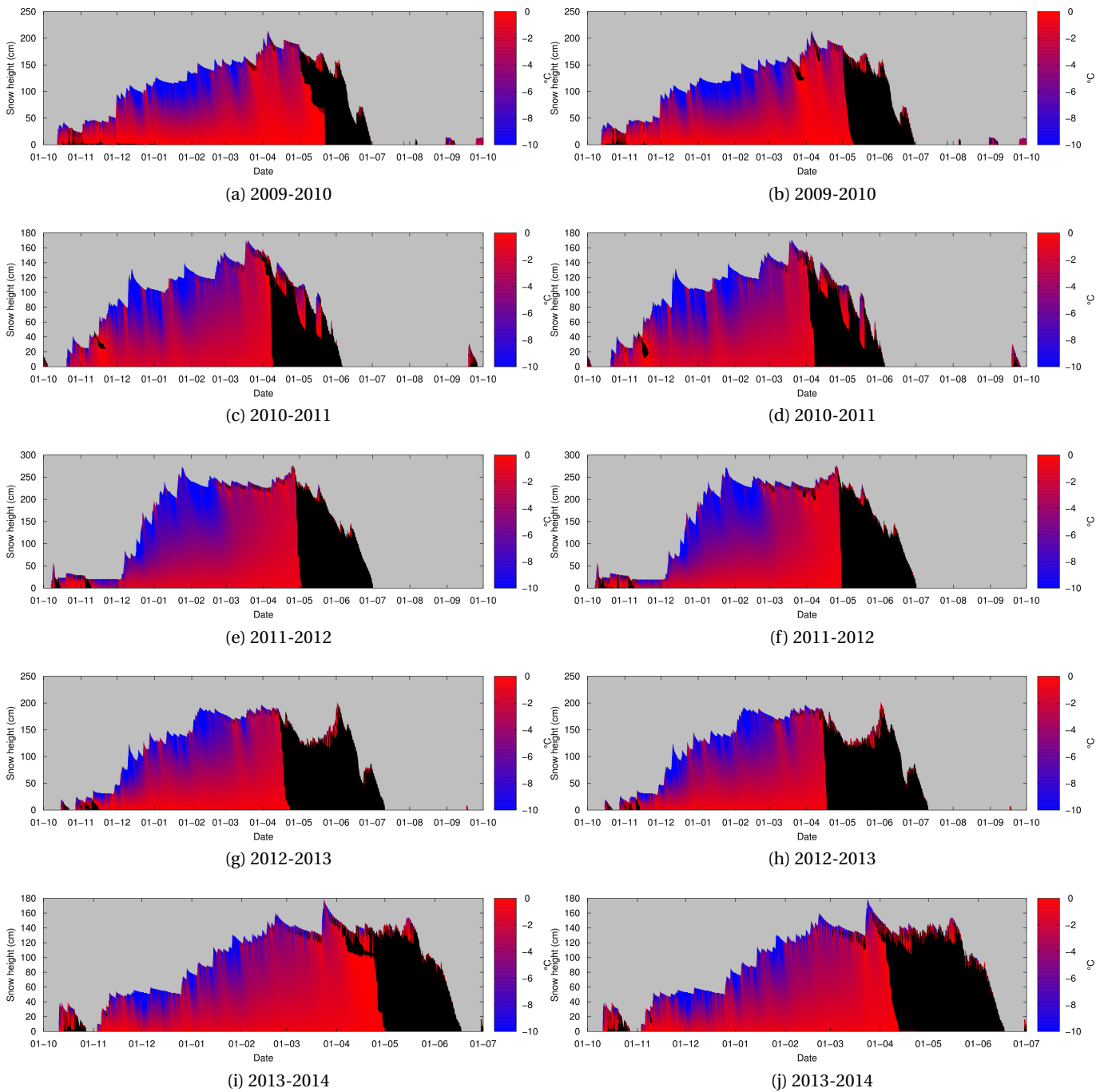
Figure 3.30: Snow temperature (°C) for the simulations with the bucket scheme (left), and with RE-Y2012AM (right), continued. Snow at exactly 0 °C coloured black to mark areas of the snowpack that are melting or wet.

(a) 1999-2000

(b) 2000-2001

(c) 2001-2002

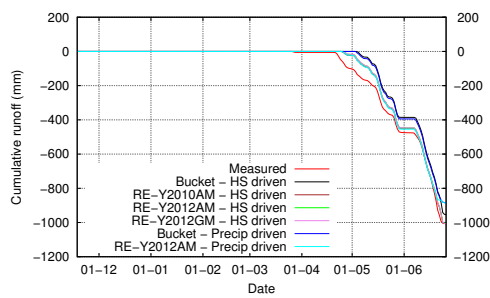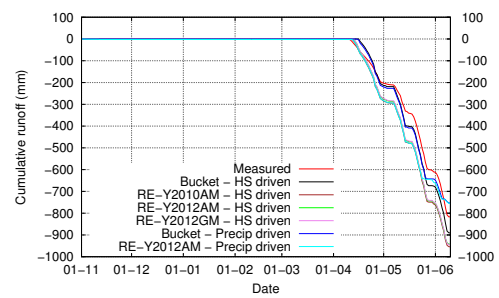(d) 2002-2003

(e) 2003-2004

(f) 2004-2005

(g) 2005-2006

(h) 2006-2007
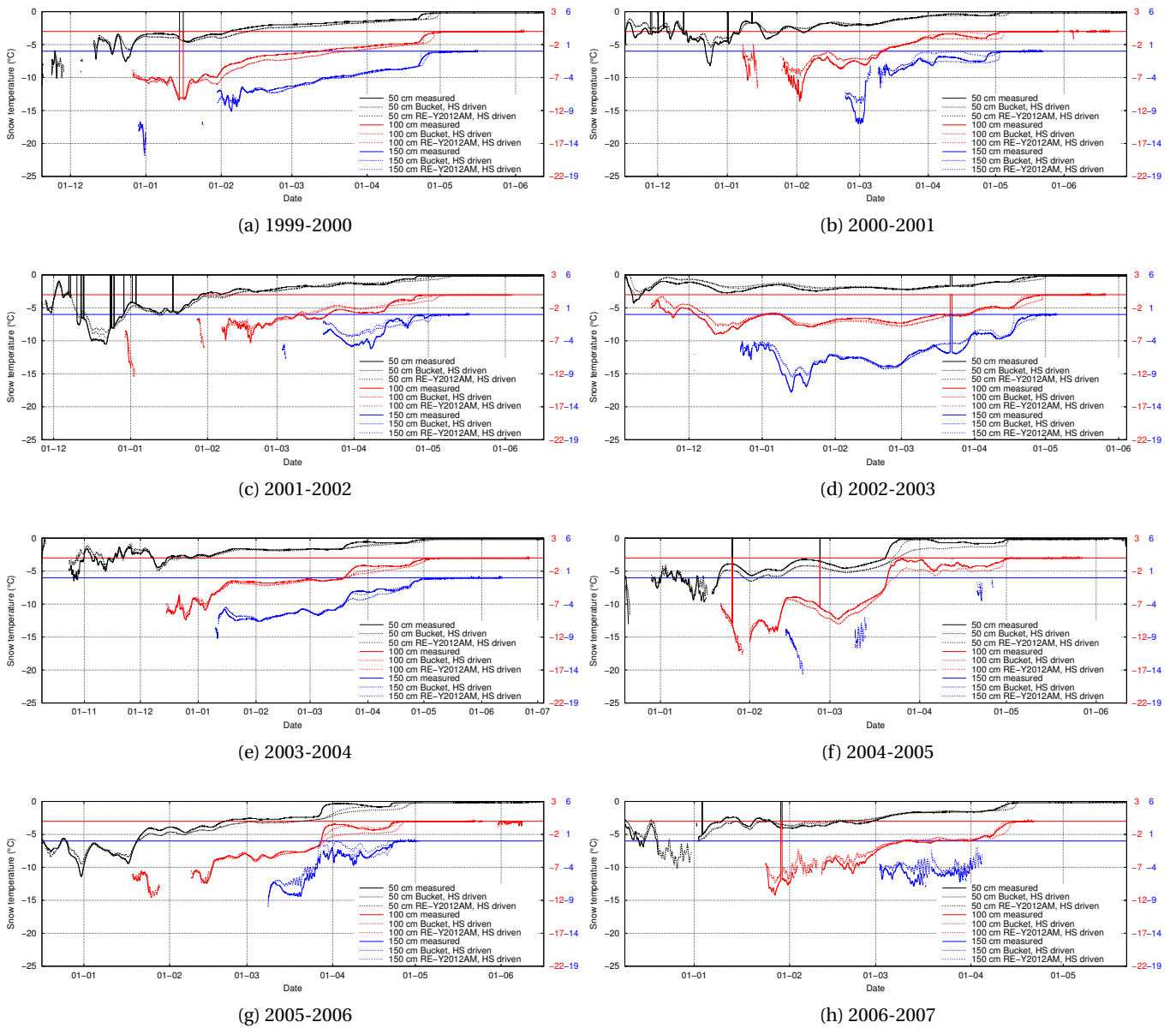
Figure 3.31: Measured and modelled snow temperatures at 50, 100 and 150 cm above the surface. Values are only plotted when the snow height was at least 20 cm more than the height of the temperature sensor.

(a) 2007-2008

(b) 2008-2009

(c) 2009-2010

(d) 2010-2011

(e) 2011-2012

(f) 2012-2013

(g) 2013-2014
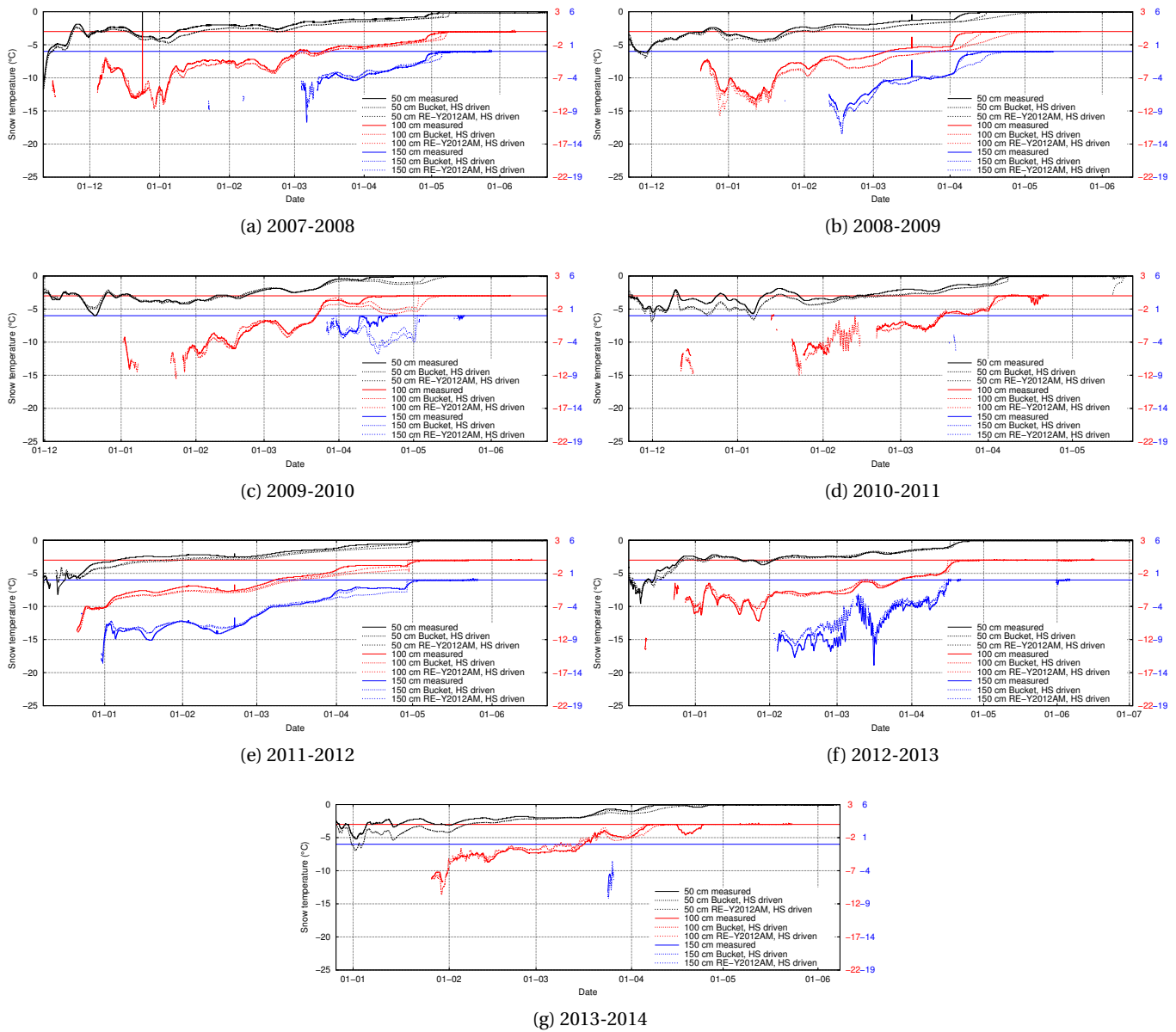
Figure 3.32: Measured and modelled snow temperatures at 50, 100 and 150 cm above the surface, continued. Values are only plotted when the snow height was at least 20 cm more than the height of the temperature sensor.

(a) 1999-2000

(b) 1999-2000

(c) 2000-2001

(d) 2000-2001

(e) 2001-2002

(f) 2001-2002

(g) 2002-2003

(h) 2002-2003

(i) 2003-2004

(j) 2003-2004
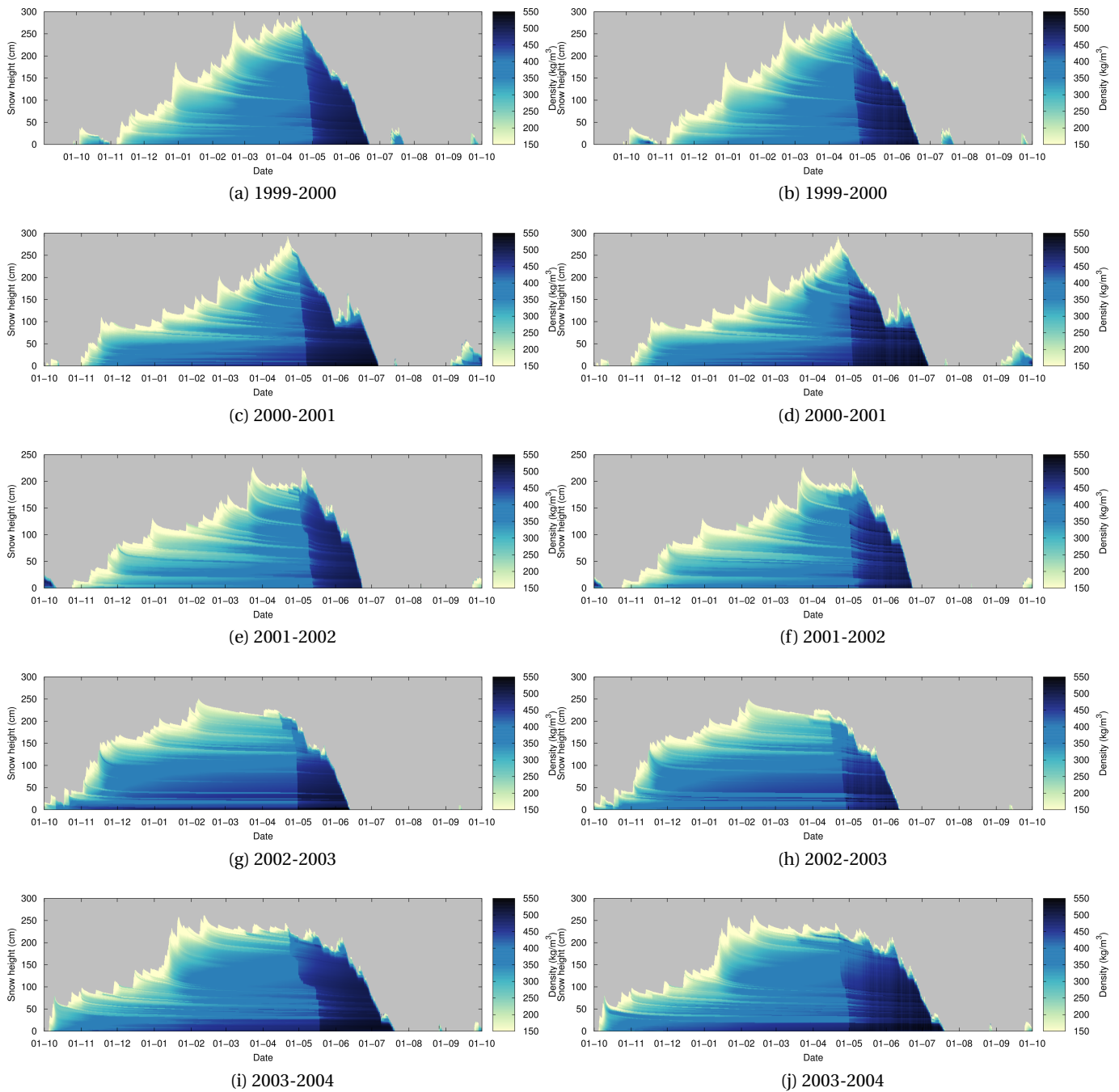
Figure 3.33: Snow density (kg m^{-3}) for the simulations with the bucket scheme (left), and with RE-Y2012AM (right).

(a) 2004-2005

(b) 2004-2005

(c) 2005-2006

(d) 2005-2006

(e) 2006-2007

(f) 2006-2007

(g) 2007-2008

(h) 2007-2008

(i) 2008-2009

(j) 2008-2009
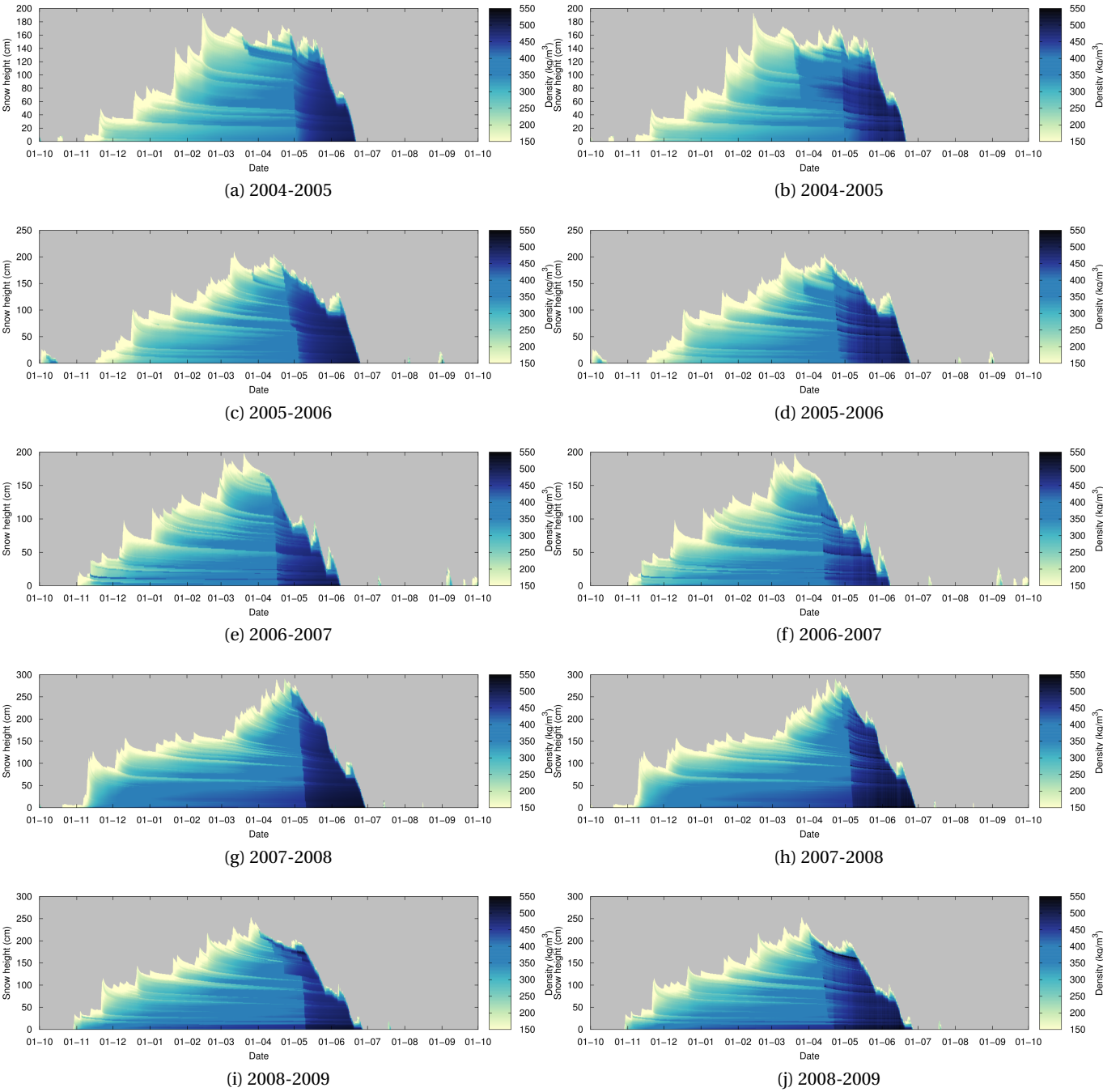
Figure 3.34: Snow density (kg m^{-3}) for the simulations with the bucket scheme (left), and with RE-Y2012AM (right), continued.

(a) 2009-2010

(b) 2009-2010

(c) 2010-2011

(d) 2010-2011

(e) 2011-2012

(f) 2011-2012

(g) 2012-2013

(h) 2012-2013

(i) 2013-2014

(j) 2013-2014
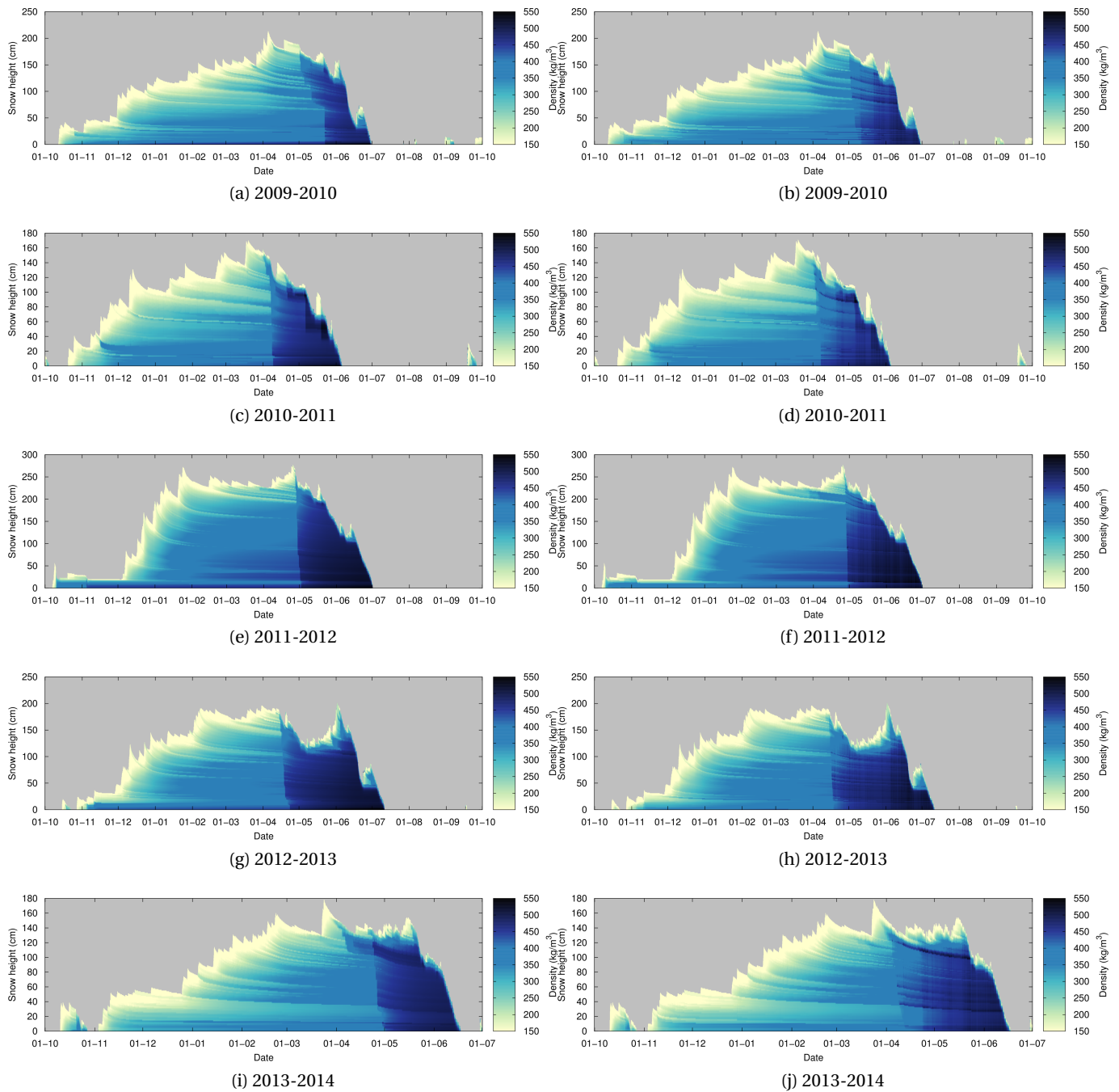
Figure 3.35: Snow density (kg m^{-3}) for the simulations with the bucket scheme (left), and with RE-Y2012AM (right), continued.

(a)

(b)
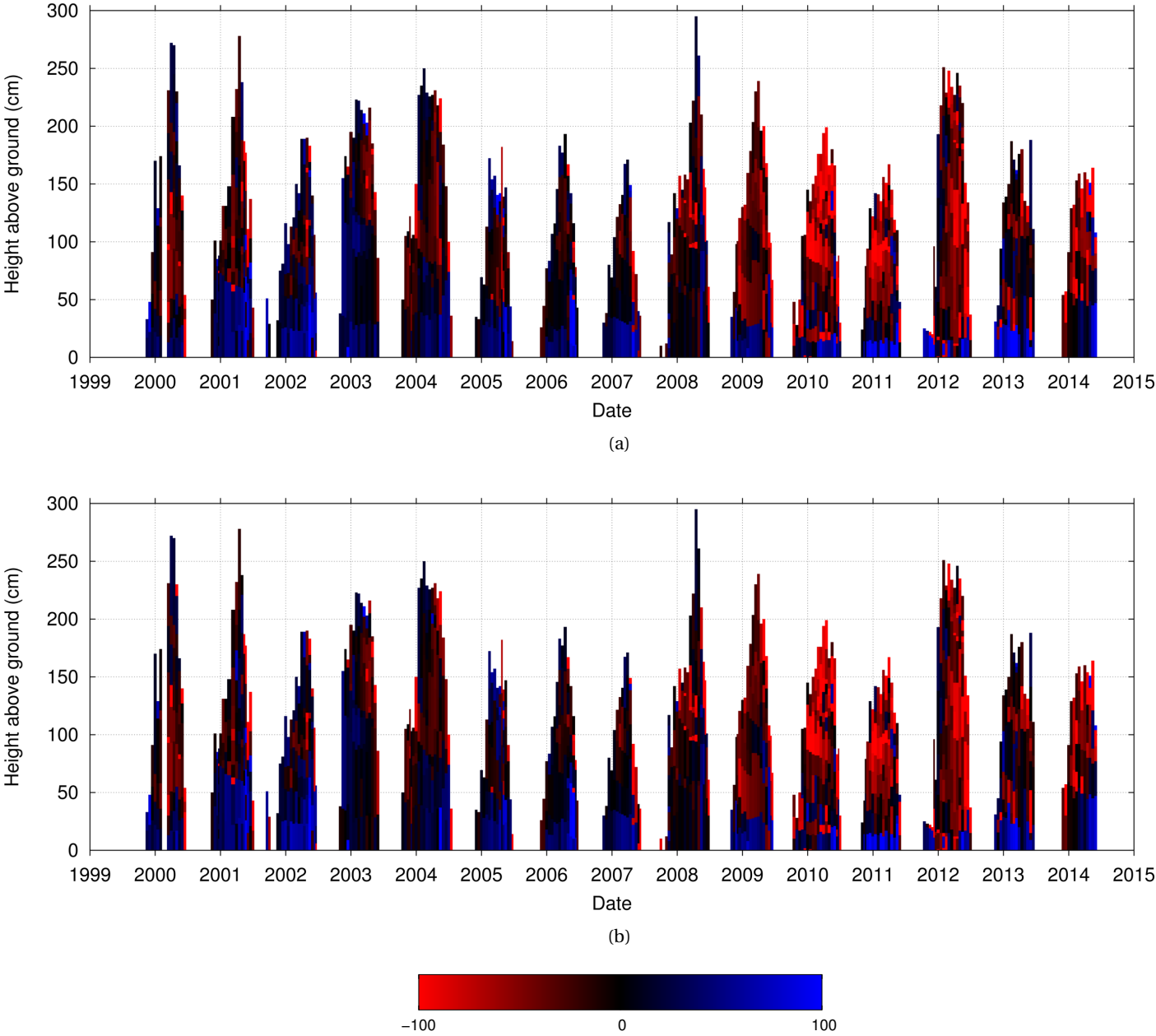
Figure 3.36: Difference between modelled and measured density (kg m^{-3}) for snow height driven simulations with the bucket scheme (a) and RE-Y2012AM (b).

Precipitation Particles

Decomposing and fragmented
precipitation particles

Rounded grains

Faceted crystals

Depth hoar

Surface hoar

Melt forms

Ice formations

Figure 3.37: Grain shapes and associated colours. Crusts and ice lenses are summarized as *Ice formations.*

(a) 1999-2000

(b) 1999-2000

(c) 2000-2001

(d) 2000-2001

(e) 2001-2002

(f) 2001-2002

(g) 2002-2003

(h) 2002-2003

(i) 2003-2004

(j) 2003-2004
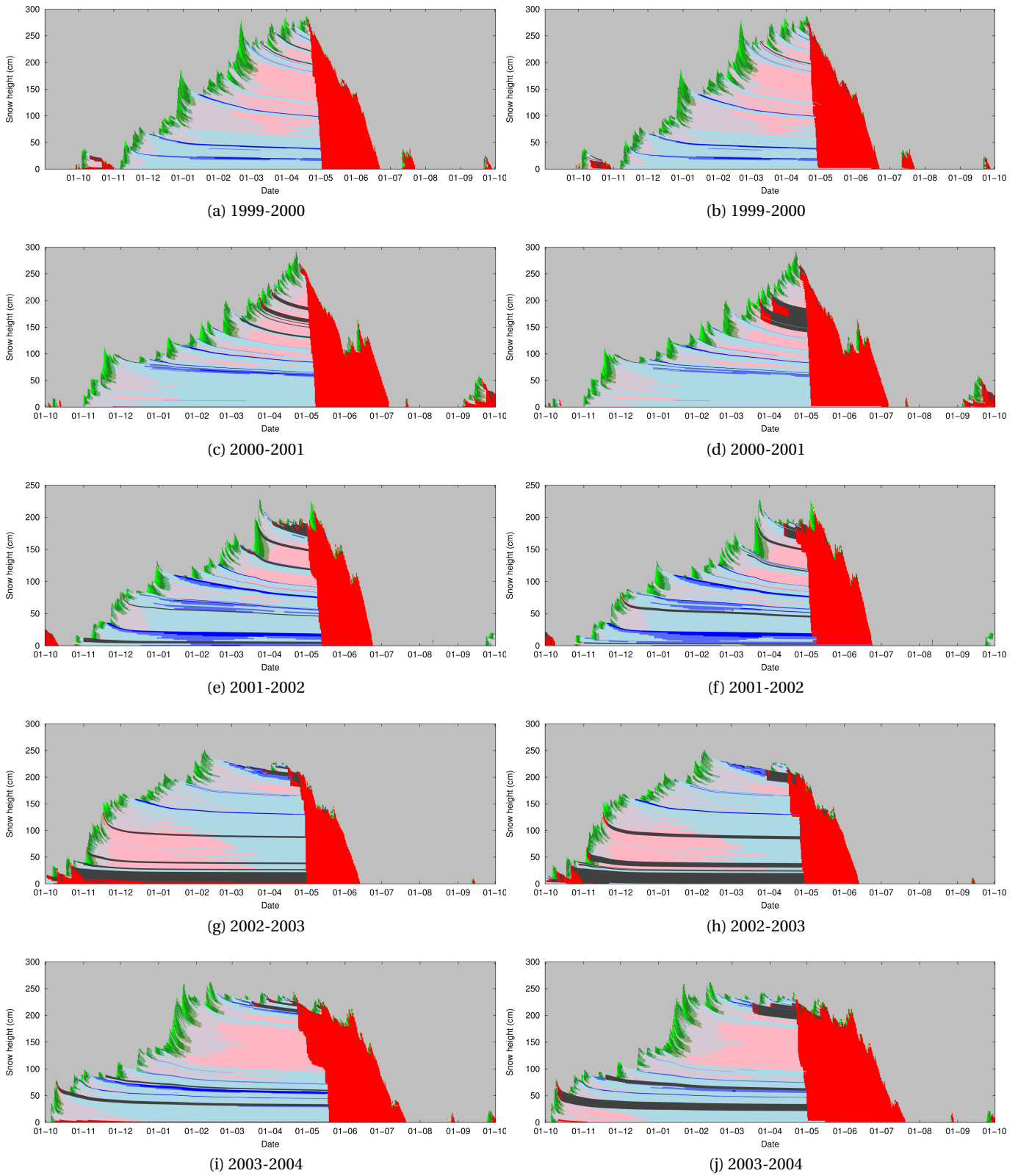
Figure 3.38: Grain shapes for the simulations with the bucket scheme (left), and with RE-Y2012AM (right). A legend is provided in Figure 3.37.

100

(a) 2004-2005

(b) 2004-2005

(c) 2005-2006

(d) 2005-2006

(e) 2006-2007

(f) 2006-2007

(g) 2007-2008

(h) 2007-2008

(i) 2008-2009

(j) 2008-2009
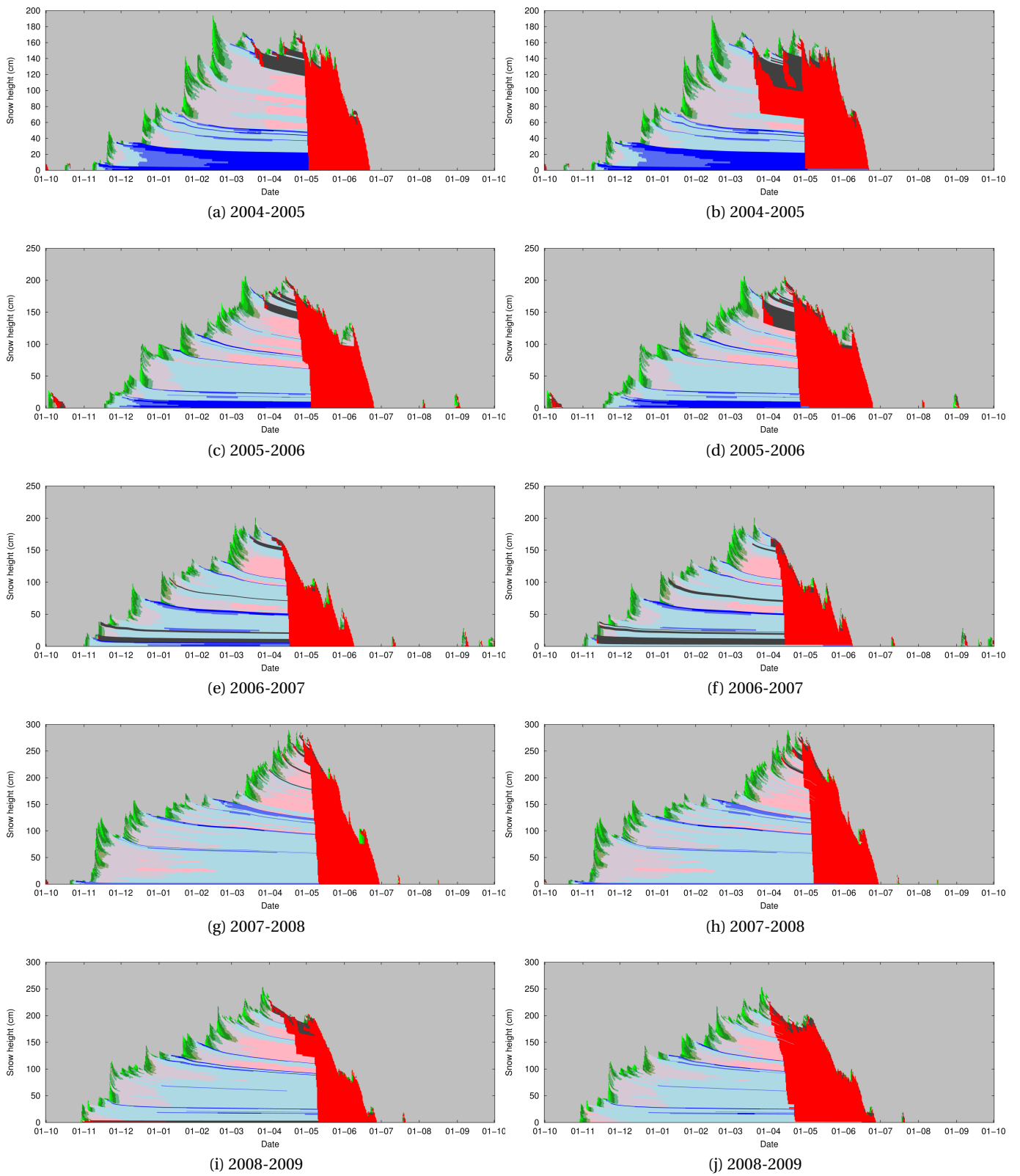
Figure 3.39: Grain shapes for the simulations with the bucket scheme (left), and with RE-Y2012AM (right), continued. A legend is provided in Figure 3.37.

(a) 2009-2010

(b) 2009-2010

(c) 2010-2011

(d) 2010-2011

(e) 2011-2012

(f) 2011-2012

(g) 2012-2013

(h) 2012-2013

(i) 2013-2014

(j) 2013-2014
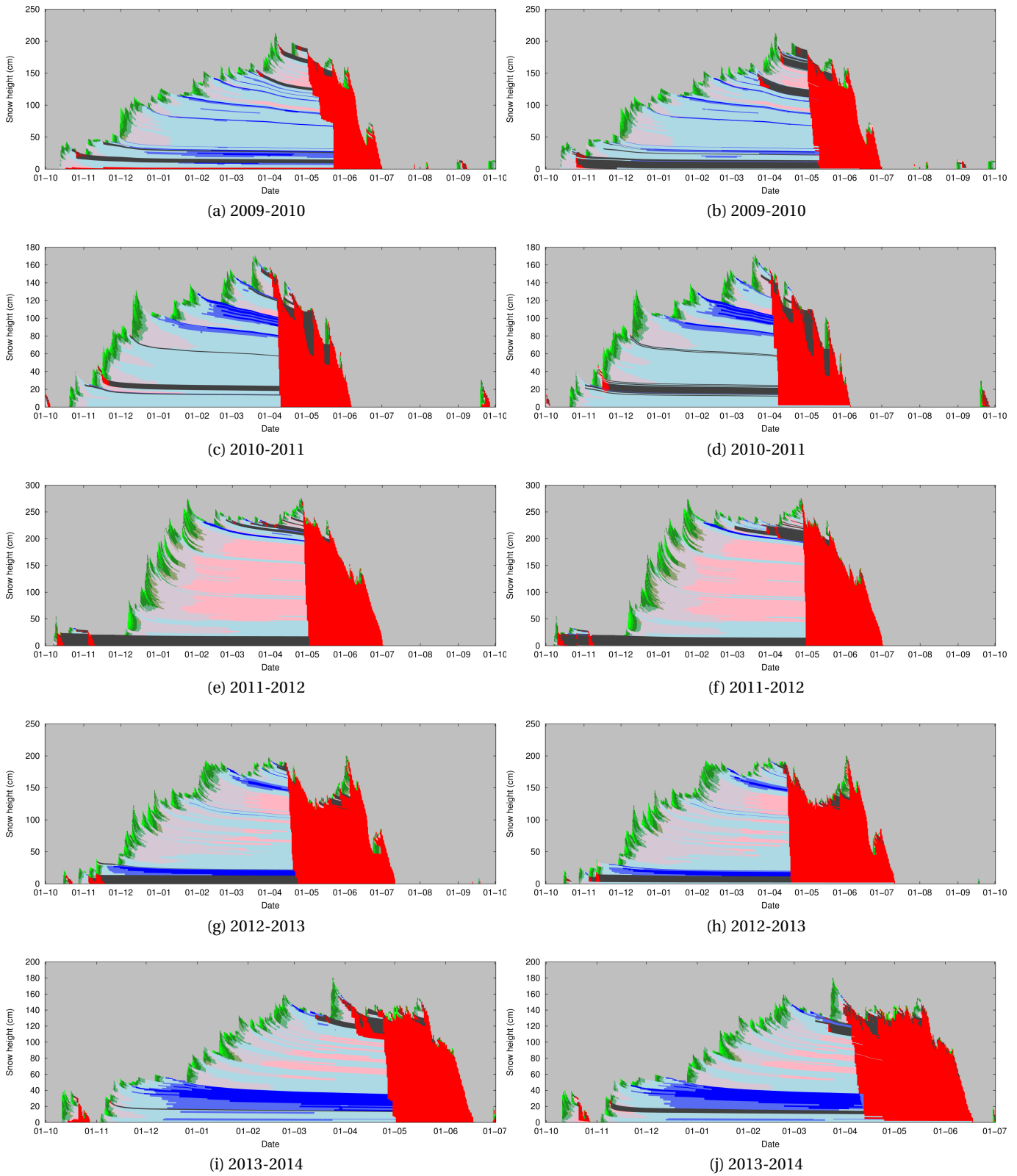
Figure 3.40: Grain shapes for the simulations with the bucket scheme (left), and with RE-Y2012AM (right), continued. A legend is provided in Figure 3.37.

(a) 1999-2000

(b) 1999-2000

(c) 2000-2001

(d) 2000-2001

(e) 2001-2002

(f) 2001-2002

(g) 2002-2003

(h) 2002-2003

(i) 2003-2004

(j) 2003-2004
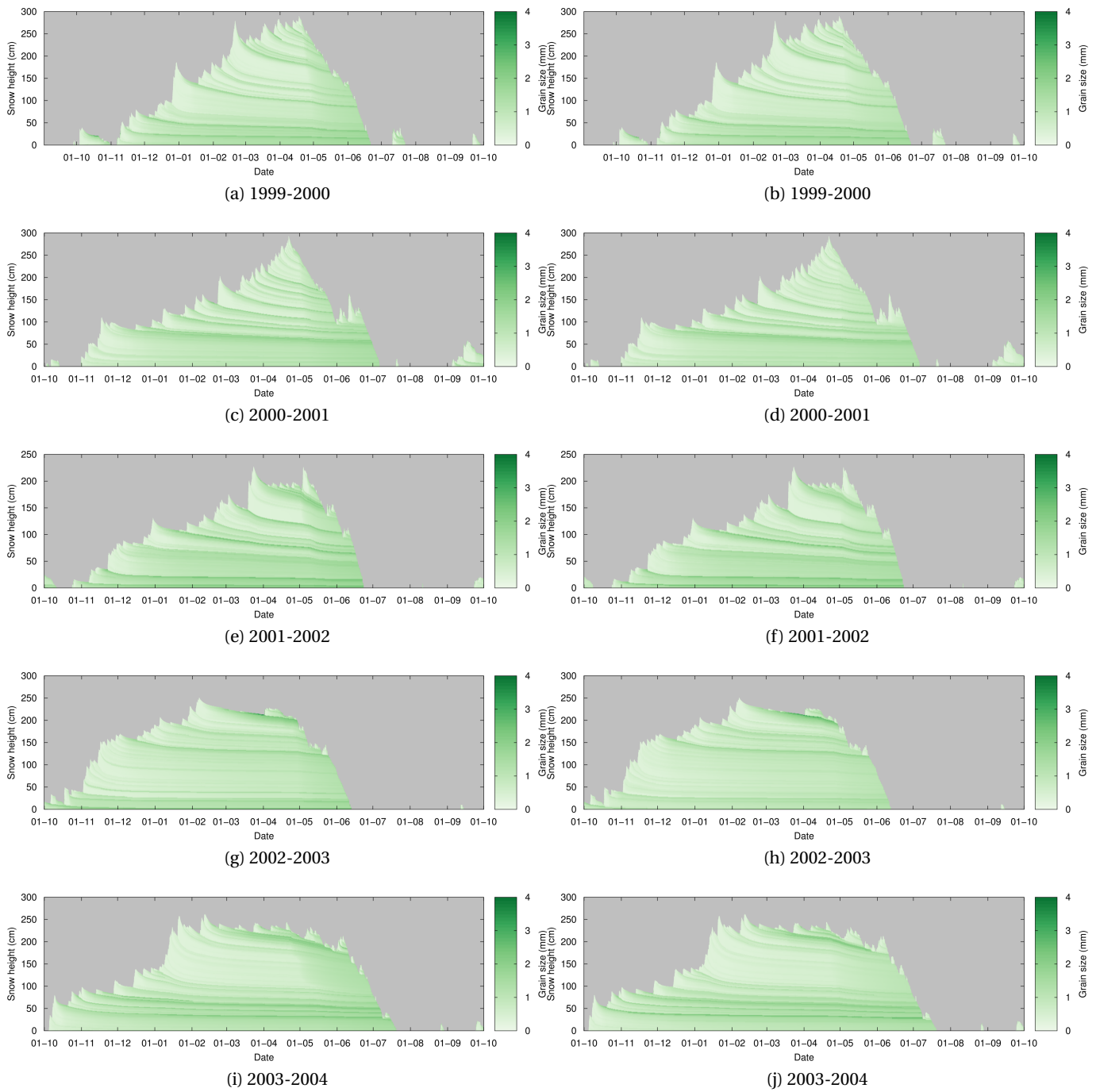
Figure 3.41: Grain size (mm) for simulations with the bucket scheme (left), and with RE-Y2012AM (right).

(a) 2004-2005

(b) 2004-2005

(c) 2005-2006

(d) 2005-2006

(e) 2006-2007

(f) 2006-2007

(g) 2007-2008

(h) 2007-2008

(i) 2008-2009

(j) 2008-2009
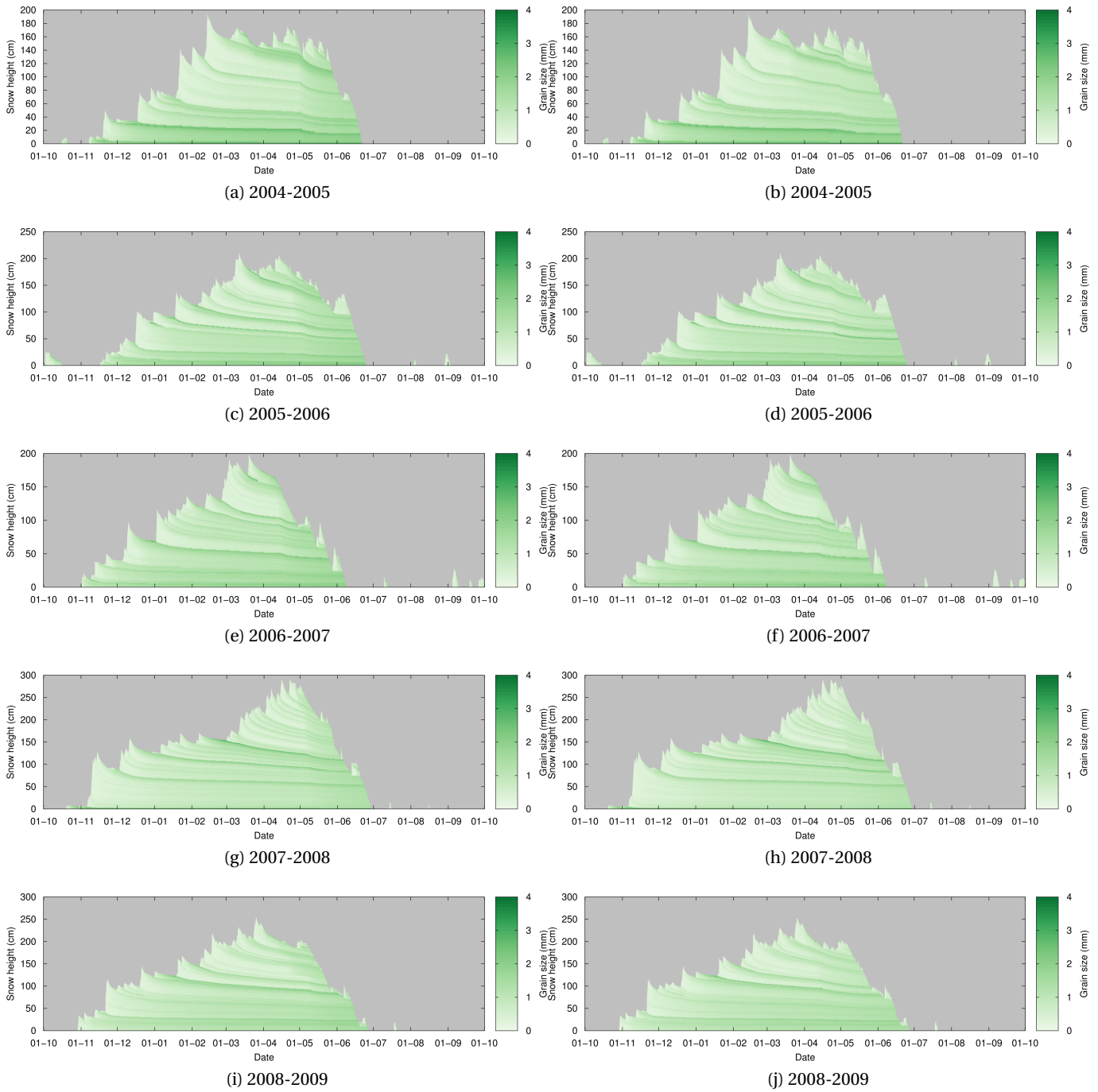
Figure 3.42: Grain size (mm) for simulations with the bucket scheme (left), and with RE-Y2012AM (right), continued.

(a) 2009-2010

(b) 2009-2010

(c) 2010-2011

(d) 2010-2011

(e) 2011-2012

(f) 2011-2012

(g) 2012-2013

(h) 2012-2013

(i) 2013-2014

(j) 2013-2014
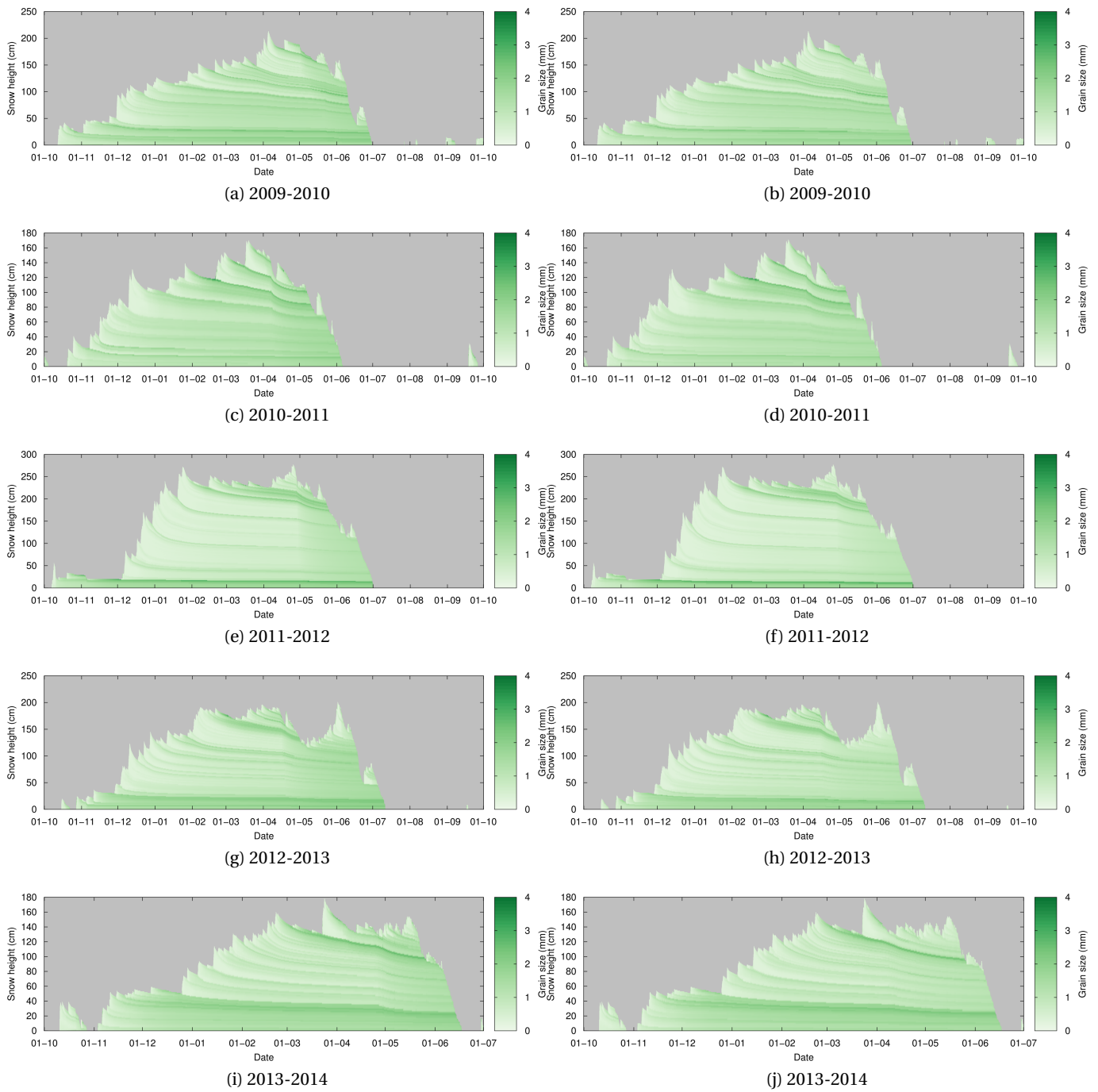
Figure 3.43: Grain size (mm) for simulations with the bucket scheme (left), and with RE-Y2012AM (right), continued.

4 Soil moisture measurements and simulations in alpine terrain using the distributed Alpine3D model

Nander Wever[1,2], Francesco Comola[2], Mathias Bavay[1], Michael Lehning[1,2]

[1] WSL Institute for Snow and Avalanche Research SLF, Davos Dorf, Switzerland.
[2] CRYOS, School of Architecture, Civil and Environmental Engineering, EPFL, Lausanne, Switzerland.

Summary

Studies have shown that the simulation of hydrological processes in alpine catchments can benefit from using a physics based snow cover model in hydrological modelling. One advantage of physical modelling lies in the potential to correctly represent spatially variable snow distribution and snow melt, which is known to impact soil moisture and streamflow. Here, the recently updated soil module of the physics based, multi-layer snow cover model SNOW-PACK is verified against soil moisture measurements at seven sites in the area around Davos, Switzerland. Using the fully distributed version of SNOWPACK, which is called Alpine3D, spatially explicit simulations of soil moisture have been performed. It was found that the most important influence on spatial variability in soil moisture is the spatial distribution of the snow cover and snowmelt. Existing cross correlations between measurement sites in soil moisture measurements were also found in the simulations, suggesting that Alpine3D is able to capture this spatial variability. In the snow-free summer months, this was not observed, and variability in simulated soil moisture was much smaller than in the measurements. This can likely be attributed to neglecting spatial variability in soil properties. Streamflow simulations using the travel time distribution approach for the outlet of the Dischma catchment provided a closer agreement with observed streamflow when using the water flux at 30 cm inside the soil, then using the water flux at the top of the soil column. This suggests that streamflow simulations using the Alpine3D model will benefit from the updated soil module of SNOWPACK.

4.1   Introduction

In many mountainous catchments, hydrological processes are strongly influenced by the presence of a snow cover for at least some part of the year. The snow cover stores precipitation over winter and provides a contribution to catchment scale runoff via meltwater in spring. During the winter months, the snow cover basically decouples the soil from the atmosphere and the upper boundary for the soil is determined by the state of the snow cover on top (*McNamara et al.*, 2005; *Kumar et al.*, 2013). Often, the hydrological processes are strongly reduced, such as groundwater flow and streamflow, until the spring snowmelt provides liquid water again to the hydrological system.

Several studies found that improved estimations of snow cover distribution and snowmelt lead to more accurate streamflow simulations (*Maurer and Lettenmaier*, 2003; *Berg and Mulroy*, 2006; *Seyfried et al.*, 2009; *Koster et al.*, 2010). However, the studies also show that accurate simulations of liquid water draining from the snowpack due to snowmelt or rainfall (snowpack runoff) are not sufficient. The degree of saturation of the soil was found to determine the eventual effect of snowpack runoff on streamflow (*McNamara et al.*, 2005; *Seyfried et al.*, 2009; *Bales et al.*, 2011). This effect is not limited to snowpack runoff, but is also found for rainfall (*Bales et al.*, 2011).

To assess the coupling between snowmelt, soil moisture and streamflow, the use of physics based models seems attractive as they should not require calibration for the specific application. In *Rigon et al.* (2006), it is shown that the physics based hydrological model GEOtop, which includes a relatively simple physics based snow scheme, is able to provide accurate streamflow simulations for small catchments, where a snow cover is present for extended periods during the winter season. On the other hand, a study by *Kumar et al.* (2013) showed that relatively simple temperature index based snowmelt models may perform well after careful calibration.

A physics based approach does not necessarily improve simulations, as an accurate physical representation of micro- or macro-scale processes does not automatically guarantee a good performance on larger scales (*Beven*, 1993). However, *Kumar et al.* (2013) also found that using a physics based model approach for snow related processes in the PIHM model achieved a slightly better performance for streamflow simulations than the temperature index approach. The results in their study suggest that this improvement is linked to the spatial variability of snow distribution and snowmelt, which provides a strong control on other components of the hydrological cycle, like soil moisture or streamflow.

In *Warscher et al.* (2013), a similar comparison was made by comparing a temperature-index approach with an energy balance approach to determine snowmelt in the physics based hydrological model WaSiM-ETH. Their results show that the energy balance approach provides improvements at the small scales, like at high alpine headwater catchments. However, the improvements rapidly decreased with increasing scale.

Table 4.1: Yearly, winter months (DJF) and summer months (JJA) precipitation sums from heated rain gauges in the area around Davos. In brackets the percentage that falls as snow, based on measured air temperature below 1.2°C.

Year	Precipitation year mm (% snow)	Precipitation DJF mm (% snow)	Precipitation JJA mm (% snow)	Precipitation year mm (% snow)	Precipitation DJF mm (% snow)	Precipitation JJA mm (% snow)
	Davos (1590 m)			Weissfluhjoch (2540 m)		
2011	999 (18%)	129 (76%)	410 (0%)	1767 (65%)	276 (100%)	536 (24%)
2012	1419 (36%)	547 (81%)	516 (0%)	2801 (73%)	1372 (100%)	755 (22%)
2013	1028 (24%)	223 (81%)	297 (0%)	2002 (66%)	565 (100%)	538 (39%)

The fully-distributed Alpine3D model is typically applied for detailed studies of small scale surface processes in alpine catchments where snow plays an important role (*Lehning et al.*, 2006; *Mott et al.*, 2008; *Groot Zwaaftink et al.*, 2013). In this study, the recent addition to the SNOWPACK model of a solver for Richards Equation for soil (see Chapter 2 and 3) is verified against soil moisture measurements in the vicinity of Davos, Switzerland. The SNOWPACK model also provides the description of soil-snow-vegetation processes in the Alpine3D model framework and here, the capabilities of Alpine3D to capture spatial variability of soil moisture is also tested. Finally, an outlook is given how the improved soil module of SNOWPACK may eventually contribute to a better simulation of streamflow.

4.2 Study Area and Data

4.2.1 Study Area

The Davos area is located in the Canton Graubünden in east Switzerland. The studied area is 21.5×21.5 km^2 and stretches over an altitudinal range from about 1250 m to 3218 m. Some small glaciers exist in the highest parts, covering about 0.86 km^2 (*Zappa et al.*, 2003). The Dischma catchment is an important catchment in the Davos area, and has been subject to previous studies concerning streamflow from the Dischma river (*Zappa et al.*, 2003; *Lehning et al.*, 2006; *Bavay et al.*, 2009). The measurement site Weissfluhjoch (WFJ), which is focussed on snow-related measurements, is located within the area, as well as several permanent meteorological stations. Figure 4.1 shows the studied area, including the measurement stations and the gauging station for streamflow measurements of the Dischmabach in the Dischma catchment. Streamflow data has been provided by the Swiss Federal Office for the Environment (FOEN). Simulations presented in this study consist of three winter seasons, from October 1, 2010 to September 30, 2013.

Snow fall plays an important role in the Davos area. Table 4.1 shows the precipitation sums for two heated rain gauges at two altitudes in the region. About 25% and 68% of all precipitation falls as snow at 1590 m and 2540 m altitude, respectively. The separation in rainfall and snowfall was determined on an hourly basis, using a temperature threshold of 1.2 °C. The winter months are dominated by snowfall at all altitudes in the area. In the summer months,
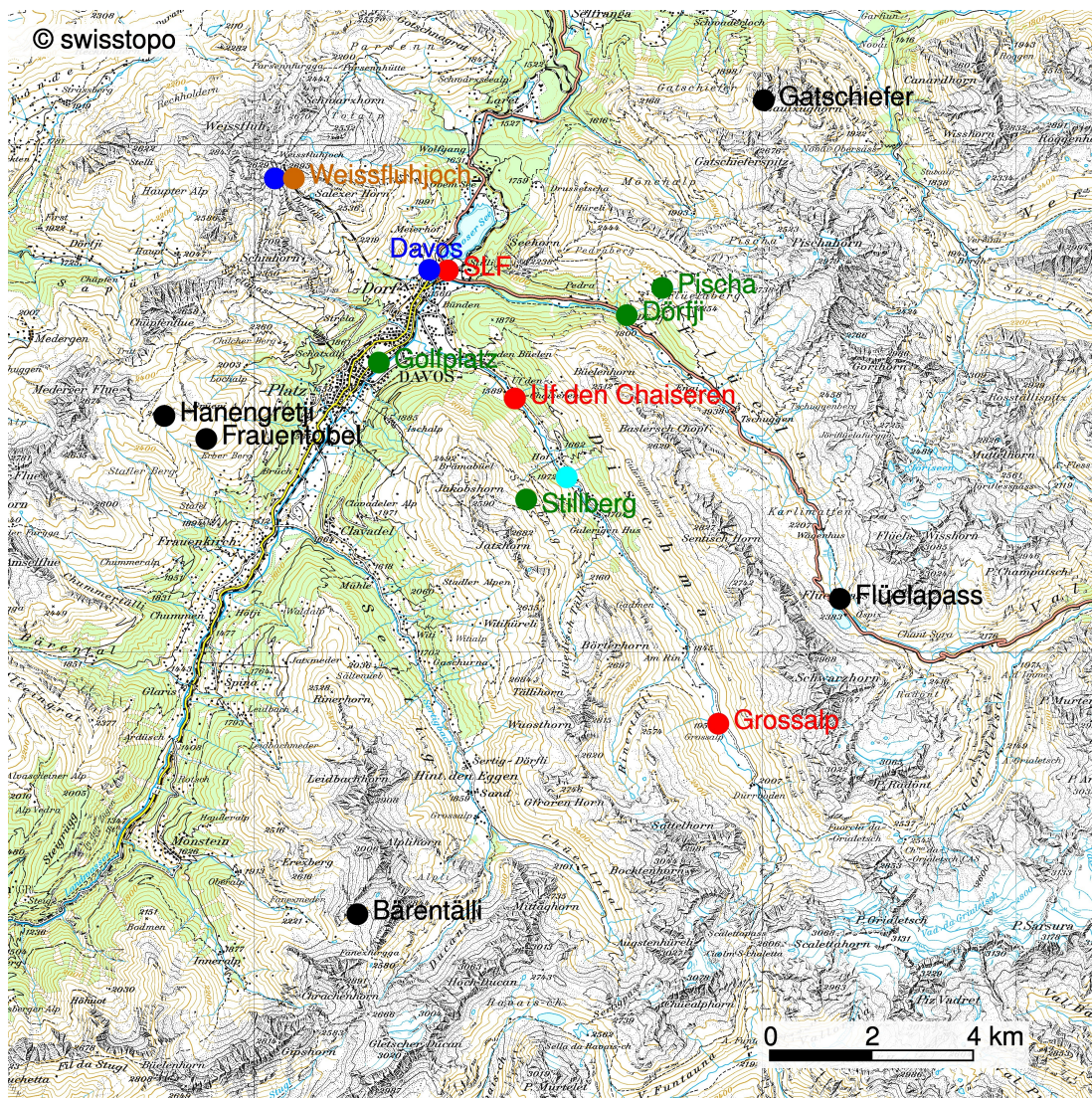
Figure 4.1: Topographical map of the simulated domain, showing the locations of the stations. IMIS stations are shown in black, IRKIS stations in red, SensorScope stations in green, SwissMetNet stations in blue and Weissfluhjoch in brown. The gauging station measuring streamflow in the Dischmabach at the outlet of the Dischma catchment is shown in cyan. Map reproduced by permission of swisstopo (JA100118).

about 25% of the precipitation amounts still consist of snowfall at 2540 m altitude. At the lower rain gauge, virtually all precipitation falls as rain in the summer months. There is a strong altitudinal gradient in precipitation amounts. At 2540 m altitude, precipitation amounts are about 1.9 times higher than at 1590 m altitude. Furthermore, the area exhibits a climatological northwest - southeast gradient in precipitation amounts (not shown).

Figures 4.2a and 4.2b show the daily temperature and precipitation amounts separated in
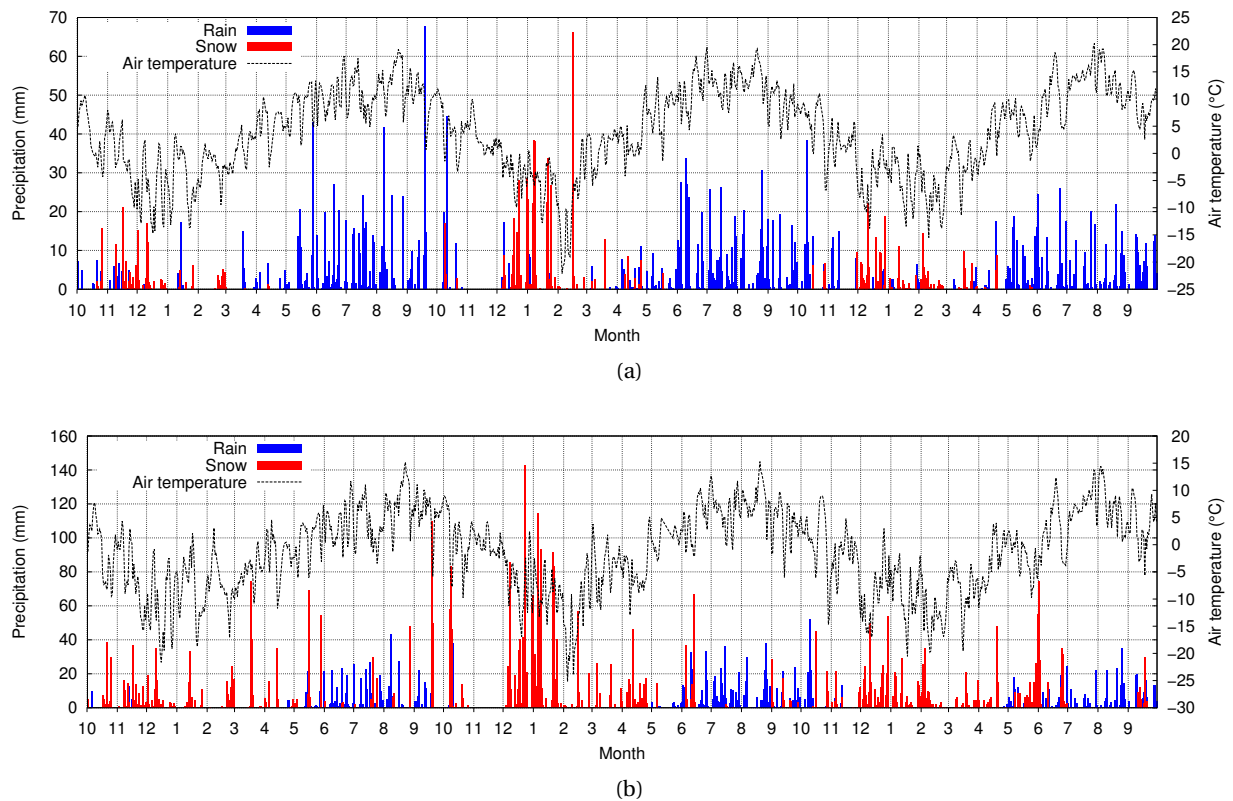
Figure 4.2: Daily rain and snowfall amounts and daily average air temperature for Davos, 1590 m (a) and Weissfluhjoch, 2540 m (b).

snowfall and rainfall, for both locations with a heated rain gauge. The yearly cycle in temperature has a similar amplitude at both altitudes. Maximum daily temperatures occasionally reached 20°C at 1590 m altitude and 15°C at 2540 m altitude. The minimum daily temperatures reached −20°C and −25°C, respectively. Note that those temperatures were reached after significant snowfall in the months before. Therefore, the isolating snow cover is expected to have prevented an impact of these cold days on soil freezing.

An important event in the meteorological forcing can be found in winter season 2011-2012, which was dominated by large snow falls in December, January and February. Maximum measured snow height was higher than in the other simulated years. Cold temperatures in those months were followed by a relatively warm spring season, resulting in relatively fast snowmelt rates. Also the spring of snow season 2010-2011 was relatively warm, compared to the spring of 2012-2013. None of the summer periods were outspokenly dry or wet, and precipitation occurred homogeneously distributed over time. Noticeable is also the dry November 2011, in which no precipitation occurred. Finally, total precipitation at WFJ in summer 2013 was equal to summer 2011, whereas the summer 2013 was rather dry in Davos.

Table 4.2: List of stations and measured quantities at the stations that are used in this study. (X): measured and used in this study, (-): not measured, (u): unventilated (temperature) or unheated (rain gauge), (v): ventilated, (h): heated rain gauge. VWC shallow denotes soil moisture sensors at 10, 30 and 50 cm depth, VWC deep denotes soil moisture sensors at 80 and 120 cm depth.

Station name	Type	Altitude (m)	TA	RH	TSS	Wind speed	Snow height	Rain gauge	ISWR	RSWR	ILWR	VWC shallow	VWC deep
Bärentalli	IMIS	2560	u	u	X	X	X	u	-	X	X	-	-
Flüelapass	IMIS	2390	u	u	X	X	X	u	-	X	X	-	-
Frauentobel	IMIS	2330	u	u	X	X	X	u	-	X	X	-	-
Gatschiefer	IMIS	2310	u	u	X	X	X	u	-	X	X	-	-
Grüniberg	IMIS	2300	u	u	X	X	X	u	-	X	X	-	-
Madrisa	IMIS	2140	u	u	X	X	X	-	-	X	X	-	-
SLF	IMIS	1560	u	u	X	X	X	-	-	X	X	X	X
Grossalp	IRKIS	1960	v	v	X	X	X	u	-	X	X	X	X
Uf den Chaiseren	IRKIS	1590	v	v	X	X	X	u	-	X	X	X	X
Dorfji	SENS[1]	1813	-	-	-	-	-	-	-	-	-	X	-
Golf Course	SENS[1]	1537	-	-	-	-	-	-	-	-	-	X	X
Pischa	SENS[1]	2156	-	-	-	-	-	-	-	-	-	X	-
Stillberg	SENS[1]	2218	-	-	-	-	-	-	-	-	-	X	-
Davos	SMN[2]	1596	-	-	-	-	-	h	X	-	X	-	-
Weissfluhjoch	COMBI[3]	2540	v	v	X	X	X	h	X	X	X	-	-

[1] SENS: Sensorscope station.

[2] SMN: SwissMetNet station (MeteoSwiss).

[3] COMBI: Combination of IMIS, SwissMetNet and other instrumentation.

4.2.2 Data

Several measurement sites are located or were temporarily installed in the vicinity of Davos. Their locations are shown in Figure 4.1 and the stations can be separated into 5 types:

(i) IMIS stations: those stations are permanently operational meteorological stations in the Swiss Alps, especially focussed on usage for avalanche warning (*Lehning et al.*, 1999). The stations are 7.5 m high, and are designed for long-term operational use. For this purpose, they receive regular maintenance and quality control. Data is collected at 30 minute intervals. One exception is SLF2 in Davos-Dorf, which is used as a test station for new sensors or hardware. For this reason, during the winter season 2011 and for a large part of winter season 2012, the relative humidity sensor was providing erroneous data. Therefore, the data from the relative humidity sensor from the Uf den Chaiseren IRKIS station (see below) was used for these periods. Relative humidity is mainly influencing the calculated latent heat flux and therefore, the possible error is expected to be small.

(ii) IRKIS stations: these stations were temporarily set up for this study. They are based on the IMIS design, although they are smaller than IMIS stations with a height of 4.5 m. The IRKIS stations were additionally equipped with soil moisture sensors at 10, 30, 50, 80 and 120 cm depth. At each depth, two sensors were installed at approximately 50 cm distance. The IRKIS station SLF2 was using the IMIS station SLF2, but soil moisture sensors were installed in close

vicinity. IRKIS stations report weather and soil moisture conditions at a time resolution of 10 minutes.

(iii) SensorScope stations: to improve the data quantity and the area covered by measurements, SensorScope stations (*Ingelrest et al.*, 2010) were installed in less accessible terrain for a period of approximately 2-3 years. Operation of these type of stations in the harsh winter conditions appeared to be more difficult than expected and the sometimes hazardous locations of the measurement sites was hindering maintenance during the winter season. Due to several outages of the stations and broken sensors, the meteorological measurement series contain many gaps and are discarded in this study. The SensorScope stations were also equipped with soil moisture sensors at 10, 30 and 50 cm depth. At the Golf Course station, sensors were additionally installed at 80 and 120 cm depth. Also here, two sensors were installed at each depth. In this study, we consider the data to be useful for validation. SensorScope stations measure at a time resolution of 1 minute, sending their data using GPRS cell phone networks.

(iv) SwissMetNet stations: the Swiss Federal Office of Meteorology and Climatology (MeteoSwiss) is operating meteorological stations in the SwissMetNet network. In the vicinity of Davos, two SissMetNet stations are present: at the WFJ (2540 m altitude) and in Davos-Dorf (1590 m altitude). They are equipped with a heated rain gauge, providing relatively accurate measurements of solid precipitation in winter, and incoming shortwave and longwave radiation sensors. To amend the data set from the SLF2 IMIS station, the heated rain gauge data for Davos-Dorf, which is collected at a distance of 350 m from the SLF2 station, was used to determine rainfall here.

(v) WFJ: this measurement site serves as the main research site for the WSL Institute for Snow and Avalanche Research SLF and is focussed on snow related processes. The site is equipped with an IMIS type station, as well as a heated rain gauge that is part of the SwissMetNet network. Furthermore, ventilated temperature and relative humidity sensors are present as well as incoming and reflected shortwave and incoming and outgoing longwave radiation sensors. Several backup sensors are present, allowing for filling data gaps.

At the soil moisture measurement sites, Decagon 10HS soil moisture sensors were installed (*Decagon Devices*, 2014). *Mittelbach et al.* (2012) presents an in-depth comparison with other types of soil moisture sensors. A few important issues related to the Decagon 10HS sensors that are relevant for this study were found. In their study, the sensors hardly registered values above 0.40 $\text{m}^3 \text{ m}^{-3}$ and it is concluded that the 10HS is showing a decreased sensitivity with increasing liquid water content and that the sensor is unable to follow fluctuations in wet soil conditions. Furthermore, the liquid water content values from the sensors exhibit a soil temperature dependency. They are favourable to use, however, due to their low cost and easy integration in existing measurement networks.

Table 4.3: List of parameters for the soil types for saturated water content (θ_s), residual water content (θ_r), the van Genuchten parameters α and n, the saturated hydraulic conductivity (K_{sat} [1]), the density of soil particles (ρ_p), the thermal conductivity of soil particles (λ) and the specific heat of soil particles (c_p).

Name	θ_s [1] $(m^3\,m^{-3})$	θ_r [1] $(m^3\,m^{-3})$	α [1] (m^{-1})	n [1] $(-)$	K_{sat} [1] $(m\,s^{-1})$	ρ_p $(kg\,m^{-3})$	λ $W\,m^{-1}\,s^{-1}$	c_p $J\,kg^{-1}\,K^{-1}$
Loamy sand	0.390	0.049	3.475	1.746	$1.22 \cdot 10^{-5}$	2600 [2]	0.9 [2]	1000 [2]
Sandy loam	0.387	0.039	2.667	1.449	$4.43 \cdot 10^{-6}$	2600 [3]	2.5 [3]	801 [3]
Silt loam	0.439	0.065	0.506	1.663	$2.11 \cdot 10^{-6}$	2700 [3]	2.5 [3]	871 [3]

[1] ROSETTA class average parameters (*Schaap et al.*, 2001).
[2] *Bachmann et al.* (2001).
[3] *Ochsner et al.* (2001).

4.3   Methods

4.3.1   Methods: SNOWPACK Simulations

SNOWPACK is a one-dimensional physics based multi-layer snow cover model (*Lehning et al.*, 2002a,b). In *Wever et al.* (2014) (see Chapter 2), an implementation for Richards Equation (RE) for snow covers is shown to improve modelling liquid water flow in snow from the perspective of snowpack runoff. The solver is also applied in soil, such that SNOWPACK solves both the heat advection equation and RE for the snow-soil continuum. In Chapter 3, the revised soil module is discussed in more detail, including the treatment of phase changes in soil. Water retention curves in the SNOWPACK model are based on the van Genuchten model (*van Genuchten*, 1980). For snow, the water retention curve from *Yamaguchi et al.* (2012) is used. For soil, the model has predefined soil types, coupled to the ROSETTA class average parameters (*Schaap et al.*, 2001).

For the stations SLF2, Uf den Chaiseren and Grossalp, a continuous, high-quality data set for meteorological conditions as well as soil moisture measurements is available. Moreover, continuous snow height measurements allow to estimate precisely the amount of snowfall in winter and, consequently, provide an accurate estimation of maximum snow water equivalent and snowmelt in spring (see Chapter 3). A limitation is that these are all valley stations. Stand-alone SNOWPACK simulations were performed for these three stations to validate the SNOWPACK model itself and the model set-up. These simulations provided the basis for setting up the Alpine3D model. When installing the soil moisture sensors, observations of soil types were made. From these, it was assumed that for the area around Davos, a top layer of 60 cm with silt loam, followed by a deeper layer of sandy loam, best describes the soil state. To determine thermal properties of the soil, literature values were taken (Table 4.3). For thermal conductivity, a wide range of values is reported and a strong dependence with water content is present. We used values corresponding to typical soil saturation values, based on work by *Ochsner et al.* (2001) and *Bachmann et al.* (2001)

Table 4.4: Land use classes and corresponding soil initialisations.

Land use class	Area (%)	Soil 0-60 cm	Soil 60-300 cm
Rock	29.2	loamy sand	loamy sand
Alpine meadow	21.1	silt loam	sandy loam
Rough pasture	15.5	silt loam	sandy loam
Mixed forest	12.9	silt loam	sandy loam
Bush	7.3	silt loam	sandy loam
Bare soil	6.0	silt loam	sandy loam
Glacier, ice, firn	3.2	ice	ice
Pasture	2.6	silt loam	sandy loam
Water	1.0	water	water
Settlements	0.8	stone	stone
Road	0.5	stone	stone
Wetland	0.1	silt loam	sandy loam
Vegetables	<0.1	silt loam	sandy loam

For the simulations, atmospheric stability was taking into account when calculating the turbulent heat fluxes, parametrising incoming longwave radiation using air temperature, relative humidity and incoming shortwave radiation following *Unsworth and Monteith* (1975). For SLF2 and Uf den Chaiseren, a roughness length of 0.015 m was used, whereas for Grossalp, a roughness length of 0.002 m was taken. The higher roughness length at SLF2 and Uf den Chaiseren is motivated by the fact that those two stations are below the tree line and have trees and buildings in close vicinity.

4.3.2 Methods: Alpine3D Simulations

Alpine3D is a model system that describes surface processes in complex terrain (*Lehning et al.*, 2006). The main component of the model consists of distributed SNOWPACK simulations for snow and soil. For describing the highly spatial variability in incoming and outgoing long and shortwave radiation, including shadowing effects and the surface reflections of shortwave radiation, a detailed energy balance module is available (*Michlmayr et al.*, 2008). An additional module considers drifting snow (*Lehning et al.*, 2008; *Mott et al.*, 2010), including sublimation processes (*Groot Zwaaftink et al.*, 2013). These drifting snow modules are not used in this study, as the location of the measurement sites are not prone to significant drifting snow effects, except for the Grossalp station. Moreover, the calculation of the wind fields and snow drift is posing a high computational demand compared to the other modules. The different modules and the coupling strategy is described in *Lehning et al.* (2006).

The Alpine3D simulations were run for a domain of 21.5 km×21.5 km with a grid cell size of 100 m×100 m, giving a total size of 215 × 215 grid cells. The model was run in hourly time steps, providing meteorological forcing data per time step for each pixel by interpolating from the meteorological stations in and just outside the Davos area using the MeteoIO library (*Bavay and Egger*, 2014). At IMIS stations and at WFJ, snowfall was determined by the increase in measured snow height (*Lehning et al.*, 1999), when a snow cover was present. Otherwise, the

heated rain gauges in Davos and Weissfluhjoch and the measured precipitation from IMIS stations that are equipped with a rain gauge were used to determine precipitation amounts. These precipitation amounts were interpolated over the grid by inverse distance weighting (IDW), taking into account the altitudinal gradient. This interpolation scheme ensures that both the altitudinal and spatial variability in precipitation patterns are present. By using a temperature threshold of 1.2 °C, precipitation was separated into rain and snowfall.

Air temperature, relative humidity and wind speed were also interpolated over the grid, using the station data as indicated in Table 4.2 and applying IDW with lapse rates calculated from the available data. Only IMIS stations were used for spatial interpolations, except for the radiation components. Incoming longwave radiation is measured at two stations, and was distributed over the grid using the same methods as mentioned before. Incoming shortwave radiation was provided by the radiation module, using the measurements from Weissfluhjoch. The radiation balance is closed by the SNOWPACK simulations at each grid points, when SNOWPACK calculates the surface temperature and surface albedo.

Two important components to initialise Alpine3D simulations are the digital elevation model (DEM) for the Davos area, provided by the Swiss Federal Office of Topography (swisstopo). Also the soil has to be initialised for each pixel, although limited information is available. We based soil properties on the land use classification, as provided by swisstopo (*Zappa et al.*, 2003). Table 4.4 lists the land use classes, the percentage of areal coverage in the simulated area and the soil initializations. Pixels that were defined as glacier, ice, firn, road, settlements, rivers and lakes (6%) were initialised in a state that represents the land use class, but liquid water transport in soil was handled by a bucket-type scheme. Those pixels are excluded from the analysis presented here. Pixels defined as rocky surface (i.e., vegetation-free) (29%) were initialised uniformly with loamy sand. This is based on observations when installing soil temperature sensors at the WFJ, which is located in the rock class. All other pixels (65%), including forests, meadows, pasture, bare soil, and occasional pixels that are defined as agricultural use were initialised using an upper layer of 60 cm consisting of silt loam and a lower layer of 240 cm consisting of sandy loam. This choice is based on observations when installing the soil moisture sensors at the IRKIS and SensorScope stations. The soil permeability classification provided by the Swiss Federal Office for Agriculture (FOAG) shows generally high permeability in the area surrounding Davos, which confirms the choice for soil types with no clay content.

A soil depth of 3 m was simulated, subdivided into 23 layers. The layer spacing was 2 cm near the surface, increasing to 40 cm at 3 m depth. The densely spaced surface layers are necessary to describe the large gradients of temperature and moisture occurring in this region. The lower boundary condition at 3 m depth was taken as a water table condition for the liquid water flow. The roughness length was defined to be 0.015 m below 1900 m altitude and 0.002 m otherwise. This division is based on the stand-alone SNOWPACK simulations and is in line with the generally rougher terrain below 1900 m, due to the presence of trees or large bushes, whereas above 1900 m, mainly meadows and scree fields are present.

Alpine3D has recently been extended with MPI support, allowing for the parallelisation of the distributed SNOWPACK and energy balance simulations. Using 36 CPU cores, the computation took on average 14 hours for a single year, mainly depending on snow height in the winter season.

4.3.3 Analysis

The soil moisture measurements series were first cleaned from erroneous data, like negative values, or data from broken sensors. Then, data was aggregated to hourly and daily time scales by calculating average soil moisture contents. To quantify the spatial variability in the soil moisture measurements, cross correlations were calculated between all soil moisture stations using daily average soil moisture. This was done for 10, 30 and 50m depth and for both sensors per depth individually. Per depth, the highest correlation found between either one of the two sensors at each site was used in further analysis.

From the simulations, the modelled soil moisture values were extracted for each depth at which also measurements were taken. The output resolution was 1 hour and also here, daily values were calculated by averaging the hourly values. The spatial variability in the simulations was also quantified by calculating cross correlations between modelled daily average soil moisture at each combination of two measurement sites.

As the area of Davos is dominated by snowfall in winter, a separation is made for yearly, summer and winter periods. The summer months are defined as the period from June through September. At the altitude of the soil moisture stations, snow fall episodes are almost absent and the winter snow cover has melted completely in these months. The winter months are defined as the period from November through May, when a snow cover is present. Note that typically, the snow cover melts away in April or May and in those months, the soil moisture is expected to be strongly influenced by the snowmelt from the snowpack.

The streamflow from the Dischmabach has been successfully simulated using the PREVAH model framework coupled to Alpine3D (*Zappa et al.*, 2003; *Lehning et al.*, 2006). Recently, a travel time distribution approach has been introduced, as outlined in *Comola et al.* (2014). In this study, the latter will be used to relate spatially explicit soil water fluxes in 55 sub-catchments to streamflow at the outlet of the Dischma catchment. Three approaches are followed: taking the water flux at the top of the soil, or the water flux in the soil at 30 or 60 cm depth as input for the travel time based water routing scheme. The travel time distribution approach separates the soil in an upper and lower component, where the upper represents the fast response and the lower the slow response. The method has three constants that require calibration: the standardized average travel time of the upper and lower soil compartment (day) and the maximum recharge rate of lower compartment from upper compartment (mm day^{-1}). Here, both approaches are independently calibrated with measured streamflow from October 2010 to September 2012, using Monte-Carlo simulations. The best combination of coefficients was determined based on the highest Nash-Sutcliffe Model Efficiency (NSE)

coefficient (*Nash and Sutcliffe*, 1970). The period from October 2012 - September 2013 was used for validation.

4.4   Results and Discussion

4.4.1   Snow Height

The upper panels in Figures 4.3, 4.4 and 4.5 show snow depth development in both the stand-alone SNOWPACK simulations as well as the Alpine3D simulations for stations SLF2, Uf den Chaiseren and Grossalp, respectively. As the stand-alone SNOWPACK simulations were snow height driven, the snow height as simulated by SNOWPACK closely follows measured snow height. Measured snow height itself is not shown. The snow height differences between SNOWPACK and Alpine3D simulations provide a validation for the interpolation scheme for precipitation used in Alpine3D.

In snow season 2011 and 2013, the snow height in the Alpine3D simulations is satisfyingly reproduced at both SLF2 and Uf den Chaiseren. The snow height at Grossalp is overestimated in all snow seasons. This is explained by the fact that that site is relatively sensitive to snow drift eroding the snow surface. Snow season 2012 is overestimated at all stations, which is related to unusual meteorological circumstances of large snow falls accompanied by strong winds. Apparently, this situation is not well captured in the interpolation scheme. Nevertheless, the snow cover development at those three sites is overall satisfactorily simulated in Alpine3D.

4.4.2   Soil Moisture Measurements and Simulations

Figures 4.3-4.9 show measured and simulated soil moisture time series at all depths for the 7 stations in the area of Davos. Temporal variations in soil moisture in the area of Davos are clearly dominated by winter periods, in which the presence of a snow cover reduces water influx at the top of the soil for several months. This phase is followed by the snowmelt phase in spring, when liquid water draining from the snowpack is providing liquid water again to the soil. The summer months are snow-free, and soil moisture measurements show fluctuations on short time scales of a few days, related to rainfall and evaporation.

At several stations, soil freezing is indicated by the soil moisture sensors. Significant soil freezing was occurring in snow season 2011, as clearly indicated at SLF2 (Figure 4.3), Uf den Chaiseren (Figure 4.4) and Stillberg (Figure 4.6). The soil freezing was promoted by a long period with no snow or only a shallow snow cover, allowing the soil to cool. For the stations SLF2 and Uf den Chaiseren, the onset of the freezing is rather well predicted in both the SNOWPACK stand-alone as the Alpine3D simulations. At most stations, the soil freezing front does not seem to reach the sensor at 30 cm. Only at Uf den Chaiseren and Stillberg, the minimum soil moisture at this depth in this particular snow season is slightly lower than in the other snow seasons, which may be indicative of slight soil freezing here.

Figure 4.3: Soil moisture measurements (denoted MSR) and simulations with SNOWPACK stand-alone (denoted SNP) and Alpine3D (denoted A3D) at the IRKIS station SLF2, for (from top to bottom) 10, 30, 50, 80 and 120 cm depth. In the upper panel, also simulated snow height is shown.

119

Figure 4.4: Soil moisture measurements (denoted MSR) and simulations with SNOWPACK stand-alone (denoted SNP) and Alpine3D (denoted A3D) at the IRKIS station Uf den Chaiseren, for (from top to bottom) 10, 30, 50, 80 and 120 cm depth. In the upper panel, also simulated snow height is shown.

Figure 4.5: Soil moisture measurements (denoted MSR) and simulations with SNOWPACK stand-alone (denoted SNP) and Alpine3D (denoted A3D) at the IRKIS station Grossalp, for (from top to bottom) 10, 30, 50, 80 and 120 cm depth. In the upper panel, also simulated snow height is shown.

Figure 4.6: Soil moisture measurements (denoted MSR) and simulations with SNOWPACK stand-alone (denoted SNP) and Alpine3D (denoted A3D) at the SensorScope station Stillberg, for (from top to bottom) 10, 30 and 50 cm depth. In the upper panel, also simulated snow height is shown.

Figure 4.7: Soil moisture measurements (denoted MSR) and simulations with SNOWPACK stand-alone (denoted SNP) and Alpine3D (denoted A3D) at the SensorScope station Pischa, for (from top to bottom) 10, 30 and 50 cm depth. In the upper panel, also simulated snow height is shown.

Figure 4.8: Soil moisture measurements (denoted MSR) and simulations with SNOWPACK stand-alone (denoted SNP) and Alpine3D (denoted A3D) at the SensorScope station Dorfji, for (from top to bottom) 10, 30 and 50 cm depth. In the upper panel, also simulated snow height is shown.
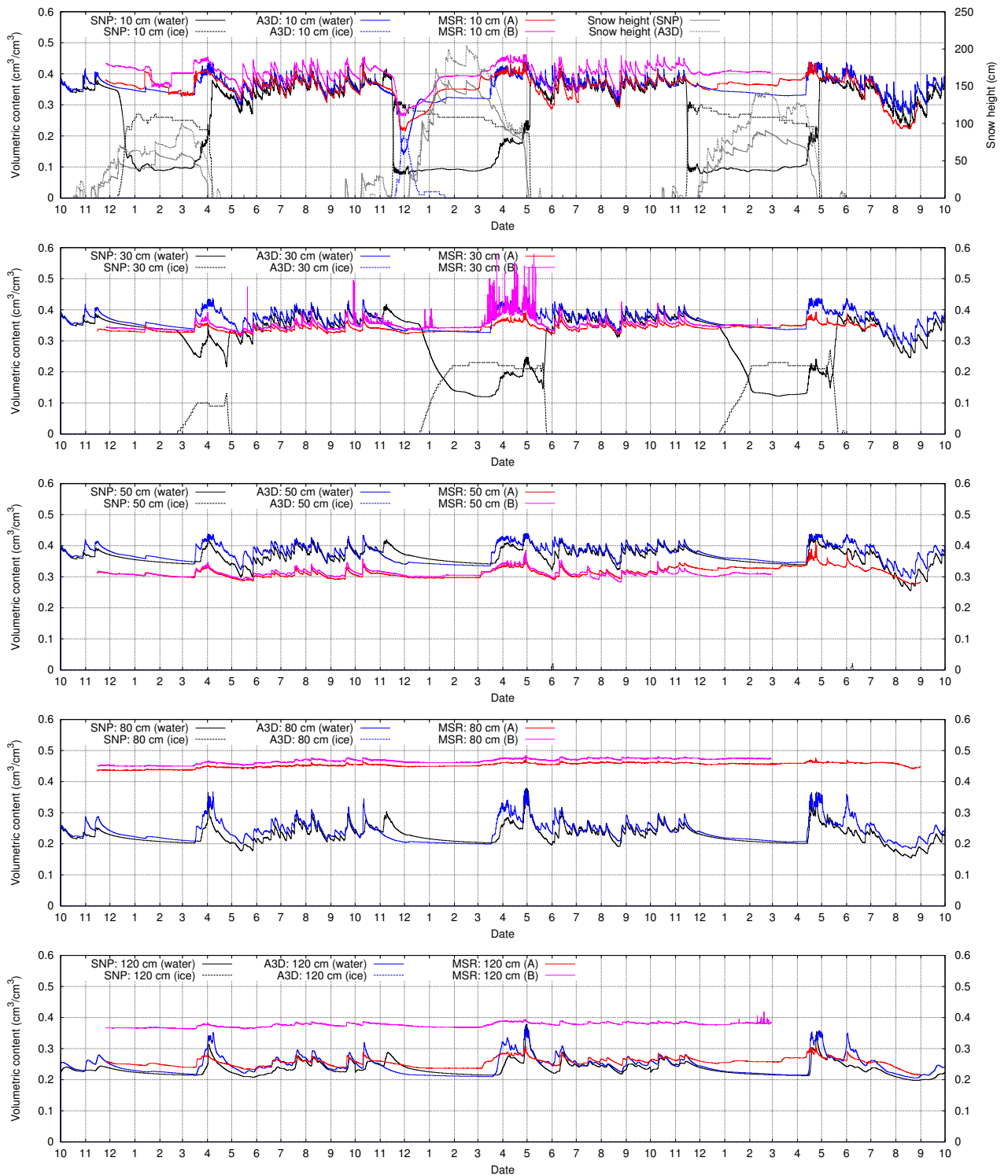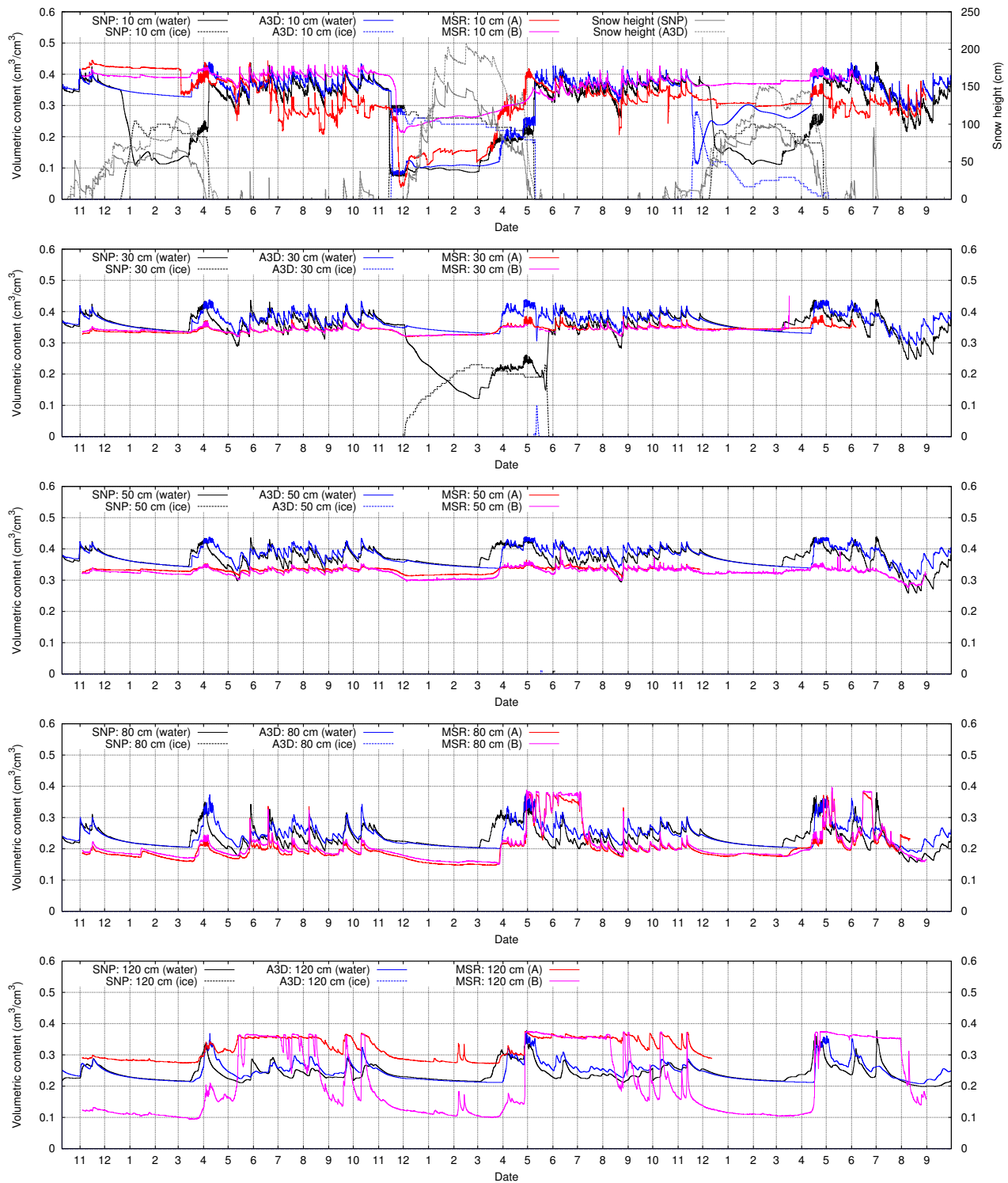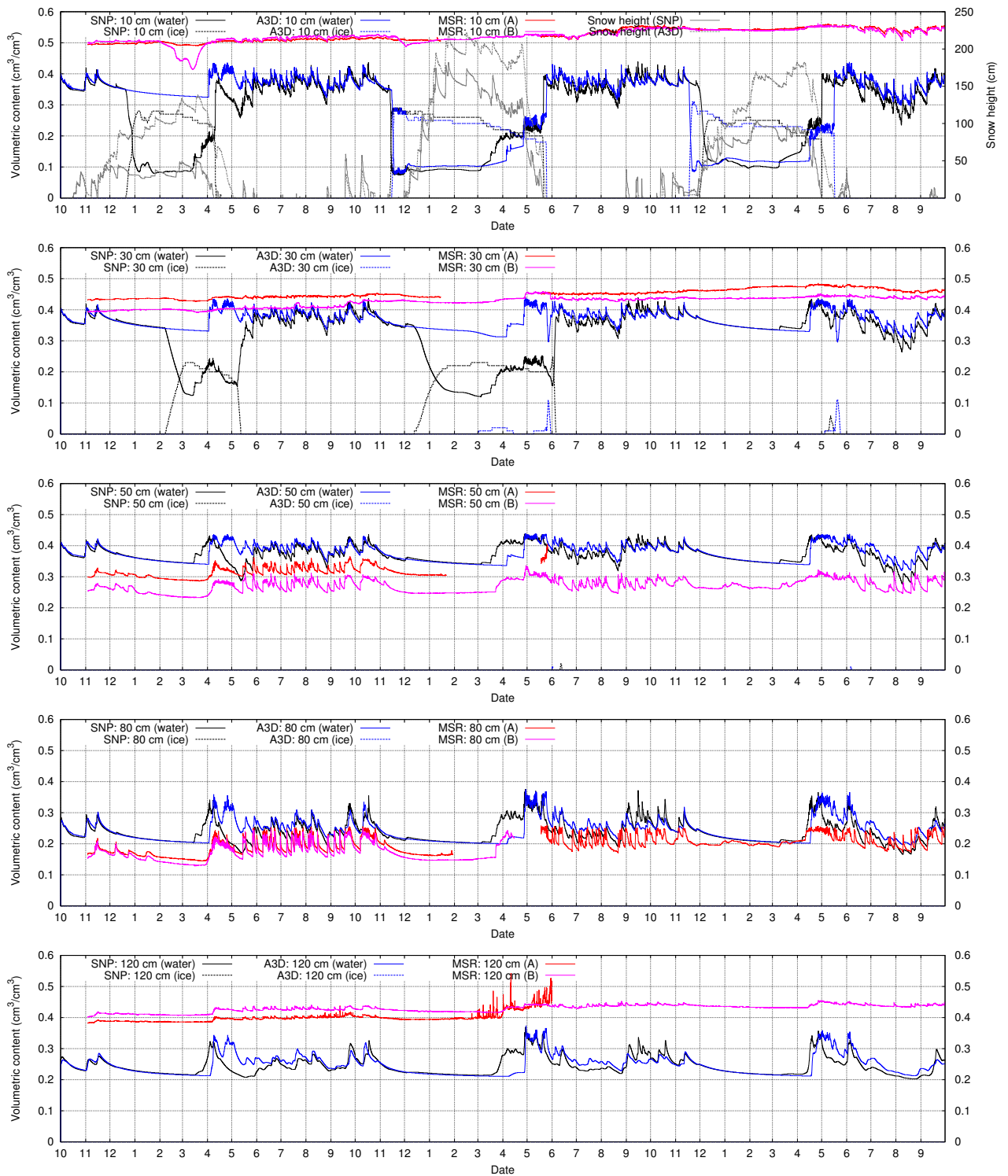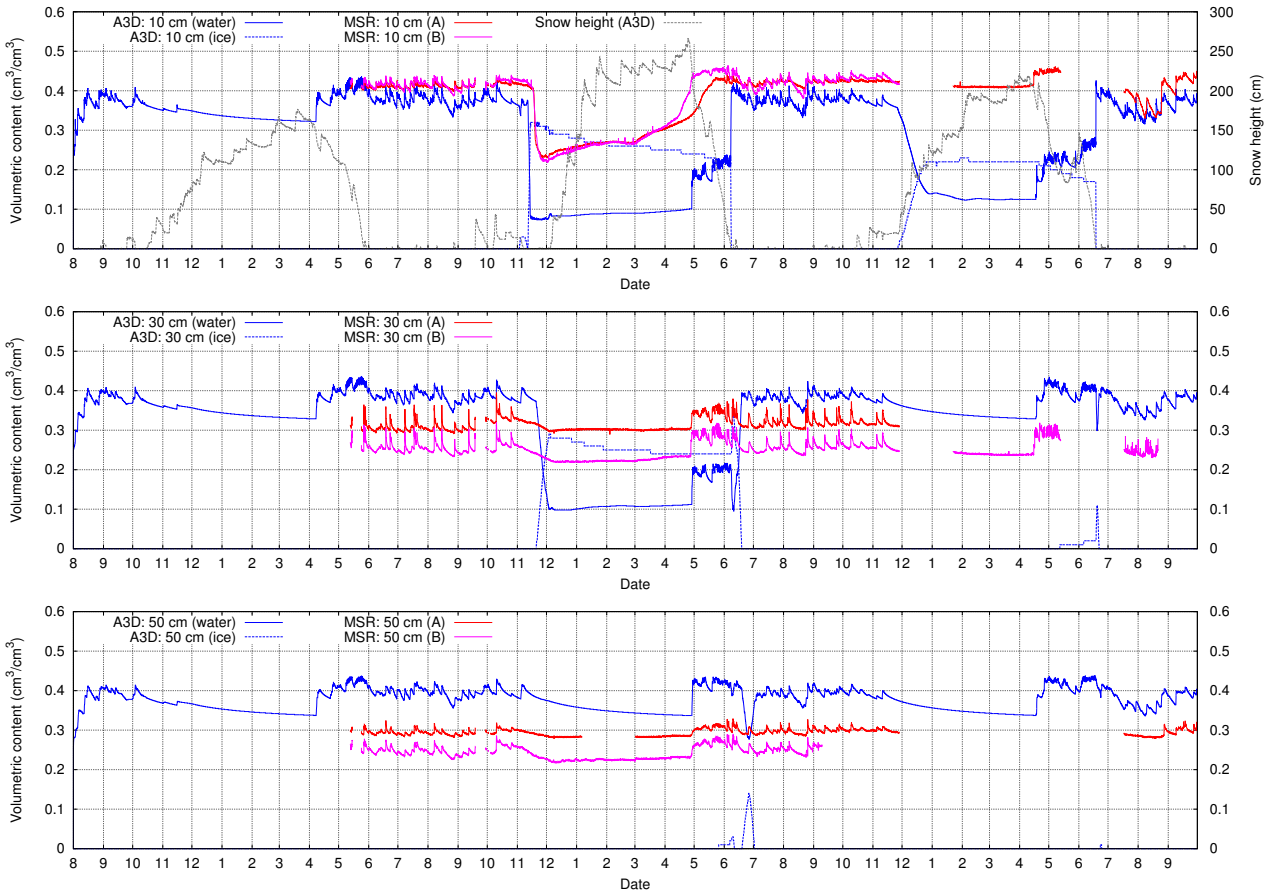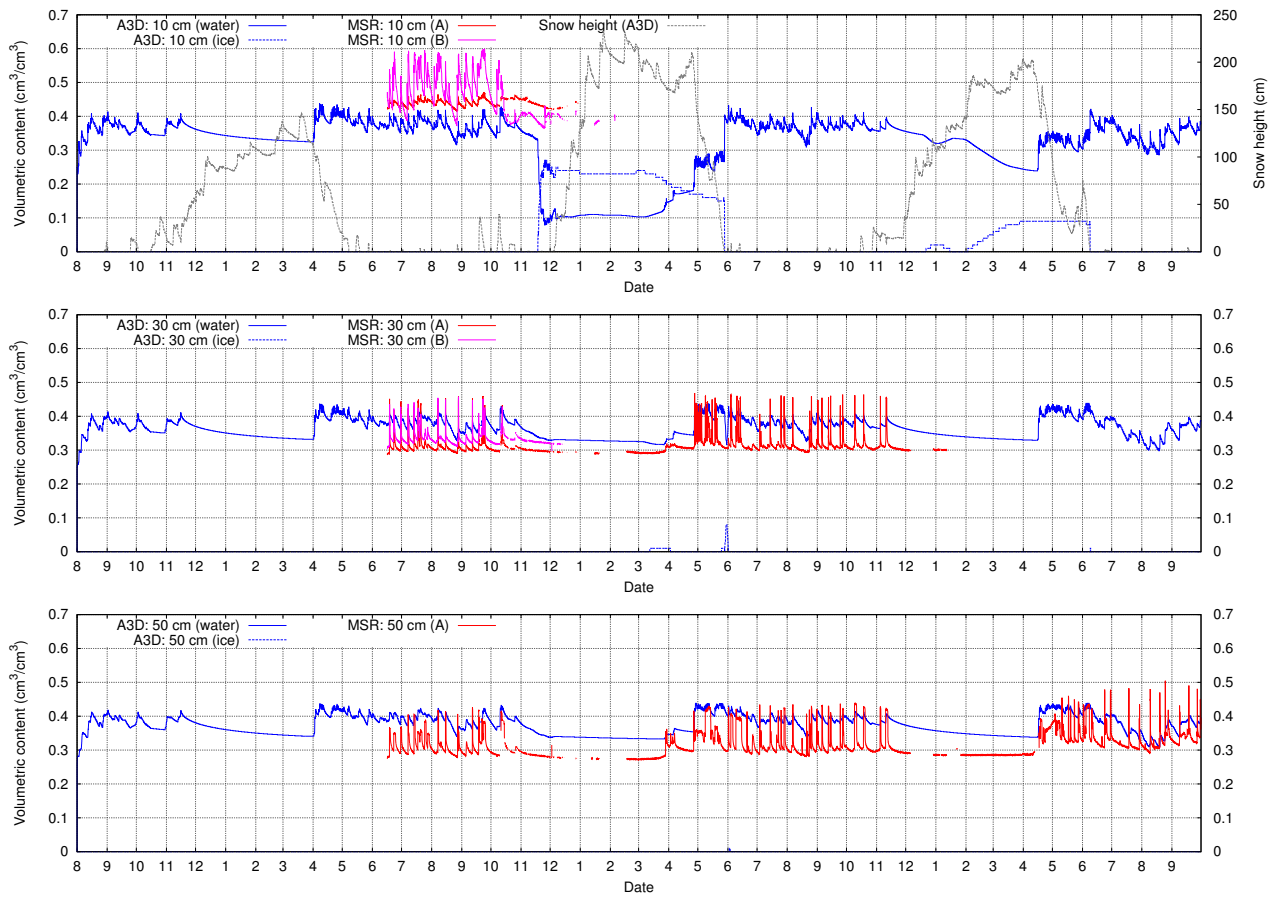
Figure 4.9: Soil moisture measurements (denoted MSR) and simulations with SNOWPACK stand-alone (denoted SNP) and Alpine3D (denoted A3D) at the SensorScope station Golf Course, for (from top to bottom) 10, 30 and 50 cm depth. In the upper panel, also simulated snow height is shown.

The simulations show soil freezing at 10 cm depth in all snow seasons at most stations, for at least a short period of time. The stand-alone SNOWPACK simulations produced more soil freezing than Alpine3D simulations. Apparently, the local atmospheric forcing at the individual sites, which is used in the SNOWPACK simulations, is favouring soil freezing conditions. As an hypothesis, cold pools that form at night near the valley bottom may not be captured by the interpolations from neighbouring stations in the Alpine3D simulations. The overestimation of soil freezing in the simulations may also be partly related to neglecting the presence of vegetation at the measurement sites. All sites are covered by grass, or rough pasture. To account for the insulating effects of the canopy, some soil freezing schemes consider the presence of a canopy when calculating soil phase changes (e.g., *Giard and Bazile* (2000)). Due to the lack of possible validation data, we did not implement this. Furthermore, the amount of soil freezing is also dependent on the amount of liquid water available. At stations Grossalp and Golf Course, the soil is wetter than simulated, which would require a higher heat flow out of the soil before freezing may start. Finally, uncertainties in soil thermal properties may play a role.

The relatively dry summer of 2013 at low altitudes, as was indicated by the difference in summer precipitation from both heated rain gauges (Table 4.1), is clearly visible in the simulations by a drop in soil moisture at all depths, reaching the lowest values of the entire measurement period. Unfortunately, soil moisture sensors had stopped working at many stations by this time, but at the site SLF2 and Stillberg, a good correspondence is found in the 10 cm soil measurement series. At the Uf den Chaiseren site, the recession curve in this summer is particularly present at the sensors at 50 and 80 cm depth, and absent in the highest sensor.

Some features are found that likely relate to hydrological processes that are not simulated in the Alpine3D and SNOWPACK models. For example, at the Uf den Chaiseren site, the soil moisture at 80 and 120 cm is clearly influenced by a rising water table in the late snowmelt season. This is indicated by the sudden rise to high values of saturation, remaining constant afterwards (Figure 4.4). The soil at the Golf Course station appeared to be close to saturation for extended periods of time (Figure 4.9. The location close to the Landwasser river, which is partly fed by meltwater from the glacierised area, supports this interpretation. The apparent interaction with ground water levels at these stations is not considered in the simulations. Similarly, the measurements at 10 and 30 cm depth at the Grossalp station also indicate high saturation of the soil, for which no source of water could be found. Due to the insensitivity of the soil moisture sensors in wet soil conditions, discrepancies between simulations and measurements as found at the sites Grossalp and Golf Course can only be assessed qualitatively and provide insights on the limitations of the measurements and simulations. In contrast with the other measurement sites, the soil moisture sensors at the Pischa station show a very dynamic response (Figure 4.7). We cannot exclude that during the installation of the sensors, the soil was disturbed in such a way that afterwards, efficient preferential flow paths occurred along the boundaries of the displaced soil layers.

In Table 4.5, the bias between measured and simulated soil moisture as well as the correlation

Table 4.5: Statistics of soil moisture simulations and measurements. The letter in the brackets denote the analysed measured soil profile. The choice was made by favouring the longest available record and/or the record showing the highest correlation.

Station	Bias	r^2	Bias	r^2	Bias	r^2
	all months		summer (Jun - Sep)		winter (Nov - May)	
10 cm, SNOWPACK stand-alone						
SLF2 (A)	-0.102	0.21 (6.78)	-0.005	0.93 (47.66)	-0.164	0.30 (7.86)
Uf den Chaiseren (B)	-0.084	0.68 (28.62)	-0.035	0.60 (12.02)	-0.110	0.64 (21.19)
Grossalp (A)	-0.252	0.12 (3.55)	-0.181	-0.06 (-1.10)	-0.314	-0.03 (-0.71)
10 cm, Alpine3D						
SLF2 (A)	-0.001	0.74 (35.28)	0.019	0.90 (37.78)	-0.011	0.80 (33.04)
Uf den Chaiseren (B)	-0.054	0.86 (51.86)	-0.007	0.33 (5.67)	-0.077	0.88 (47.02)
Grossalp (A)	-0.220	-0.23 (-7.29)	-0.159	-0.07 (-1.35)	-0.271	-0.53 (-14.13)
Dorfji (A)	0.018	0.05 (1.29)	0.089	0.74 (16.85)	-0.042	0.32 (6.43)
Golf Course (A)	-0.028	0.66 (14.41)	-0.032	0.53 (5.62)	-0.026	0.66 (12.02)
Pischa (A)	-0.109	0.58 (9.59)	-0.068	0.76 (11.88)	-0.230	0.85 (10.39)
Stillberg (A)	-0.119	0.70 (26.92)	-0.043	0.39 (7.52)	-0.197	0.63 (15.49)
50 cm, SNOWPACK stand-alone						
SLF2 (A)	0.049	0.59 (23.28)	0.049	0.63 (15.00)	0.047	0.61 (19.25)
Uf den Chaiseren (B)	0.041	0.69 (30.33)	0.027	0.83 (27.21)	0.047	0.63 (20.49)
Grossalp (A)	0.052	0.54 (13.57)	0.054	0.78 (13.52)	0.052	0.27 (4.77)
50 cm, Alpine3D						
SLF2 (A)	0.062	0.54 (20.25)	0.073	0.62 (14.58)	0.055	0.59 (18.08)
Uf den Chaiseren (B)	0.051	0.78 (40.10)	0.057	0.89 (36.07)	0.047	0.72 (25.83)
Grossalp (B)	0.107	0.71 (33.19)	0.113	0.74 (20.87)	0.103	0.68 (23.22)
Dorfji (A)	0.154	0.52 (15.50)	0.156	0.61 (11.82)	0.150	0.50 (10.97)
Golf Course (A)	-0.037	0.63 (20.93)	-0.031	0.48 (8.31)	-0.040	0.59 (14.65)
Pischa (A)	0.062	0.69 (25.86)	0.061	0.42 (8.75)	0.062	0.85 (29.38)
Stillberg (B)	0.137	0.76 (25.35)	0.141	0.41 (6.56)	0.133	0.86 (24.79)

coefficients are shown for daily average values. It clearly shows that soil moisture is simulated with varying degrees of success at the various sites. At 50 cm depth, all correlation coefficients are significantly positive for both summer and winter periods as well as for the full years, showing that the simulations capture the variations in soil moisture adequately. The simulated soil moisture at this depth is generally overestimated, as indicated by a positive bias.

At 10 cm depth, results are mixed. Only the Grossalp stations has no statistical significant and even a negative correlation between simulations and measurements for both seasons. This is likely related to the local wetness of the soil, as discussed earlier. All other stations show significant correlations in the summer or winter season. At the Dorfji station, the correlation for the complete period is not significant. This is in line with the results for the other stations, that show a lower correlation coefficient for the complete period, compared to the summer or winter period individually. Apparently, the simulations are less capable of reproducing the difference between winter and summer, compared to temporal variations in either the winter and melt period or the summer period. The soil at 10 cm depth is generally slightly dryer in the simulations than observed, but typically, stations with a high correlation coefficient show a smaller bias at 10 cm than at 50 cm depth.

The discrepancies in soil freezing are causing typically a higher bias in winter than in summer.
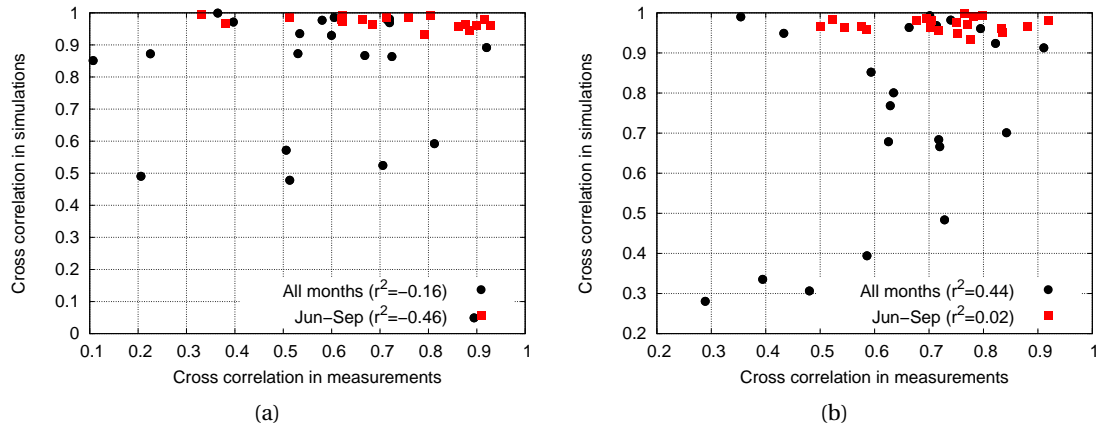
Figure 4.10: Cross correlations between sites for measurements and simulations, for 10 cm depth (a) and 30 cm depth (b). The r^2 values denote the correlation coefficients between the cross-correlations from the measurements and simulations, between the measurement sites. Only the r^2 value for 30 cm depth for all months tested significant at the 95% confidence interval using a t-test.

Nevertheless, they generally do not impact the correlation coefficients. At some stations, the correlation coefficients are even higher for the winter months, suggesting that the soil moisture variations due to the presence of a snow cover and snowmelt are better simulated than those due to rainfall and evaporation in summer.

Interestingly, stand-alone SNOWPACK simulations do not consistently provide better results than the Alpine3D simulations, even though the former uses local meteorological forcing. Alpine3D simulations typically show a higher agreement in winter, possibly related to the better agreement in soil freezing. In summer, stand-alone SNOWPACK simulations tend to provide a better agreement, which possibly is caused by using locally measured precipitation as input. In contrast, at 50 cm depth, correlation coefficients are generally higher for Alpine3D simulations than SNOWPACK simulations, also in summer. As the stand-alone SNOWPACK simulations are using locally measured meteorological conditions, a higher accuracy in soil moisture simulations should be expected. However, incoming shortwave and longwave radiation are not measured at the sites and are determined by either albedo or the *Unsworth and Monteith* (1975) parametrisation, respectively. The primary reason for this unexpected result may therefore be related to a better representation of incoming shortwave and longwave radiation by the Alpine3D model, which is using measured values inside the domain to interpolate the radiation components over the grid.

4.4.3 Spatial Variability

In Figures 4.10a and 4.10b, the cross correlations of soil moisture measurements and simulations between the 7 sites are shown for 10 and 30 cm depth, respectively. In the measurements, cross correlations vary for both the full period and the summer months only, whereas in the simulations, cross correlations only vary significantly for the full period. This strongly suggests that the spatial variability that is reproduced by Alpine3D on the yearly time scale is dominated by snow distribution and snowmelt, whereas in the summer months, spatial variability is very limited. The larger variability for the cross correlations in the measurements in the full period compared to the summer months indicates that also the soil moisture measurements exhibit a strong spatial variability based on snow cover distribution and snowmelt. However, the measurements exhibit also a clear variability in summer that is absent in the simulations.

The correlation coefficient for the cross correlation in measurements and simulations is not significant at 10 cm depth, neither for the full period, nor for only the summer period. However, at 30, and also at 50 cm depth (the latter is not shown), the correlation coefficient is significant for the full period. This indicates that the spatial variability simulated by the Alpine3D model is in agreement with the measurements. The absence of a significant correlation in the summer months strongly suggests that spatial variability in simulated soil moisture is mainly governed by processes in the winter season, i.e. snow accumulation and snowmelt. As identified above, these processes pose a strong control on the temporal evolution of measured soil moisture.

The contrasting result between 10 cm depth on the one hand and 30 and 50 cm depth on the other hand may be attributed to the overestimation of soil freezing in the simulations at 10 cm depth. Furthermore, the fast soil moisture dynamics due to large moisture and temperature gradients close to the surface as well as the influence of vegetation on soil moisture may also play a role. Another source of error may be related to the soil moisture measurements. The soil at this depth seems to exhibit high saturation at some stations (e.g., Grossalp, Golf Course and Stillberg), which is known to negatively impact the sensitivity of the Decagon 10HS sensor to soil moisture fluctuations, as discussed before.

As we determined that Alpine3D is mainly capturing the effect of spatial patterns in snow distribution and snowmelt on soil moisture, we used correlation maps to visualise this dependency for the simulated area. We considered the grid cells that represent Stillberg and SLF2, as the former is the highest soil moisture station and the latter is one of the lowest. Furthermore, Stillberg is located at a northeast slope, whereas SLF2 is on a flat site. Figure 4.11 shows the correlation map for snowpack runoff, using the grid cell representing Stillberg as the correlation point in Figure 4.11a and SLF2 in Figure 4.11b, respectively. Additionally, the correlation map for soil moisture in the top 20 cm is shown in Figures 4.11c and 4.11c for Stillberg and SLF2, respectively. Although the absolute values of the correlation coefficients differ, there is a clear correspondence in spatial patterns between the correlation maps for snowpack runoff and soil moisture. Especially flat areas (the valley bottoms) and south facing slopes are correlating with the SLF2 grid cell, for both soil moisture in the top soil layers as
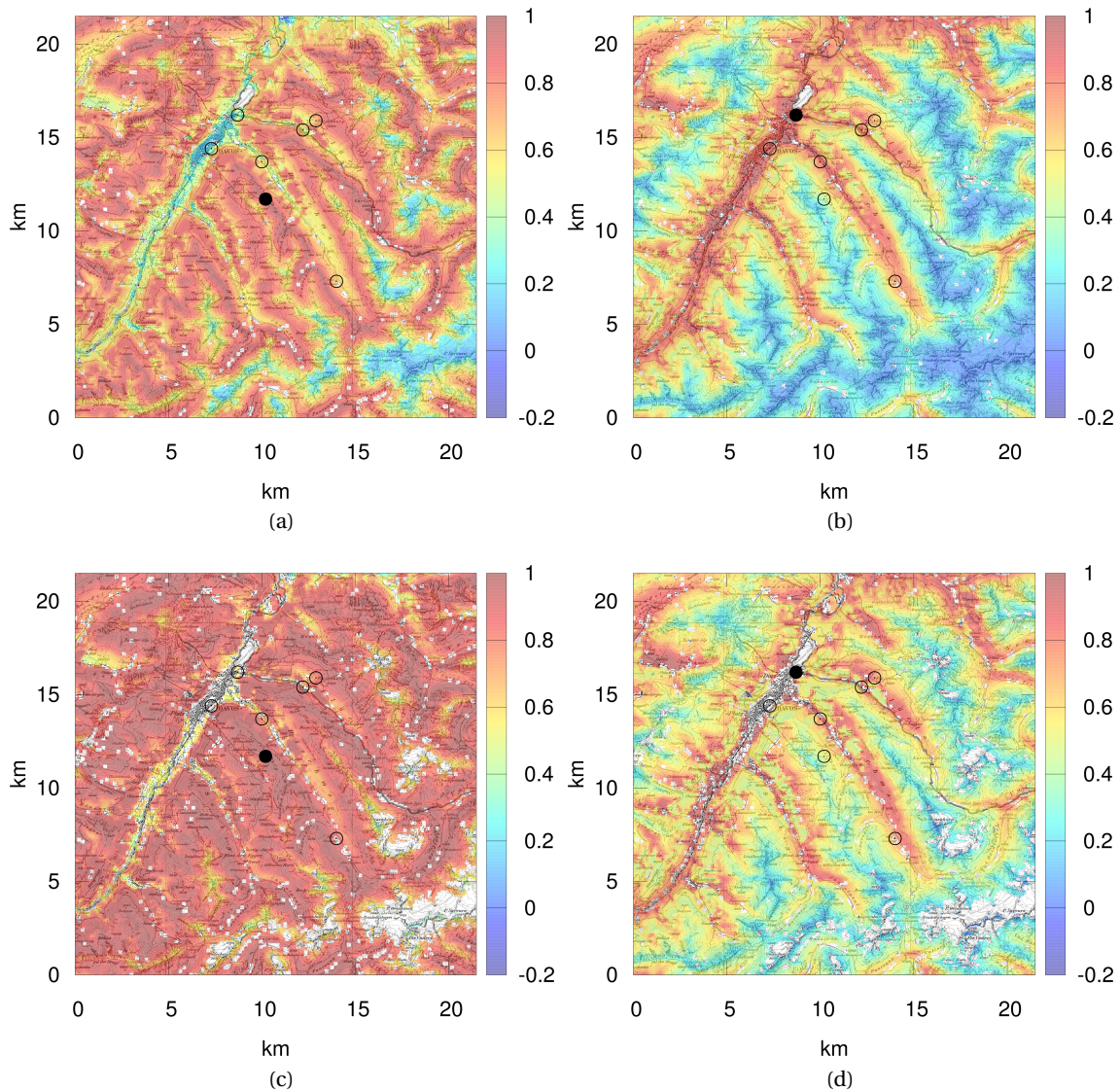
Figure 4.11: Correlation map for snowpack runoff (a, b) and soil moisture in the top 20 cm (c, d), using the grid cell representing Stillberg as correlation point (a, c) or SLF2 (b, d). The colour scale denotes the correlation coefficients. The station used as correlation station is denoted with a filled circle, the other sites with an open circle.

snowpack runoff, whereas for the Stillberg station, north facing and high altitude areas are correlating for both variables.

Interestingly, the low absolute variability in correlation coefficients for soil moisture at the Stillberg grid cell suggests that the soil moisture measurements here may be regarded representative for a much larger area than the measurements at SLF2. This conclusion is based on
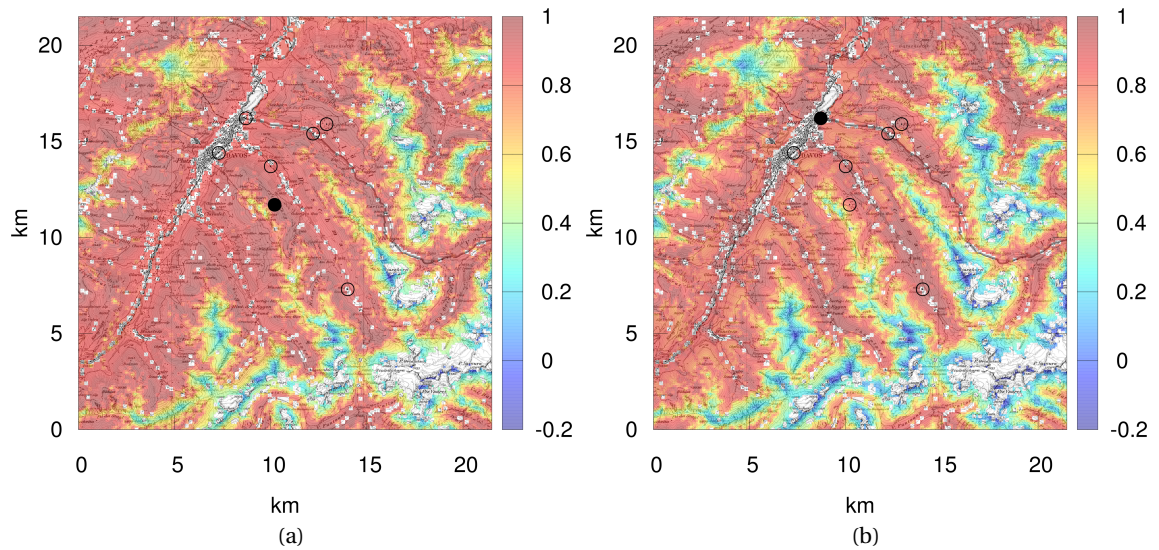
Figure 4.12: Correlation map for soil moisture in the top 20 cm in the summer months (Jun-Sep), using the grid cell representing Stillberg as correlation point (a) or SLF2 (b). The colour scale denotes the correlation coefficients. The station used as correlation station is denoted with a filled circle, the other sites with an open circle.

the simulations only, and is likely related to the fact that Stillberg is much closer to the average altitude of the simulated area than SLF2, providing a closer agreement with the average precipitation in the area.

The correlation maps for soil moisture in only the summer months (see Figures 4.12a and 4.12b) show smaller differences between the maps from both sites. This confirms the earlier conclusion that in the current model setup, Alpine3D especially captures spatial variability due to snow distribution and snowmelt. The correlation maps show that in the summer months, the spatial variability seems to be governed by altitudinal differences, which strongly suggest that vertical gradients in precipitation play a role here. However, the soil moisture measurement sites used in this study are probably spanning a too small altitudinal range to verify this result experimentally. Furthermore, the lack of spatial explicit information about soil properties is likely one of the most important error sources.

4.4.4 Streamflow

Figure 4.13 shows the measured and simulated streamflow at the outlet of the Dischmabach in the Dischma catchment. The winter periods are clearly identifiable by the hydrograph falling back to baseflow. Furthermore, high discharge is particularly found in spring, during the snowmelt season (May to July). In spring 2013, the snowmelt was interrupted by a short cooler period in June (Figure 4.2). During the summer period, streamflow slowly decreases,
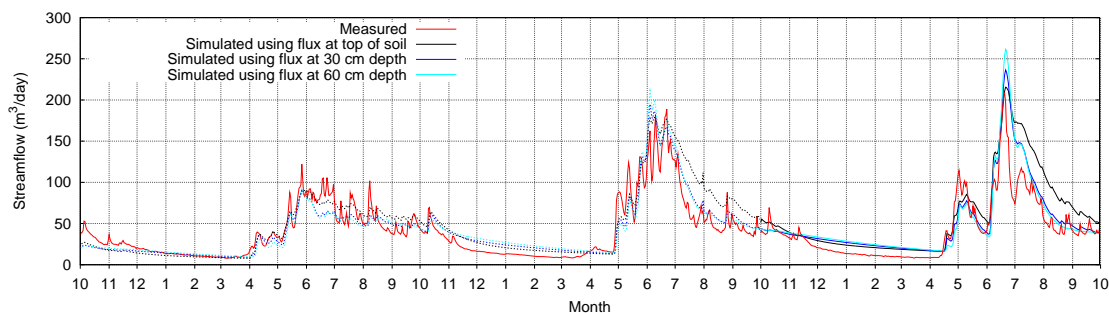
Figure 4.13: Measured and simulated daily streamflow for the outlet of the Dischmabach. Dashed lines denote the calibration period, solid lines denote the validation period.

interrupted regularly with peaks in streamflow due to rainfall. These general discharge patterns are well captured in the simulations, although the fast dynamics on daily time scales in the Dischmabach streamflow is missed in the simulations.

The three simulations of streamflow differ in the water input used for the travel time distribution approach. The main differences arise after the main snowmelt season is over, when the simulations using the water flux at 30 cm depth in the soil provide a closer agreement with the observed streamflow than the simulations using the water influx at the top of the soil. This is also expressed by the difference in overall NSE coefficient of 0.80 and 0.64, respectively. For the validation period, NSE coefficients are 0.71 and 0.45, respectively. Using the soil water flux at 60 cm depth provides an almost similar result as at 30 cm, although the NSE coefficients are slightly lower. The results suggests that the updated soil module of SNOWPACK is contributing to a better prediction of streamflow. However, the underestimation of the dynamic response on short time scales in the simulations deserves further investigation.

4.5 Conclusions

Simulations with the spatially explicit Alpine3D model were performed for the area of Davos, in which the SNOWPACK model provided the surface scheme. The recent update of the soil module of SNOWPACK shows satisfactory results for simulating soil moisture at 7 stations with soil moisture measurements in the area around Davos. The comparison included measurements at 10, 30 and 50 cm depth, and at 4 stations also at 80 and 120 cm depth. For three sites, stand alone SNOWPACK simulations were performed, using locally measured meteorological conditions. These simulations could be used to set up and validate the Alpine3D model. For those stations, simulations with both models showed a similar level of agreement with the measurements. Overall, correlation coefficients are significantly positive for most sites, showing that generally, the temporal variability is adequately captured. However, often a bias between simulated and measured soil moisture was found.

In winter, the amount of soil freezing was higher in the stand-alone SNOWPACK than in the Alpine3D simulations. The amount of soil freezing in both models seems to be overestimated compared to indications from the field data. The soil moisture measurements also provide some clear indications of fluctuations in ground water level. Ground water dynamics is not taken into account in the model. Also uncertainties in soil properties and measurements likely play an important role in discrepancies between simulations and measurements.

By analysing cross-correlations of soil moisture measurements and simulations between stations, it was found that Alpine3D is able to provide explicit information of spatial variability in soil moisture that corresponds with measurements, but that this is closely related to snow distribution and snowmelt. This is supported by a high correspondence in spatial patterns in correlation maps for snowpack runoff and soil moisture in the top of the soil. The spatially explicit information in summer is much smaller in the simulations than suggested by the cross-correlations of the measurements. In the soil moisture simulations by Alpine3D, an altitudinal gradient could be identified in summer, likely related to the altitudinal gradient in precipitation.

Attempts to relate the outflow at 30 and 60 cm depth in the soil to streamflow in the Dischma catchment using a travel time distribution approach provided a higher agreement with observed streamflow than directly using the water flux at the top of the soil. This suggests that the soil module of SNOWPACK is an important component for streamflow simulations. However, the Dischmabach exhibits strong dynamics on daily time scales, that is poorly captured in the simulations.

Acknowledgements

5 Model simulations of the modulating effect of the snow cover in a rain-on-snow event

[1] WSL Institute for Snow and Avalanche Research SLF, Davos Dorf, Switzerland.

[2] CRYOS, School of Architecture, Civil and Environmental Engineering, EPFL, Lausanne, Switzerland.

Summary

In October 2011, the Swiss Alps underwent a marked rain-on-snow (ROS) event when a large snowfall on 8 and 9 October was followed by intense rain on 10 October. This resulted in severe flooding in some parts of Switzerland. Model simulations were carried out for 14 meteorological stations in two affected regions of the Swiss Alps using the detailed physics-based snowpack model SNOWPACK. We also conducted an ensemble sensitivity study, in which repeated simulations for a specific station were done with meteorological forcing and rainfall from other stations. This allowed the quantification of the contribution of rainfall, snow melt and liquid water storage on generating snowpack runoff. In the simulations, the snowpack produced runoff about 4–6 h after rainfall started, and total snowpack runoff became higher than total rainfall after about 11–13 h. These values appeared to be strongly dependent on snow depth, rainfall and melt rates. Deeper snow covers had more storage potential and could absorb all rain and meltwater in the first hours, whereas the snowpack runoff from shallow snow covers reacts much more quickly. However, the simulated snowpack runoff rates exceeded the rainfall intensities in both snow depth classes. In addition to snow melt, the water released due to the reduction of liquid water storage contributed to excess snowpack runoff. This effect appears to be stronger for deeper snow covers and likely results from structural changes to the snowpack due to settling and wet snow metamorphism. These results are specifically valid for the point scale simulations performed in this study and for ROS events on relatively fresh snow.

5.1 Introduction

For mountain regions, the presence of a snow cover is an important factor in hydrological processes. One type of event that is still poorly understood is the behaviour of a snow cover during rainfall. These rain-on-snow (ROS) events are often accompanied by strong snow melt, due to high latent heat exchange and incoming long-wave radiation (ILWR) that reduces the radiative cooling of the snowpack (*Marks et al.*, 2001; *Mazurkiewicz et al.*, 2008). These effects increase the water available for outflow from the snowpack, which hereafter we will refer to as snowpack runoff. In this way, heavy precipitation can more easily lead to flooding events in mountainous terrain due to the additional snow melt (*Pradhanang et al.*, 2013; *Sui and Koehler*, 2001). Furthermore, rainfall reduces snowpack stability, resulting in stronger wet snow avalanche activity (*Conway and Raymond*, 1993).

This study focuses on the dynamical snowpack behaviour during a ROS event in October 2011 in the Swiss Alps. The event is described in detail in *Badoux et al.* (2013). During 8 October 2011, the passage of a cold front brought significant snowfall amounts on the north side of the Swiss Alps at altitudes above 800 m, accompanied by a strong drop in air temperature. During 9 October, the precipitation faded and cold weather remained. In the night of 9 to 10 October, the passage of a warm front brought new precipitation, mainly rain, this time accompanied by a strong increase in air temperature. The snowfall limit finally increased up to 3000 m on 10 October. This ROS event is very suitable for a case study, because it occurred on a large scale and is well captured at many measurement sites. Furthermore, the fact that it caused widespread flooding shows that the event was extreme. One region, where the snow cover was relatively shallow, was more strongly affected by flooding than a region with a deep snow cover at the onset of rain (*Badoux et al.*, 2013). An important question that arose from the event is whether there is a difference in snowpack behaviour for a shallow and a deep snow cover that may explain the difference in hydrological response in those two areas. The differences in streamflow response (*Badoux et al.*, 2013), in terms of return period, would suggest that deep snowpacks can better dampen peak outflows than shallow ones.

Studies modelling ROS events mostly analyse the daily to weekly timescales and successfully reproduce the temporal evolution of snow water equivalent over several days (*Marks et al.*, 1998, 2001). This suggests that snowpack-related processes during ROS events are sufficiently understood. Consequently, one can estimate rather precisely how much water will be available for snowpack runoff (*Marks et al.*, 1998; *Mazurkiewicz et al.*, 2008), but the temporal dynamics of the release of meltwater on the sub-daily timescales has seldom been investigated in detail. This knowledge is essential, however, to estimate the response in streamflow discharge in catchments and to assess flood risks from ROS events. In *Rössler et al.* (2014), the meteorological circumstances leading to this event have been studied in combination with a hydrological catchment scale model to simulate streamflow discharge in one of the affected areas. To reproduce the rapid peak discharge in the event, considerable recalibration of the hydrological model setup was required. For example, relatively simple single layer snow models, which are often used in hydrological model frameworks, were unable to follow the snow cover dynamics

without significant calibration of snow-related parameters for this particular situation (*Rössler et al.*, 2014).

The exact behaviour of the snow cover during ROS events is governed by complex interactions between several processes. A cold snow cover can store rain water by capillary suction and, to a lesser extent, freezing the liquid water. These processes depend on the state of the snow cover before the onset of rain. As soon as the snow cover becomes wet, strong settling has been observed (*Marshall et al.*, 1999). This settling, combined with a destruction of the snow matrix by melt, reduces the storage capacity, which may increase snowpack runoff. These counteracting processes are difficult to assess without the use of a physics-based snow cover model that includes a representation of the above processes. Here, the detailed multi-layer snow cover model SNOWPACK (*Lehning et al.*, 2002a,b) is used. The SNOWPACK model has been extended recently with a solver for the Richards equation, which provides a demonstrable improvement in modelling liquid water flow through the snow cover, especially on the sub-daily timescale (*Wever et al.*, 2014). This study aims to simulate the snow cover dynamics at individual snow stations during this event, to better understand the snowpack behaviour with respect to the production of snowpack runoff.

5.2 Methods and Data

The results in this study are achieved by simulations with the SNOWPACK model, using measurements from automated meteorological stations in the affected areas. First, the SNOWPACK model will be discussed, focusing in particular on the treatment of snow melt and liquid water flow in the model. Then the available data sets are discussed, followed by how the SNOWPACK model was set up to simulate the event using the measured meteorological data. Finally, we discuss the methods used for carrying out an ensemble sensitivity analysis and subsequent regression analysis to better understand the dynamics of snowpacks in this ROS event as simulated by the model.

5.2.1 SNOWPACK model

The physics-based snowpack model SNOWPACK was used to simulate the development of the snow cover as a 1D-column, forced with the meteorological conditions as measured by meteorological stations. The model simulates snow cover development, e.g. temperature and density profiles, phase changes, microstructural parameters, liquid water infiltration and snowpack runoff (*Lehning et al.*, 2002b,a). The simulations were done using SNOWPACK version 3.2.0 in which the solver for the Richards equation was introduced (*Wever et al.*, 2014). Furthermore, improvements were made in the treatment of the boundary conditions for the energy balance and accompanying phase changes, which may explain some discrepancies with model results presented in *Badoux et al.* (2013).

Snow melt is an important source of liquid water in the snowpack. In the SNOWPACK model,

snow melt occurs at a specific depth when the local temperature is 0 °C and excess energy is added at this depth either by heat conduction in the snow matrix or by a divergent short-wave radiation flux penetrating the snow. At the top of the snowpack, the model prescribes the energy flux as a Neumann boundary condition in the case of melting conditions in the top snow element or else as a Dirichlet boundary condition, prescribing the measured snow surface temperature. The latter ensures a better assessment of the cold content of the snowpack, although it may result in small discrepancies between changes in internal energy and the diagnosed energy balance. Prescribing the upper or lower boundary temperature may result in changes in internal energy between time steps that are not accounted for by the diagnosed top and bottom energy flux from the preceding time step.

The heat flux that is used to force the model at the top of the snowpack can be expressed as (*Lehning et al.*, 2002b):

$$Q_{\text{sum}} = Q_{\text{LWnet}} + Q_{\text{S}} + Q_{\text{L}} + Q_{\text{P}}, \tag{5.1}$$

where Q_{sum} is the prescribed flux (W m^{-2}) for the Neumann boundary condition at the upper boundary, Q_{LWnet} is the net long-wave radiation (W m^{-2}), Q_{S} is the sensible heat (W m^{-2}), Q_{L} is the latent heat (W m^{-2}) and Q_{P} is the heat advection by liquid precipitation (W m^{-2}). The net short-wave radiation absorbed by the snowpack is not incorporated in the Neumann boundary condition for the temperature equation, as it is modelled as a source term in the top layers of the snowpack to reflect the penetration of short-wave radiation in the snowpack.

Water transport in snow is governed by capillary suction and gravitational drainage (*Marsh*, 2006). Two common model approaches for liquid water flow in snow are the so-called bucket scheme and Richards equation (*Wever et al.*, 2014). In the bucket scheme, downward water transport is determined by the presence of an excess liquid water content above a defined threshold water content in a specific layer. This excess water is transported downwards regardless of the storage capacity of lower layers. In the Richards equation, the balance between gravity and capillary suction is explicitly calculated. It yields performance improvement over the bucket approach on both daily and hourly timescales (*Wever et al.*, 2014). However, solving the Richards equation may be expected to especially improve the simulation of water flow in seasonal snow covers, where snow stratigraphy can have a marked influence on the water flow. Differences in grain sizes can lead to capillary barriers and ice lenses may block the water flow, resulting in ponding (*Marsh*, 1999; *Hirashima et al.*, 2010a). For this ROS event, the snow cover built up in two days, leading to a very homogeneous stratification.

The hydraulic properties of the snowpack, as used for solving the Richards equation, are expected to have changed as follows due to the wet snow metamorphism of the initially fresh, dry snow:

- Fresh, dry snow has generally a dendritic structure and thereby a high capillary suction. Old and wet snow on the other hand has coarse, rounded grains accompanied by lower capillary suction. In the water retention curve proposed by *Yamaguchi et al.* (2010), dendricity is not explicitly taken into account. However, SNOWPACK initialises new snow layers with small grains and these layers thereby exhibit also higher suction than melt forms or old snow in the simulations.

- The saturated hydraulic conductivity increases with grain size, but decreases with density. In wet snow metamorphism, both grain growth and densification are occurring. However, in the simulations in this study, saturated hydraulic conductivity following *Calonne et al.* (2012) was increasing during the event (not shown).

- Snow melt destroys the ice matrix locally and in wet snow, also settling and densification occur. When the matrix to store water is decreasing in volume due to snow melt and/or settling, this leads to a decrease in storage capacity and is expected to cause additional snowpack runoff.

5.2.2 Data

The behaviour of the snow cover during this ROS event is studied for two parts of the Swiss Alps: the Bernese Oberland and Glarner Alpen (Fig. 5.1). These areas were chosen because in particular the Bernese Oberland and to a lesser extent the Glarner Alpen experienced serious flooding (*Badoux et al.*, 2013). The studied areas are both about $1000\,km^2$. Both areas are located on the north side of the Alps and extend more or less over a similar altitude range, with glaciated areas in the highest parts. They are about $100\,km$ apart, and, as will be shown, have experienced different meteorological forcing conditions.

In both areas, several automated weather stations are operated in the IMIS network. The stations measure meteorological and snow cover conditions at $0.5\,h$ resolution. They are equipped with wind speed and direction, temperature, relative humidity, surface temperature, soil temperature, reflected short-wave radiation and snow height sensors. The stations are also equipped with an unheated rain gauge, which makes the precipitation measurements at the stations unreliable in case of snowfall and mixed precipitation. In both the Bernese Oberland and Glarner Alpen, seven stations were selected for this study (14 in total), as shown in Fig. 5.1 and listed in Table 5.1. These particular stations were selected because they represent the altitudinal gradient in the two regions and had limited missing values during the event. The sites are located in relatively flat terrain. The data have been quality checked manually and missing values were interpolated from neighbouring stations (*Badoux et al.*, 2013). Most corrections were needed for wind speed, as the relatively wet snow caused the wind speed

sensor to freeze at some stations. For interpreting the results, it is important to note that the average altitude of the analysed stations in the Glarner Alpen is about 270 m lower than in the Bernese Oberland.

For this study, the model was forced to interpret increases in measured snow height at the IMIS stations as snowfall (following *Lehning et al.*, 1999), deriving the new snow density from a parameterised relationship with wind speed, temperature and relative humidity (*Schmucki et al.*, 2014). The unheated rain gauges at the IMIS stations are not useful during these types of events, so to estimate rainfall, a different approach was followed. The Swiss Federal Office of Meteorology and Climatology (MeteoSwiss) is operating weather stations with a heated rain gauge (SwissMetNet stations). Combined with several totalisers for precipitation, which are read off once per day, these precipitation measurements are compiled in a gridded data set (RhiresD, *MeteoSwiss*, 2013) at 2 km resolution with daily precipitation sums (06:00–06:00 UTC). To estimate the liquid precipitation input at an IMIS station, the daily sum derived from the nine grid points closest to the IMIS station in the RhiresD gridded data was distributed over the day by using the relative amounts of precipitation registered by the closest SwissMetNet station. The rainfall started after 18:00 UTC on 9 October and consequently, all precipitation values before this time are set to zero, as snowfall is determined separately from the snow height measurements.

To validate the model performance for the chosen methods and data preparation procedures, data from the experimental site Weissfluhjoch (WFJ), located at 2540 m altitude in east Switzerland near Davos (Fig. 5.1), were also used in this study. The course of the ROS event at this measurement site was quite similar to the 14 chosen IMIS stations, although both snowfall and rainfall amounts were smaller. At WFJ, both incoming and outgoing long- and short-wave radiation are available in addition to the default IMIS-type station setup, enabling a full assessment of the surface energy balance (abbreviated below as full EB). Furthermore, the site is equipped with a heated rain gauge that is part of the SwissMetNet network and a snow lysimeter that measures snowpack runoff (*Wever et al.*, 2014), enabling the validation of simulated snowpack runoff.

5.2.3 Model Setup

The model was initialised with 10 soil layers of 1 cm each. This allows the measured soil temperature at the lower boundary to be prescribed and, thereby, an estimate of the soil heat flux to be achieved. To allow for a spin-up period, the model simulations were started at 2 September, 6 weeks before the event. We consider this to be sufficient time for a soil of 10 cm depth. For soil parameters, typical values for very coarse material were chosen (similar to *Wever et al.*, 2014). Furthermore, a free drainage lower boundary condition was used. This combination prevents liquid water ponding in the soil or snow. We hypothesise that this is generally not happening in the sloped terrain in the Swiss Alps, where liquid water that cannot directly infiltrate the soil is expected to leave the snowpack downslope, instead of ponding
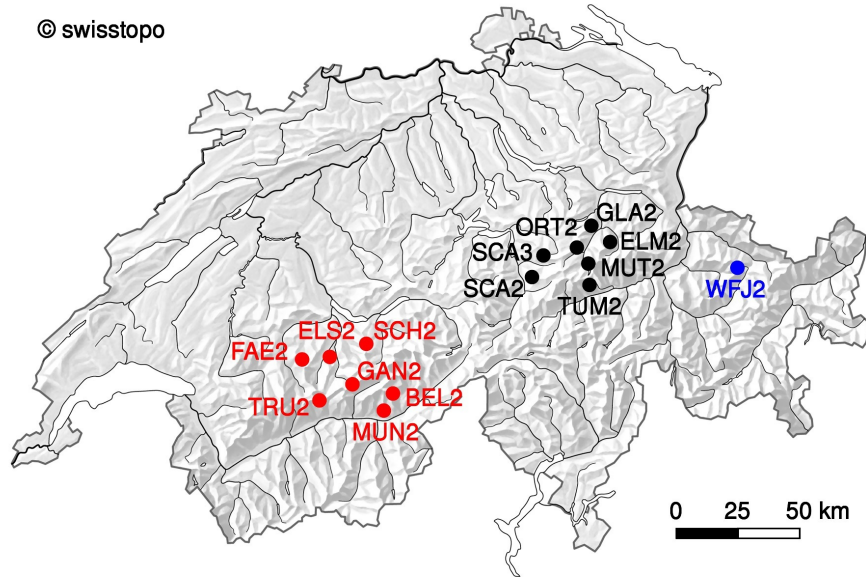
Figure 5.1: Map of Switzerland showing the locations of the stations used in this study in Bernese Oberland (red), Glarner Alpen (black) and the verification station Weissfluhjoch (blue). Reproduced by permission of swisstopo (JA100118).

inside the snowpack.

A temperature threshold of 0.0 °C is used to determine whether precipitation should be considered rain (from RhiresD) or snow (from the snow height sensors). This threshold is determined by comparing the ventilated and unventilated temperature sensor at WFJ during this particular event. It was found that during the onset of rain, the ventilated sensor was close to 1.2 °C when the unventilated IMIS type sensor was measuring around 0.0 °C. This discrepancy may have arisen from bad ventilation due to wet snow collected onto the sensor hut, or condensation from the moist air on the temperature sensor itself. Because the onset of rain was accompanied by a strong and quick increase in air temperature, the influence of the choice of threshold on the results is small. In the case of snowfall, a snow element is added to the model domain for each 2 cm of new snow. In the case of rainfall, the water flux is either added to the top element (bucket scheme) or applied as a Neumann boundary condition (Richards equation).

For calculating the heat fluxes in Eq. (5.1), a neutral atmospheric stratification was assumed, which is likely an appropriate assumption because of the windy conditions during the event. The turbulent heat fluxes were calculated following a standard Monin–Obukhov parameterisation (*Lehning et al.*, 2002a), using a roughness length z_0 of 0.002 m. The net radiation is approximated by using the measured reflected short-wave radiation and a parameterised albedo (*Schmucki et al.*, 2014). Because the IMIS stations do not measure ILWR, this was approximated by the *Omstedt* (1990) parameterisation, using an estimated cloud cover. Based on observations of cloudiness at the MeteoSwiss station at Jungfraujoch, cloudiness was set

Table 5.1: List of station abbreviations, station names, station altitudes and statistics for the two study areas and the verification station. The statistics denoted with Event are determined over the period 9 October, 18:00 UTC–11 October, 00:00 UTC. The bracketed sign before the root mean square error (RMSE) of snow height denotes whether modelled snow height is on average higher (+) or lower (−) than measured snow height. Time lag is the lag between the start of rain and the start of snowpack runoff and time runoff > rain denotes the time it took before cumulative snowpack runoff exceeded cumulative rainfall; w.e., water equivalent.

stn	name	altitude	max snow height 6-14 Oct.	RMSE snow height Event	rainfall Event	deposition Event	snowmelt Event	snowpack runoff Event	cold content	time lag	time runoff > rain
		(m)	(cm)	(cm)	(mm)	(mm w.e.)	(mm w.e.)	(mm w.e.)	(kJ/m^3)	(hours)	(hours)
Bernese Oberland											
FAE2	Faermel	1970	39	(+) 4.6	63	1.0	29	97	6	1.8	4.8
ELS2	Elsige	2140	44	(+) 2.4	59	1.3	34	94	33	3.5	6.2
MUN2	Mund	2210	53	(+) 3.4	34	2.3	45	78	94	3.0	7.0
SCH2	Schilthorn	2360	70	(-) 4.0	88	0.5	14	95	387	4.8	19.5
TRU2	Trubelboden	2480	37	(+) 3.7	84	0.8	22	106	68	3.8	9.8
BEL2	Belalp	2556	51	(+) 6.5	43	0.2	5	44	166	2.8	18.8
GAN2	Gandegg	2717	103	(+) 18.4	75	0.4	2	63	1265	10.0	-
average all		2348	57	(+) 6.1	64	0.9	21	82	288	4.2	11.0
Glarner Alpen											
GLA2	Glaernisch	1630	99	(+) 4.4	72	0.7	36	97	294	7.5	14.5
ORT2	Ortstock	1830	108	(-) 4.2	76	3.8	70	142	798	7.5	12.5
SCA2	Schächental	2030	73	(-) 6.4	75	2.5	71	146	330	5.5	9.8
ELM2	Elm	2050	90	(-) 3.1	53	1.0	24	67	559	5.2	13.0
TUM2	Tumpiv	2195	93	(-) 2.0	41	0.6	33	67	662	5.0	10.8
SCA3	Schächental	2330	90	(-) 7.1	81	1.6	23	95	972	5.2	14.8
MUT2	Muttsee	2474	92	(-) 4.8	63	0.7	10	61	932	7.0	-
average all		2077	92	(-) 4.6	66	1.5	38	96	649	6.1	12.5
Verification station											
WFJ	Weissfluhjoch	2540	48	(+) 2.4	33	1.1	18	47	799	4.8	11.2

to 1.0 in the period from 7 October to 9 October, 10:00 UTC and from 9 October, 17:00 to 11 October, when there was either solid or liquid precipitation, and 0.5 (half cloudy) for all other times.

5.2.4 Methods

To investigate the factors influencing the response of the snow cover during the ROS event, we added a sensitivity study by also forcing the SNOWPACK model for each station with the meteorological conditions from all the other stations. Snow melt is mainly governed by atmospheric conditions (temperature, relative humidity and wind speed), whereas liquid precipitation causes relatively little melt. Therefore, we consider atmospheric conditions and liquid precipitation as independent forcings during the event and treat them separately. The meteorological forcing, excluding the liquid precipitation, at the 14 stations represents 14 different melt scenarios. For liquid precipitation, we also have 14 more or less unique scenarios, although the temporal distribution over the day is based on eight SwissMetNet stations only. However, the scenarios provide differences in rainfall amounts due to the spatial distribution as captured in the RhiresD data set by spatial interpolations and climatological lapse rates. So for each of the 14 stations, with its own unique maximum snow height, we performed an ensemble of 2744 simulations (14 × 14 × 14) with the SNOWPACK model, with every combination of melt and liquid precipitation scenario for statistical analysis. By replacing time series at

a measurement site with a time series from another site, self-consistent series with real meteorological conditions that occurred during the event were created to act on the snow cover existing at the site. The original meteorological measurements at each station were used to force the model up to the moment on which the rainfall started on 9 October. From this specific time onwards, the meteorological and precipitation forcing was replaced by forcings from other stations. The starting time for these replacement series was taken as the moment on which rainfall started at these other stations.

To analyse possible different effects on snowpack runoff for shallow and deep snow covers, the 14 IMIS stations were divided into a shallow and deep snow cover class, depending on being above or below the median of maximum snow height during the event. The stations in Bernese Oberland are all present in the shallow snow cover class, except for GAN2, and all stations in Glarner Alpen are in the deep snow cover class, except SCA2. Per class, we determined a best fit by the linear regression for a given cumulative period using all ensemble simulations in the respective class:

$$Q_{\text{cum}} = \alpha P_{\text{cum}} + \beta M_{\text{cum}} + b, \tag{5.2}$$

where Q_{cum} is the cumulative snowpack runoff sum (mm w.e.), P_{cum} is the cumulative precipitation sum (mm), α is the linear regression coefficient for precipitation, M_{cum} is the cumulative snow melt sum (mm w.e.), β is the linear regression coefficient for snow melt and b is the intercept. In this context, b can be interpreted as the change in liquid water storage in the snow cover. As a positive value of b describes the snowpack runoff in the absence of any rain or snow melt, it can be assumed to reflect the recession curve and the effect of a decreasing water holding capacity, for example due to snow settling, wet snow metamorphism or changing hydraulic conductivity.

The dependence of the fit coefficients α, β and b over varying cumulative periods can reveal how the snow cover is modulating precipitation input and snow melt when generating snowpack runoff. These coefficients will be used on the original simulations to attribute the individual contributions of snow melt, precipitation and the intercept (change in storage) to the modelled snowpack runoff. The linear regression was done for cumulative periods of 0–1 to 0–24 h with two approaches: (i) taking the onset of rain at the stations as the start of the cumulative period and (ii) taking the onset of snowpack runoff as the start of the cumulative period. The latter was determined by both an increase of snowpack runoff by a factor of 2 compared to the snowpack runoff at the onset of rain and a modelled snowpack runoff larger than 0.5 mm in 15 min.

5.3 Results

5.3.1 Verification

Before discussing the simulations for the two study regions, the results for the verification station WFJ will be presented. Figure 5.2 shows the modelled and measured snowpack runoff at the WFJ for the ROS event, starting shortly before the onset of rain. The measured snowpack runoff started shortly after midnight on 10 October, although this involved only marginal amounts, most likely related to snow melt at the snowpack base due to the ground heat flux. The measured snowpack runoff strongly increased just before 06:00 UTC, which we associate with the arrival of the liquid water added to the snowpack by rainfall and snow melt near the snow surface. This particular moment is found 1.5 (for RE with IMIS type setup) to 3.5 h (for bucket with full EB type setup) later in the simulations. Here, the neglect of preferential flow in the model probably plays a role. There is strong observational evidence for preferential flow paths in snow that transport liquid water down efficiently (*Kattelmann*, 1985; *Marsh*, 2006; *Katsushima et al.*, 2013), but currently, a modelling concept for this process is not available.

Nevertheless, solving liquid water flow in the snow cover with the Richards equation is providing a closer agreement with observed snowpack runoff than with the bucket scheme concerning the timing of the start of snowpack runoff. Both models are overestimating the snowpack runoff rate, as shown by the steeper cumulative curve, although this overestimation is larger with the bucket scheme. In contrast, the total runoff sum at the end of the day is overestimated more in simulations with the Richards equation than with the bucket scheme. Because of the focus on snowpack runoff dynamics during the event in this study, we chose to do all further calculations with the Richards equation only. It should be noted, however, that several parameterisations are not yet verified with the Richards equation (metamorphism, snow settling, etc.).

In spite of some differences between the full energy balance station from WFJ and the IMIS-type setup from WFJ, it can be seen that the approach of parameterising ILWR and deriving precipitation from the RhiresD data and the SwissMetNet stations is providing reasonable results. It shows that the methods used in this study are suitable for analysing the dynamical snowpack behaviour at the IMIS stations in the two study areas. It should be noted, however, that the timing of precipitation for WFJ is very accurate, because a heated SwissMetNet rain gauge is located at this site, whereas for other stations, the closest SwissMetNet station is generally several kilometres away.

5.3.2 Event Description

The event started with snowfall above 800 m altitude on 7 October. Figure 5.3 shows the temporal development of snow cover height in the two study regions. The snowfall was quite continuous and the maximum snow height averaged over all stations was reached around 9 October, 12:00 UTC. Table 5.1 shows that the average maximum snow height at the seven
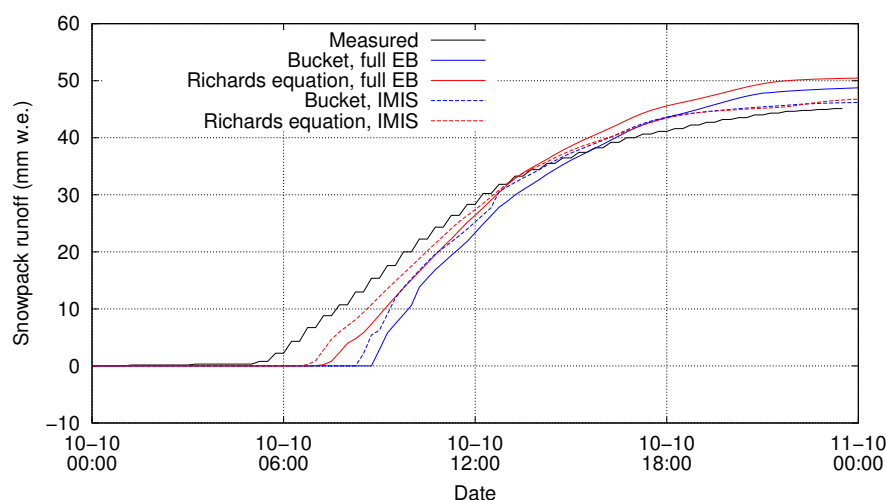
Figure 5.2: Comparison of modelled snowpack runoff using the bucket scheme or Richards equation for liquid water transport in the snowpack with measured snowpack runoff by a snow lysimeter for the station Weissfluhjoch, for October 10. Simulations are done with either the full energy balance meteorological forcing (solid lines) or the forcing available for IMIS-type stations (dashed lines).

IMIS stations in Bernese Oberland was 57 cm, less than the 92 cm in the Glarner Alpen. In Bernese Oberland, snowfall amounts tended to increase with altitude, whereas interestingly, this trend was absent in the Glarner Alpen.

After the maximum snow height was reached, the snow height started decreasing, although rain and surface snow melt had not started yet. This decrease can be attributed mainly to settling of the snowpack and melt at the snowpack base by the ground heat flux. The following precipitation event started after 18:00 UTC on 9 October, and consisted purely of rainfall (except for very high altitudes). It was accompanied by a rapid increase of the 0 °C-isotherm to 3000 m altitude. The rainfall lasted until 15:00 UTC on 10 October, with an average rainfall sum of about 65 mm for both areas (Table 5.1). This gives a higher precipitation rate during the rainfall period than during the snowfall period.

The rainfall in the first hours was not accompanied by significant snowpack runoff (Fig. 5.3). This means that liquid water was stored in the snow cover by capillary suction and refreezing inside the snowpack. Refreezing was especially occurring at high altitude and at stations in Glarner Alpen, given the high cold content of those snow covers at the onset of rain (Table 5.1). Note that for typical snowpack conditions present at the onset of the rainfall, the amount of rain water needed to warm the snowpack to 0 °C is in the order of 5 mm for the typical cold contents reported in Table 5.1. For this event, this is less than 10 % of the total rainfall amounts. In the model, snowpack runoff started approximately 4–6 h after the onset of rain, depending on snow depth (Table 5.1). The amount of snow melt during the rainfall period was rather small compared to the rainfall amounts. Table 5.1 shows that the total amount of snow melt
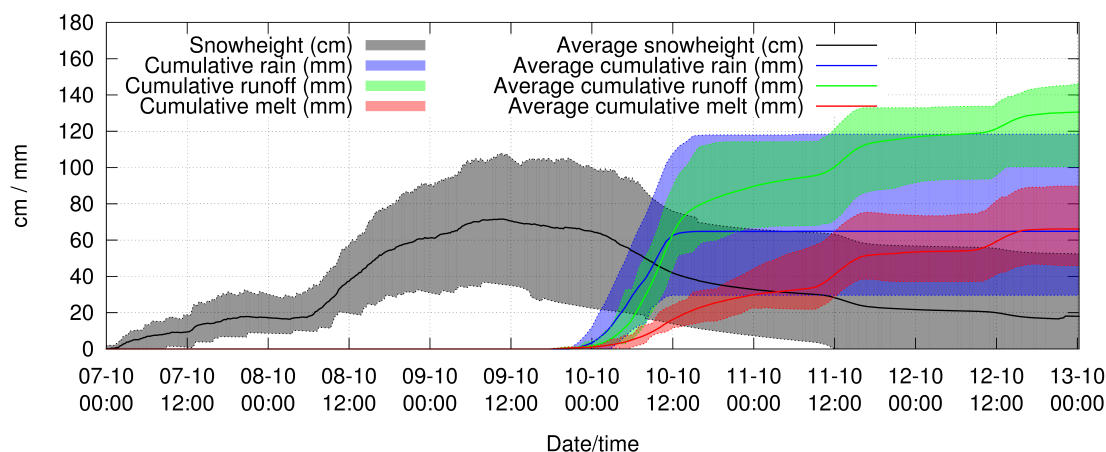
Figure 5.3: Overview of the simulation results of the temporal evolution of the ROS event between October 7 and 13. Shown is the range of absolute minimum and maximum modelled snow height, cumulative precipitation, cumulative snowpack runoff and cumulative melt over the 14 stations. The solid lines denote the average values. The accumulation for precipitation and melt was calculated from October 9, 18:00 onwards.

during the event was almost twice as large in Glarner Alpen as in Bernese Oberland, although this is partly caused by the lower average altitude of the stations in the Glarner Alpen and the exact values are strongly dependent on the choice of period. We can see that the average snowpack runoff curve is getting steeper during the rain episode and eventually becomes steeper than the rain curve (Fig. 5.3). After the rain stopped, snow melt continued due to the sensible heat flux provided by the increased air temperature. The snow melt exhibited a clear daily cycle on 11 and 12 October (Fig. 5.3), with a peak in the afternoon hours, associated with a high short-wave radiation input and a high air temperature.

To verify the snowpack simulations, the RMSE of measured and modelled snow height was calculated for the period 9 October, 18:00 UTC–11 October, 00:00 UTC (Table 5.1). Although snow water equivalent would be the preferred way to validate the simulations, as it better reflects the processes of snow melt, rainfall and liquid water flow than snow height, this is not possible due to the lack of validation data. However, measured snow height is generally considered an adequate estimate of snow water equivalent in physics-based models (*Sturm et al.*, 2010). Because the simulations were forced by measured snow height, a high agreement between measured and modelled snow height is present for the accumulation phase. By focusing solely on the ROS period itself, the RMSE values are indicative for the melt phase only. Most stations have an RMSE value below 5 cm, indicating a satisfying agreement between measured and modelled snow height in the melt phase. The largest discrepancy is found for the highest station in the study, where the snow height is overestimated with an RMSE value of 18 cm. Interestingly, the snow height is generally overestimated in the Bernese Oberland, whereas the opposite is found for the Glarner Alpen. Main reasons for this discrepancy may
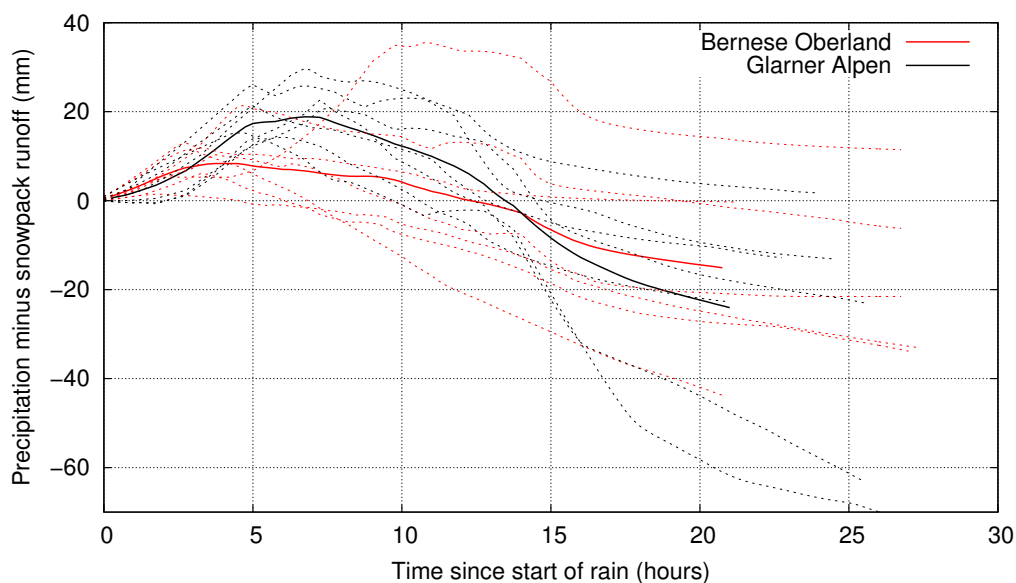
Figure 5.4: Cumulative rainfall minus cumulative modelled snowpack runoff during the event, starting at the onset of rain for each individual station (dashed lines) and for area averages (solid lines).

be an underestimation or overestimation, respectively, of snow melt, or an overestimation or underestimation, respectively, of new snow density and thus snow water equivalent.

In Fig. 5.4, the cumulative difference between rainfall and snowpack runoff is shown, starting from the onset of rain at the individual stations. When the curve is increasing, precipitation amounts exceed snowpack runoff, denoting storage of liquid water in the snowpack. A decreasing curve shows that the snowpack runoff is exceeding precipitation. The model results suggest that the snow cover was storing liquid water after the onset of the rainfall at all stations, dampening the effect of rain in the first few hours of the event. The initially dry and cold snow cover used the latent heat from refreezing rain water to get isothermal and also rain water was stored additionally in the snow cover by capillary suction. The shallow snow cover at the stations in the Bernese Oberland could retain less water than the deeper snow cover at the stations in Glarner Alpen. Furthermore, the tipping point where a net storage of liquid water in the snow cover changed into a net release of liquid water from the snow cover was reached earlier in Bernese Oberland (4 h) than in Glarner Alpen (7 h). Table 5.1 shows the time needed before cumulative snowpack runoff exceeded cumulative rainfall, which is generally shorter in Bernese Oberland than in Glarner Alpen. However, it still took on average 11–13 h from the start of rainfall before the total snowpack runoff exceeded total rainfall. This shows that the dampening effect of the rainfall by the snow cover was quite strong and persisted for several hours. Figure 5.4 also shows a wide spread between individual stations, related to variations in rainfall and snow melt rates. This motivated us to carry out the ensemble simulations that will be discussed later.

Table 5.2: Energy balance at the stations for the period October 9, 18:00 - October 11, 00:00. The energy fluxes are expressed as an equivalent snow melt energy in mm w.e. for understanding the magnitude of the energy fluxes, although snow melt should not necessarily have occurred.

Stn	Altitude (m)	Rnet (mm w.e.)	Rain energy (mm w.e.)	Latent heat flux (mm w.e.)	Sensible heat flux (mm w.e.)	Soil heat flux (mm w.e.)	Total energy (mm w.e.)
Bernese Oberland							
FAE2	1970	1	5	8	9	6	28
ELS2	2140	-1	4	10	12	5	30
MUN2	2210	-3	1	17	24	4	44
SCH2	2360	-3	4	4	8	1	14
TRU2	2480	-2	6	6	15	-1	24
BEL2	2556	-5	1	1	3	1	1
GAN2	2717	-6	1	3	6	0	4
average all	2348	-3	3	7	11	2	21
Glarner Alpen							
GLA2	1630	2	6	5	8	11	31
ORT2	1830	-0	6	30	37	12	85
SCA2	2030	-1	6	18	38	6	69
ELM2	2050	-1	3	7	7	6	22
TUM2	2195	-0	3	4	13	11	32
SCA3	2330	-4	3	12	13	1	25
MUT2	2474	-6	1	5	8	1	10
average all	2077	-1	4	12	18	7	39
Verification station							
WFJ	2540	-6	0	8	14	0	17

5.3.3 Energy Balance

A net positive energy balance for the surface will first result in a heating of the snowpack (reducing the cold content), followed by melt. Table 5.2 shows the individual terms of the energy balance at the stations, expressed as mm w.e. melt potential as if the energy would be solely used for snow melt or freezing. The time period denoted as "Event" in Tables 5.1 and 5.2 is arbitrarily chosen to contain at least the complete rainfall, but longer or shorter time periods may have a significant effect on the relative contribution of the terms. A comparison with the amount of snow melt provided in Table 5.1 reveals that at all stations, most energy was used for snow melt. For stations with a high cold content, the net energy is partly used for heating of the snowpack. The contribution of net radiative energy, if not negative, and rain energy is fairly small. Most energy was delivered by heat release due to condensation during the ROS event and sensible heat. *Mazurkiewicz et al.* (2008) also found a strong contribution of latent heat to snow melt during ROS events. This is in contrast with typical clear sky spring snow melt situations, where the two terms often have opposite sign (*Mott et al.*, 2013). Note that small discrepancies between total heat and snow melt (with more snow melt occurring than total heat provided) are due to small errors in the diagnosed energy balance as a result of the Dirichlet boundary condition at the upper and lower boundaries, as described before.

5.4 Ensemble Simulations

Figure 5.5 shows the time lag between the onset of rain and the arrival of meltwater at the bottom of the snowpack as a function of snow height for the ensemble simulations. A general tendency of an increasing time lag with deeper snow covers is found, consistent with a longer travel time. However, the spread, caused by variations in rainfall and snow melt amounts, is
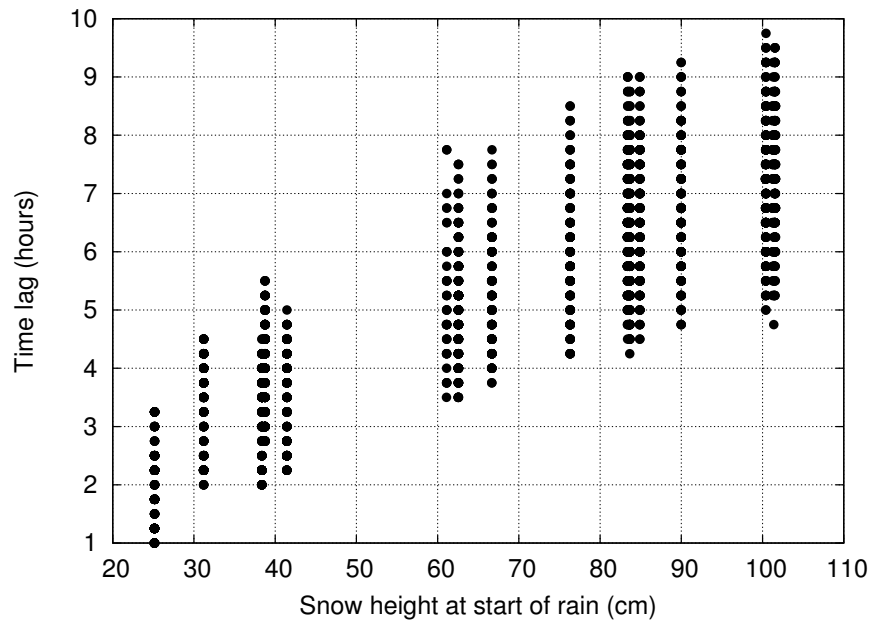
Figure 5.5: Time lag between the start of rain and the modelled start of snowpack runoff as a function of the snow height at the onset of rain for the ensemble simulations.

very large. In Fig. 5.6, the snow height is divided by the time lag to get an approximation of the simulated velocity of the water movement in the snow cover. There is a clear dependency of the sum of rainfall and snow melt rate on flow velocity. Simulated water flow velocities range from $0.07 \, \mathrm{m \, h^{-1}}$ for low rainfall and snow melt rates up to 0.20–$0.25 \, \mathrm{m \, h^{-1}}$ for the highest rates. These modelled values and the correlation with rainfall and snow melt rates match well with earlier published results: *Jordan* (1983b) reports experimental values of $0.22 \, \mathrm{m \, h^{-1}}$, and also shows that earlier studies found values ranging from 0.04 to $0.6 \, \mathrm{m \, h^{-1}}$. The value of $0.22 \, \mathrm{m \, h^{-1}}$ was determined for spring snow melt conditions, and is at the upper limit of what was simulated in this model study. The lower values in the simulations are likely associated with the state of the snow cover during this event. The relatively freshly fallen snow is generally fine grained, associated with a lower hydraulic conductivity than for spring snow. The upward trend with increasing rainfall and snow melt rates is associated with higher hydraulic conductivities as a result of a higher saturation inside the snow cover. Furthermore, in the presence of liquid water, wet snow metamorphism is rapid, resulting in grain growth, rounding, and consequently, an increase in hydraulic conductivity. In *Singh et al.* (1997), a very high velocity of $6 \, \mathrm{m \, h^{-1}}$ was found for very high precipitation rates in a study with artificially created rainfall. In that study, it was concluded that the formation of efficient preferential flow paths (not considered in the SNOWPACK model) is likely contributing to this high average velocity.
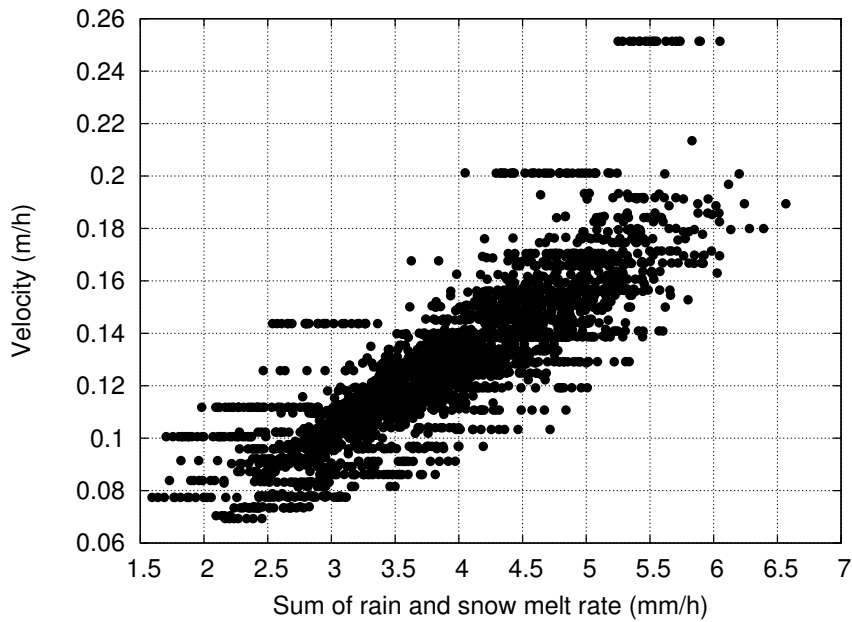
Figure 5.6: Simulated water velocity in the snow cover as a function of the sum of rain and snow melt in the first 5 hours since the start of rain for the ensemble simulations.

5.4.1 Regression Analysis

The regression analysis, as described by Eq. (5.2), was carried out to investigate the temporal evolution of the contribution of the different mechanisms in producing snowpack runoff. Figure 5.7a shows the regression coefficients of Eq. (5.2) for both the shallow and deep snow cover class as a function of cumulative period since the start of rain. In the shallow snow cover class, rain is correlated to snowpack runoff after 2 h already, whereas in the deep snow cover class, the first non-zero regression coefficient is found after 5 h. This illustrates that the retardation between rainfall and snowpack runoff is dependent on snow depth. Furthermore, the coefficient for snow melt is higher in the shallow snow cover class than in the deep one in the early hours since the onset of snowpack runoff. The coefficient in the deep snow cover class is below 1.0 for several hours, denoting that 1.0 mm of additional snow melt would result in less than 1.0 mm extra snowpack runoff. This is caused by the long travel time needed by the liquid water arising from snow melt that occurred mostly near the surface. Only the part of the total snow melt near the base of the snowpack could have contributed to snowpack runoff in the first hours after the onset of rainfall.

After approximately 15 h from the start of rain, there is almost no difference in regression coefficient for snow melt and rain between the shallow and deep snow cover class. Then, the coefficient for rain is almost equal to 1.0, indicating that 1.0 mm of additional precipitation in this period would result in 1.0 mm extra snowpack runoff and the dampening effect of the snow cover has disappeared. Interestingly, the coefficient for snow melt is about 1.1,

150

suggesting that there was approximately 10 % more snowpack runoff from the snow cover than the amount of snow melt alone. We attribute this to the destruction of the snow matrix by snow melt, which reduced the storage capacity of the snowpack for liquid water. The intercept term clearly demonstrates that the deep snow covers had more storage capacity for meltwater, as the minimum is smaller than in the shallow snow cover class. This results in a longer delay between the onset of rain and the actual snowpack runoff. The intercept term is still negative after 24 h, denoting that the effect of the storage capacity is noticeable over long periods.

In Fig. 5.7b, the regression coefficients are shown for cumulative periods starting at the onset of snowpack runoff. Expectedly, the intercept term changes sign: once snowpack runoff started, there was a contribution from the intercept. The intercept term is larger in the deep snow cover class than in the shallow one, indicating that in the simulations, deep snow covers produced more snowpack runoff, independent of snow melt or rainfall. This contribution consists of the snow melt and precipitation prior to the onset of snowpack runoff. Furthermore, settling may cause a reduction in storage capacity of the snow cover.

The stations in the shallow snow cover class have a higher coefficient for precipitation and snow melt in the short cumulative periods, denoting a stronger correlation of both variables with snowpack runoff shortly after the onset of runoff. We suggest that this is caused by short travel times through the snowpack in shallow snow covers. The difference with the deep snow cover class is decreasing with increasing time. After about 13 h, the regression coefficients appear to remain fairly constant. Interestingly, for a deep snow cover, snow melt has a lower regression coefficient than for a shallow one while this is opposite for rain, for which we cannot offer an explanation. Another contrasting effect is that the regression coefficients for precipitation and snow melt show a larger increase with increasing cumulative period in the deep snow cover class than in the shallow one. This points towards a dynamic effect in the snowpack, likely associated with changing snowpack microstructure and associated hydraulic properties.

5.4.2 Attribution

In Fig. 5.8, the individual terms (precipitation, snow melt and intercept) and the sum (snow-pack runoff) of the linear regression (Eq. 5.2) are shown, using the coefficients for both classes and the average rain and snow melt for each of the respective classes. Also drawn is the average modelled snowpack runoff. The almost perfect match between the modelled snowpack runoff and the sum of the linear regression terms shows that the regression analysis performs well. In both classes, the modelled cumulative snowpack runoff curve is steeper than the cumulative rainfall curve and it is steeper in the deep snow cover class than in the shallow one. From the individual terms of the regression analysis, it can be derived that this is caused not only by the contribution of snow melt, but also by the decrease in the (negative) contribution of the snow storage, denoted by the intercept term. The results also suggest that the rainfall provided a stronger contribution in the deep snow cover class than in the shallow one, as expressed
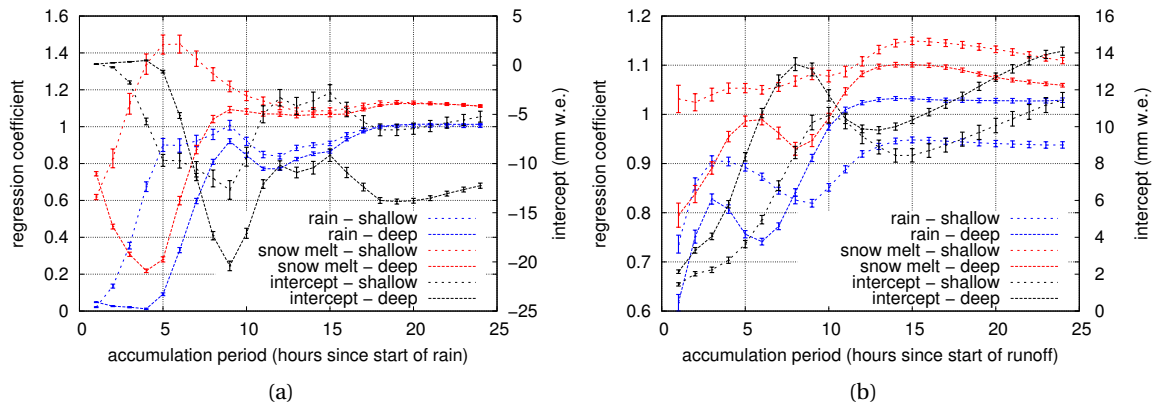
Figure 5.7: Regression coefficients as a function of cumulative period, since the start of rain (a) or start of snowpack runoff (b), for rain, snow melt and the intercept (mm w.e.) for both the shallow and deep snow cover class.

by the steeper curve of the rain term. The intercept term shows that there was a stronger dampening in the deep snow cover class than in the shallow one, although apparently it did not compensate the rainfall and snow melt contributions.

Figure 5.8 also shows that the time since the start of the rainfall after which the contribution of rainfall flattens out and the increase in snowpack runoff decreases (around 80 mm w.e.) lies for both snow depth classes around 16 h. However, the modelled onset of snowpack runoff, and thus the onset of the individual terms in the regression analysis, was about 3 h later in the deep snow cover class than in the shallow one. This clearly illustrates that the model simulates a higher snowpack runoff rate in the deep snow cover class once snowpack runoff starts. To assess the relationship with snow cover depth, Fig. 5.9 shows the snowpack runoff sums in the first hours after the start of snowpack runoff and the maximum peak snowpack runoff sum over the first 24 h after the onset of rain, averaged over all 196 simulations per individual station (associated with a specific snow depth). In the first hours of modelled snowpack runoff, snowpack runoff rates show a clear increase with snow depth, whereas the trend is almost absent for the maximum peak snowpack runoff rates. The reason for the latter is that peak snowpack runoff is likely achieved in a kind of steady state situation when incoming rainfall and snow melt are in balance with snowpack runoff. The fact that this value is almost constant with snow depth is a consequence of the ensemble simulation setup, where all precipitation and melt scenarios are present for each station.

The simulations suggest that deep snow covers initially produced more snowpack runoff than shallow snow covers and that this effect is partly caused by hydraulic effects inside the snowpack and partly by higher snow melt amounts. In Fig. 5.10, the percentages of respectively intercept, snow melt and rainfall contributions to snowpack runoff are shown for increasing cumulative periods, as determined by the regression analysis. This confirms the
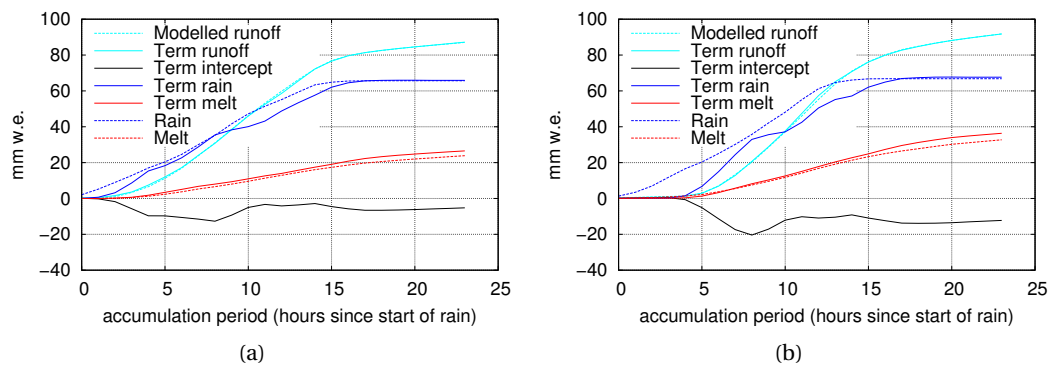
Figure 5.8: Modelled snowpack runoff, measured rainfall and modelled snow melt together with the terms of the linear regression for both the shallow (a) and the deep (b) snow cover class. Note that the blue, red and black solid lines sum up to the cyan line.

earlier conclusions. The contribution of the storage is varying between 15 and 20 % and is higher in the deep snow cover class. The contribution of snow melt is almost doubling from 15 and 20 % to 30 and 3 8% between 1 and 24 h cumulative periods for the shallow and deep snow covers, respectively. The higher amount of snow melt experienced at the stations in the deeper snow cover class is likely unrelated to the deeper snow cover, whereas the higher contribution of the intercept term for the deeper snow cover class should be truly connected to the deeper snow cover.

5.5 Discussion

The response of the snowpack during a ROS event has been studied here using a physics-based snow cover model. The results depict how the SNOWPACK model simulates the influence of rainfall and snow melt on producing snowpack runoff and consequently, the conclusions drawn here are strongly dependent on a sufficient process representation in the SNOWPACK model. The comparison with snow lysimeter measurements at WFJ indicated that average velocity with which liquid water is routed through the snowpack in SNOWPACK was slightly underestimated, most likely due to neglecting preferential flow paths. This would imply that the time lag between the onset of rainfall and the onset of snowpack runoff is overestimated in the model. A preferential flow path formulation for physics-based snowpack models is not yet available and, to our knowledge, preferential flow paths are neglected in most physics-based models. It is difficult to speculate on the influence of preferential flow on the results presented here, in particular for contrasts between shallow and deep snow covers. However, the role of preferential flow in homogeneous layered snowpacks, as was the case in this particular event, may be limited. The snow at the onset of this ROS event had fallen during cold conditions in the 3 days prior to the event. We can thus assume that the initial snowpack was rather homogeneous with relatively small grains. In laboratory experiments, preferential flow was
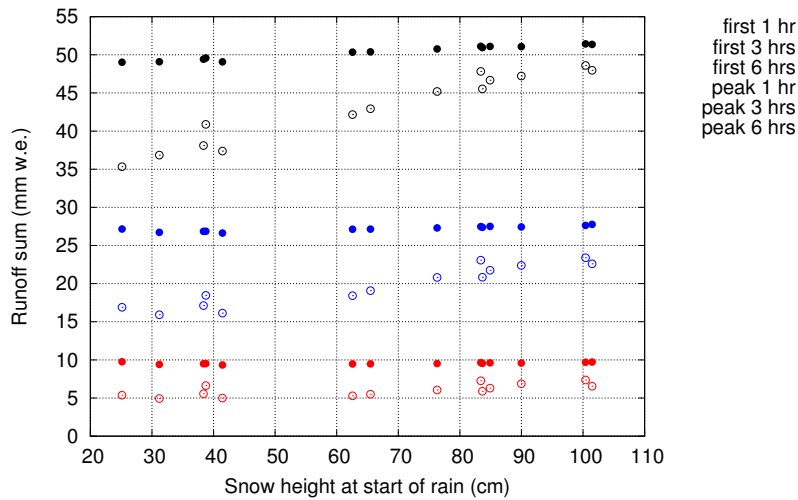
Figure 5.9: Average maximum cumulative snowpack runoff (denoted peak) and average cumulative snowpack runoff in the first hours after the start of snowpack runoff (denoted first), averaged over all ensemble simulations.

not observed for small grain sizes (*Katsushima et al.*, 2013). From those experiments, the role of water ponding at strong transitions in snow properties between snow layers for the formation of preferential flow was also identified. These water accumulations may also trigger significant amounts of lateral flow, for example over ice layers inside the snowpack. However, it is unlikely that these inhomogeneities were present in the snow cover in this particular event.

Other discrepancies were found between measured and modelled snow height, which may be caused by underestimations or overestimations of snow settling and/or snow melt. However, typical RMSE for snow height was less than 5 cm, which is around 2 mm w.e., dependent on snow density. Using the ensemble and regression analysis, the individual contributions of snow melt, rainfall and snow storage have been quantified by using melt scenarios from all stations. The higher snowpack runoff rates found in the simulations for deep snow covers were found to be not only dependent on snow melt, but also due to the effects of rainfall on deeper snow covers and the reaction of the snow storage. We therefore conclude that these discrepancies have only a small influence on the general validity of the results, even though the comparison of measured and modelled snow height suggested a consistent underestimation of snow melt in the Bernese Oberland and a consistent overestimation in the Glarner Alpen.

5.6 Conclusions

Model simulations of a ROS event in October 2011 for 14 meteorological stations in two regions of the Swiss Alps have shown that the snowpack runoff dynamics from the snow cover is strongly dependent on the snow depth at the onset of the rain. Deeper snow covers had
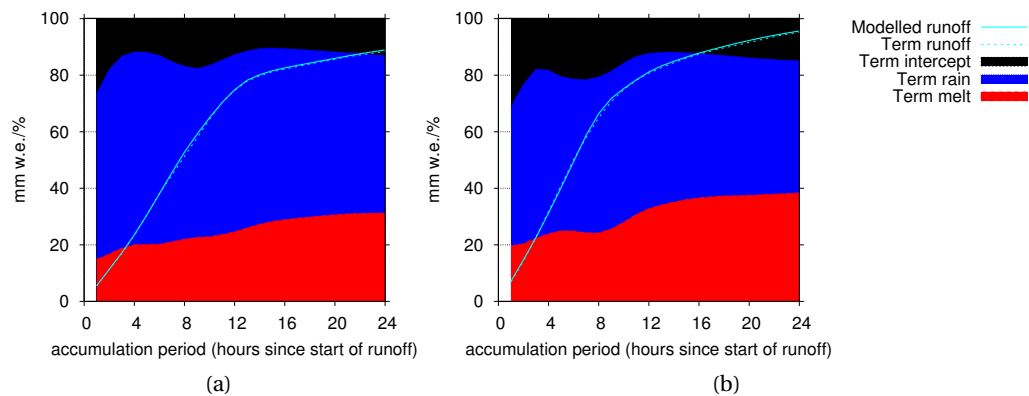
Figure 5.10: Cumulative snowpack runoff (from model and from regression analysis) and the terms of the linear regression for both the shallow (a) and the deep (b) snow cover class.

more storage and absorbed all rain and meltwater in the first hours, whereas the modelled snowpack runoff from shallow snow covers reacted much more quickly to the onset of rainfall. The modelled time lag between the onset of rain and the onset of snowpack runoff ranged from 2.2 to 10 h, depending on snow depth and cold content of the snowpack at the onset of rainfall, with an average around 4–5 h. In this event, cumulative modelled snowpack runoff became higher than cumulative rainfall as a result of additional snow melt after on average 11–13 h.

An ensemble of simulations was carried out where meteorological and precipitation forcing conditions were interchanged between stations. It was found that the time lag between the onset of rainfall and snowpack runoff in the model study depends not only on snow height but also on the sum of rainfall and melt rates. Simulated flow rates of liquid water in the snowpack were smaller than observations in spring snow, which can be attributed to the structure of the snowpack that consisted of small grains with a high suction and low hydraulic conductivity.

A regression analysis on the ensemble simulations has shown that deep snow covers generated more snowpack runoff, in the first hours after snowpack runoff started. The analyses suggested that this was caused by a higher release of liquid water from the storage in deep snow covers than in shallow ones. The quicker depletion of the storage in deep snow covers is partly driven by snowpack settling and partly by recession processes.

Note that these conclusions were derived for a ROS event during which the amount of rainfall largely exceeded the storage capacity of the snow, generating large amounts of snowpack runoff, even at locations with a deep snow cover. The effect of initial snow depth may be fundamentally different for ROS events in which rain falls on spring snow, where most settling has already occurred and liquid water is already present in the snowpack.

Given that the snow cover was deeper in Glarner Alpen than in Bernese Oberland, these

differences in snowpack behaviour in terms of time lag between the onset of rain and the onset of snowpack runoff may have contributed to the differences found in streamflow discharge. In Bernese Oberland, streams reacted quickly on the onset of rain, whereas in Glarner Alpen, where the snow cover was thicker, flooding occurred mainly in the late afternoon of 10 October after most rainfall occurred (*Badoux et al.*, 2013). On the other hand, the model results in this study have shown that once the snowpack produces runoff, the modelled snowpack runoff is higher in the deep snow cover class than in the shallow one. The validity of this conclusion depends on the adequacy of the representation of liquid water flow in the SNOWPACK model, as snow lysimeter measurements to support this result are lacking.

Acknowledgements

Edited by: H.-J. Hendricks Franssen

6 Discussion and Outlook

In this thesis, it is discussed that solving RE for snow improves the simulation of liquid water flow through snow. Furthermore, the continuum approach for the snow-soil column, seems to be able to adequately describe soil moisture states in the upper soil layers in alpine terrain. SNOWPACK provides now a better process representation for snow, soil and the interaction processes between them. Those play not only an important role in hydrological processes in mountainous terrain, but also in large flat snow covered areas. Here, it will be discussed what the limitations are from the modelling perspective used in this thesis. The discussion and outlook on future research will mainly focus on point scale simulations (albeit not necessarily one-dimensional) with the SNOWPACK model. It is beyond doubt that a better description of hydrological processes at the catchment scale is not only limited to the process representation in the SNOWPACK model. For example, the studies presented in this thesis did not focus on streamflow from catchments, overland flow or ground water flow. These processes are nevertheless essential to improve the understanding of catchment scale hydrology, and research activities are underway focussing on these issues in the context of the Alpine3D and SNOWPACK model framework (e.g., *Comola et al.* (2014)). However, an in-depth discussion on these topics is considered outside the scope of this thesis. Other issues, like the spatial variability of soil parameters and a generally poor knowledge of them will also not be discussed further. The discussion and outlook focusses on the topics that were defined as the motivation for the studies in this thesis (Section 1.1).

6.1 Non-Equilibrium Flow and Preferential Flow

Is RE an adequate description of liquid water flow in snow or soil? This question gets a lot of attention in the soil community (see the extended discussions by *Parlange et al.* (2002); *Beven and Germann* (2013) and references therein). RE was derived on the basis that gravity and capillary forces are in balance. This assumption requires that no acceleration is present and that flow velocities are zero. For small flow velocities, this may still be a good approximation. However, in saturated snow samples, flow velocities in the order of 1 cm s^{-1} have been observed (*Walter et al.*, 2013). These velocities would cause dynamic effects on the flow that

are not accounted for by RE. Furthermore, the equation relates water flow to gradients in pressure head. This requires differentiable pressure head and hydraulic conductivity in the porous medium, which would only be found in media that are homogeneous on small scales. In snow, this assumption may be severely violated at adjacent layers with marked differences in microstructural snow properties, like depth hoar and ice lenses in the snow cover.
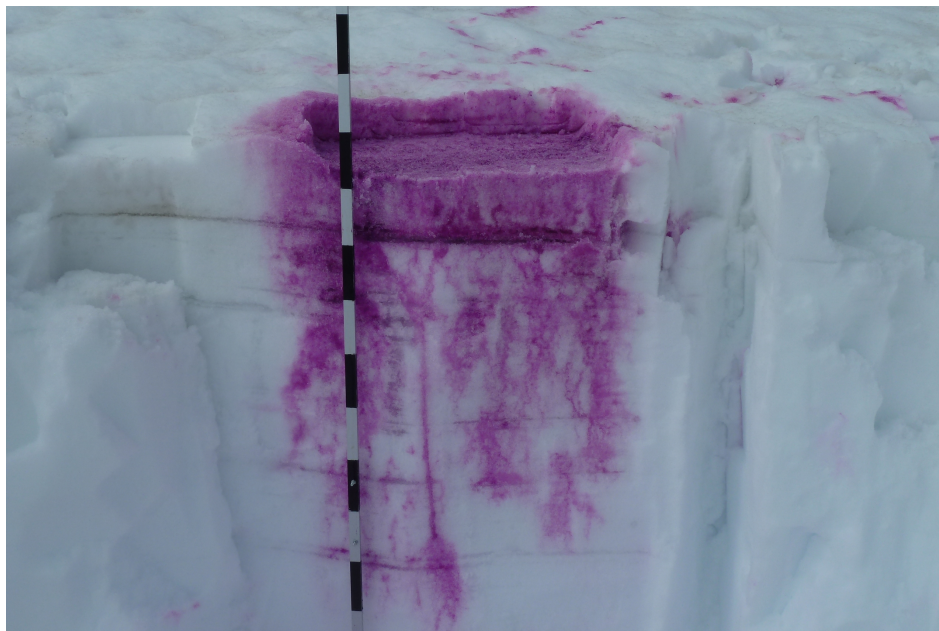
Figure 6.1: Dye-tracer experiment on liquid water flow in spring snow at the forefield of the Tiefen Glacier on June 15, 2012, clearly revealing preferential flow (experiment and photo: J. Zeyer and A. Lazzaro, ETHZ).

6.1.1 Observations of Non-Equilibrium or Preferential Flow

What observational evidence is there for the importance of non-equilibrium and preferential flow? In many studies, it has been found that soils not only violate the assumptions of homogeneity and equilibrium, but also that the discrepancies arising from that are noticeable large. In particular, discrepancies in observed dispersion of pollutants in soils and ground water with simulations based on RE, show that RE is not the suitable description for these type of problems. In soils, preferential flow paths through macropores have long been recognized as important and efficient water transport mechanisms, in addition to matrix flow. They are often associated with growth and decay of roots, burrowing animals, cracks in soil, etc. (for example, see *Beven and Germann* (1982) and reference therein). Another preferential flow mechanism arises from unstable wetting fronts, which results in flow fingering (see for a discussion *Parlange et al.* (2002) and references therein). Unstable wetting fronts are considered to originate from self-maintaining instabilities in the matrix flow rather than from macropores or other pre-existing structures in the matrix, although phase changes and wet snow metamorphism may alter the snow matrix after the first wetting.

There is also substantial observational evidence that liquid water flow in snow may exhibit strong inhomogeneities. For example, dye tracer experiments have shown typical flow patterns in snowpacks which point to non-equilibrium flow and preferential flow paths (*Schneebeli*, 1995; *Waldner et al.*, 2004; *Techel et al.*, 2011; *Katsushima et al.*, 2013). Figure 6.1 shows the result of a dye-tracer experiment in a natural snowpack which clearly shows inhomogeneous flow patterns, like preferential flow paths. Also ponding can be seen at transitions between layers, similar to what is found in snowpack simulations using RE (for example, see Figure 1.3).

It is described now how the formation of preferential flow paths in snow is thought to develop, based on studies by *Katsushima et al.* (2013); *Hirashima et al.* (2014). Normally, there exists some degree of spatial variability in snow properties, like grain size and bulk density. This variability is present across several scales. On the micro-scale, bulk density looses its meaning, but differences in grain size still occur. When liquid water is added to the snow, either due to snowmelt, or to rainfall, water starts to accumulate at certain layers, most likely at capillary barriers. Due to the spatial variability in snow properties, and thus capillary suction, there is a spot where water is first able to infiltrate the dry, possibly below freezing, lower layers. This set in action positive feedback mechanisms. The infiltrating water in the lower layer enhances the hydraulic conductivity at this point and the water that was ponding in the layer on top, will flow to the same spot, even further increasing the hydraulic conductivity locally. It has been hypothesized that the temperature and moisture gradients that build up where the liquid water starts infiltrating the lower layer, is initialising fast wet snow metamorphism (*Wakahama*, 1968). The grains at the gradient become larger and rounded. This basically separates the wet snow from the dry snow, and as more water is draining from the upper layer, the water flow propagates vertically. The role of ponding in the formation of preferential flow has been found in experiments by *Katsushima et al.* (2013), but can also be identified in the dye-tracer experiment in Figure 6.1, where preferential flow paths form below a layer with high water content.

By the end of this process, a preferential flow path has formed. Often, the flow path extends either to the ground, or to the next marked transition of snow properties inside the snowpack. Here, again ponding and associated lateral water flow may occur, as observed by *Techel et al.* (2011). With the wet snow metamorphism causing structural changes to the snowpack, preferential flow paths may get fixed in the snowpack microstructure. Even when no new melt water is added, the preferential flow paths remain, as has been observed in the field (*Kattelmann*, 1985). That means that in the next wetting cycle, the same preferential flow path may be used, and the processes described above may even make the flow path more pronounced. However, in other studies, the opposite has been observed when different preferential flow paths formed during different melt episodes (*Schneebeli*, 1995). In spring conditions, when the snowpack is isothermal and wet, it may be hypothesized that the preferential flow paths that could form during the day, may collapse when the wet snow gets cohesionless and, consequently, preferential flow may play a less pronounced role here. On the other hand, the experiments shown in Figure 6.1 were done in spring snow and clearly show preferential flow patterns.

The visual observations of preferential flow in snow as shown in Figure 6.1 seem to bear strong correspondence with observations of finger flow in soils (for example, see *Hill and Parlange* (1972)). The correspondence is also confirmed by notions that flow fingering in soils particularly form for relatively fine grained material on top of a relatively course grained one and that ponding in the upper layer is identified as triggering the flow finger formation (for soil, see *Hill and Parlange* (1972); for snow, see *Wakahama* (1963); *Katsushima et al.* (2013)), although these conditions might not be required (*Selker et al.*, 1992). Flow fingering is particularly pronounced in course grained soils (*Parlange and Hill*, 1976), which corresponds with a typical snow matrix. In the experiments by *Katsushima et al.* (2013), preferential flow was only observed in snow samples with a grain diameter larger than 0.25 mm. Describing preferential flow in snow as a flow fingering process rather than macropore flow may be motivated by arguing that in the build up phase of a natural snowpack, snowpack characteristics are homogeneous on macro-scales and no predisposition for future preferential flow paths exists. In soils on the other hand, some preferential flow channels exist most of the time, caused by roots, worm holes, or cracks in the soil. In fact, also for snow, wet snow metamorphism in flow fingers may locally introduce structural changes to the snowpack that are favoured locations for water infiltration in the next wetting cycle, resembling macropore flow.

For wet snow avalanche formation, studies clearly indicate that preferential flow paths are essential in understanding the formation process (e.g., *Kattelmann* (1984)). However, when snowpack runoff is considered for simulations of hydrological processes, the results are less clear. For example, in Chapter 2 it is shown that there is a significant underestimating of the arrival time of melt water at the base of the snowpack, in both the bucket scheme and RE. This suggests that preferential flow paths are present. However, the results also indicate that the amount of water that leaves the snowpack in the early phase, is about 5% of total seasonal snowpack runoff. For catchment scale hydrological processes, one could consider this amount to be of minor importance. Furthermore, lag correlations between simulated and measured snowpack runoff are in the order of half an hour to one hour. For Weissfluhjoch, the lag correlation is typically negative, denoting a too early release of melt water during the day in the simulations, whereas for CDP, the lag correlation tends to be positive. This result makes it unclear what the discrepancy caused by neglecting preferential flow paths actually is.

6.1.2 Modelling of Non-Equilibrium or Preferential Flow

How can numerical models treat non-equilibrium or preferential flow? Most studies addressing possible modelling concepts for preferential flow are coming from the field of the soil sciences. *Gerke* (2006) provides an overview of various methods to implicitly or explicitly account for preferential flow. Most of them are focussed on the dispersion of pollutants and solutes, where neglecting preferential flow becomes most apparent.

In some models, preferential flow is simulated by modifying the hydraulic conductivity curve in near-saturated conditions. By increasing the hydraulic conductivity locally, a preferential

flow effect is mimicked (*Beven and Germann*, 2013). The idea is to describe the hydraulic conductivity function for a heterogeneous pore structure by overlapping two hydraulic conductivity curves, each one accounting for either the small pores or the large pores (*Durner*, 1994).

Another approach is two separate the domain in a dual-domain approach. In principle, the domain remains one-dimensional, but two sub-domains are defined. Then, several variants have been developed (*Šimůnek et al.*, 2003; *Beven and Germann*, 2013): (i) one of the sub-domains is considered immobile, the other one is solved by RE, (ii) both domains are solved with RE, but the domains differ in permeability, (iii) a combination of either an immobile or RE domain, and a domain in which water flow is governed by some form of kinematic equation. In all approaches, additional factors or functions are used to relate both domains with one another. Although the approaches sound attractive, as the simulations remain relatively simple and one-dimensional, it should be mentioned that they all require an additional set of parameters and exchange coefficients between sub-domains. This means that calibration is necessary in order to get good results, and, as will be discussed below, it seems delicate to collect a dataset from which preferential flow effects can be quantified. Furthermore, the methods described above basically treat preferential flow as resulting from macropores or other structural features in the matrix, which is questionable in the case of snow.

As argued above, the flow fingering process, which is considered an instability of the wetting front, may be more applicable to snow. However, a one-dimensional model approach will be inadequate to describe this process in a physics based approach. A very interesting pioneering study by *Hirashima et al.* (2014) has shown that RE was able to simulate the development of preferential flow paths in a 3-dimensional snow cover model, given two constraints: the implementation of a water entry suction threshold and spatially variable snow properties (and thus hydraulic properties). The model simulations were able to successfully simulate the laboratory experiments on preferential flow paths by *Katsushima et al.* (2013), regarding the density and size of preferential flow paths formed. Interestingly in this context is that *Hirashima et al.* (2014) achieved the simulation of preferential flow paths, without considering phase changes and snow metamorphism processes. This result suggests that mainly instabilities related to the flow processes (flow fingering) are responsible for the formation of preferential flow paths. Hysteresis in the water retention curve seems to be important for the formation of flow fingers. In laboratory experiments, it has been found that lateral flow that could potentially merge flow fingers is reduced because the core of the flow finger is on the drying curve of the water retention curve, whereas the surrounding matrix is on the wetting curve (*DiCarlo et al.*, 1999). At the same matric potential, the core of the flow finger has a higher water content than the surrounding matrix, while lateral flow is inhibited by the absence of a gradient in matric potential. Multiple studies have shown hysteresis in water retention curves in soils (e.g., *Topp* (1969)) and snow (e.g., *Wankiewicz* (1976); *Adachi et al.* (2012)). Although hysteresis was not considered by *Hirashima et al.* (2014), it may be that the water entry suction threshold mimics the effects of hysteresis in their simulations.

Finally, a complete understanding of preferential flow in snow possibly requires a combined treatment of preferential flow, phase changes and snow metamorphism. Preferential flow is known to be an important mechanism to infiltrate snow that is below freezing. When those preferential flow paths reach capillary barriers, they may form ice lenses inside the snowpack, between layers that are still below freezing.

6.1.3   Implications for Snow Cover Modelling

What is preferential flow in snow models supposed to explain? As discussed above, for runoff amounts and timing on the sub-daily time scale, the effect seems relatively small and inconsistent. The clearest signal of the possible effect of neglecting preferential flow paths is found in the seasonal dynamics of snowpack runoff. As hydraulic properties are often derived from experimental work on macro-scale soil or snow samples, possibly the effects of preferential flow is partly present in samples and aggregated into the parametrisations. Preferential flow paths may indeed occur at high spatial density, as for example shown in dye-tracer experiments on natural snowpacks in *Techel et al.* (2011). Furthermore, the current implementation in SNOWPACK, where the residual water content is always kept below the actual water content (see Chapter 2), results in all liquid water actively participating in liquid water transport. Whether or not this is the case (see Section 6.3), this approach may, as a side effect, partly represent preferential flow processes. Finally, discrepancies between simulated and measured snowpack runoff seems to be limited, in spite of neglecting preferential flow, for typical alpine snow covers of 2-3 m. This may be different in very deep snow covers.

The data from the upward looking ground penetrating radar provides also an excellent illustration of the diffuse picture regarding the topic of preferential flow, as discussed in Chapter 3. For example, in snow season 2010-2011, high amounts of snowpack runoff are measured by the snow lysimeter, although both the modelled and measured position of the melt water front is still high up in the snowpack. In other years, the moment the melt water front reaches the bottom of the snowpack in simulations with RE coincide well with the onset of snowpack runoff (e.g., 2011-2012 or 2013-2014). From the 4 years of upward looking ground penetrating radar data only, it is difficult to extract the factors governing these discrepancies.

It has become clear that before implementing an approach to model preferential flow in snow, it is very important to define what the preferential flow should explain. Subsequently, an adequate dataset to answer the question needs to be collected. From a hydrological point of view, neglecting preferential flow paths seems to play a minor role. For wet snow avalanche formation, a direct comparison between wet snow avalanche release and the liquid water flow is helpful and constructing such a dataset is encouraged. As preferential flow is thought to reach capillary barriers (that often form weak layers) in the snowpack earlier than matrix flow, one would expect to find a consistent tendency for an earlier avalanche release than expected based on modelled liquid water flow. Promising is also the data from the upward looking ground penetrating radar, where a direct comparison can be made to the position of

the melt water front in the snowpack and snowpack runoff. However, the four snow seasons studied here showed all a different melt water front dynamics in spring, and various degrees of congruence with model simulations and measured snowpack runoff. This suggests that a much longer time series is required for quantifying the contribution of preferential flow to total water flow in snow.

6.2 Wet Snow Avalanche Formation

In simulations of liquid water flow in snow with RE, strong accumulations of liquid water at inhomogeneities in the snow cover arose. For example at the Weissfluhjoch (Figure 3.5b) in new snow on top of old snow, or at Uf den Chaiseren at a surface hoar layer (Figure 1.3a). The latter is particularly identified as loosing its strength when wetted for the first time (*Techel et al.*, 2011). In the simulations, values typically rose to 10% volumetric contents in those water accumulations. These water accumulations are also observed in field studies, measuring spatial variability of liquid water in snow (*Techel and Pielmeier*, 2011). A comparison between field measurements and the simulations should be able to confirm that the accumulations of liquid water found in field measurements indeed coincide with capillary barriers in the simulations.

The simulations also reveal that those accumulations are especially outspoken when the snow gets wet for the first time in the season. Once melt water breaks through the capillary barrier, the hydraulic conductivity of the lower layers increases. The reduced gradient in hydraulic conductivity at the capillary barrier reduces its workings as a barrier. It would offer an explanation of why the avalanche risk increases at the first wetting, and decreases afterwards again. Currently, the avalanche warning service for Switzerland uses a liquid water content index based on the average liquid water content of the snowpack to help evaluating wet snow avalanche risks. The index typically works well for finding the onset of periods with wet snow avalanche activity, yet is unable to predict the decrease of activity again. The simulations and field observations suggest that the index may be improved by incorporating a measure of variance (e.g., standard deviation) of the vertical distribution of liquid water.

6.3 The Dry Limit

6.3.1 Dry Limit of Water Retention Curves

A water retention curve describes the relation between pressure head (h) and liquid water content (θ) of the porous medium under investigation. In this study, the van Genuchten model (*van Genuchten*, 1980) was used to describe the water retention curve. Another commonly applied model is the Brooks-Corey model (*Brooks and Corey*, 1964). Both models have the asymptotic limit for the water content for infinitely small pressure head not at 0, but at a residual water content (θ_r). Sometimes, θ_r is considered the amount of water that is held by adsorptive forces and cannot be extracted from the medium, sometimes it is considered a

fitting parameter and in other studies, it is noted that the liquid water content of a medium may eventually become 0 (*Peters*, 2013). For snow, a liquid water decrease below the residual water content is easily achieved by freezing, when the liquid water becomes part (again) of the snow matrix. Even at very low water contents, below what is generally considered the residual water content, water movement through porous media has been observed, for example by film flow (for example, in soil: *Lenormand* (1990), in snow: *de Quervain* (1973)).

Modifications of the water retention curve and hydraulic conductivity have been developed. *Hirashima et al.* (2010a) implements a pragmatic approach by linear interpolating the water retention curve from $\theta = 1.01 \cdot \theta_\mathrm{r}$ to $\theta = 0$, using the derivative of the water retention curve at $\theta = 1.01 \cdot \theta_\mathrm{r}$. In Chapter 2, another pragmatic approach is proposed. A more physics based approach is described in *Peters* (2013). He separates the hydraulic conductivity and the water saturation in a part for adsorptive forces (film flow) and a part for capillary dominated flow. Although in principle, the approach should be easy to implement in existing numerical models, a drawback is that either the approach is not consistent for small pore size distributions (values of parameter n close to 1.0), or the hydraulic conductivity function has no analytical solution and needs to be calculated by numerical integration. Finally, it should not be forgotten that all approaches are mainly for convenience, as RE is not valid for dry conditions, when the liquid water content is so low, that capillary pressure is not continuously defined anymore.

6.3.2 Water Vapour Flux

Apart from liquid water flow, water vapour transport has also been identified as an important process in soils (*Cahill and Parlange*, 1998) and snow (*Sturm and Benson*, 1997), especially in near-dry conditions. Water vapour transport may be described as the resulting process from a gradient in pressure head (isothermal) and in temperature (thermal) (*Philip and De Vries*, 1957). In fact, even when considering liquid water flow, a thermal gradient effect is present on the flow. This is due to the fact that surface tension, and thus capillary pressure, exhibits a temperature dependency (*Philip and De Vries*, 1957). The effect in snow is negligible, as either snow is wet, and temperature gradients are absent, or snow is dry and water vapour transport is the governing mass transfer process. Even for most soil conditions, the term generally is very small and plays a minor role in liquid water flow (*Philip and De Vries*, 1957).

Consider the liquid water flow in variably saturated porous media as originally described by RE (*Richards*, 1931):

$$\frac{\partial \theta}{\partial t} - \frac{\partial}{\partial z}\left(K(\theta)\left(\frac{\partial h}{\partial z} + \cos\gamma \right) \right) + s = 0, \tag{6.1}$$

where θ is the volumetric liquid water content (m^3 m^{-3}), K is the hydraulic conductivity (m s^{-1}), h is the pressure head (m), z is the vertical coordinate (m, positive upwards and perpendicular to the slope), γ is the slope angle and s is a source/sink term (m^3 m^{-3} s^{-1}).

For numerical models, *Saito et al.* (2006) proposed to extend Equation 6.1 to also include

vapour transport, by considering the gradient in pressure head (isothermal) and the gradient in temperature (thermal):

$$\frac{\partial \theta_{\mathrm{T}}}{\partial t} - \frac{\partial}{\partial z}\left(K_{\mathrm{T}h}(\theta)\frac{\partial h}{\partial z} + K_{\mathrm{L}h}\cos\gamma + K_{\mathrm{T}T}\frac{\partial T}{\partial z}\right) + s = 0, \tag{6.2}$$

where θ_{T} is the sum of liquid water and water vapour (m^3 m^{-3}), $K_{\mathrm{T}h}$ is the total hydraulic conductivity of the isothermal part (m s^{-1}), $K_{\mathrm{T}T}$ the total hydraulic conductivity of the thermal part (m s^{-1}) and $K_{\mathrm{L}h}$ is the hydraulic conductivity of the isothermal part for liquid water (m s^{-1}). Note that $K_{\mathrm{L}h}$ equals K in Equation 6.1. In this approach, the hydraulic conductivity $K_{\mathrm{T}h}$ for the isothermal part can be considered as a combination of the vapour ($K_{\mathrm{v}h}$) and liquid water part ($K_{\mathrm{L}h}$):

$$K_{\mathrm{T}h} = K_{\mathrm{L}h} + K_{\mathrm{v}h}. \tag{6.3}$$

Similarly for the hydraulic conductivity $K_{\mathrm{T}T}$ for the thermal part:

$$K_{\mathrm{T}T} = K_{\mathrm{L}T} + K_{\mathrm{v}T}, \tag{6.4}$$

where $K_{\mathrm{L}T}$ and $K_{\mathrm{v}T}$ are the hydraulic conductivities for the liquid water flow and vapour flux, respectively, under a thermal gradient. Note that the term $K_{\mathrm{L}T}$ is often small and negligible, as discussed above.

When vapour fluxes are present, latent heat is transferred as a consequence. Currently, SNOW-PACK does factor in the latent heat transfer due to vapour transport when calculating thermal conductivity. In wet snow, the thermal conductivity is artificially increased in adjacent dry layers to simulate the latent heat flux due to evaporation.

Combing the above methods, a complete numerical description for the processes of liquid water flow and vapour flow for the full range from dry to wet snowpack conditions is provided. However, it would involve several additional parameters and also validation may become difficult.

6.3.3 Implications for Snow Cover Modelling

There are indications that liquid water and vapour transport in the dry limit of snow has noticeable influences on the snow cover. For example, the average observed snow density at the base of the snowpack (<30 cm) at the measurement site WFJ shows a decreasing trend during a short period of the winter season, although liquid water is absent in this period (see Figure 6.2). The snow profiles also indicate that the snow metamorphism is producing depth hoar at the snowpack base (see Figure 3.13a). This suggests that the mass flux is directed upward inside the snowpack and significant mass transfer is taking place. However, SNOWPACK is designed around the idea that water vapour is indeed influencing snow metamorphism and produces depth hoar, yet the vapour flux is only considered in an element, i.e., the location of

mass remains constant during this process. This is also indicated by the fact that the simulated average snow density is continuously increasing during the main winter season as a result of continuous settling of the snowpack due to regular snow falls adding mass on top (Figure 6.2). The assumption that in deep alpine snow covers, temperature gradients remain relatively moderate, the moisture flux from the soil is relatively small and therefore also the vapour flux is negligible, is challenged by this figure.

The process may be even more important for situations where a significant source of water vapour is present at the lower boundary of the snowpack and the snowpack is shallow. For example, on sea ice, the formation of frost flowers on snow-free sea ice (*Massom et al.*, 2001) is a clear indication that vapour transport takes place through sea ice, especially via the brine channels. Brine is formed when sea salt is rejected from freezing ocean water and small droplets with high salinity are formed inside the sea ice. Sea ice is generally considered to become permeable when the brine volume exceeds 5% and the ice temperature is above −5°C (*Golden et al.*, 1998). The combination of a shallow snowpack, the possible low air temperatures (resulting in high temperature gradients) and a source of water vapour at the bottom of the snowpack results in the formation of depth hoar. This is generally observed in snowpacks at sea ice (*Massom et al.*, 2001). Snow on sea ice is also exposed to flooding, which occurs partly by the load of the snowpack exceeding the buoyancy of the sea ice, or by other processes, like swell (*Massom et al.*, 1997). Upward movement of sea water in snow by capillary suction up to 10-20 cm has been observed (*Massom et al.*, 2001) and is considered to be an important transport mechanisms of sea salt in the snowpack over sea ice (*Domine et al.*, 2004). The SNOWPACK model should be able to simulate this process when using the solver for the full RE. A further improved process representation in the dry limit would make SNOWPACK more suitable for snow on sea ice simulations. Another example can be found in snow covered subarctic or tundra areas. Also there, soil moisture provides a source of water vapour, and the temperature gradients in the generally shallow snow cover (typically less than 1 m), drive moisture transport inside the snowpack. This leads to significant formations of depth hoar, as found in a study by *Sturm and Benson* (1997). They also showed that layers where depth hoar formed, were subject to significant mass loss, whereas upper layers of the snowpack gained mass. This is a clear indication that vapour transport between snow layers needs to be taken into account for these type of snowpack conditions.

6.4 The Wet Limit

Typical values of volumetric liquid water content for snow are around 4%, which corresponds with saturation values around 10% (*Coléou and Lesaffre*, 1998). Compared to typical values for soil, wet snow may still be considered rather dry. For hydrological processes at the catchment scale, groundwater flow, subsurface lateral flow or overland flow are considered to be important processes. *Kampf et al.* (2014) found indications that subsurface lateral flow was occurring on steep hillslopes during snowmelt, yet soil moisture measurements provided a rather inconsistent picture.

166
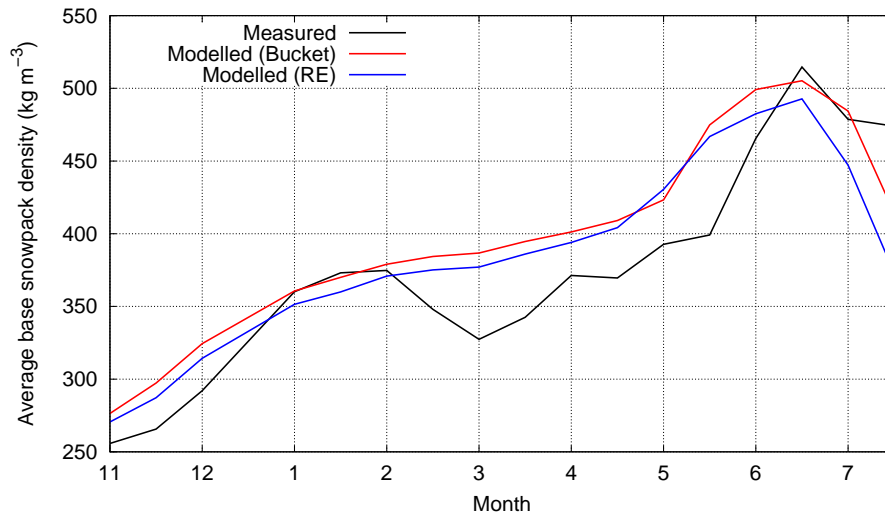
Figure 6.2: Snowpack density of the base of the snowpack from the lowest density measurement (< 30 cm), averaged from the bi-weekly profiles from 1999-2013 and the corresponding densities from SNOWPACK simulations with either the Bucket scheme or RE for simulating liquid water flow.

For snow, lateral flow normally is considered to play a minor role. Typical soils in alpine terrain have a high permeability and liquid water draining from the snowpack is normally able to infiltrate the underlying soil. Some exceptions can be made here. If melt water leaving the snowpack has difficulties infiltrating the underlying soil, lateral flow may occur. This has been observed when soil is frozen (*Johnsson and Lundin*, 1991; *Bayard et al.*, 2005). Simulations with RE suggest that this could potentially also occur when the underlying soil is relatively impermeable due to its composition (Figure 1.3b). The brownish water found at the snowpack base of glide snow avalanches also suggests that lateral flow may have occurred here (Figure 1.2). In this case, the long, dry grass may have also acted as a capillary barrier causing accumulations of liquid water at the base of the snowpack. Furthermore, crusts, ice layers or capillary barriers may also form a surface above which lateral flow may occur, because the downward water motion is severely hindered (*Peitzsch et al.*, 2008; *Techel et al.*, 2011).

In the rain-on-snow event discussed in Chapter 5, the streams reacted with unprecedented increases in streamflow after the onset of rain (*Badoux et al.*, 2013; *Rössler et al.*, 2014). In the hydrological model system used by *Rössler et al.* (2014), significant recalibration of parameters relating liquid water in the snowpack to runoff was required for simulating the observed response in streamflow for this event. The role of lateral flow in the snowpack or at the snow-soil interface has been hypothesized, although neither the snow, nor the predisposition of the soil would indicate this. For example, the snow cover is not expected to have had capillary barriers or ice lenses which may have favoured preferential flow. Rather, the snow cover was built up by approximately continuous snowfall and the stratification is expected to be homogeneous. The underlying soil was not unusual wet, or frozen, which could have caused

preferential flow at the snow-soil boundary. So far, it remains an unresolved question what the role of lateral flow in the snowpack or at the snow-soil interface has been (*Badoux et al.*, 2013).

A problem with modelling strategies for lateral flow is that in most hydrological models, calibration factors are present which are optimized for a particular catchment, often calibrated using streamflow. It is to be expected that lateral flow processes are described implicitly by the calibration. In some hydrological models, RE is solved in 3 dimensions for the unsaturated zone of the soil, which, in theory, should be able to explicitly simulate lateral flow processes. However, several problems may be identified with this approach. First of all, if grid spacing is large, the model is supposed to simulate average flow behaviour for a large grid cell. However, it does not seem possible to describe the response of spatially variable parameters (e.g., hydraulic conductivity) with a single consistent effective parameter (*Beven*, 1989). The Alpine3D simulations discussed in Chapter 4 were run with a grid cell size of 100x100 m^2. Another problem is that on these scales, concepts like gradients in pressure head loose its meaning (*Beven*, 1989). Taking these factors into account, one would expect that a useful grid size would be rather in the order of 1 m, which poses an infeasible computationally demand for Alpine3D in the near future, not to mention that a realistic initialization of surface and soil properties on these scales also seem problematic.

Nevertheless, possible lateral flow processes in snow may still be assessed with the Alpine3D model. As discussed above, the most important component of liquid water flow in snow is normally formed by the gravity component. In sloped terrain, the main component of lateral liquid water flow is expected to be in the direction of gravity. Therefore, the SNOWPACK model needs to separate the gravity component of liquid water flow in a component perpendicular to the slope and one parallel to the slope. Currently, only the perpendicular component is used in the calculations. However, the information about the parallel component can be used to move liquid water downslope from grid cell to grid cell. The source/sink term of RE (Equation 6.1) can be used to simulate downslope moving liquid water.

A remaining technical issue in the SNOWPACK model is that simulations are aborted when positive pressure heads due to ponding inside the model domain arise. This happens when the snow or soil is fully saturated and additional water is added (e.g., by rainfall). As more water is added than there is a room for in the matrix, the solver cannot find a solution anymore. This particular situation is now prevented by limiting the maximum allowed incoming flux to a value where the upper node is still able to handle the water. In alpine snow covers, the situation is occurring rather seldom, due to the high permeable soils and sloped terrain. For the application of SNOWPACK for different situations, like sea ice, or tundra, ponding on top of the snow cover may be an important process to consider. This could be incorporated in the SNOWPACK model by enabling a water layer on top of the snow-soil continuum, from which the pressure head exerted by its depth can be assigned as a Dirichlet boundary condition for pressure head on top of the snowpack.

Appendix

Figure A1 provides a flow chart of the SNOWPACK model, with a special focus on the water transport schemes.

SNOWPACK time step flow chart

Add **new snow** in case of snowfall	
Determine **boundary conditions** for temperature equation	
Solve **temperature** profile	
Perform **phase changes**	
Perform l**iquid water flow**	

Bucket and NIED schemes — **Richards equation**

Apply sublimation, deposition, evaporation and condensation: adjust top element ice matrix and water content

Apply sublimation, deposition: adjust ice matrix

Apply evaporation, condensation and rainfall: add to upper boundary flux

Remove and merge thin elements and elements with low ice content

Remove and merge thin elements and elements with low ice content

Initialize per snow layer: water retention curve and saturated hydraulic conductivity

Add rain water in case of rainfall

Melt ice matrix to match specified minimum initial pressure head

Determine and set boundary conditions for liquid water flow

Solve Picard iteration

Assess heat advection by liquid water flow in soil and soil freezing and thawing

Check convergence of Picard iteration

Picard iterations

Route liquid water in snow and/or soil with bucket or NIED scheme

Time step control: optimize Richards equation time steps

Richards equation time steps

Perform **phase changes** (for refreezing percolating water)

Calculate snowpack creep (settling)

Calculate snowpack microstructure

Combine and split snow elements to optimize computational load
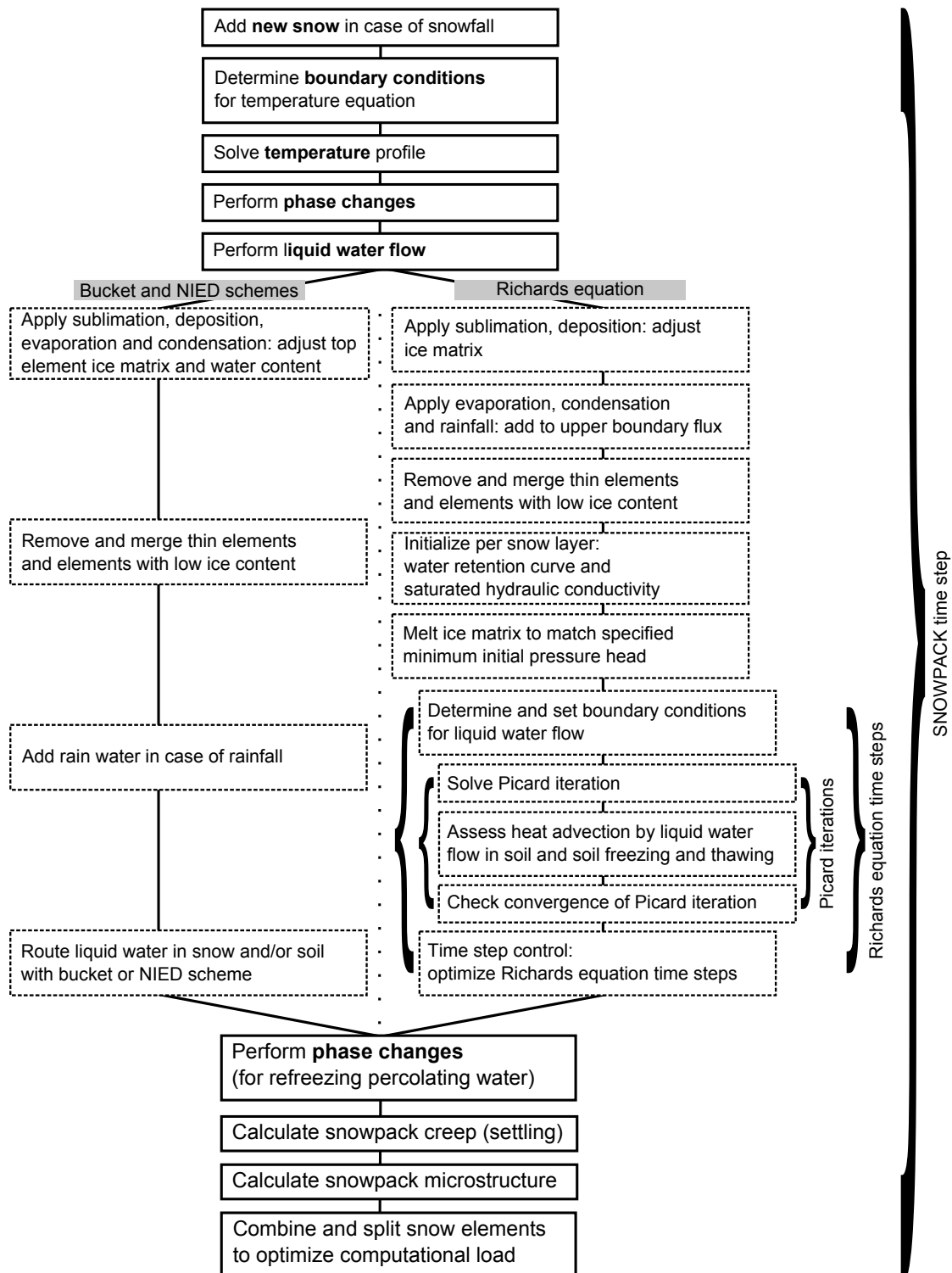
SNOWPACK time step

Figure A1: Flow chart for one time step of the SNOWPACK model, with a special focus on the water transport schemes.

Bibliography

Adachi, S., S. Yamaguchi, T. Ozeki, and K. Kose (2012), Hysteresis in the water retention curve of snow measured using an MRI system, in *Proceedings of the 2012 International Snow Science Workshop*.

Ambroise, B., J. Freer, and K. Beven (1996), Application of a generalized TOPMODEL to the Small Ringelbach Catchment, Vosges, France, *Water Resour. Res.*, *32*(7), 2147–2159, doi:10.1029/95WR03715.

Avanzi, F., M. Caruso, C. Jommi, C. D. Michele, and A. Ghezzi (2014), Continuous-time monitoring of liquid water content in snowpacks using capacitance probes: A preliminary feasibility study, *Adv. Water Resour.*, *68*, 32–41, doi:10.1016/j.advwatres.2014.02.012.

Bachmann, J., R. Horton, T. Ren, and R. R. van der Ploeg (2001), Comparison of the thermal properties of four wettable and four water-repellent soils, *Soil Sci. Soc. Am. J.*, *65*(6), 1675–1679, doi:10.2136/sssaj2001.1675.

Badoux, A., M. Hofer, and T. Jonas (Eds.) (2013), *Hydrometeorologische Analyse des Hochwasser-ereignisses vom 10. Oktober 2011*, Birmensdorf, Swiss Federal Institute for Forest, Snow and Landscape Research WSL; Davos, WSL-Institute for Snow and Avalanche Research SLF; Zürich, Federal Office of Meteorology and Climatology MeteoSwiss; Bern, geo7 geowissenschaftliches Büro; Bern, Federal Office for the Environment FOEN, in German.

Baggi, S., and J. Schweizer (2009), Characteristics of wet-snow avalanche activity: 20 years of observations from a high alpine valley (Dischma, Switzerland), *Nat. Hazards*, *50*(1), 97–108, doi:10.1007/s11069-008-9322-7.

Bales, R. C., J. W. Hopmans, A. T. O'Geen, M. Meadows, P. C. Hartsough, P. Kirchner, C. T. Hunsaker, and D. Beaudette (2011), Soil moisture response to snowmelt and rainfall in a Sierra Nevada mixed-conifer forest, *Vadose Zone J.*, *10*(3), 786–799, doi:10.2136/vzj2011.0001.

Bartelt, P., and M. Lehning (2002), A physical SNOWPACK model for the Swiss avalanche warning Part I: Numerical model, *Cold Reg. Sci. Technol.*, *35*(3), 123–145, doi:10.1016/S0165-232X(02)00074-5.

Basso, S., and G. Botter (2012), Streamflow variability and optimal capacity of run-of-river hydropower plants, *Water Resour. Res.*, *48*(10), doi:10.1029/2012WR012017.

Baunach, T., C. Fierz, P. K. Satyawali, and M. Schneebeli (2001), A model for kinetic grain growth, *Ann. Glaciol.*, *32*(1), 1–6, doi:10.3189/172756401781819427.

Bavay, M., and T. Egger (2014), MeteoIO 2.4.2: a preprocessing library for meteorological data, *Geosci. Model Dev. Discuss.*, *7*(3), 3595–3645, doi:10.5194/gmdd-7-3595-2014.

Bavay, M., M. Lehning, T. Jonas, and H. Löwe (2009), Simulations of future snow cover and discharge in Alpine headwater catchments, *Hydrol. Proc.*, *23*(1), 95–108, doi:10.1002/hyp.7195.

Bavay, M., T. Grünewald, and M. Lehning (2013), Response of snow cover and runoff to climate change in high Alpine catchments of Eastern Switzerland, *Adv. Water Resour.*, *55*, 4–16, doi:10.1016/j.advwatres.2012.12.009.

Bayard, D., M. Stähli, A. Parriaux, and H. Flühler (2005), The influence of seasonally frozen soil on the snowmelt runoff at two Alpine sites in Southern Switzerland, *J. Hydrol.*, *309*(1-4), 66–84, doi:10.1016/j.jhydrol.2004.11.012.

Berg, A. A., and K. A. Mulroy (2006), Streamflow predictability in the Saskatchewan/Nelson River basin given macroscale estimates of the initial soil moisture status, *Hydrolog. Sci. J.*, *51*(4), 642–654, doi:10.1623/hysj.51.4.642.

Beven, K. (1989), Changing ideas in hydrology – The case of physically-based models, *J. Hydrol.*, *105*(1–2), 157–172, doi:10.1016/0022-1694(89)90101-7.

Beven, K. (1993), Prophecy, reality and uncertainty in distributed hydrological modelling, *Adv. Water Resour.*, *16*(1), 41–51, doi:10.1016/0309-1708(93)90028-E, research Perspectives in Hydrology.

Beven, K., and P. Germann (1982), Macropores and water flow in soils, *Water Resour. Res.*, *18*(5), 1311–1325, doi:10.1029/WR018i005p01311.

Beven, K., and P. Germann (2013), Macropores and water flow in soils revisited, *Water Resour. Res.*, *49*(6), 3071–3092, doi:10.1002/wrcr.20156.

Boone, A., and P. Etchevers (2001), An intercomparison of three snow schemes of varying complexity coupled to the same land surface model: Local-scale evaluation at an Alpine site, *J. Hydrometeor.*, *2*(4), 374–394, doi:10.1175/1525-7541(2001)002<0374:AIOTSS>2.0.CO;2.

Bormann, K. J., S. Westra, J. P. Evans, and M. F. McCabe (2013), Spatial and temporal variability in seasonal snow density, *J. Hydrol.*, *484*(0), 63–73, doi:10.1016/j.jhydrol.2013.01.032.

Brooks, R., and A. Corey (1964), Hydraulic properties of porous media, *Hydrological Papers, 3*, (Colorado State

Bibliography

University).

Brun, E., E. Martin, V. Simon, C. Gendre, and C. Coléou (1989), An energy and mass model of snow cover suitable for operational avalanche forecasting, *J. Glaciol.*, *35*(121), 333–342.

Cahill, A. T., and M. B. Parlange (1998), On water vapor transport in field soils, *Water Resour. Res.*, *34*(4), 731–739, doi:10.1029/97WR03756.

Calonne, N., C. Geindreau, F. Flin, S. Morin, B. Lesaffre, S. Rolland du Roscoat, and P. Charrier (2012), 3-D image-based numerical computations of snow permeability: links to specific surface area, density, and microstructural anisotropy, *Cryosphere*, *6*(5), 939–951, doi:10.5194/tc-6-939-2012.

Carmagnola, C. M., S. Morin, M. Lafaysse, F. Domine, B. Lesaffre, Y. Lejeune, G. Picard, and L. Arnaud (2014), Implementation and evaluation of prognostic representations of the optical diameter of snow in the SURFEX/ISBA-Crocus detailed snowpack model, *Cryosphere*, *8*(2), 417–437, doi:10.5194/tc-8-417-2014.

Celia, M. A., E. T. Bouloutas, and R. L. Zarba (1990), A general mass-conservative numerical solution for the unsaturated flow equation, *Water Resour. Res.*, *26*(7), 1483–1496, doi:10.1029/WR026i007p01483.

Cohen, J., and D. Rind (1991), The effect of snow cover on the climate, *J. Climate*, *4*(7), 689–706, doi:10.1175/1520-0442(1991)004<0689:TEOSCO>2.0.CO;2.

Colbeck, S. (1979), Grain clusters in wet snow, *J. Colloid Interface Sci.*, *72*(3), 371–384, doi:10.1016/0021-9797(79)90340-0.

Colbeck, S. C. (1972), A theory of water percolation in snow, *J. Glaciol.*, *11*(63), 369–385.

Colbeck, S. C. (1974), The capillary effects on water percolation in homogeneous snow, *J. Glaciol.*, *13*(67), 85–97.

Colbeck, S. C. (1982), An overview of seasonal snow metamorphism, *Rev. Geophys.*, *20*(1), 45–61, doi:10.1029/RG020i001p00045.

Colbeck, S. C. (1997), A review of sintering in seasonal snow., *CRREL report 97-10*, US Army Cold Regions Research and Engineering Laboratory.

Coléou, C., and B. Lesaffre (1998), Irreducible water saturation in snow: experimental results in a cold laboratory, *Ann. Glaciol.*, *26*, 64 – 68.

Comola, F., B. Schaefli, A. Rinaldo, and M. Lehning (2014), Flow and temperature dynamics in the hydrologic response: Travel time formulation and application to Alpine catchments, *Submitted to: Water Resour. Res.*

Conway, H., and R. Benedict (1994), Infiltration of water into snow, *Water Resour. Res.*, *30*(3), 641–649, doi:10.1029/93WR03247.

Conway, H., and C. F. Raymond (1993), Snow stability during rain, *J. Glaciol.*, *39*(133), 635–642.

Daanen, R., and J. Nieber (2009), Model for coupled liquid water flow and heat transport with phase change in a snowpack, *J. Cold Reg. Eng.*, *23*(2), 43–68, doi:10.1061/(ASCE)0887-381X(2009)23:2(43).

Dall'Amico, M., S. Endrizzi, S. Gruber, and R. Rigon (2011), A robust and energy-conserving model of freezing variably-saturated soil, *Cryosphere*, *5*(2), 469–484, doi:10.5194/tc-5-469-2011.

Davis, R. E., R. Jordan, S. Daly, and G. G. Koenig (2001), *Model Validation: Perspectives in Hydrological Science*, John Wiley & Sons Ltd.

de Quervain, M. (1973), Snow structure, heat, and mass flux through snow, in *The Role of Snow and Ice in Hydrology*, vol. 1, chap. Snow structure, heat and mass flux through snow, pp. 203–206, International Association of Hydrological Sciences (IAHS), report 107.

Decagon Devices (2014), 10HS soil moisture sensor, *Tech. rep.*

Dekker, T. J. (1969), Finding a zero by means of successive linear interpolation, in *Constructive Aspects of the Fundamental Theorem of Algebra*, edited by B. Dejon and P. Henrici, Wiley-Interscience.

Denoth, A. (1982), The pendular-funicular liquid transition and snow metamorphism, *J. Glaciol.*, *28*(99), 357–364.

Denoth, A. (1994), An electronic device for long-term snow wetness recording, *Ann. Glaciol.*, *19*, 104–106.

DiCarlo, D. A., T. W. J. Bauters, C. J. G. Darnault, T. S. Steenhuis, and J.-Y. Parlange (1999), Lateral expansion of preferential flow paths in sands, *Water Resour. Res.*, *35*(2), 427–434, doi:10.1029/1998WR900061.

Disse, M., and H. Engel (2001), Flood events in the Rhine basin: Genesis, influences and mitigation, *Nat. Hazards*, *23*(2-3), 271–290, doi:10.1023/A%3A1011142402374.

Domine, F., R. Sparapani, A. Ianniello, and H. J. Beine (2004), The origin of sea salt in snow on Arctic sea ice and in coastal regions, *Atmos. Chem. Phys.*, *4*(9/10), 2259–2271, doi:10.5194/acp-4-2259-2004.

Domine, F., S. Morin, E. Brun, M. Lafaysse, and C. M. Carmagnola (2013), Seasonal evolution of snow permeability under equi-temperature and temperature-gradient conditions, *Cryosphere*, *7*(6), 1915–1929, doi:10.5194/

tc-7-1915-2013.

Durner, W. (1994), Hydraulic conductivity estimation for soils with heterogeneous pore structure, *Water Resour. Res.*, *30*(2), 211–223, doi:10.1029/93WR02676.

Edwards, A. C., R. Scalenghe, and M. Freppaz (2007), Changes in the seasonal snow cover of alpine regions and its effect on soil processes: A review, *Quat. Int.*, *162–163*, 172–181, doi:10.1016/j.quaint.2006.10.027.

Endrizzi, S., S. Gruber, M. Dall'Amico, and R. Rigon (2013), GEOtop 2.0: simulating the combined energy and water balance at and below the land surface accounting for soil freezing, snow cover and terrain effects, *Geosci. Model Dev. Discuss.*, *6*(4), 6279–6341, doi:10.5194/gmdd-6-6279-2013.

Essery, R., and P. Etchevers (2004), Parameter sensitivity in simulations of snowmelt, *J. Geophys. Res.*, *109*(D20), doi:10.1029/2004JD005036.

Essery, R., S. Morin, Y. Lejeune, and C. B. Ménard (2013), A comparison of 1701 snow models using observations from an alpine site, *Adv. Water Resour.*, *55*(0), 131 – 148, doi:10.1016/j.advwatres.2012.07.013.

Federal Office for Water and Geology (2002), *Hochwasser 2000 - Ereignisanalyse/Fallbeispiele*, Berichte des BWG, Serie Wasser Nr. 2 - Bern, in German.

Fierz, C., R. Armstrong, Y. Durand, P. Etchevers, E. Greene, D. McClung, K. Nishimura, P. Satyawali, and S. Sokratov (2009), The International Classification for Seasonal Snow on the Ground (ICSSG), *Tech. rep.*, IHP-VII Technical Documents in Hydrology No. 83, IACS Contribution No. 1, UNESCO-IHP.

Fily, M., J. Dedieu, and Y. Durand (1999), Comparison between the results of a snow metamorphism model and remote sensing derived snow parameters in the Alps, *Remote Sens. Environ.*, *68*(3), 254–263, doi:10.1016/S0034-4257(98)00116-3.

Fink, A., U. Ulbrich, and H. Engel (1996), Aspects of the January 1995 flood in Germany, *Weather*, *51*(2), 34–39, doi:10.1002/j.1477-8696.1996.tb06182.x.

Flerchinger, G. N., and K. E. Saxton (1989), Simultaneous heat and water model of a freezing snow-residue-soil system: I. Theory and development., *Trans. Amer. Soc. Agric. Engr.*, *32*(2), 565–571.

Fontaine, T., T. Cruickshank, J. Arnold, and R. Hotchkiss (2002), Development of a snowfall-snowmelt routine for mountainous terrain for the soil water assessment tool (SWAT), *J. Hydrol.*, *262*(1–4), 209–223, doi:10.1016/S0022-1694(02)00029-X.

Førland, E., P. Allerup, B. Dahlström, E. Elomaa, T. Jónsson, H. Madsen, Perälä, P. Rissanen, H. Vedin, and F. Vejen (1996), Manual for operational correction of Nordic precipitation data, *Tech. Rep. 24/96*, Norske Meteorologiske Institutt.

Forster, F., and C. Hegg (2000), The flood events of May 1999: an analysis based on hydrologic measurements in small catchments, *Schweizerische Zeitschrift für Forstwesen*, *151*(6), 183–191, doi:10.3188/szf.2000.0183, in German.

Gerke, H. H. (2006), Preferential flow descriptions for structured soils, *J. Plant Nutr. Soil Sci.*, *169*(3), 382–400, doi:10.1002/jpln.200521955.

Giard, D., and E. Bazile (2000), Implementation of a new assimilation scheme for soil and surface variables in a global NWP model, *Mon. Wea. Rev.*, *128*(4), 997–1015, doi:10.1175/1520-0493(2000)128<0997:IOANAS>2.0.CO;2.

Golden, K. M., S. F. Ackley, and V. I. Lytle (1998), The percolation phase transition in sea ice, *Science*, *282*(5397), 2238–2241, doi:10.1126/science.282.5397.2238.

Goodison, B., P. Louie, and D. Yang (1998), WMO Solid precipitation measurement intercomparison, Final Report, *Tech. rep.*, World Meteorological Organization (WMO).

Groot Zwaaftink, C. D., A. Cagnati, A. Crepaz, C. Fierz, G. Macelloni, M. Valt, and M. Lehning (2013), Event-driven deposition of snow on the Antarctic Plateau: analyzing field measurements with SNOWPACK, *Cryosphere*, *7*(1), 333–347, doi:10.5194/tc-7-333-2013.

Hansson, K., J. Šimůnek, M. Mizoguchi, L.-C. Lundin, and M. T. van Genuchten (2004), Water flow and heat transport in frozen soil, *Vadose Zone J.*, *3*(2), 693–704.

Haverkamp, R., and M. Vauclin (1979), A note on estimating finite difference interblock hydraulic conductivity values for transient unsaturated flow problems, *Water Resour. Res.*, *15*(1), 181–187, doi:10.1029/WR015i001p00181.

Heilig, A., M. Schneebeli, and O. Eisen (2009), Upward-looking ground-penetrating radar for monitoring snowpack stratigraphy, *Cold Reg. Sci. Technol.*, *59*(2-3), 152–162, doi:10.1016/j.coldregions.2009.07.008, International Snow Science Workshop (ISSW) 2008.

Heilig, A., O. Eisen, and M. Schneebeli (2010), Temporal observations of a seasonal snowpack using upward-looking

GPR, *Hydrol. Proc.*, *24*(22), 3133–3145, doi:10.1002/hyp.7749.

Hill, D. E., and J.-Y. Parlange (1972), Wetting front instability in layered soils, *Soil Sci. Soc. Am. J.*, *36*, 697–702, doi:10.2136/sssaj1972.03615995003600050010x.

Hirashima, H., S. Yamaguchi, A. Sato, and M. Lehning (2010a), Numerical modeling of liquid water movement through layered snow based on new measurements of the water retention curve, *Cold Reg. Sci. Technol.*, *64*(2), 94 – 103, doi:10.1016/j.coldregions.2010.09.003.

Hirashima, H., I. Kamiishi, S. Yamaguchi, A. Sato, and M. Lehning (2010b), Application of a numerical snowpack model to estimate full-depth avalanche danger, in *Proceedings of the 2010 International Snow Science Workshop*.

Hirashima, H., S. Yamaguchi, and T. Katsushima (2014), A multi-dimensional water transport model to reproduce preferential flow in the snowpack, *Cold Reg. Sci. Technol.*, in press.

Hock, R. (1999), A distributed temperature-index ice- and snowmelt model including potential direct solar radiation, *J. Glaciol.*, *45*(149), 101–111.

Hock, R. (2003), Temperature index melt modelling in mountain areas, *J. Hydrol.*, *282*(1-4), 104–115, doi:10.1016/S0022-1694(03)00257-9.

Huang, K., B. Mohanty, and M. van Genuchten (1996), A new convergence criterion for the modified Picard iteration method to solve the variably saturated flow equation, *J. Hydrol.*, *178*(1-4), 69 – 91, doi:10.1016/0022-1694(95)02799-8.

Illangasekare, T. H., R. J. Walter, Jr., M. F. Meier, and W. T. Pfeffer (1990), Modeling of meltwater infiltration in subfreezing snow, *Water Resour. Res.*, *26*(5), 1001–1012, doi:10.1029/WR026i005p01001.

Ingelrest, F., G. Barrenetxea, G. Schaefer, M. Vetterli, O. Couach, and M. Parlange (2010), SensorScope: Application-specific sensor network for environmental monitoring, *ACM Trans. Sens. Netw.*, *6*(2), doi:{10.1145/1689239.1689247}.

Ippisch, O., H.-J. Vogel, and P. Bastian (2006), Validity limits for the van Genuchten-Mualem model and implications for parameter estimation and numerical simulation, *Adv. Water Resour.*, *29*(12), 1780 – 1789, doi:10.1016/j.advwatres.2005.12.011.

Jin, J., X. Gao, Z.-L. Yang, R. C. Bales, S. Sorooshian, R. E. Dickinson, S. F. Sun, and G. X. Wu (1999), Comparative analyses of physically based snowmelt models for climate simulations, *J. Climate*, *12*(8), 2643–2657, doi:10.1175/1520-0442(1999)012<2643:CAOPBS>2.0.CO;2.

Johnsson, H., and L.-C. Lundin (1991), Surface runoff and soil water percolation as affected by snow and soil frost, *J. Hydrol.*, *122*(1-4), 141–159, doi:10.1016/0022-1694(91)90177-J.

Jonas, T., C. Marty, and J. Magnusson (2009), Estimating the snow water equivalent from snow depth measurements in the Swiss Alps, *J. Hydrol.*, *378*(1-2), 161–167, doi:10.1016/j.jhydrol.2009.09.021.

Jordan, P. (1983a), Meltwater movement in a deep snowpack: 2. Simulation model, *Water Resour. Res.*, *19*(4), 979–985, doi:10.1029/WR019i004p00979.

Jordan, P. (1983b), Meltwater movement in a deep snowpack: 1. Field observations, *Water Resour. Res.*, *19*(4), 971–978, doi:10.1029/WR019i004p00971.

Jordan, R. (1991), A one-dimensional temperature model for a snow cover: Technical documentation SNTHERM.89, *Tech. Rep. Spec. Rep. 657*, U.S. Army Cold Reg. Res. Eng. Lab., Hanover, NH.

Jordan, R. (1996), Effects of capillary discontinuities on water flow and water retention in layered snowcovers., in *Proceedings of the International Symposium on Snow and Related Manifestations.*, vol. 94, edited by K. C. Agrawal, pp. 157–170, Snow and Avalanche Study Establishment, Manali, India.

Kampf, S., J. Markus, J. Heath, and C. Moore (2014), Snowmelt runoff and soil moisture dynamics on steep subalpine hillslopes, *Hydrol. Proc.*, doi:10.1002/hyp.10179.

Kapnick, S. B., and T. L. Delworth (2013), Controls of global snow under a changed climate, *J. Climate*, *26*(15), 5537–5562, doi:10.1175/JCLI-D-12-00528.1.

Katsushima, T., S. Yamaguchi, T. Kumakura, and A. Sato (2013), Experimental analysis of preferential flow in dry snowpack, *Cold Reg. Sci. Technol.*, *85*, 206–216, doi:10.1016/j.coldregions.2012.09.012.

Kattelmann, R. (1984), Wet slab instability, in *Proceedings of the 1984 International Snow Science Workshop*.

Kattelmann, R. (1985), Macropores in snowpacks of Sierra Nevada, *Ann. Glaciol.*, *6*, 272–273.

Kattelmann, R. (2000), Snowmelt lysimeters in the evaluation of snowmelt models, *Ann. Glaciol.*, *31*(1), 406–410, doi:10.3189/172756400781820048.

Koster, R. D., S. P. P. Mahanama, B. Livneh, D. P. Lettenmaier, and R. H. Reichle (2010), Skill in streamflow forecasts

derived from large-scale estimates of soil moisture and snow, *Nature Geosci.*, *3*(9), 613–616, doi:10.1038/ngeo944.

Kumar, M., D. Marks, J. Dozier, M. Reba, and A. Winstral (2013), Evaluation of distributed hydrologic impacts of temperature-index and energy-based snow models, *Adv. Water Resour.*, *56*(0), 77–89, doi:10.1016/j.advwatres.2013.03.006.

Lehning, M., P. Bartelt, B. Brown, T. Russi, U. Stöckli, and M. Zimmerli (1999), SNOWPACK calculations for avalanche warning based upon a new network of weather and snow stations, *Cold Reg. Sci. Technol.*, *30*(1–3), 145–157, doi:10.1016/S0165-232X(99)00022-1.

Lehning, M., C. Fierz, and C. Lundy (2001), An objective snow profile comparison method and its application to SNOWPACK, *Cold Reg. Sci. Technol.*, *33*(2-3), 253–261, doi:10.1016/S0165-232X(01)00044-1, International Snow Science Workshop (ISSW) 2000.

Lehning, M., P. Bartelt, B. Brown, C. Fierz, and P. Satyawali (2002a), A physical SNOWPACK model for the Swiss avalanche warning Part II. Snow microstructure, *Cold Reg. Sci. Technol.*, *35*(3), 147 – 167, doi:10.1016/S0165-232X(02)00073-3.

Lehning, M., P. Bartelt, B. Brown, and C. Fierz (2002b), A physical SNOWPACK model for the Swiss avalanche warning Part III: Meteorological forcing, thin layer formation and evaluation, *Cold Reg. Sci. Technol.*, *35*(3), 169 – 184, doi:10.1016/S0165-232X(02)00072-1.

Lehning, M., I. Völksch, D. Gustafsson, T. A. Nguyen, M. Stähli, and M. Zappa (2006), ALPINE3D: a detailed model of mountain surface processes and its application to snow hydrology, *Hydrol. Proc.*, *20*(10), 2111–2128, doi:10.1002/hyp.6204.

Lehning, M., H. Löwe, M. Ryser, and N. Raderschall (2008), Inhomogeneous precipitation distribution and snow transport in steep terrain, *Water Resour. Res.*, *44*(7), W07404, doi:10.1029/2007WR006545.

Lenormand, R. (1990), Liquids in porous media, *J. Phys.: Condens. Matter*, *2*, SA79–SA88, doi:10.1088/0953-8984/2/S/008.

Luetschg, M., V. Stoeckli, M. Lehning, W. Haeberli, and W. Ammann (2004), Temperatures in two boreholes at Flüela pass, Eastern Swiss Alps: the effect of snow redistribution on permafrost distribution patterns in high mountain areas, *Permafrost Periglacial Process.*, *15*(3), 283–297, doi:10.1002/ppp.500.

Mahanama, S. P., B. Livneh, R. Koster, D. Lettenmaier, and R. Reichle (2012), Soil moisture, snow, and seasonal streamflow forecasts in the United States, *J. Hydrometeor.*, *13*(1), 189/203, doi:{10.1175/JHM-D-11-046.1}.

Marks, D., J. Kimball, D. Tingey, and T. Link (1998), The sensitivity of snowmelt processes to climate conditions and forest cover during rain-on-snow: a case study of the 1996 Pacific Northwest flood, *Hydrol. Proc.*, *12*(10-11), 1569–1587, doi:10.1002/(SICI)1099-1085(199808/09)12:10/11<1569::AID-HYP682>3.0.CO;2-L.

Marks, D., J. Domingo, D. Susong, T. Link, and D. Garen (1999), A spatially distributed energy balance snowmelt model for application in mountain basins, *Hydrol. Proc.*, *13*(12-13), 1935–1959, doi:10.1002/(SICI)1099-1085(199909)13:12/13<1935::AID-HYP868>3.0.CO;2-C.

Marks, D., T. Link, A. Winstral, and D. Garen (2001), Simulating snowmelt processes during rain-on-snow over a semi-arid mountain basin, *Ann. Glaciol.*, *32*(1), 195–202, doi:10.3189/172756401781819751.

Marsh, P. (1991), *Water flux in melting snow covers, Advances in Porous Media*, vol. 1, pp. 61–124, Elsevier, Amsterdam.

Marsh, P. (1999), Snowcover formation and melt: recent advances and future prospects, *Hydrol. Proc.*, *13*(14-15), 2117–2134, doi:10.1002/(SICI)1099-1085(199910)13:14/15<2117::AID-HYP869>3.0.CO;2-9.

Marsh, P. (2006), *Encyclopedia of Hydrological Sciences.*, chap. 161: Water Flow Through Snow and Firn, pp. 1–14, John Wiley & Sons, Ltd, Chichester, England, doi:10.1002/0470848944.hsa167.

Marshall, H., H. Conway, and L. Rasmussen (1999), Snow densification during rain, *Cold Reg. Sci. Technol.*, *30*(1–3), 35–41, doi:10.1016/S0165-232X(99)00011-7.

Massom, R. A., M. R. Drinkwater, and C. Haas (1997), Winter snow cover on sea ice in the Weddell Sea, *J. Geophys. Res.*, *102*(C1), 1101–1117, doi:10.1029/96JC02992.

Massom, R. A., H. Eicken, C. Hass, M. O. Jeffries, M. R. Drinkwater, M. Sturm, A. P. Worby, X. Wu, V. I. Lytle, S. Ushio, K. Morris, P. A. Reid, S. G. Warren, and I. Allison (2001), Snow on Antarctic sea ice, *Rev. Geophys.*, *39*(3), 413–445, doi:10.1029/2000RG000085.

Maurer, E. P., and D. P. Lettenmaier (2003), Predictability of seasonal runoff in the Mississippi River basin, *J. Geophys. Res.*, *108*(D16), doi:10.1029/2002JD002555.

Mazurkiewicz, A. B., D. G. Callery, and J. J. McDonnell (2008), Assessing the controls of the snow energy balance

Bibliography

and water available for runoff in a rain-on-snow environment, *J. Hydrol.*, *354*(1–4), 1–14, doi:10.1016/j.jhydrol.2007.12.027.

McClung, D., and P. A. Schaerer (2006), *The Avalanche Handbook*, 3 ed., The Mountaineers Books.

McCord, J. T. (1991), Application of second-type boundaries in unsaturated flow modeling, *Water Resour. Res.*, *27*(12), 3257–3260, doi:10.1029/91WR02158.

McCuen, R., Z. Knight, and A. Cutter (2006), Evaluation of the Nash-Sutcliffe Efficiency Index, *J. Hydrol. Eng.*, *11*(6), 597–602, doi:10.1061/(ASCE)1084-0699(2006)11:6(597).

McNamara, J. P., D. Chandler, M. Seyfried, and S. Achet (2005), Soil moisture states, lateral flow, and streamflow generation in a semi-arid, snowmelt-driven catchment, *Hydrol. Proc.*, *19*(20), 4023–4038, doi:10.1002/hyp.5869.

MeteoSwiss (2013), Documentation of MeteoSwiss grid-data products, daily precipitation (final analysis): RhiresD, *Tech. rep.*, Federal Office of Meteorology and Climatology MeteoSwiss, Zürich, Switzerland.

Michlmayr, G., M. Lehning, G. Koboltschnig, H. Holzmann, M. Zappa, R. Mott, and W. Schöner (2008), Application of the Alpine 3D model for glacier mass balance and glacier runoff studies at Goldbergkees, Austria, *Hydrol. Proc.*, *22*(19), 3941–3949, doi:10.1002/hyp.7102.

Mittelbach, H., I. Lehner, and S. I. Seneviratne (2012), Comparison of four soil moisture sensor types under field conditions in Switzerland, *J. Hydrol.*, *430–431*(0), 39–49, doi:10.1016/j.jhydrol.2012.01.041.

Mitterer, C., H. Hirashima, and J. Schweizer (2011a), Wet-snow instabilities: comparison of measured and modelled liquid water content and snow stratigraphy, *Ann. Glaciol.*, *52*(58), 201–208, doi:10.3189/172756411797252077.

Mitterer, C., A. Heilig, J. Schweizer, and O. Eisen (2011b), Upward-looking ground-penetrating radar for measuring wet-snow properties, *Cold Reg. Sci. Technol.*, *69*(2-3), 129–138, doi:10.1016/j.coldregions.2011.06.003, International Snow Science Workshop (ISSW) 2010.

Morin, S., Y. Lejeune, B. Lesaffre, J.-M. Panel, D. Poncet, P. David, and M. Sudul (2012), An 18-yr long (1993–2011) snow and meteorological dataset from a mid-altitude mountain site (Col de Porte, France, 1325 m alt.) for driving and evaluating snowpack models, *Earth System Science Data*, *4*(1), 13–21, doi:10.5194/essd-4-13-2012.

Mott, R., F. Faure, M. Lehning, H. Löwe, B. Hynek, G. Michlmayer, A. Prokop, and W. Schöner (2008), Simulation of seasonal snow-cover distribution for glacierized sites on Sonnblick, Austria, with the Alpine3D model, *Ann. Glaciol.*, *49*(1), 155–160, doi:10.3189/172756408787814924.

Mott, R., M. Schirmer, M. Bavay, T. Grünewald, and M. Lehning (2010), Understanding snow-transport processes shaping the mountain snow-cover, *Cryosphere*, *4*(4), 545–559, doi:10.5194/tc-4-545-2010.

Mott, R., C. Gromke, T. Grünewald, and M. Lehning (2013), Relative importance of advective heat transport and boundary layer decoupling in the melt dynamics of a patchy snow cover, *Adv. Water Resour.*, *55*(0), 88–97, doi:10.1016/j.advwatres.2012.03.001.

Mualem, Y. (1976), A new model for predicting the hydraulic conductivity of unsaturated porous media, *Water Resour. Res.*, *12*(3), 513–522, doi:10.1029/WR012i003p00513.

Nash, J., and J. Sutcliffe (1970), River flow forecasting through conceptual models part I - A discussion of principles, *J. Hydrol.*, *10*(3), 282 – 290, doi:10.1016/0022-1694(70)90255-6.

Niu, G.-Y., C. Paniconi, P. A. Troch, R. L. Scott, M. Durcik, X. Zeng, T. Huxman, and D. C. Goodrich (2014), An integrated modelling framework of catchment-scale ecohydrological processes: 1. Model description and tests over an energy-limited watershed, *Ecohydrol.*, *7*(2), 427–439, doi:10.1002/eco.1362.

Ochsner, T. E., R. Horton, and T. Ren (2001), A new perspective on soil thermal properties, *Soil Sci. Soc. Am. J.*, *65*(6), 1641–1647, doi:10.2136/sssaj2001.1641.

Okorn, R., G. Brunnhofer, T. Platzer, A. Heilig, L. Schmid, C. Mitterer, J. Schweizer, and O. Eisen (2014), Upward-looking L-band FMCW radar for snow cover monitoring, *Cold Reg. Sci. Technol.*, *103*, 31–40, doi:10.1016/j.coldregions.2014.03.006.

Omstedt, A. (1990), A coupled one-dimensional sea ice-ocean model applied to a semi-enclosed basin, *Tellus A*, *42*(5), 568–582, doi:10.1034/j.1600-0870.1990.t01-3-00007.x.

Paniconi, C., and M. Putti (1994), A comparison of Picard and Newton iteration in the numerical solution of multi-dimensional variably saturated flow problems, *Water Resour. Res.*, *30*(12), 3357–3374, doi:10.1029/94WR02046.

Parlange, J. Y., and D. E. Hill (1976), Theoretical analysis of wetting front instability in soils, *Soil Science*, *122*(4).

Parlange, J.-Y., T. S. Steenhuis, L. Li, D. A. Barry, and F. Stagnitti (2002), Column flow in stratified soils and fingers in Hele-Shaw cells: A review, in *Geophys. Monogr. Ser.*, vol. 129, pp. 79–85, AGU, Washington, DC, doi:10.1029/129GM08.

Peitzsch, E., B. Karl, and H. Kathy. (2008), Water movement and capillary barriers in a stratified and inclined snowpack, in *Proceedings Whistler 2008 International Snow Science Workshop September 21-27, 2008*, pp. 179–187.

Peters, A. (2013), Simple consistent models for water retention and hydraulic conductivity in the complete moisture range, *Water Resour. Res.*, *49*(10), 6765–6780, doi:10.1002/wrcr.20548.

Philip, J. R., and D. A. De Vries (1957), Moisture movement in porous materials under temperature gradients, *Eos Trans. AGU*, *38*(2), 222–232, doi:10.1029/TR038i002p00222.

Pradhanang, S. M., A. Frei, M. Zion, E. M. Schneiderman, T. S. Steenhuis, and D. Pierson (2013), Rain-on-snow runoff events in New York, *Hydrol. Proc.*, *27*(21), 3035–3049, doi:10.1002/hyp.9864.

Rathfelder, K., and L. M. Abriola (1994), Mass conservative numerical solutions of the head-based Richards equation, *Water Resour. Res.*, *30*(9), 2579–2586, doi:10.1029/94WR01302.

Richards, L. (1931), Capillary conduction of liquids through porous mediums, *J. Appl. Phys.*, *1*(5), 318–333, doi:10.1063/1.1745010.

Rigon, R., G. Bertoldi, and T. M. Over (2006), GEOtop: A distributed hydrological model with coupled water and energy budgets, *J. Hydrometeor.*, *7*(3), 371–388, doi:10.1175/JHM497.1.

Rössler, O., P. Froidevaux, U. Börst, R. Rickli, O. Martius, and R. Weingartner (2014), Retrospective analysis of a nonforecasted rain-on-snow flood in the Alps – a matter of model limitations or unpredictable nature?, *Hydrol. Earth Syst. Sci.*, *18*(6), 2265–2285, doi:10.5194/hess-18-2265-2014.

Saito, H., J. Šimůnek, and B. P. Mohanty (2006), Numerical analysis of coupled water, vapor, and heat transport in the vadose zone, *Vadose Zone J.*, *5*, 784–800, doi:10.2136/vzj2006.0007.

Schaap, M. G., F. J. Leij, and M. T. van Genuchten (2001), ROSETTA: a computer program for estimating soil hydraulic parameters with hierarchical pedotransfer functions, *J. Hydrol.*, *251*(3–4), 163–176, doi:10.1016/S0022-1694(01)00466-8.

Schirmer, M., M. Lehning, and J. Schweizer (2009), Statistical forecasting of regional avalanche danger using simulated snow-cover data, *J. Glaciol.*, *55*(193), 761–768, doi:10.3189/002214309790152429.

Schmid, L., A. Heilig, C. Mitterer, J. Schweizer, H. Maurer, R. Okorn, and O. Eisen (2014), Continuous snowpack monitoring using upward-looking ground-penetrating radar technology, *J. Glaciol.*, *60*(221), 509–525, doi:10.3189/2014JoG13J084.

Schmucki, E., C. Marty, C. Fierz, and M. Lehning (2014), Evaluation of modelled snow depth and snow water equivalent at three contrasting sites in switzerland using SNOWPACK simulations driven by different meteorological data input, *Cold Reg. Sci. Technol.*, *99*(0), 27–37, doi:10.1016/j.coldregions.2013.12.004.

Schneebeli, M. (1995), Development and stability of preferential flow paths in a layered snowpack, in *Biogeochemistry of Seasonally Snow-Covered Catchments (Proceedings of a Boulder Symposium July 1995)*, edited by K. Tonnessen, M. Williams, and M. Tranter, p. 89–95, AHS Publ. no. 228.

Selker, J. S., T. S. Steenhuis, and J.-Y. Parlange (1992), Wetting front instability in homogeneous sandy soils under continuous infiltration, *Soil Sci. Soc. Am. J.*, *56*, 1346–1350, doi:10.2136/sssaj1992.03615995005600050003x.

Seyfried, M. S., L. E. Grant, D. Marks, A. Winstral, and J. McNamara (2009), Simulated soil water storage effects on streamflow generation in a mountainous snowmelt environment, Idaho, USA, *Hydrol. Proc.*, *23*(6), 858–873, doi:10.1002/hyp.7211.

Shanley, J. B., and A. Chalmers (1999), The effect of frozen soil on snowmelt runoff at Sleepers River, Vermont, *Hydrol. Proc.*, *13*(12-13), 1843–1857, doi:10.1002/(SICI)1099-1085(199909)13:12/13<1843::AID-HYP879>3.0.CO;2-G.

Shimizu, H. (1970), *Air permeability of deposited snow*, 32 pp., Institute of Low Temperature Science, Sapporo, Japan.

Sihvola, A., and M. Tiuri (1996), Snow Fork for field determination of the density and wetness profiles of a snow pack, *IEEE T. Geosci. Remote*, *GE-24*, 717–721.

Singh, P., G. Spitzbart, H. Hübl, and H. Weinmeister (1997), Hydrological response of snowpack under rain-on-snow events: a field study, *J. Hydrol.*, *202*(1–4), 1–20, doi:10.1016/S0022-1694(97)00004-8.

Stössel, F., M. Guala, C. Fierz, C. Manes, and M. Lehning (2010), Micrometeorological and morphological observations of surface hoar dynamics on a mountain snow cover, *Water Resour. Res.*, *46*(4), doi:10.1029/2009WR008198.

Sturm, M., and C. S. Benson (1997), Vapor transport, grain growth and depth-hoar development in the subarctic snow, *J. Glaciol.*, *43*(143), 42–59.

Bibliography

Sturm, M., B. Taras, G. E. Liston, C. Derksen, T. Jonas, and J. Lea (2010), Estimating snow water equivalent using snow depth data and climate classes, *J. Hydrometeor.*, *11*(6), 1380–1394, doi:10.1175/2010JHM1202.1.

Sui, J., and G. Koehler (2001), Rain-on-snow induced flood events in Southern Germany, *J. Hydrol.*, *252*(1-4), 205–220, doi:10.1016/S0022-1694(01)00460-7.

Szymkiewicz, A., and R. Helmig (2011), Comparison of conductivity averaging methods for one-dimensional unsaturated flow in layered soils, *Adv. Water Resour.*, *34*(8), 1012 – 1025, doi:10.1016/j.advwatres.2011.05.011.

Tarboton, D. G., and C. H. Luce (1996), *Utah energy balance snow accumulation and melt model (UEB). Computer model technical description and users guide.*, Utah Water Research Laboratory, Utah State University and USDA Forest Service Intermountain Research Station.

Techel, F., and C. Pielmeier (2011), Point observations of liquid water content in wet snow – investigating methodical, spatial and temporal aspects, *Cryosphere*, *5*(2), 405–418, doi:10.5194/tc-5-405-2011.

Techel, F., C. Pielmeier, and M. Schneebeli (2011), Microstructural resistance of snow following first wetting, *Cold Reg. Sci. Technol.*, *65*(3), 382–391, doi:10.1016/j.coldregions.2010.12.006.

Topp, G. C. (1969), Soil-water hysteresis measured in a sandy loam and compared with the hysteretic domain model, *Soil Sci. Soc. Am. J.*, *33*, 645–651, doi:10.2136/sssaj1969.03615995003300050011x.

Unsworth, M. H., and J. L. Monteith (1975), Long-wave radiation at the ground I. Angular distribution of incoming radiation, *Q. J. Roy. Meteor. Soc.*, *101*(427), 13–24, doi:10.1002/qj.49710142703.

van Genuchten, M. T. (1980), A closed-form equation for predicting the hydraulic conductivity of unsaturated soils, *Soil Sci. Soc. Am. J.*, *44*(5), 892–898, doi:10.2136/sssaj1980.03615995004400050002x.

Vionnet, V., E. Brun, S. Morin, A. Boone, S. Faroux, P. Le Moigne, E. Martin, and J.-M. Willemet (2012), The detailed snowpack scheme Crocus and its implementation in SURFEX v7.2, *Geosci. Model Dev.*, *5*(3), 773–791, doi:10.5194/gmd-5-773-2012.

Viviroli, D., H. H. Dürr, B. Messerli, M. Meybeck, and R. Weingartner (2007), Mountains of the world, water towers for humanity: Typology, mapping, and global significance, *Water Resour. Res.*, *43*(7), n/a–n/a, doi:10.1029/2006WR005653.

Šimůnek, J., N. J. Jarvis, M. van Genuchten, and A. Gärdenäs (2003), Review and comparison of models for describing non-equilibrium and preferential flow and transport in the vadose zone, *J. Hydrol.*, *272*(1-4), 14–35, doi:10.1016/S0022-1694(02)00252-4, soil Hydrological Properties and Processes and their Variability in Space and Time.

Wakahama, G. (1963), The infiltration of melt water into snow cover I., *Low Temp. Sci. Ser. A, 21*, 45–74, in Japanese, with English abstract.

Wakahama, G. (1968), The metamorphism of wet snow, *Tech. rep.*, International Association of Scientific Hydrology, publication 79.

Waldner, P. A., M. Schneebeli, U. Schultze-Zimmermann, and H. Flühler (2004), Effect of snow structure on water flow and solute transport, *Hydrol. Proc.*, *18*(7), 1271–1290, doi:10.1002/hyp.1401.

Walter, B., S. Horender, C. Gromke, and M. Lehning (2013), Measurements of the pore-scale water flow through snow using Fluorescent Particle Tracking Velocimetry, *Water Resour. Res.*, *49*(11), 7448–7456, doi:10.1002/2013WR013960.

Walter, M. T., E. S. Brooks, D. K. McCool, L. G. King, M. Molnau, and J. Boll (2005), Process-based snowmelt modeling: does it require more input data than temperature-index modeling?, *J. Hydrol.*, *300*(1-4), 65–75, doi:10.1016/j.jhydrol.2004.05.002.

Wankiewicz, A. C. (1976), Water percolation within a deep snowpack: Field investigations at a site on Mt. Seymour, British Columbia, Ph.D. thesis, Univ. of British Columbia.

Warscher, M., U. Strasser, G. Kraller, T. Marke, H. Franz, and H. Kunstmann (2013), Performance of complex snow cover descriptions in a distributed hydrological model system: A case study for the high Alpine terrain of the Berchtesgaden Alps, *Water Resour. Res.*, *49*(5), 2619–2637, doi:10.1002/wrcr.20219.

Waterhouse, R. W., and L. Bunten (1969), Permeability and strength of aging snow, *Special Report 124*, US Army Cold Regions Research and Engineering Laboratory.

Weingartner, R., M. Barben, and M. Spreafico (2003), Floods in mountain areas–an overview based on examples from Switzerland, *J. Hydrol.*, *282*(1–4), 10–24, doi:10.1016/S0022-1694(03)00249-X.

Wever, N., C. Fierz, C. Mitterer, H. Hirashima, and M. Lehning (2014), Solving Richards Equation for snow improves snowpack meltwater runoff estimations in detailed multi-layer snowpack model, *Cryosphere*, *8*(1), 257–274,

doi:10.5194/tc-8-257-2014.

Winstral, A., K. Elder, and R. E. Davis (2002), Spatial snow modeling of wind-redistributed snow using terrain-based parameters, *J. Hydrometeor.*, *3*(5), 524–538, doi:10.1175/1525-7541(2002)003<0524:SSMOWR>2.0.CO;2.

Yamaguchi, S., T. Katsushima, A. Sato, and T. Kumakura (2010), Water retention curve of snow with different grain sizes, *Cold Reg. Sci. Technol.*, *64*(2), 87 – 93, doi:10.1016/j.coldregions.2010.05.008.

Yamaguchi, S., K. Watanabe, T. Katsushima, A. Sato, and T. Kumakura (2012), Dependence of the water retention curve of snow on snow characteristics, *Ann. Glaciol.*, *53*(61), 6–12, doi:10.3189/2012AoG61A001.

Yang, Z.-L., and G.-Y. Niu (2003), The versatile integrator of surface and atmosphere processes: Part 1. Model description, *Global Planet. Change*, *38*(1-2), 175–189, doi:10.1016/S0921-8181(03)00028-6.

Zanotti, F., S. Endrizzi, G. Bertoldi, and R. Rigon (2004), The GEOTOP snow module, *Hydrol. Proc.*, *18*(18), 3667–3679, doi:10.1002/hyp.5794.

Zappa, M., F. Pos, U. Strasser, P. Warmerdam, and J. Gurtz (2003), Seasonal water balance of an Alpine catchment as evaluated by different methods for spatially distributed snowmelt modelling, *Nord. Hydrol.*, *34*(3), 179–202, doi:10.2166/nh.2003.012.

Curriculum Vitae

Name: Nander Wever

Date and place of birth: 21 April 1982, The Hague, the Netherlands

Nationality: Dutch

1994-2000:	Pre-university education at Stedelijk Gymnasium Leiden, the Netherlands.
2000-2007:	Study Meteorology and Physical Oceanography at Utrecht University, the Netherlands. Master thesis: "Sublimation during drifting and blowing snow events".
2007-2010:	Research scientist at the Royal Netherlands Meteorological Institute (KNMI), de Bilt, the Netherlands. Research topics: wind climatology and climate change.
2010-2014:	PhD at École Polytechnique Fédérale de Lausanne (EPFL), Lausanne, Switzerland and the WSL Institute for Snow and Avalanche Research SLF, Davos Dorf, Switzerland.

Publications:

– Wever, N., Jonas, T., Fierz, C. and Lehning, M. (2014) Model simulations of the modulating effect of the snow cover in a rain-on-snow event, *Hydrol. Earth Syst. Sci.*, 18, 4657-4669, doi: 10.5194/hess-18-4657-2014.

– Wever, N., Fierz, C., Mitterer, C., Hirashima, H., and M. Lehning (2014) Solving Richards Equation for snow improves snowpack meltwater runoff estimations in detailed multi-layer snowpack model, *Cryosphere*, 8, 257-274, doi: 10.5194/tc-8-257-2014.

– Wever, N. (2012), Quantifying trends in surface roughness and the effect on surface wind speed observations, *J. Geophys. Res.*, 117, D11104, doi:10.1029/2011JD017118.

– Caires, S., de Waal, H., Groeneweg, J. Groen, G., Wever, N., Geerse C., and Bottema, M. (2012) Assessing the uncertainties of using land-based wind observations for determining extreme open-water winds, *J. Wind Eng. Ind. Aerodyn.*, 110, 70-85, doi: 10.1016/j.jweia.2012.07.009.

– Wever, N., Lehning, M., Clifton, A., Rüedi, J.-D., Nishimura, K., Nemoto, M., Yamaguchi, S., and Sato, A. (2009) Verification of moisture budgets during drifting snow conditions in a cold wind tunnel, *Water Resour. Res.*, 45, W07423, doi:10.1029/2008WR007522.